AD-A099 406 SCIENCE APPLICATIONS INC MCLEAN VA F/G 20/1
EFFECTS OF THE GULF STREAM ON ACOUSTIC PROPAGATION.(U)
JUL 80 A D'AMICO N00014-79-C-0481
UNCLASSIFIED SAI-81-221-WA NL

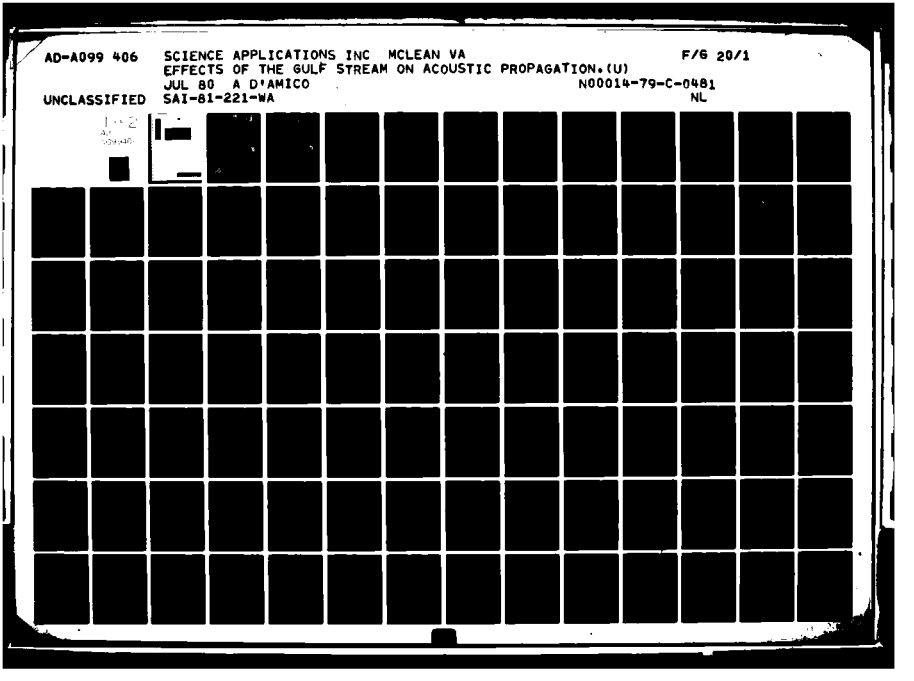

LEVEL II

EFFECTS OF THE GULF STREAM ON ACOUSTIC PROPAGATION

SAI-81-221-WA

SAI
ATLANTA • ANN ARBOR • BOSTON • CHICAGO • CLEVELAND • DENVER • HUNTSVILLE • LA JOLLA
LITTLE ROCK • LOS ANGELES • SAN FRANCISCO • SANTA BARBARA • TUCSON • WASHINGTON

SECURITY CLASSIFICATION OF THIS PAGE (When Data Entered)

REPORT DOCUMENTATION PAGE

READ INSTRUCTIONS BEFORE COMPLETING FORM

1. REPORT NUMBER: SAI-81-221-WA	2. GOVT ACCESSION NO.: AD A099406
3. RECIPIENT'S CATALOG NUMBER	
4. TITLE (and Subtitle): Effects of the Gulf Stream on Acoustic Propagation.	5. TYPE OF REPORT & PERIOD COVERED: Final rept.
	6. PERFORMING ORG. REPORT NUMBER: SAI-81-221-WA
7. AUTHOR(s): Angela D'Amico	8. CONTRACT OR GRANT NUMBER(s): N00014-79-C-0481
9. PERFORMING ORGANIZATION NAME AND ADDRESS: Science Applications, Inc. 1710 Goodridge Dr. McLean, VA 22102	10. PROGRAM ELEMENT, PROJECT, TASK AREA & WORK UNIT NUMBERS
11. CONTROLLING OFFICE NAME AND ADDRESS: Office of Naval Research 800 N Quincy Street Arlington, VA. 22217	12. REPORT DATE: Jul 1981; NUMBER OF PAGES: 154, 142
14. MONITORING AGENCY NAME & ADDRESS (if different from Controlling Office): NORDA Code 500 Naval Ocean Research & Development Activity NSTL Station, Bay St Louis, MS 39529	15. SECURITY CLASS. (of this report): Unclassified
	15a. DECLASSIFICATION DOWNGRADING SCHEDULE: N/A

16. DISTRIBUTION STATEMENT (of this Report)

DISTRIBUTION STATEMENT A
Approved for public release;
Distribution Unlimited

Unlimited to qualified DTIC users.

DTIC ELECTE MAY 27 1981 S C D

17. DISTRIBUTION STATEMENT (of the abstract entered in Block 20, if different from Report)

Abstract unlimited

18. SUPPLEMENTARY NOTES

19. KEY WORDS (Continue on reverse side if necessary and identify by block number)

Acoustic propagation	Transmission Loss
Fronts	Surface Ducts
Gulf Stream	Convergence Zones
Tactical Sonar Systems	Ray Models
	Wave Models

20. ABSTRACT (Continue on reverse side if necessary and identify by block number)

This report investigates the effect of the Gulf Stream frontal system on acoustic propagation relative to tactical sonar systems (.1-20 HKZ). An oceanographic description of the Gulf Stream frontal system is included. Two ray models (MPP and GRASS) and one wave model (PE) were compared against measured acoustic data. The appendix contains ray plots and transmission loss estimated for many source/receiver geometries across the Gulf Stream.

DD FORM 1 JAN 73 1473 EDITION OF 1 NOV 65 IS OBSOLETE

408404

UNCLASSIFIED

SECURITY CLASSIFICATION OF THIS PAGE (When Data Entered)

EFFECTS OF THE GULF STREAM ON ACOUSTIC PROPAGATION

SAI-81-221-WA

July 1980

Final Report

Contract N00014-79-C-0481

Prepared for:

Naval Ocean Research and
Development Activity
Code 500

Prepared by:

Angela D'Amico

821-5752

SCIENCE APPLICATIONS, INC.
1710 Goodridge Drive
McLean, Virginia 22102
(703) 821-4300

ACKNOWLEDGEMENTS

Appreciation is extended to Jim Lewis who is responsible, in part, for Section 2 of this report. The author would like to acknowledge the technical assistance of J. S. Hanna and other members of the Acoustics Division of SAI who are too numerous to mention individually.

TABLE OF CONTENTS

LIST OF FIGURES

LIST OF FIGURES (Continued)

Section 1
INTRODUCTION

The objective of this work is to investigate the effects of the Gulf Stream frontal system on acoustic propagation relative to tactical sonar systems. To accomplish this, two Gulf Stream data sets were considered. The first data set, provided by the U.S. Naval Oceanographic Office, was used in a comparative model study. The second, provided by the Naval Underwater Systems Center (NUSC), was used to characterize the environmental acoustic parameters of the Gulf Stream frontal system in the detail needed for systems utilizing ranges of second convergence zone or less. Transmission loss estimates have been obtained from range dependent acoustic propagation models for source and receiver geometries of tactical importance relative to features associated with this frontal system.

The characterization of acoustic propagation through a front involves several problems at frequencies of tactical systems (.1 - 20 kHz). These include convergence zone structure, leakage from surface ducts and reinsonification of surface ducts near convergence zones. Convergence zone structure can be determined from a ray model. Leakage from a range dependent surface duct and reinsonification of a surface duct near a convergence zone can best be handled by a wave model, although for the frequencies of interest a wave model is limited. Two ray models (MPP and GRASS) and one wave model (PE) were used in this analysis. The primary disadvantage of ray models is their inadequacy for handling

diffraction and leakage. The primary disadvantage of PE is the practical limitation on the combination of frequency and depth which can be handled. At the high frequency end, the propagation of interest is via direct and surface ducted paths. The diffracted field at these frequencies does not have an important effect, so a ray model should adequately handle the direct paths. A ray model may be limited in its handling of ducted paths. These limitations are discussed in the model evaluation.

The study of acoustic propagation through the Gulf Stream leads to questions concerning the position and temperature of the stream, as well as the variations of these characteristics with time. A brief discussion of the oceanographic characteristics of the Gulf Stream is found in the next section. Subsequent sections contain the technical approach, the model evaluation, and the acoustic implications of this model study.

Section 2
GULF STREAM ENVIRONMENT

In the region of the Gulf Stream, temperature variations are large when compared to salinity variations. This is due largely to the annual heating and cooling of the slope and the shelf waters. Since temperature variations are of greater importance with respect to acoustic propagation, the literature was reviewed for those studies dealing with long-term vertical temperature sampling across the Gulf Stream.

In October 1969 a program was initiated by the Naval Oceanographic Office to monitor the thermal structure of the water column between New York and Bermuda. The basic results of the study were: 1) the seasonal heating and cooling extended only to the upper 200 m of the ocean, and 2) the north wall position (defined as the maximum horizontal temperature gradient at 200 m) can be estimated from the maximum surface temperature. The minimum temperatures occurred in March/April while the maximum temperatures occured in August/September at the surface and September/October in the near-surface waters. The typical surface temperature change across the transits was 3^{o} - $4^{o}C$ in summer and as much as $15^{o}C$ in winter. Shelf and Sargasso Sea surface temperatures were approximately $24^{o}C$ and $27^{o}C$ for the summer, and $6^{o}C$ and $18^{o}C$ for the winter. In terms of sound velocities (using a constant salinity of 35 $^{o}/oo$), the typical surface velocity change across the transits was 8 m/sec in summer and 30 m/sec in winter.

Considering the data further, an annual pattern emerges which is depicted in Figure 1. During the coldest part of the year (Figure 1A), the 15° - 19°C isotherms of the north wall intersect the surface almost directly above the north wall, with the 19° isotherm leveling off at a depth of 300 m. During April/May, the 15°C isotherm begins to make its way shoreward, and the Sargasso Sea water becomes warmer. By the time of maximum surface temperatures (Figure 1B), the 15° - 25°C isotherms have formed a seasonal pycnocline north of the Gulf Stream, and the Gulf Stream itself has warmed to 27°C. The pycnocline begins to deteriorate by mid-fall (Figure 1C), with the cooling of the Gulf Stream waters and the seaward movement of the 17° - 19°C isotherms. By early winter, the 17° and 19°C isotherms are back in positions similar to that of the coldest part of the year and the 15°C isotherm has begun working its way seaward.

The variation of this annual pattern is dependent on the variations of the heating and cooling periods of the year. For example, the depth of the 19°C isotherm in the Sargasso Sea will be a function of the amount of 18°C Sargasso Sea water formed during the winter. This water, with an average temperature of 17.9°C and salinity of 36.5 °/oo, appears south of the Gulf Stream in late winter. This layer exhibits remarkable stability; temperature variations of 0.3°C and salinity variations of 0.1 °/oo are observed. This water has been called the 18° water by Worthington (1959) and Istoshin (1961). The northern and western limit of the 18°C water is the Gulf Stream which transports surface water of 20°C or warmer at all seasons.

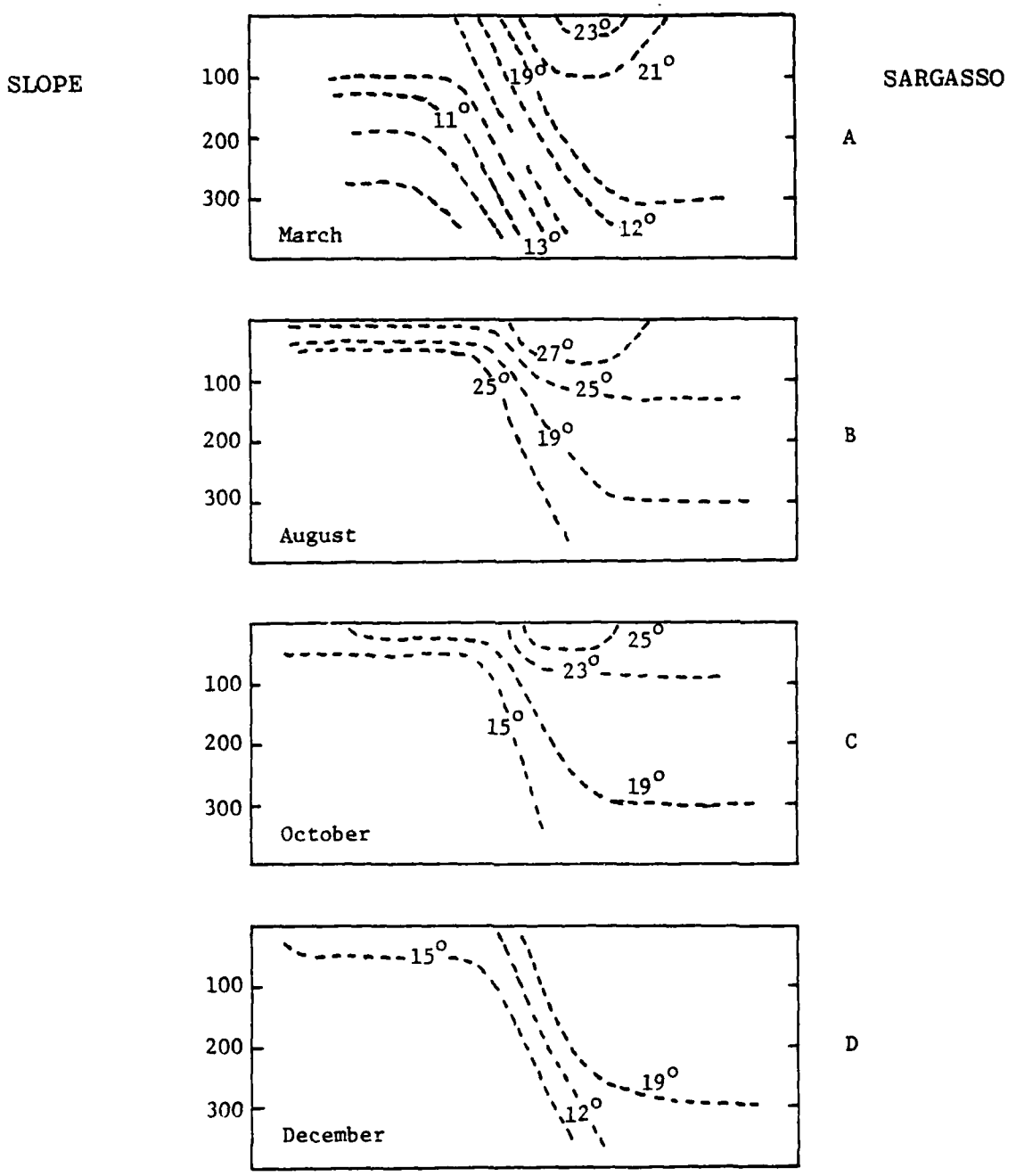

Figure 1. Seasonal Temperature Sections across the Gulf Stream.

The southern limit is around 33°N, where the surface minimum air temperature never drops below 19°C. The eastern limit is approximately in the vicinity of the Mid-Atlantic ridge, although it has been noted that the thickness of the layer decreases toward the east (Worthington, 1959). The formation of this 18°C water mass is thought to be due to outbreaks of cold, dry continental polar air that flow over the Sargasso Sea in late winter. This water mass is formed in superabundance in the Northwestern Sargasso Sea and flows southward along the density surface of $\sigma_t = 26.4$ while warm water is advected northward on the surface to replace it (Worthington, 1972). Surface warming in late spring and summer causes the formation of a seasonal thermocline, with this isothermal layer sandwiched between the seasonal and permanent thermocline.

Another factor which may influence the north wall characteristics is the entrainment of shelf water along the north edge of the Gulf Stream near Cape Hatteras (Kupperman and Garfield, 1977). This entrainment can occur above and below the shelf thermocline and results in surface and subsurface bands of fresher water found along the shoreward edge of the Gulf Stream off the northeastern United States. During periods when the shelf water is warmer than the offshore slope water, the subsurface low salinity band also appears as a temperature inversion along the north wall (Kupperman and Garfield, 1977). An intrusion of low salinity water that is cooler than the slope water can result in an increased horizontal temperature gradient at the north wall (Cheney, 1978). The horizontal scale of

these low salinity bands varies from 2 - 5 km while being 60 - 75 m thick (Kupperman and Garfield, 1977; Cheney, 1978), but little is known as to variations of these dimensions. Lower salinity of the shelf water tends to maintain the layer's vertical stability and allows it to be advected hundreds of kilometers downstream before being mixed with surrounding water (Cheney, 1978).

The acoustic environment of the Gulf Stream region can be evaluated by examining the sound velocity structure for the different water masses. Figure 2a shows typical late spring conditions in the slope water. The deep sound channel axis occurs at 500 m. The upper portion of this profile changes seasonally. Deep mixing due to winter storms results in an isothermal layer forming a surface duct. The sound velocity structure of the North Wall (Figure 2b) is primarily downward refracting. The entrained shelf water along the North Wall results in a sharp near surface sound velocity minimum. The warm core (Figure 2c) is also characterized by a sharply downward refracting region. The deep sound channel axis is deeper than the slope water. The Sargasso Sea water, like the Slope Water, is characterized by deep mixed layers in the winter and surface warming in the summer. The profile in Figure 2d shows the effects of surface warming and the remains of the surface duct formed by the 18°C water. The deep sound channel axis is at 1200 m and the channel is much wider - characteristic of warmer water.

The effect of this environment on tactical systems depends on specific source receiver geometries. In the warm core, much of the acoustic energy is refracted

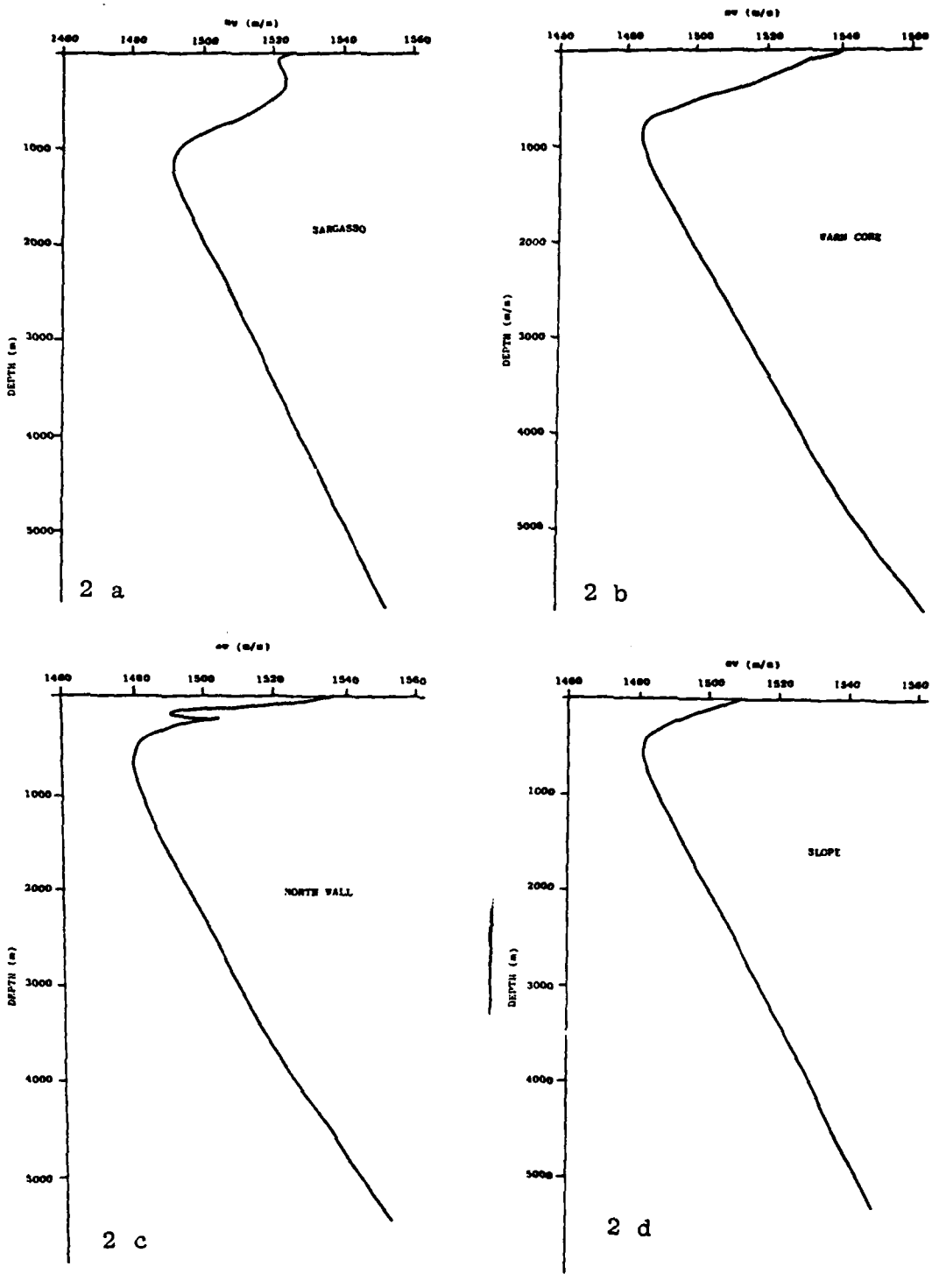

Figure 2 Four representative sound velocity profiles across the Gulf Stream

downward, into the bottom. For a receiver in the warmer Sargasso water, a signal enhancement at low frequencies can be expected for a source moving across the Gulf Stream. This results from the narrowing and rising of the deep sound channel. Detailed discussions of these effects are found in Section 5.

Section 3
TECHNICAL APPROACH

To investigate the effects of the Gulf Stream frontal system on acoustic propagation relative to tactical sonar systems a model study was performed. Transmission loss estimates from the Parabolic Equation Model (a wave model) and two ray models, GRASS (Germinating Ray Acoustics Stimulation System) and MPP (Multiple Profile Program) were compared to measured low-frequency transmission loss in the Gulf Stream. A subset of these models was used for high frequency transmission loss estimates. A discussion of the features of each model and its applicability to the analysis of the experimental data follows.

C-Field

The C-Field model permits the establishment of a continuous sound velocity field for a particular environment. Given the sound speed profiles along the track, C-Field uses a system of triangular interpolation and sound speed gradient matching to create a continuous sound speed field between any two sound velocity profiles. In this manner, sound velocity as a function of depth and range is formulated for the length of the track.

Parabolic Equation

The Parabolic Equation (PE) Model, developed by Tappert and Hardin (Tappert and Hardin, 1973; Tappert, 1974; Brock, 1978), provides an approximate solution to the

elliptical wave equation. Its primary advantage is the ability to treat range-dependent environments; secondary advantages include accuracy of solutions and ease of use. The model utilizes an environment specified by the following parameters:

- sound speed profiles
- bathymetry
- receiver depths
- source depth
- source frequency
- maximum range of interest

The PE model yields transmission loss estimates as a function of range as well as the distribution of energy as a function of depth and range along the track. These capabilities and its inherent flexibility of usage make the PE model an invaluable tool in analytic and predictive acoustical research.

The parabolic approximation method has been a powerful contribution to predictive numerical propagation models. The model is limited in its ability to treat severely varying bathymetric conditions. The measured transmission loss data considered in this study was taken by a receiver mounted on a slope which tends to reflect

incident energy. For the purposes of this study, only the waterborne energy was considered. That is, the PE calculation was made with an absorbing bottom, and any energy incident on the bottom was eliminated. The ray models were also restricted to include only energy from totally waterborne paths. In this way, the levels of predicted transmission loss can be compared and the complications in handling a slope site are avoided.

Multiple Profile Program

The Multiple Profile Program (MPP) (Spofford, 1973) uses the same range dependent environment as used by the PE model. MPP allows a visualization of sound propagation using ray tracing techniques. MPP determines ray trajectories and intensities which delineate the acoustic field of interest. For transmission loss calculations, the model uses a multipass system which first computes ray parameters, then makes an additional pass through the data to generate a smoothed range derivative function and carry out additional caustic corrections. Transmission loss estimates obtained in this study are for waterborne energy only. To accomplish this, only the angular aperture corresponding to waterborne energy is used in the calculation.

Germinating Ray Acoustic Simulation System

The Germinating Ray Acoustic Simulation System (GRASS) (Cornyn , J. J., 1973) utilizes a ray tracing technique involving iteration along the ray path. This ray tracing technique is applicable to a variable environment

with changing bottom depth, velocity profile, and sea surface conditions. The propagation loss values represent the expected value for propagation in the ocean in the context of making a series of measurements for approximately similar oceanographic conditions.

The version of GRASS used in this study is resident at the Naval Underwater Systems Center (NUSC), New London. This model uses the same range dependent track as PE and MPP but does not use the C-Field format. The model was run with a very high bottom loss so that any energy incident on the bottom was eliminated. This allowed only the waterborne energy to be used in the calculation.

At low frequencies, the PE model should provide the best approximation since the diffracted field is important. Verification of ray model results can be made by comparing the predicted transmission loss estimates with PE for these frequencies. The overall levels should agree, although the PE model should show more structure. For frequencies of tactical sonar systems, the diffracted field is less important and ray theory, which is not frequency limited, should provide a good approximation.

Section 4
ACOUSTIC MODEL COMPARISON

Environmental Description

During May 1978, the U.S. Naval Oceanographic Office conducted an exercise in which simultaneous environmental and propagation loss measurements were made along a track extending from Slope Water, through the Gulf Stream, and into the Sargasso Sea. The concurrent oceanographic and acoustic data collected during these exercises provide an excellent data set for the model evaluation to be performed in this study. Figure 3 shows the track from this experiment (I) in close proximity to the track of interest for the tactical system study. The measured transmission loss was for long range and low frequency. Under these conditions, the PE model should provide the best approximation. Transmission loss estimates from the ray models should approximate the measured transmission loss levels but should not include detailed propagation structure. As the frequency increases, the agreement between the transmission loss estimates from the ray model and wave model should increase since the diffracted field at these frequencies is less important and the ray solution should approach the wave solution.

Environmental station data were collected by the USNS BARTLETT with salinity/temperature/depth (STD) system casts to 3000 m. The USNS LYNCH followed the same track at an average speed of 14.8 km per hour while towing an omnidirectional 88.8 Hz CW projector 30 m deep. Expendable bathythermograph (XBT) measurements, from the

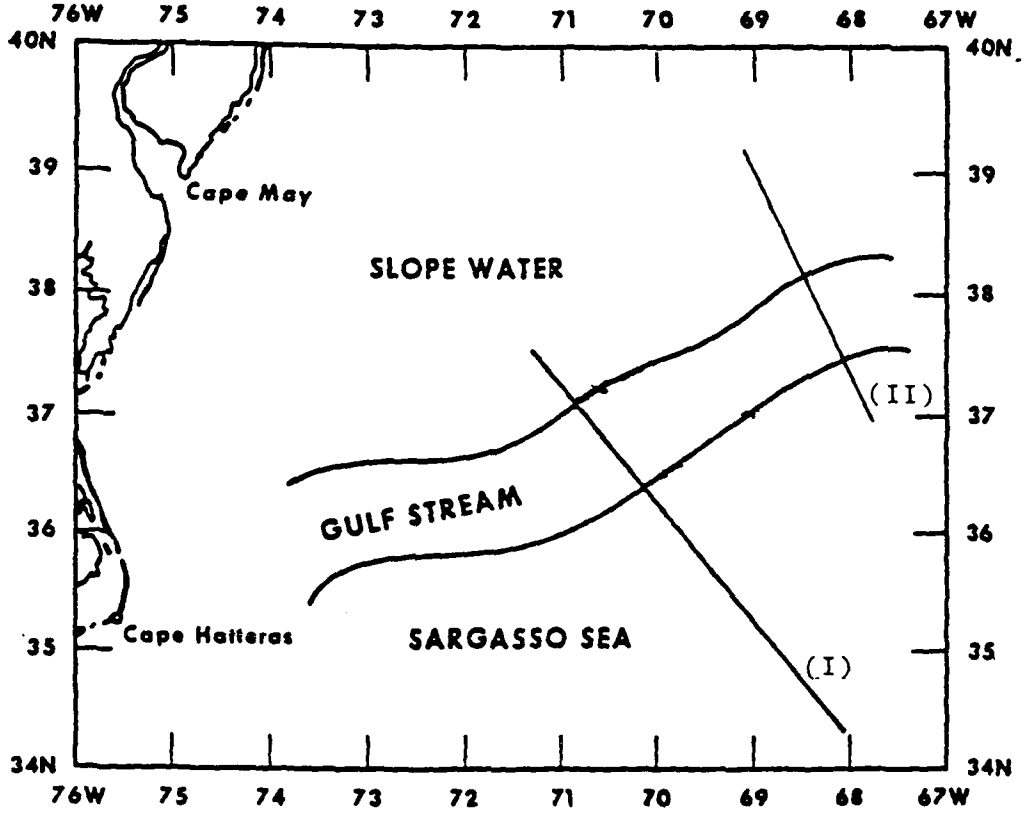

Figure 3. Track from May experiment (I)
Track from December experiment (II)
(from Gold et al., 1979).

surface to 760 m depth, were made every 1.5 km in the Gulf Stream. These densely spaced XBT's were used along with the STD's to determine the environment along the track. Transmission loss data were measured through a bottom - mounted, omnidirectional hydrophone situated near the Deep Sound Channel (DSC) axis off Bermuda. A more detailed description of this experiment and subsequent data analysis can be found in Gold et al. (1979). Both the measured transmission loss and the environmental data from this study were provided by the U.S. Naval Oceanographic Office.

Figure 4 (Gold, 1979) presents a cross section of temperature from the BARTLETT track. The Gulf Stream, indicated by the steeply sloping isotherms, extends to a depth of 3000 m. The warm core of the Gulf Stream, defined as that water with a temperature greater than 25°C is apparent in this figure. The entrained shelf water runs along the northern edge of the Gulf Stream between depths of 50 and 350 m.

Variations in temperature and salinity gradients occuring over small spatial scales have been shown to affect long range acoustic propagation (D'Amico and Blumen, 1979; Khedouri and Cheney, 1978; Fenner 1978; Gemill and Kheduri, 1974). A linear track was constructed to determine the effects of the Gulf Stream on sound transmission. The acoustic and bathymetric environment along the track is shown in Figure 5. Sound velocity profiles in the Sargasso Sea show a wide DSC with its axis at about 1200 m. Proceeding to the northwest, the deep sound channel narrows and the

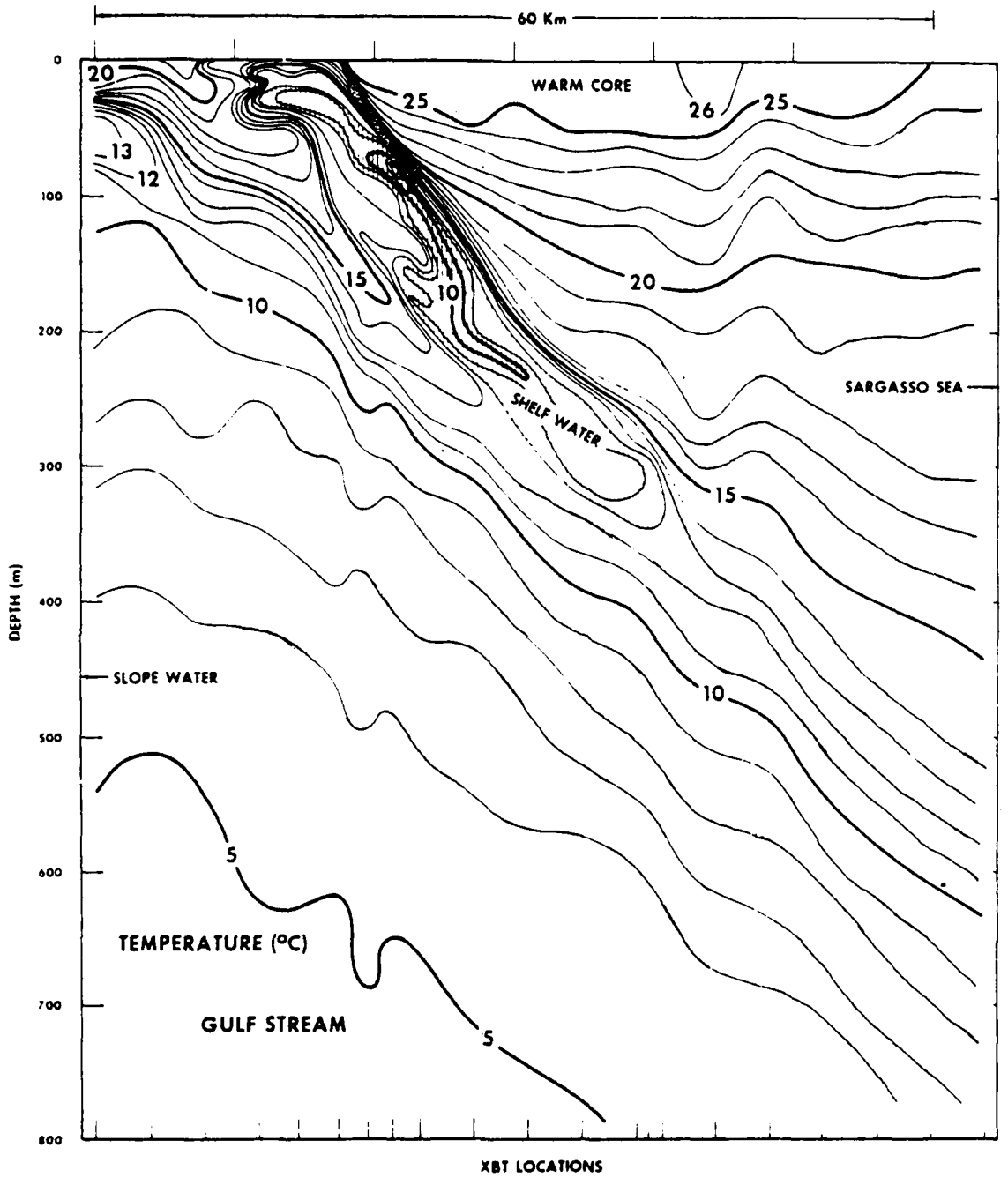

Figure 4. Gulf Stream temperature section. The North Wall, Warm Core and South Wall are illustrated (from Gold et al., 1979).

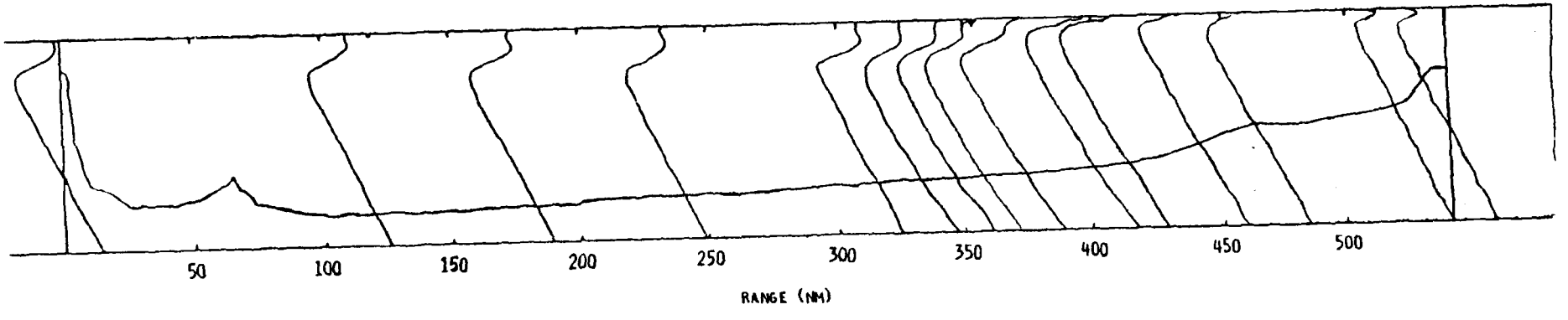

Figure 5. Acoustic and bathymetric environment along the May Gulf Stream track.

axis rises to a depth of about 500 m. The narrowing of the deep sound channel serves to focus the propagating acoustic rays in this region. The Gulf Stream is seen as a strongly downward refracting region. The bathymetry along the track becomes progressively shallower over the continental slope. The downward refracting region of the Gulf Stream causes energy to interact with the bottom. This study is concerned with only waterborne energy and these bottom interacting paths are not considered.

Acoustic Ray Paths

Acoustic ray paths have been traced outward from the receiver for the entire length of the track. These ray paths have been broken up into families that experience similar bottom and surface interactions. Only positive angles are considered since the receiver is bottom mounted. For illustrative purposes, the bottom is considered to be wholly refracting for the first 20 nm of the track. This enables all the rays to get off the slope directly in front of the receiver and propagate out in range. The bottom is totally absorbing for the remainder of the track, so that any rays incident on the bottom are eliminated from the problem.

Figure 6 shows the acoustic propagation paths for an angular aperture of 0^{o} - 3^{o}. These paths experience minimal interaction with the slope and become totally waterborne refracted-refracted (RR) paths. The structure of these paths changes upon entering the Gulf Stream (390 nm) and upon crossing the north wall (405 nm). The shoaling of

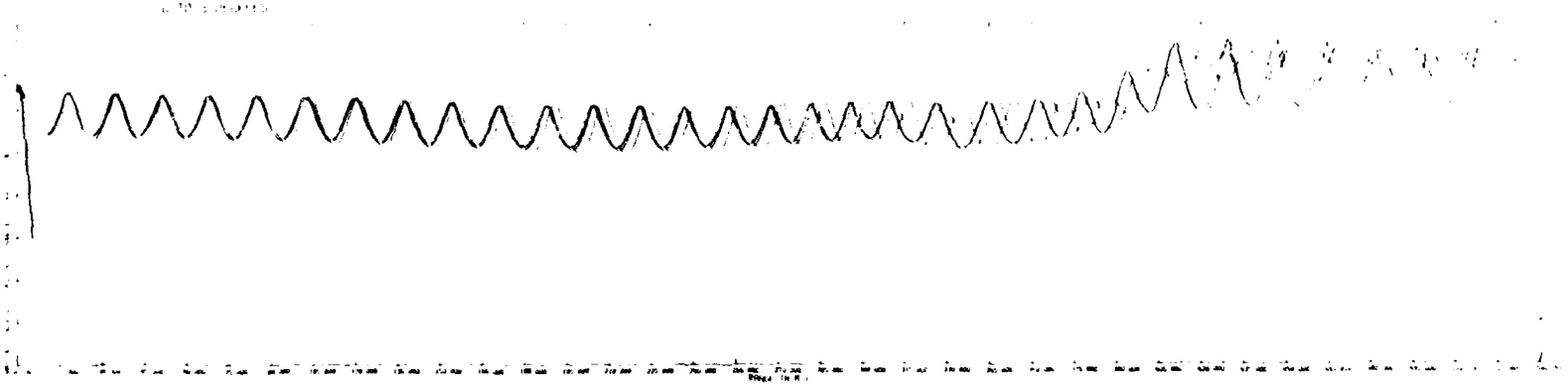

Figure 6. Acoustic ray paths (0^{o}-3^{o}) along the track - Waterborne paths.

the sound channel attributable to the presence of the front is graphically depicted by the upward migration of these paths. Figure 7 shows the ray paths associated with angles 4^{o} - 12^{o}. These paths do not interact with the slope and are totally waterborne. Again, there is a marked change in the ray structure upon entering the Gulf Stream. This family of rays also rises with the deep sound channel and there is an evident narrowing of these paths corresponding to the narrowing of the deep sound channel. Ray paths from steeper angles are shown in Figure 8. Angles from 17^{o} to 24^{o} are plotted, although this family includes angles 13^{o} to 16^{o} as well. These paths interact with the slope once and become waterborne. Changes due to the Gulf Stream crossing are not as apparent in these higher angle paths. Some of these paths interact with the absorbing bottom before crossing the north wall and lose their energy. Acoustic ray paths from very steep angles are shown in Figure 9. These paths interact with the slope twice and then interact with the bottom further out in range. These high angle paths experience many bottom interactions and do not contribute significant energy to the problem.

In summary, acoustic ray paths determine what families of rays contribute energy to the environment under consideration. The bottom type of the slope in front of the array is unknown. For purposes of illustration, it was assumed to be a perfect reflector for the first 20 nm so that the effects of the Gulf Stream on acoustic ray paths could be determined. It was shown that the ray paths from 4^{o} to 12^{o} are totally waterborne. This ray family contributes most of the energy to the problem and is modeled most accurately.

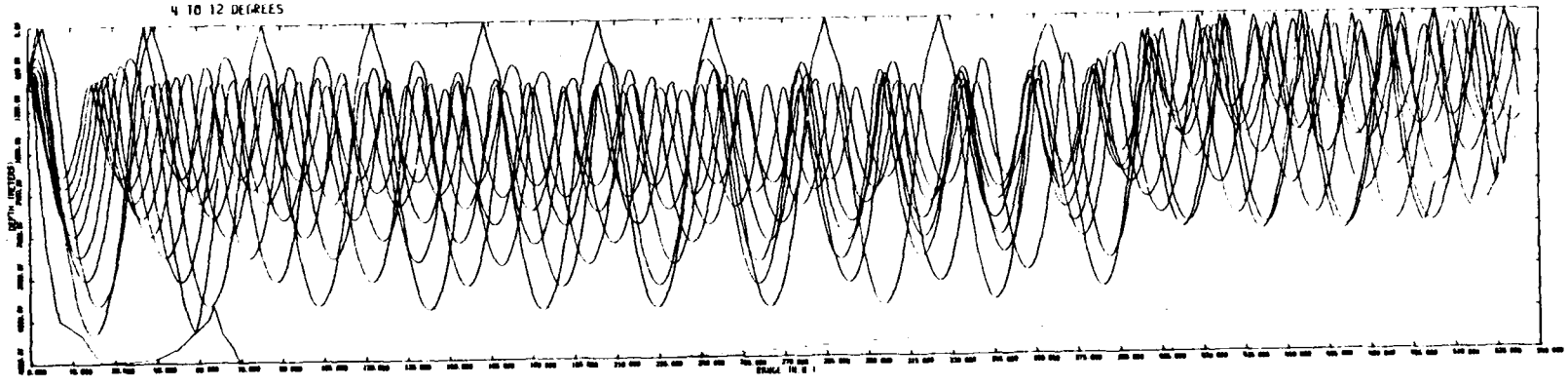

Figure 7. Acoustic ray paths (4^{o}-12^{o}) along the track - Waterborne paths.

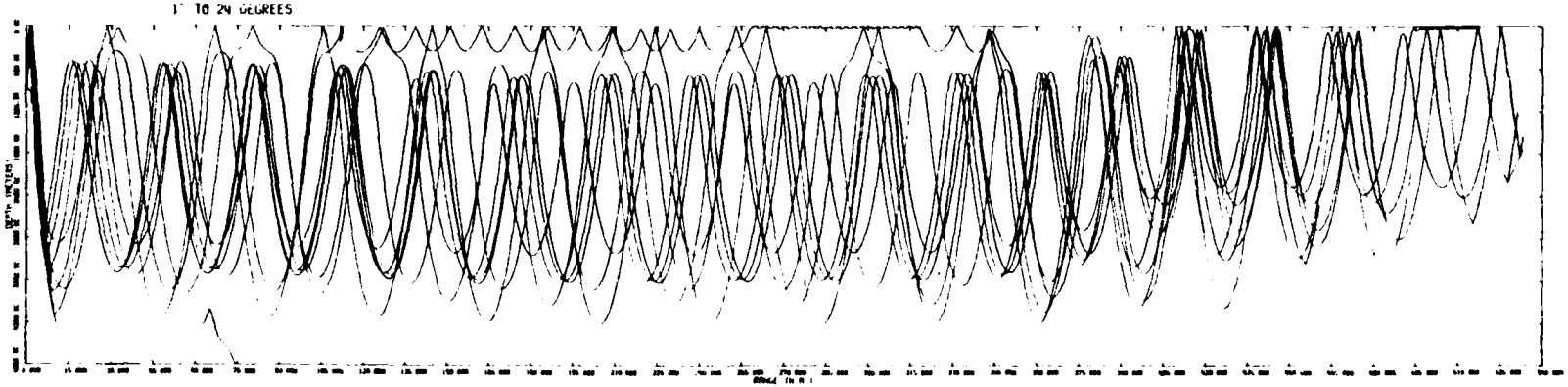

Figure 8. Acoustic ray paths (17^{o}-24^{o}) along the track - One slope interaction.

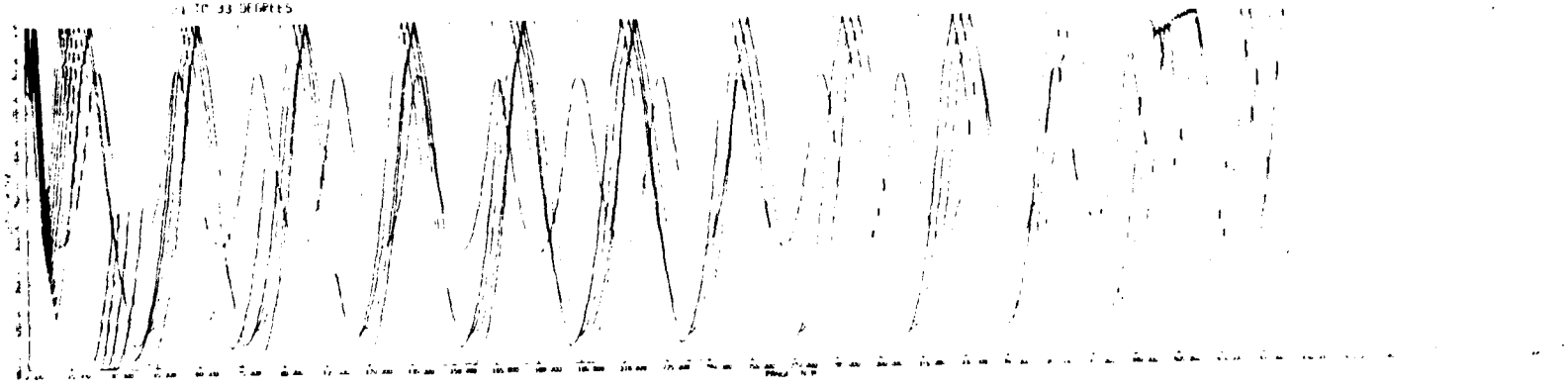

Figure 9. Acoustic ray paths (24^{O}-33^{O}) along the track - Two slope interactions.

Transmission Loss Estimates

Acoustic propagation paths as determined by geometric ray tracing techniques provide a physical justification of the distribution of energy. Transmission loss estimates from three acoustic models are compared to measured transmission loss data. In this model evaluation, only the waterborne energy is considered. This is accomplished by adjusting the environmental input to each model. PE is run with an absorbing bottom so that any energy incident on the bottom is eliminated. Input to MPP is restricted to only the waterborne paths, 4^{o} - 12^{o}. GRASS is run with a very high loss bottom which limits its effective angular aperture to 4^{o} - 12^{o} also. Transmission loss estimates for the bottom-mounted receiver and a 30 m/89 Hz source were made, using each of these three models. These were compared with measured transmission loss from the bottomed array.

Figure 10 shows transmission loss estimates from the PE model. The significant loss of energy seen at ranges 650 to 750 km results from the downward refracting region of the Gulf Stream. The marked signal enhancement occuring at 750 km corresponds to the rise and concurrent narrowing of the deep sound channel across the North Wall of the Gulf Stream. When this transmission loss estimate is compared to measured transmission loss from the bottomed array (Figure 11), it is seen that the levels of energy compare quite well. The measured transmission loss shows an additional family of paths, in the range interval from 650 to 750 km, that is not evident in the PE calculation. The major difference between these curves occurs in the region of the warm core of the Gulf Stream, where measured

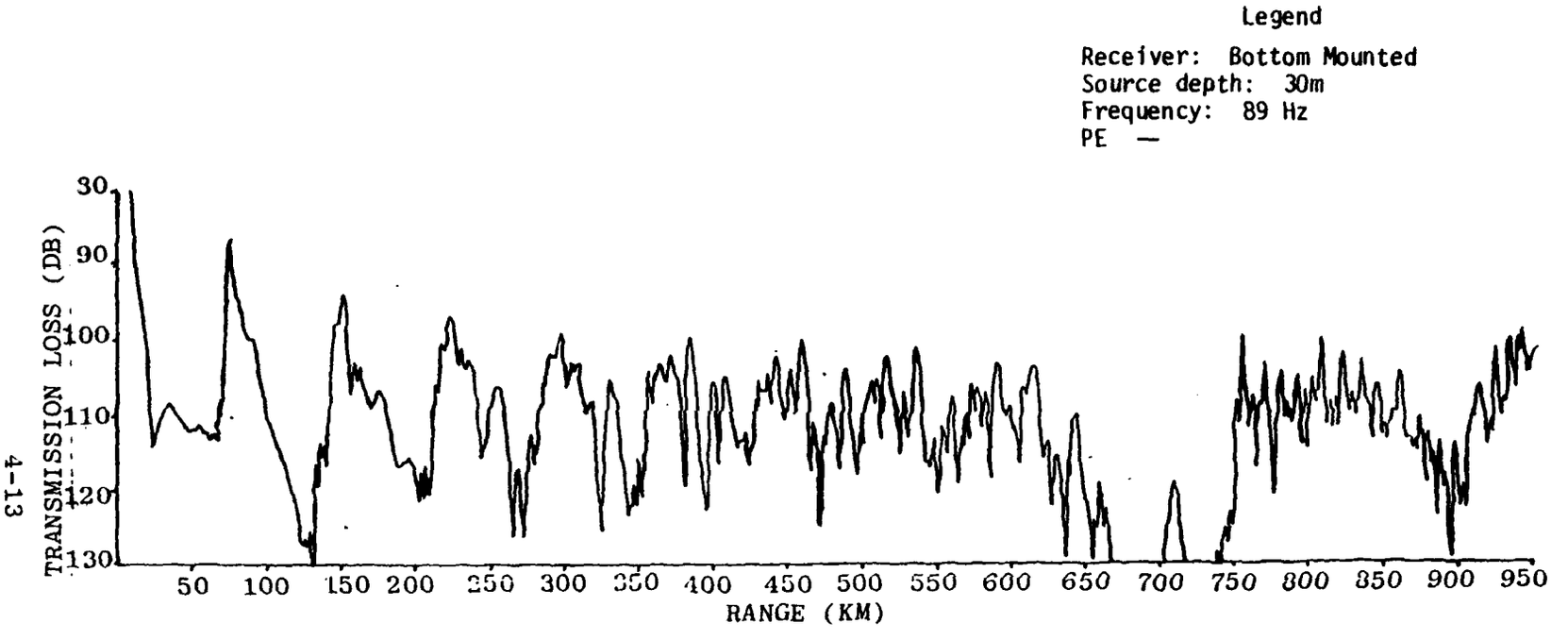

Figure 10 Transmission Loss vs. Range
May Track
PE Calculation

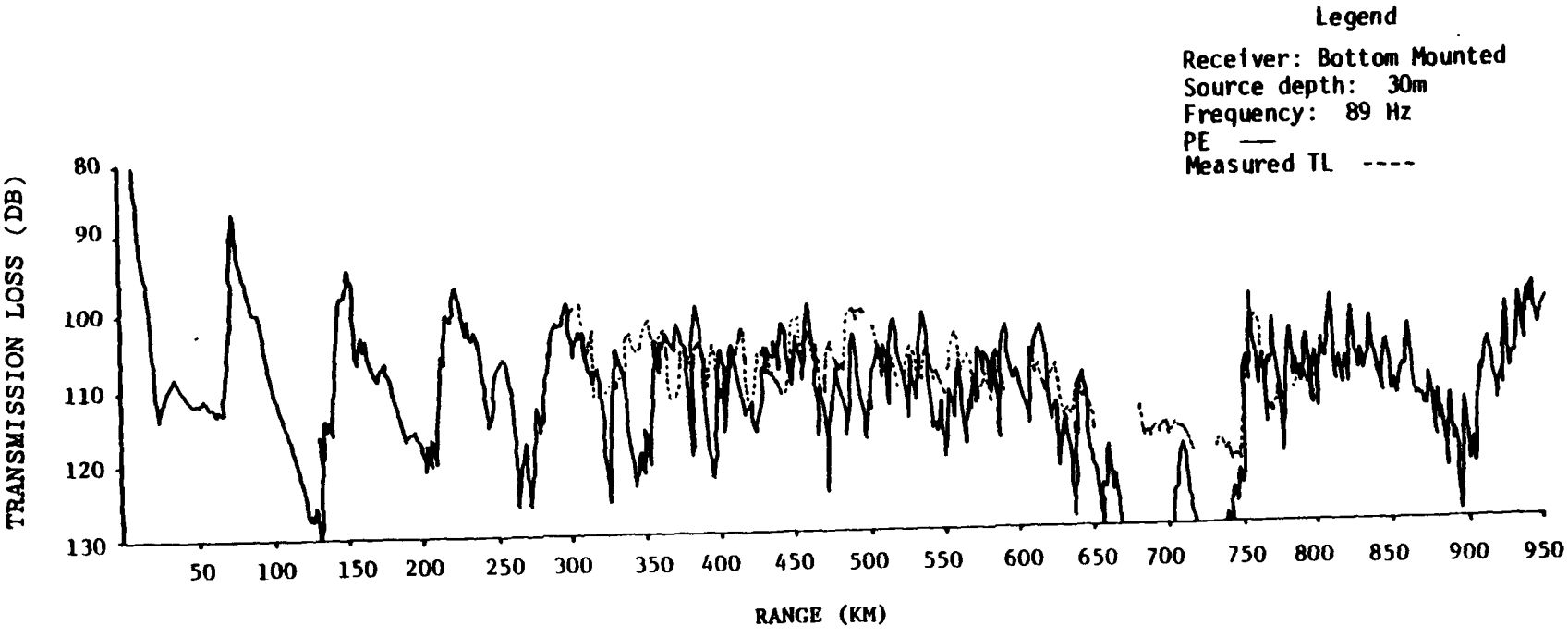

Figure 11 Transmission Loss vs. Range
May Track
PE Calculation vs. Measured Transmission Loss

transmission loss levels are much higher than the PE calculation. These differences are due to slope reflected paths that are not considered in the PE calculation. These paths account for the additional energy seen in the warm core and for the structure differences found between the two curves.

The measured data are compared with the transmission loss predicted by the GRASS model in Figure 12. The GRASS prediction shows about 6 dB less loss than the measured acoustic data. In addition, this calculation does not show the signal enhancement resulting from crossing the Gulf Stream. This indicates that this version of the GRASS code is not sensitive to range dependence and therefore should not be used in a predictive mode for rapidly changing thermohaline features such as the Gulf Stream.

The predicted transmission loss from the MPP model is compared with the measured transmission loss in Figure 13. It is seen that the levels agree quite well, yet significant differences occur in the Gulf Stream. Once again, these differences are accounted for by the presence of slope reflected energy not included in the MPP calculation. It has been shown that the PE and MPP calculations agree quite well with the measured transmission loss. An additional comparison between these two model predictions (Figure 14) shows that they agree very well in level and overall structure. The PE model shows much more detailed structure because PE is a wave solution and MPP combines the various ray paths incoherently.

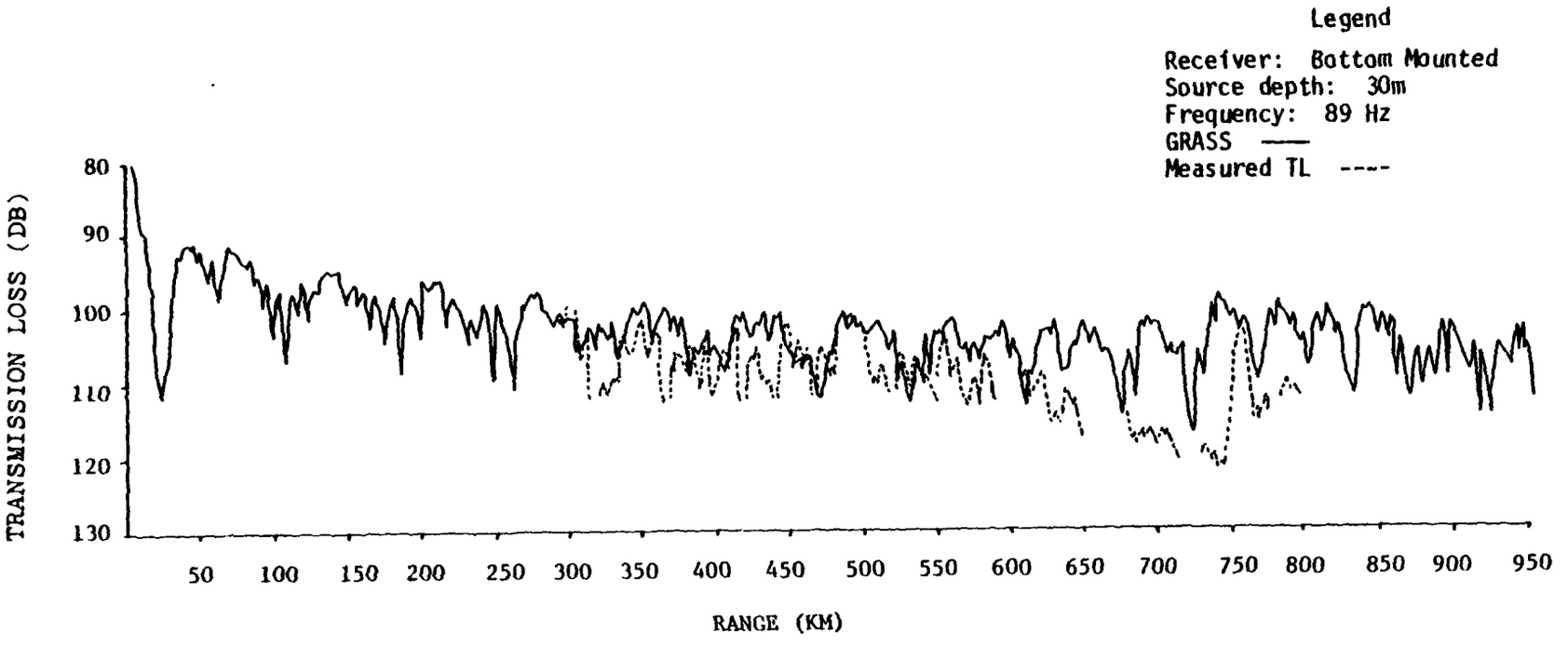

Figure 12 Transmission Loss vs. Range
May Track
GRASS Calculation vs. Measured Transmission Loss

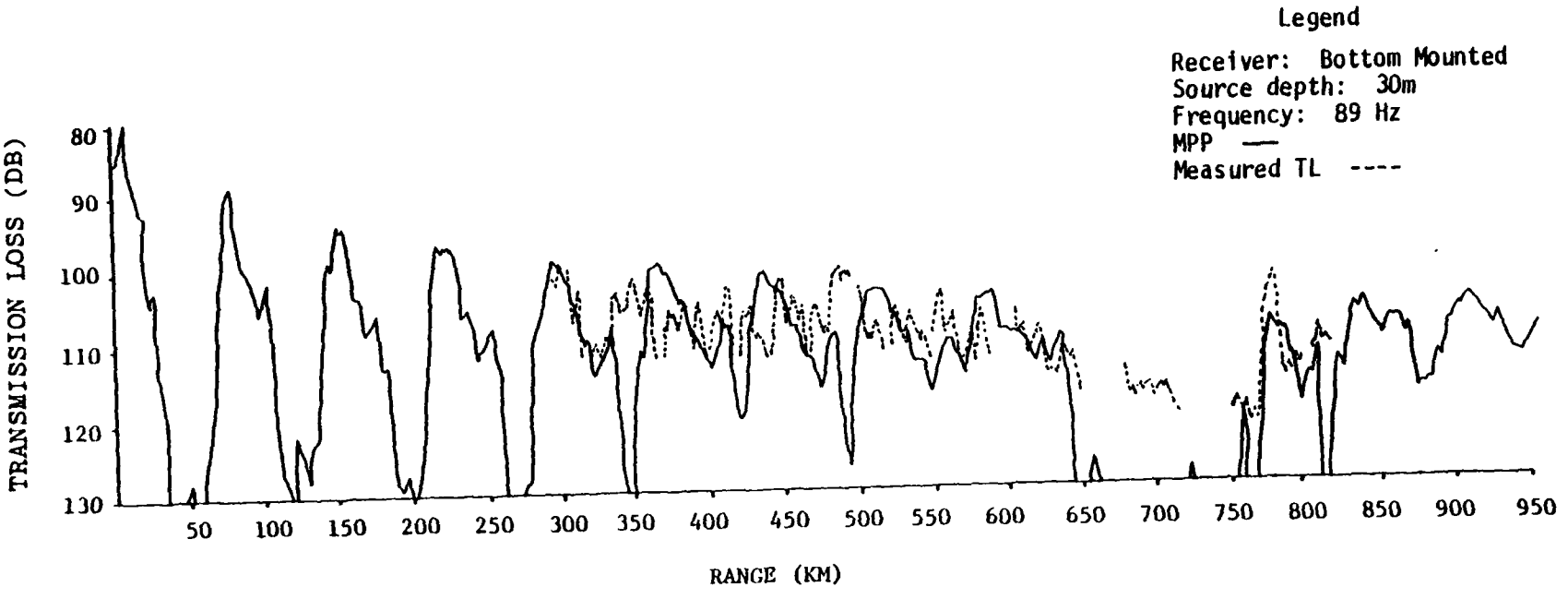

Figure 13 Transmission Loss vs. Range
May Track
MPP Calculation vs. Measured Transmission Loss

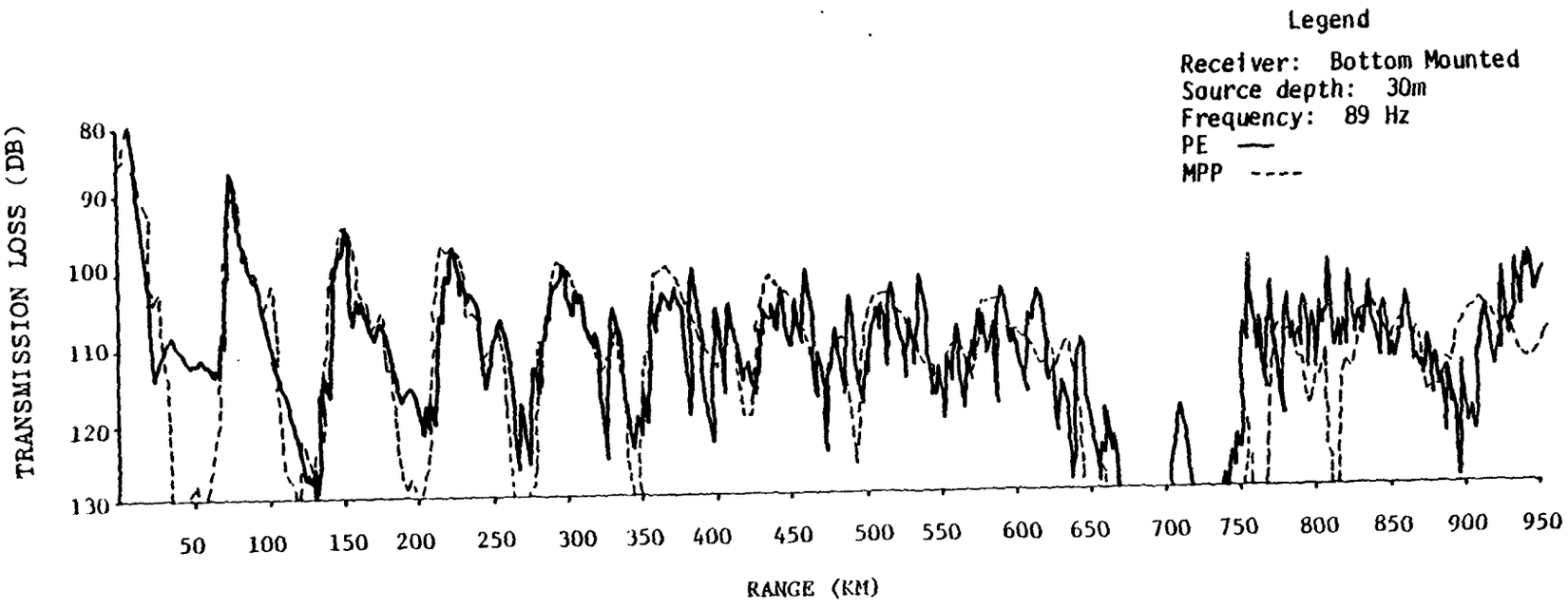

Figure 14 Transmission Loss vs. Range
May Track
PE Calculation vs. MPP Calculation

The results obtained in this comparative study indicate that both MPP and PE agree well with the measured transmission loss data. For the high frequencies of interest for tactical sonar, it was decided to use the MPP model for transmission loss estimates. This model has been shown to be accurate at low frequencies. One additional high frequency comparison is made between PE and MPP on the second Gulf Stream data set. This comparison is discussed in the next section.

Section 5
TRANSMISSION LOSS ESTIMATES FOR TACTICAL SONAR SYSTEMS

Environmental Description

The environmental data along the second Gulf Stream track (II), shown in Figure 3, were provided by NUSC, Newport. These data were collected by a NUSC-Woods Hole Oceanographic Institute cruise conducted in December, 1976. Thirty ship-dropped T-7 XBT's (750 m) were taken along a 180 km track. The sound velocity structure along the track was generated by the ICAPS deep merge routine. Figure 15 shows representative sound velocity profiles as well as the bathymetry along the track. The track is similar to the Gulf Stream tracks previously discussed. The track is representative of winter conditions, which accounts for differences found in the near surface layers. The presence of a strong surface duct is evident in the Sargasso Sea profiles. This duct is 140 m deep and extends for a distance of 85 km. The duct gradually becomes shallower and disappears in the warm core. Once across the North Wall, the surface duct reappears in the colder Slope Water. This duct is not as deep as the one in the Sargasso, reaching only a depth of 80 m and extending for 75 km.

Several source-receiver positions relative to the Gulf Stream were considered. Source-receiver depths of tactical importance (10 m, 140 m, and 300 m) were used. The frequencies of interest were 50 Hz, 3 KHz, and 20 KHz. These span the range important to tactical sonar systems. The cases considered are too numerous to discuss each one in detail and are included in Appendix A.

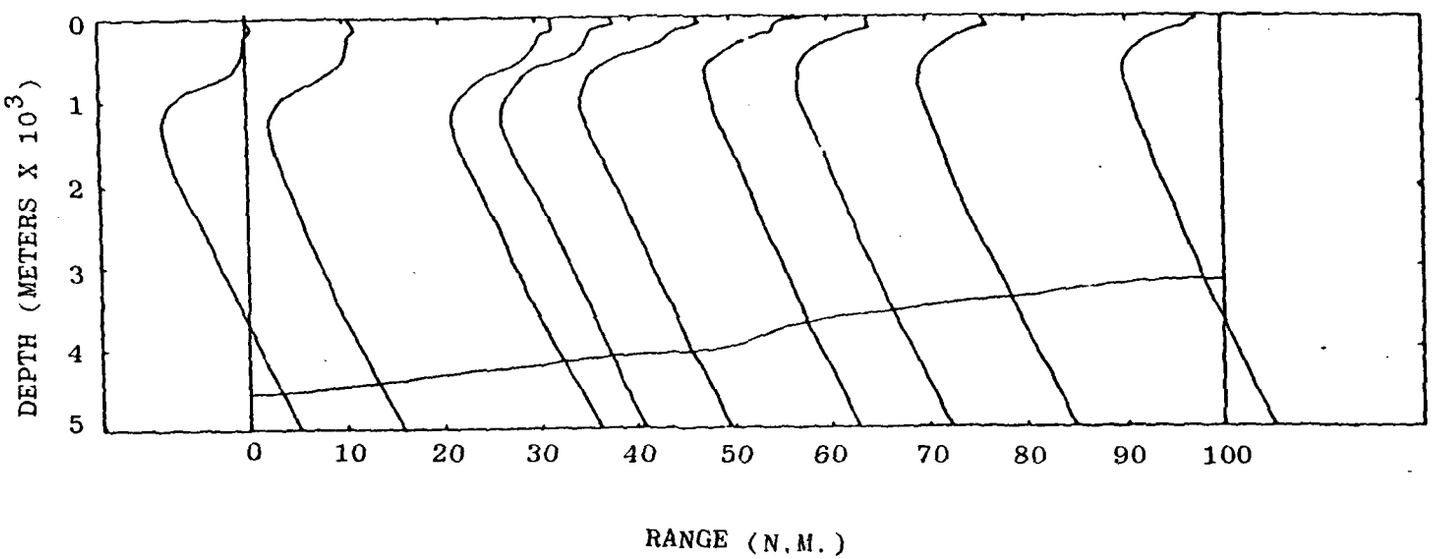

Figure 15 Bathymetric and Acoustic Environment along the December Gulf Stream Track

High Frequency Model vs. Model Comparison

The comparative model study suggested that the PE model should be used for the low frequency (50 Hz) runs and that MPP should be used for the high frequency (3 KHz, 20 KHz) cases. Measured transmission loss data were not available so that a high frequency model vs. data comparison could not be made. To compensate for this, one additional test case was constructed for the December track. Transmission loss estimates for a 1 KHz run along the entire track from the Sargasso to the Slope Water were obtained from both the PE and MPP models. This frequency was chosen since it approaches the upper limit of frequencies that PE can handle. The estimates obtained from PE were considered "true" and the MPP estimates were then compared to PE.

A test case was run for a 140 m receiver depth and for three source depths of 10 m, 140 m, and 300 m. Transmission loss estimates for the 10 m source are shown in Figure 16. Significant differences between the curves occur at 30 nm and from 45 - 65 nm. The PE calculation shows much more energy than the MPP estimate. A superposition of the ray trace and the PE energy contour (Figure 17) shows the distribution of energy as a function of range and depth along the track. This figure shows the rays from -5^{o} to 5^{o} (not including the 1^{o} ray) plotted in a solid line and the ducted paths, from $1/2^{o}$ to 1^{o} plotted in a dashed line. The PE model energy contours clearly define the presence of caustics-regions predicted by classical ray-tracing to have infinite intensity. The MPP model contains a caustic correction that approximates energy associated with strong caustics. The benefits of this

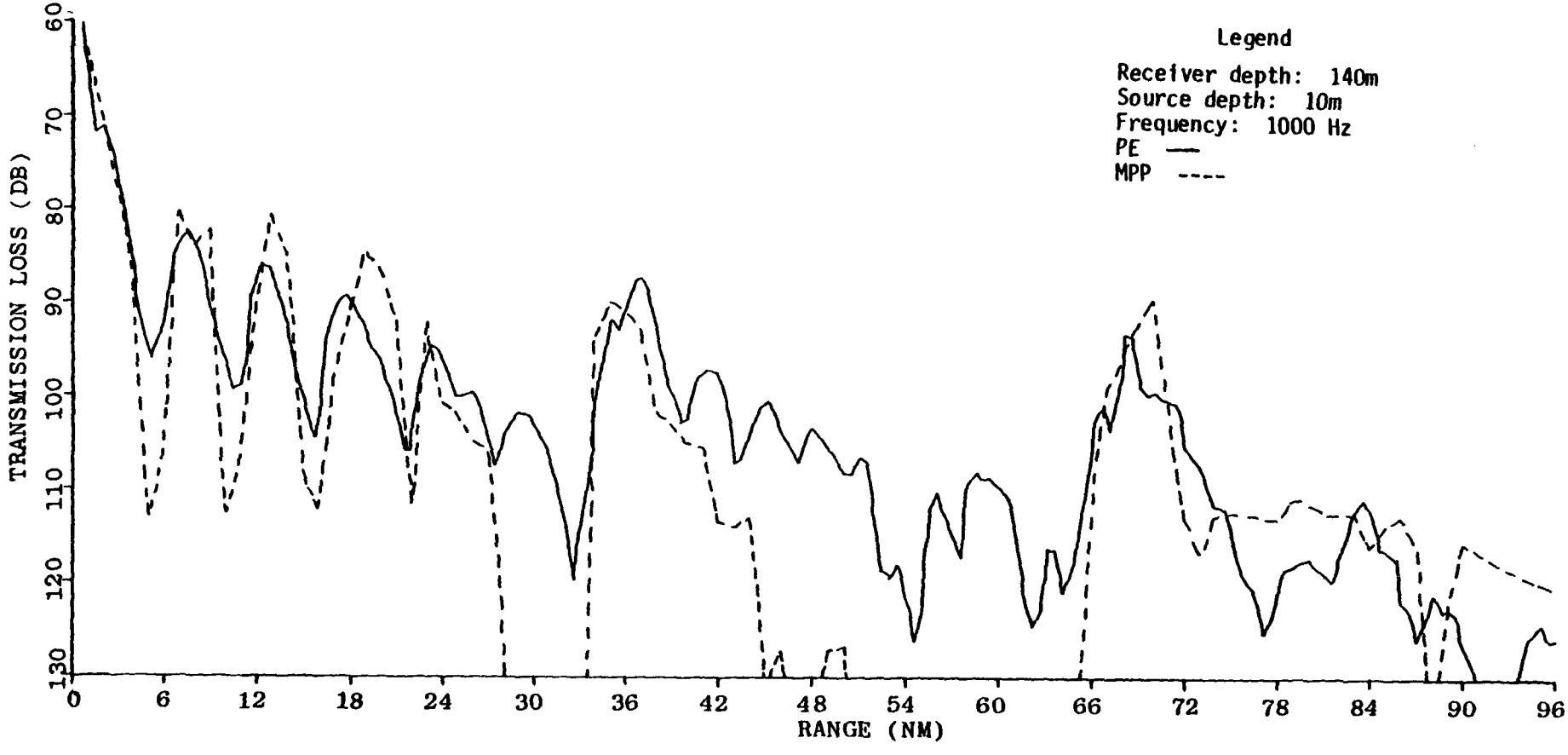

Figure 16 Transmission Loss vs. Range
December Track
PE Calculation vs. MPP Calculation

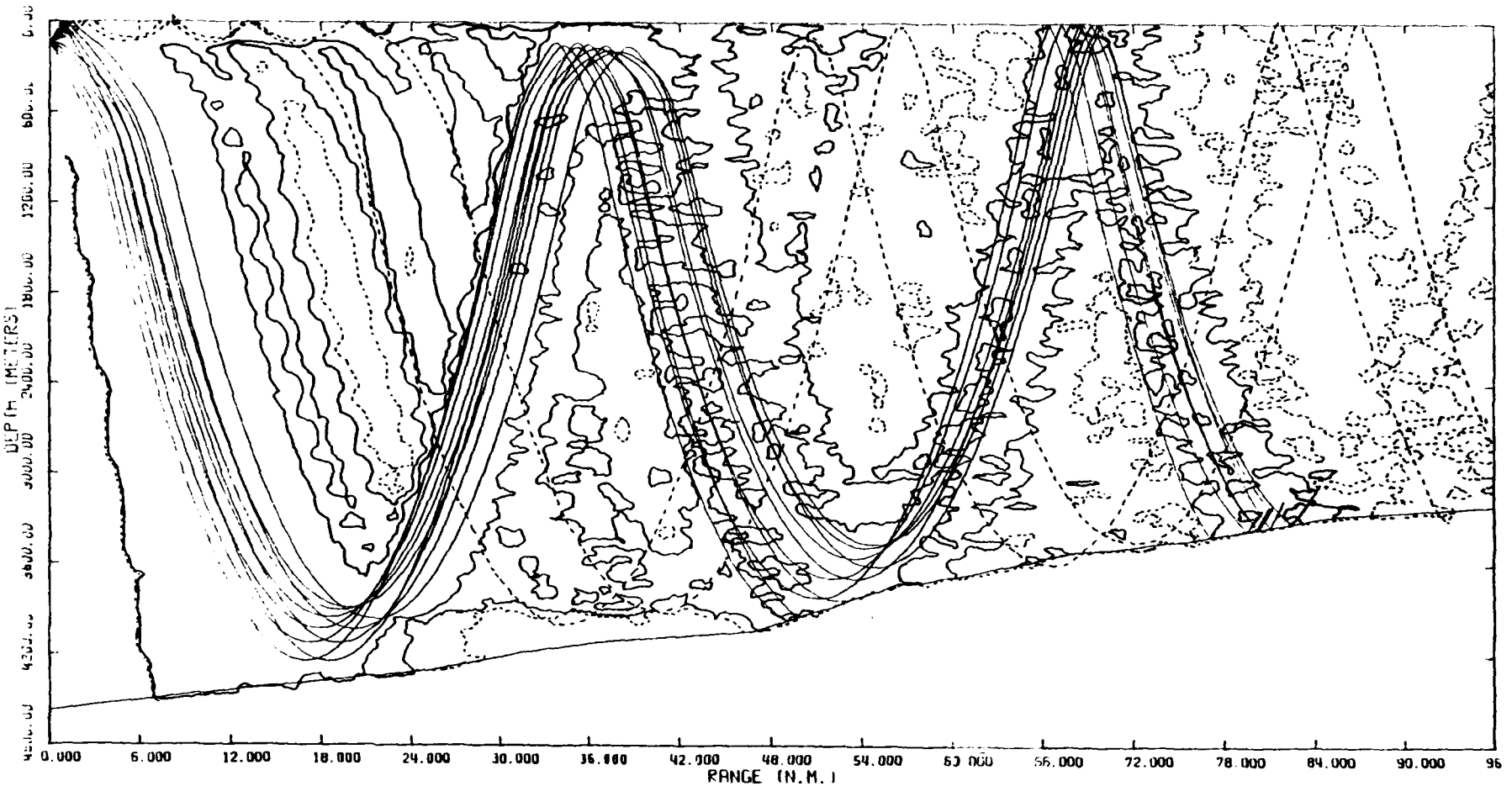

Legend

PE contour levels — 100 dB
— 110 dB
····· 120 dB

Waterborne paths —

Ducted paths ·····

Figure 17 PE energy contours and acoustic ray paths

correction are apparent at the range from 32 - 40 nm. The PE and MPP transmission loss estimates for a 10 m source 140 m receiver (Figure 16) agree quite well even though the ray trace (Figure 17) shows no energy at this depth. At the range 30 nm, the energy found in the transmission loss plot also results from the diffracted field associated with the caustic centered around 36 nm. For a source at 10 m, MPP predicts no energy for the region not directly above the caustic. At range 45 - 65 nm, energy shown in the PE calculation results from the diffracted field associated with the ducted paths. This family of paths, between $1/2^{o}$ and 1^{o}, are trapped by the strong surface duct in the Sargasso. This energy falls out of the duct when the Gulf Stream is encountered at a range of 24 nm. This energy, associated with the convergence zone centered at 36 nm, is reinsonified back into the duct past the convergence zone, at ranges 45 - 65 nm. MPP does not calculate this energy for a 10 m source since this family of rays represents a very weak caustic, and MPP only estimates energy very close to strong caustics. As the source depth increases, the differences between the PE and MPP calculations decrease since the source now couples into the propagating ray paths. This can be seen in Figure 18 for a 140 m source. MPP shows increased levels of energy at the ranges previously discussed. The differences between the two curves continue to decrease, as evident in the transmission loss estimate for the 300 m source (Figure 19).

This comparison, while providing justification for the accuracy of MPP at high frequencies, also demonstrates the limitations of ray theory in cases where leakage from a range dependent surface duct and reinsonification of a

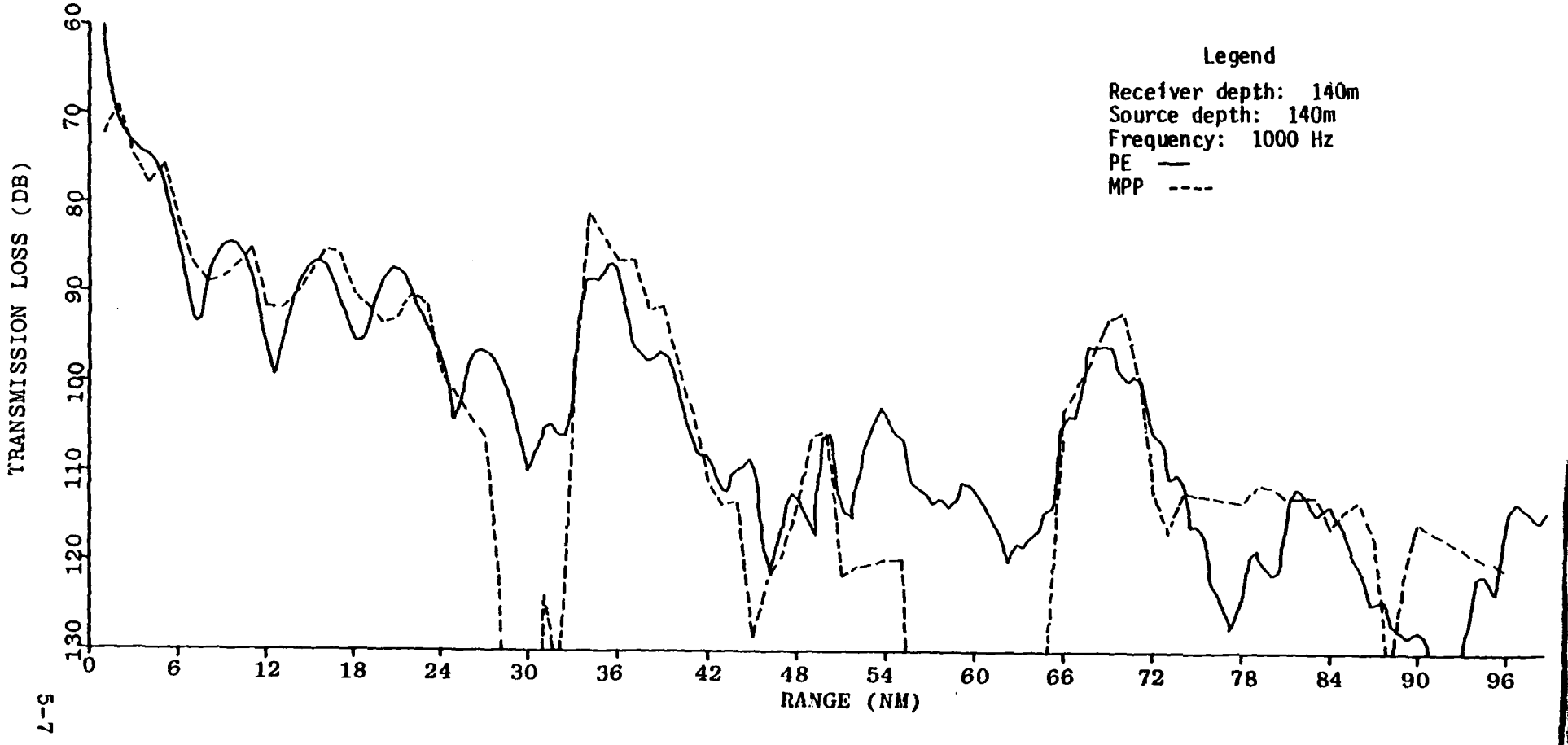

Figure 18 Transmission Loss vs. Range
December Track
PE Calculation vs. MPP Calculation

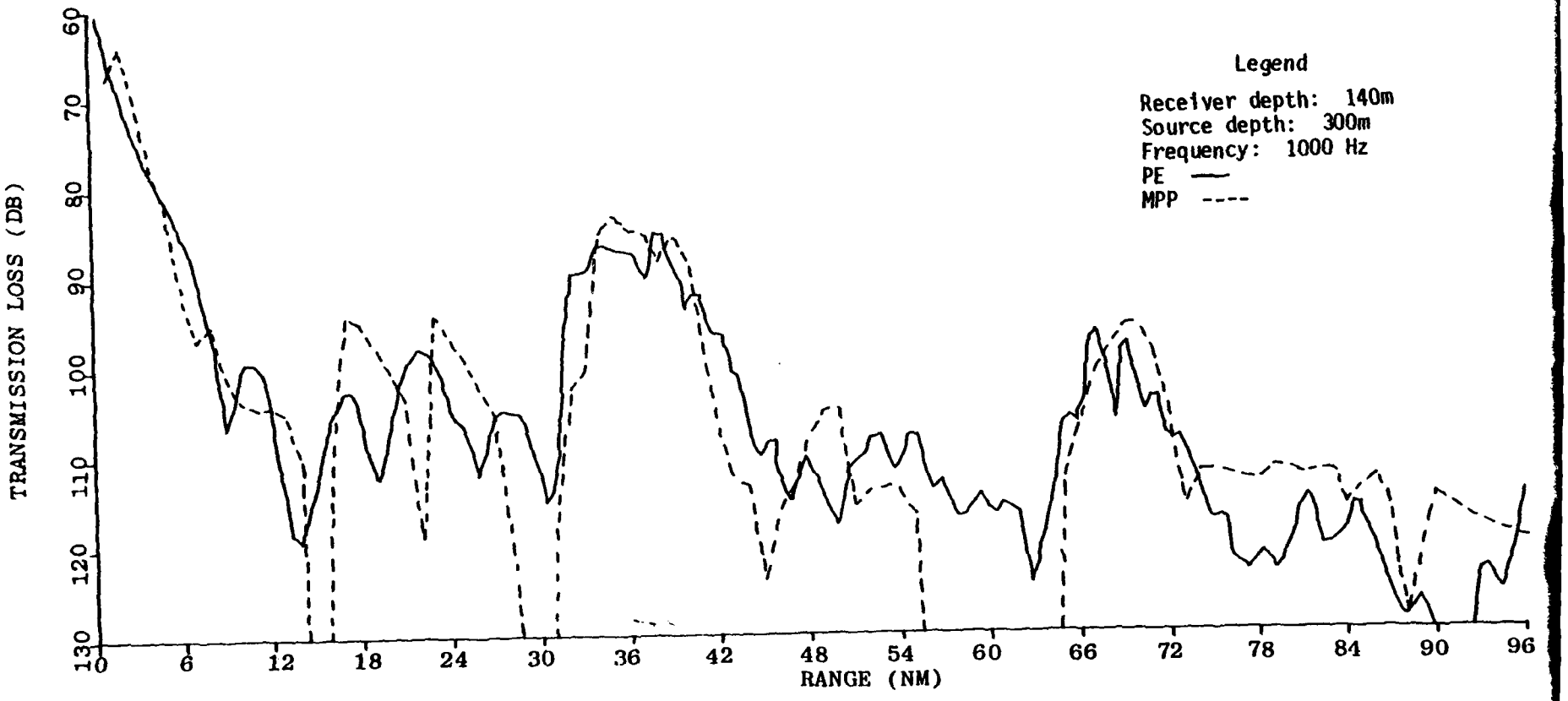

Figure 19 Transmission Loss vs. Range
December Track
PE Calculation vs. MPP Calculation

surface duct near a convergence zone occurs. Another limitation of ray theory occurs when only the source or receiver (but not both) is in the duct. These cases cannot be treated by ray theory for the frequencies of interest since the field is dominated by leakage from the duct.

Tactical Sonar Systems

MPP has been shown to be a valuable tool in providing high-frequency transmission loss estimates. The limitations of the model must be considered when using it in a predictive mode. Acoustic propagation for several sections of the track was determined. These paths included: Sargasso to the Slope Water, Warm Core to the Sargasso, Warm Core to the Slope Water, the North Wall to the Sargasso and the North Wall to the Slope Water. For each section of the track, transmission loss estimates were obtained for 50 Hz, 3 KHz, and 20 KHz. Acoustic ray paths were determined for many source-receiver geometries. The low-frequency transmission loss estimates were obtained from the PE model, while high-frequency estimates were obtained from MPP. These source-receiver geometries were determined by NUSC to have tactical importance. Source-receiver combinations that involved cross duct propagation for high frequencies were not considered.

Appendix A creates a data base of tactical interest for acoustic propagation in the Gulf Stream environment. Only waterborne energy is treated in the model calculations, and any bottom effects that may occur in this region are not considered.

Section 6
CONCLUSIONS

The Gulf Stream environment is a region of strong temperature variations. These result from seasonal heating and cooling in the upper 200 m of the ocean. The temperature fluctuations directly affect the sound velocity structure and resulting acoustic propagation.

Long-range, low-frequency propagation through the Gulf Stream can be efficiently modeled by the PE model. For high frequencies of interest to tactical sonar systems, the PE model is extremely limited. At these frequencies, the diffracted field is less important and ray theory, which is not frequency limited, provides an alternate means of obtaining transmission loss estimates. Evaluation of two ray models demonstrated that transmission loss estimates obtained from MPP agreed well with measured transmission loss for low frequency and with PE at a higher frequency.

The results of these comparative studies provided justification for using MPP in a predictive mode for frequencies of tactical importance. Transmission loss estimates from MPP were obtained for many source-receiver geometries in the Gulf Stream environment. In addition, low-frequency transmission loss estimates from PE have been included for these cases. These estimates, as well as corresponding ray plots, have been assembled in Appendix A. This appendix provides a readily available reference for users involved with tactical sonar systems.

APPENDIX A

This Appendix contains transmission loss estimates and ray plots for all the source-receiver geometries along the December Gulf Stream track. The location of the sections along the track and the source-receiver geometry relative to the environment along the track are shown. For the SLOPE/SARGASSO plots and the SARGASSO/SLOPE plots, the receiver is located at range zero. For the runs originating in the WARM CORE or NORTH WALL, the receiver is located at the beginning of the curve for the ray plots and 1 nm before this for the transmission loss plots.

RAY PLOTS

The rays drawn are spaced at 1^{o} and are measured from the horizontal. All rays begin at the receiver and propagate outward (invoking the principle of acoustic reciprocity). Most ray plots are for the 10 m and 140 m receiver. The source depth used for all ray plots was 140 m. The range scale is equivalent to 6 nm/unit. The depth scale is equivalent to 600 m/unit.

TRANSMISSION LOSS

The range scale on all transmission loss plots is 6 nm/unit. The 50 Hz transmission loss estimates are obtained from the PE model. The 3,000 Hz and 20,000 Hz estimates are obtained from the MPP model. For all runs, the fixed point (at zero range) is considered the receiver. In the color plots, transmission loss plots for all three source depths.

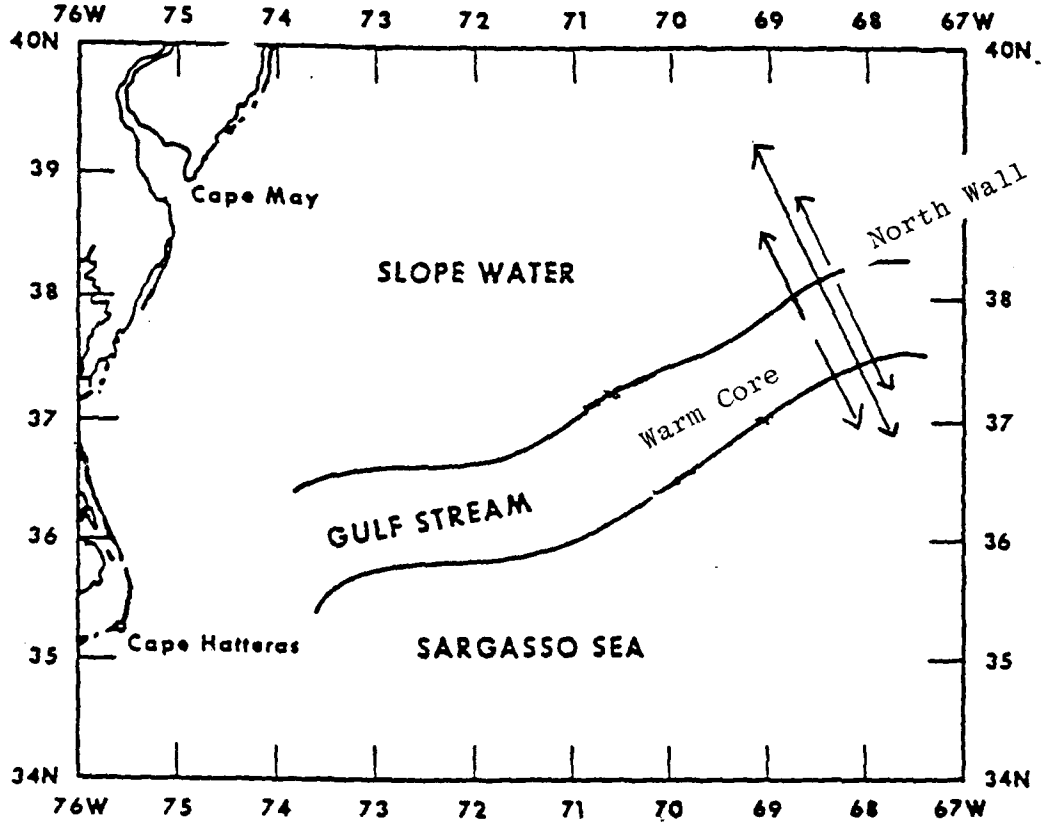

Figure A-1 Track from December experiment
Schematic track for transmission loss runs

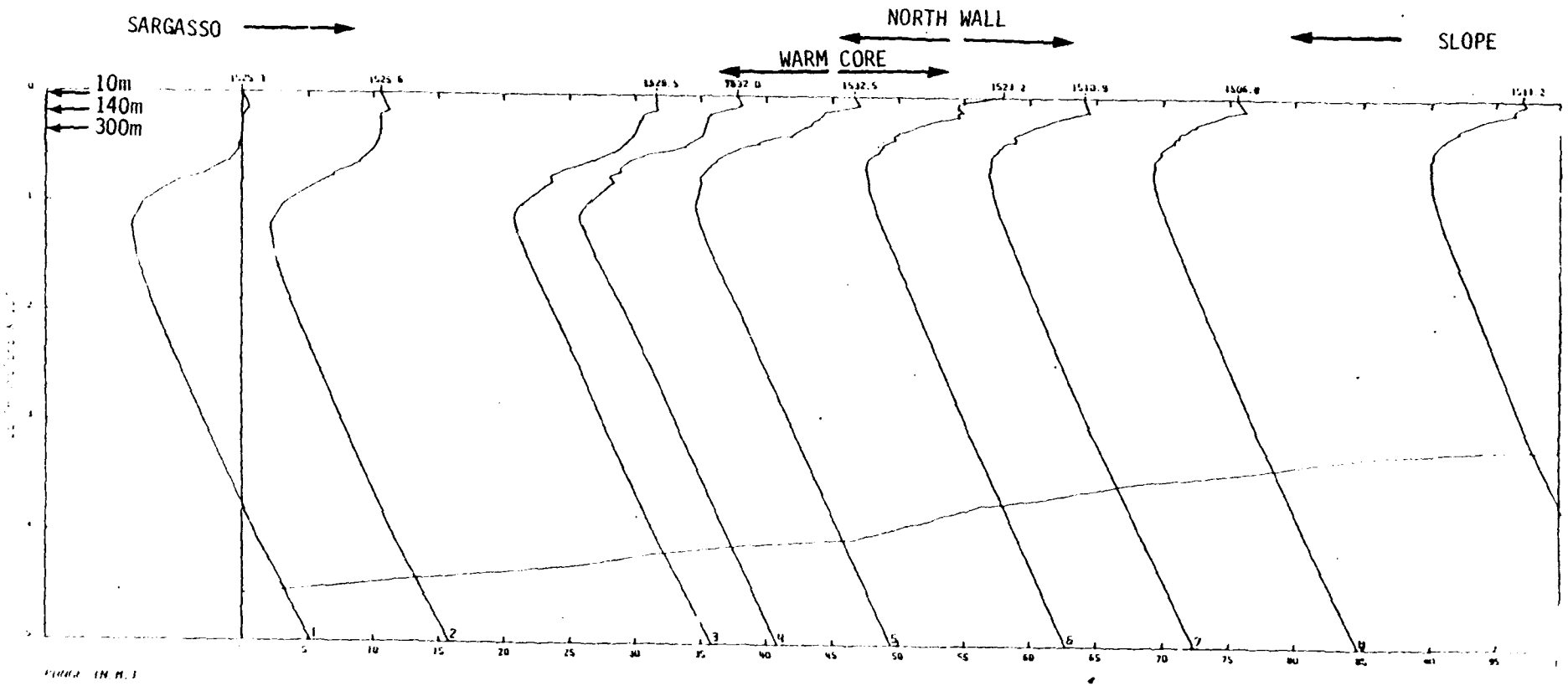

Figure A-2 Acoustic Environment along the December track
10m, 140m, 300m depths are shown
Approximate starting points of runs shown

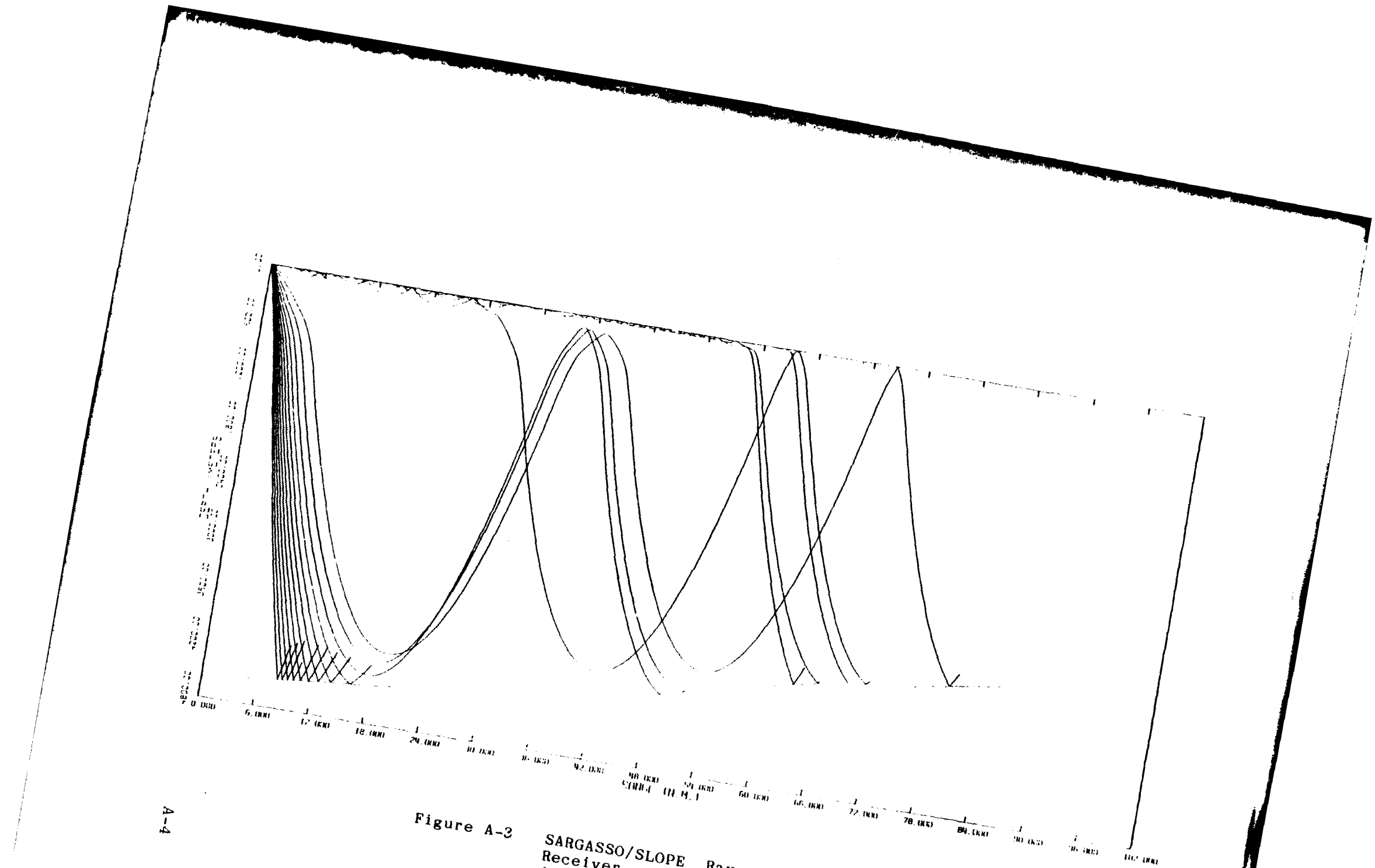

Figure A-3 SARGASSO/SLOPE Ray plot
Receiver = 10 m, Source = 140 m
Angles plotted 0o-150

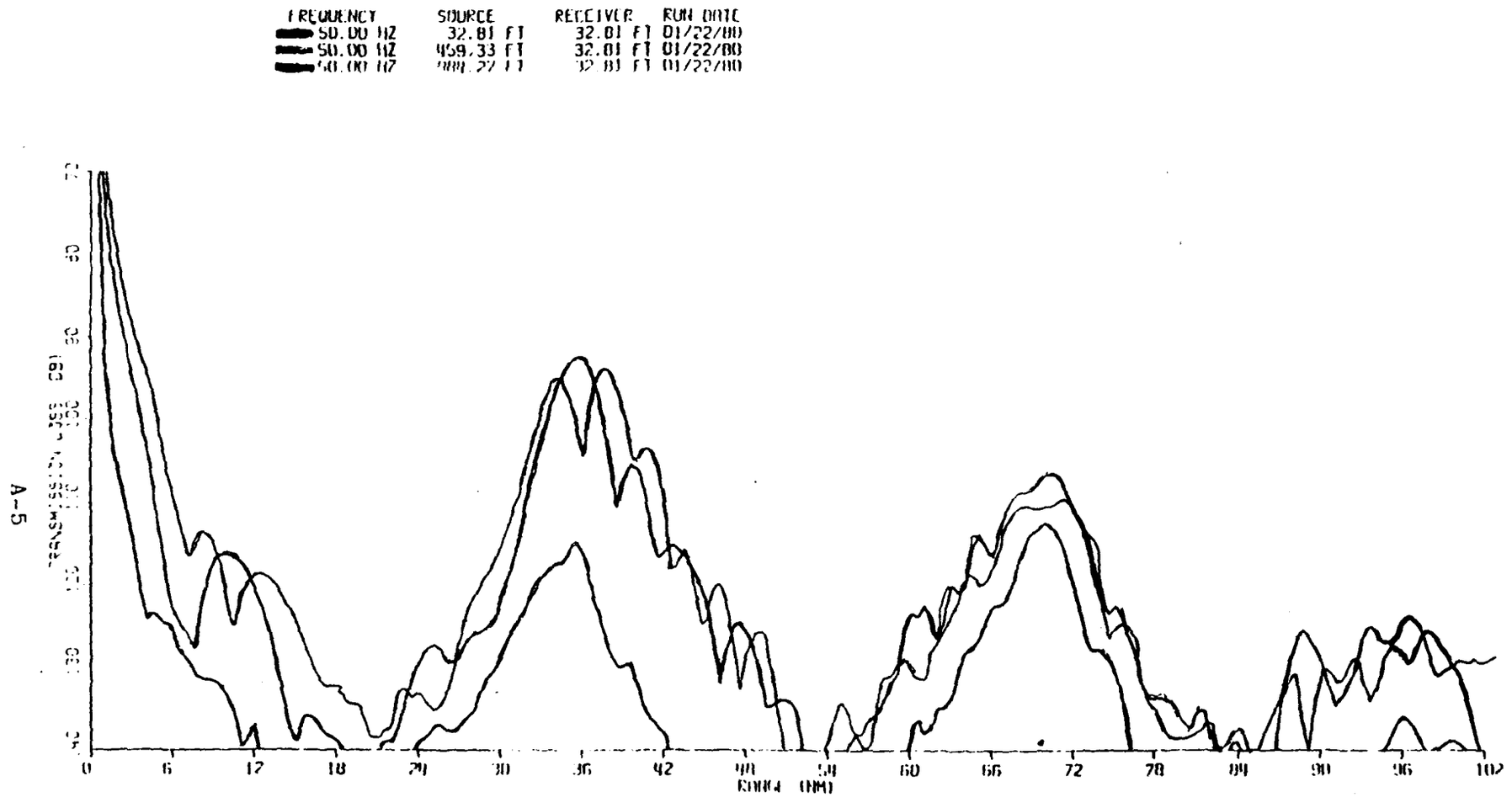

Figure A-4 SARGASSO/SLOPE Transmission Loss (PE)
Receiver = 10 m, 50 Hz

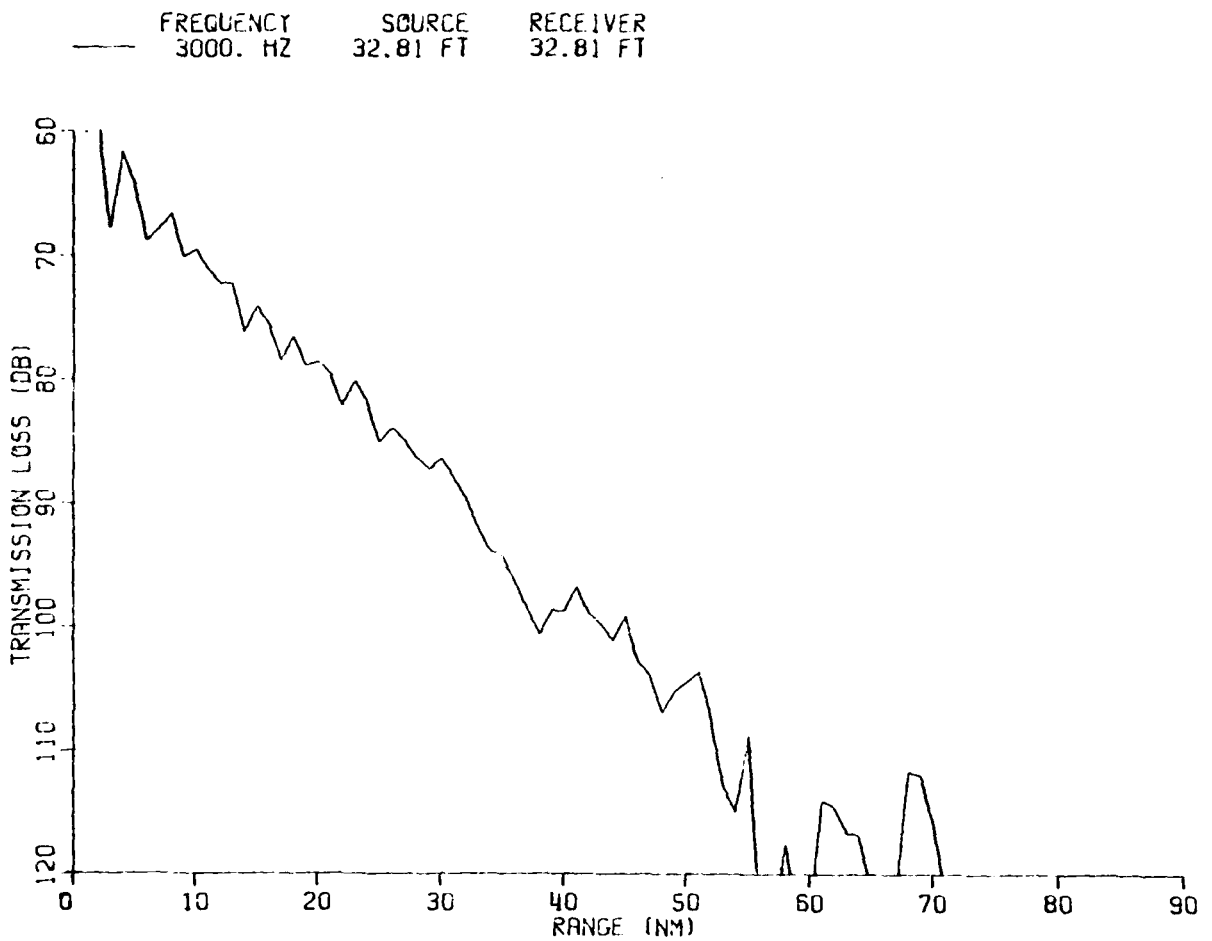

Figure A-5 SARGASSO/SLOPE Transmission Loss (MPP)
Receiver = 10 m, 3000 Hz

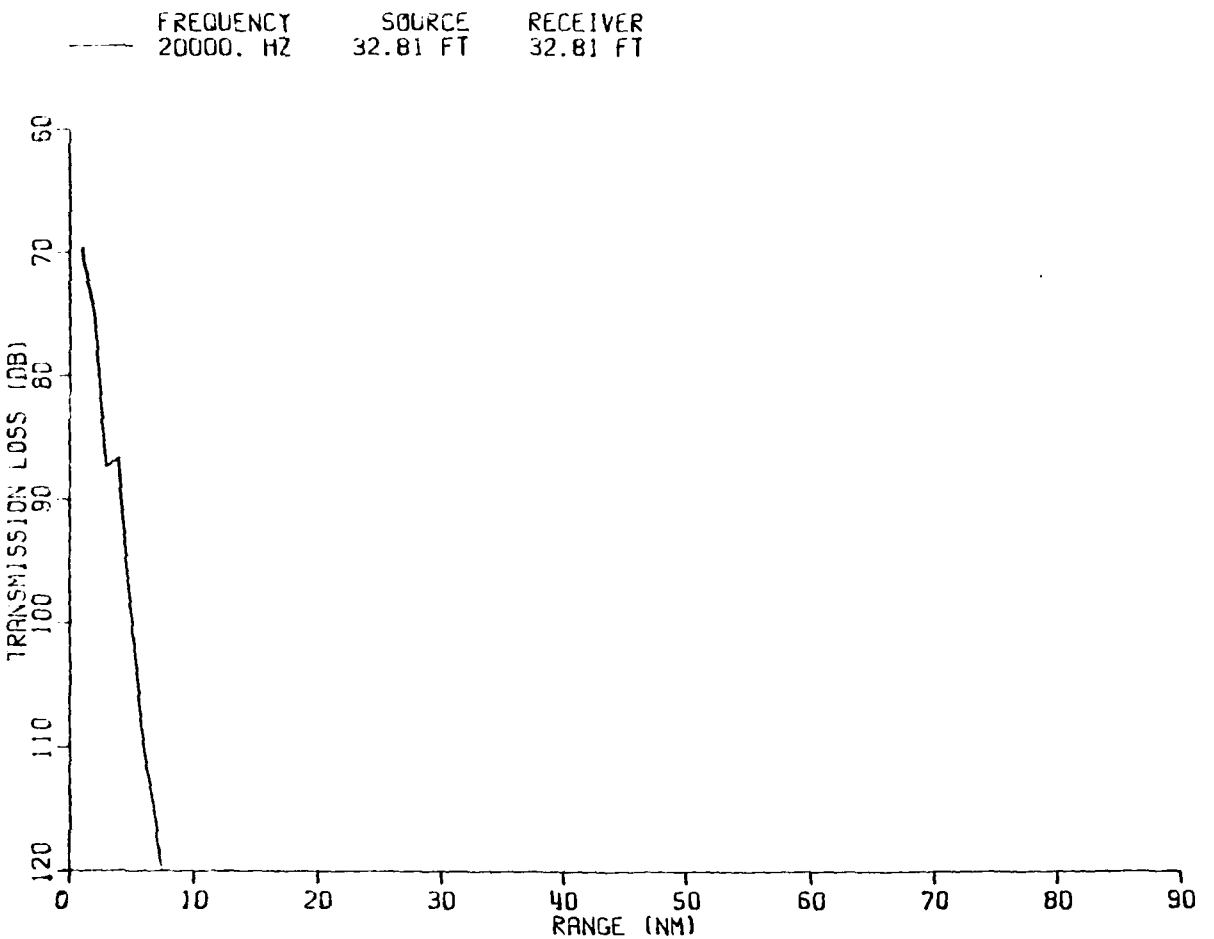

Figure A-6 SARGASSO/SLOPE Transmission Loss (MPP)
Receiver = 10 m, 20,000 Hz

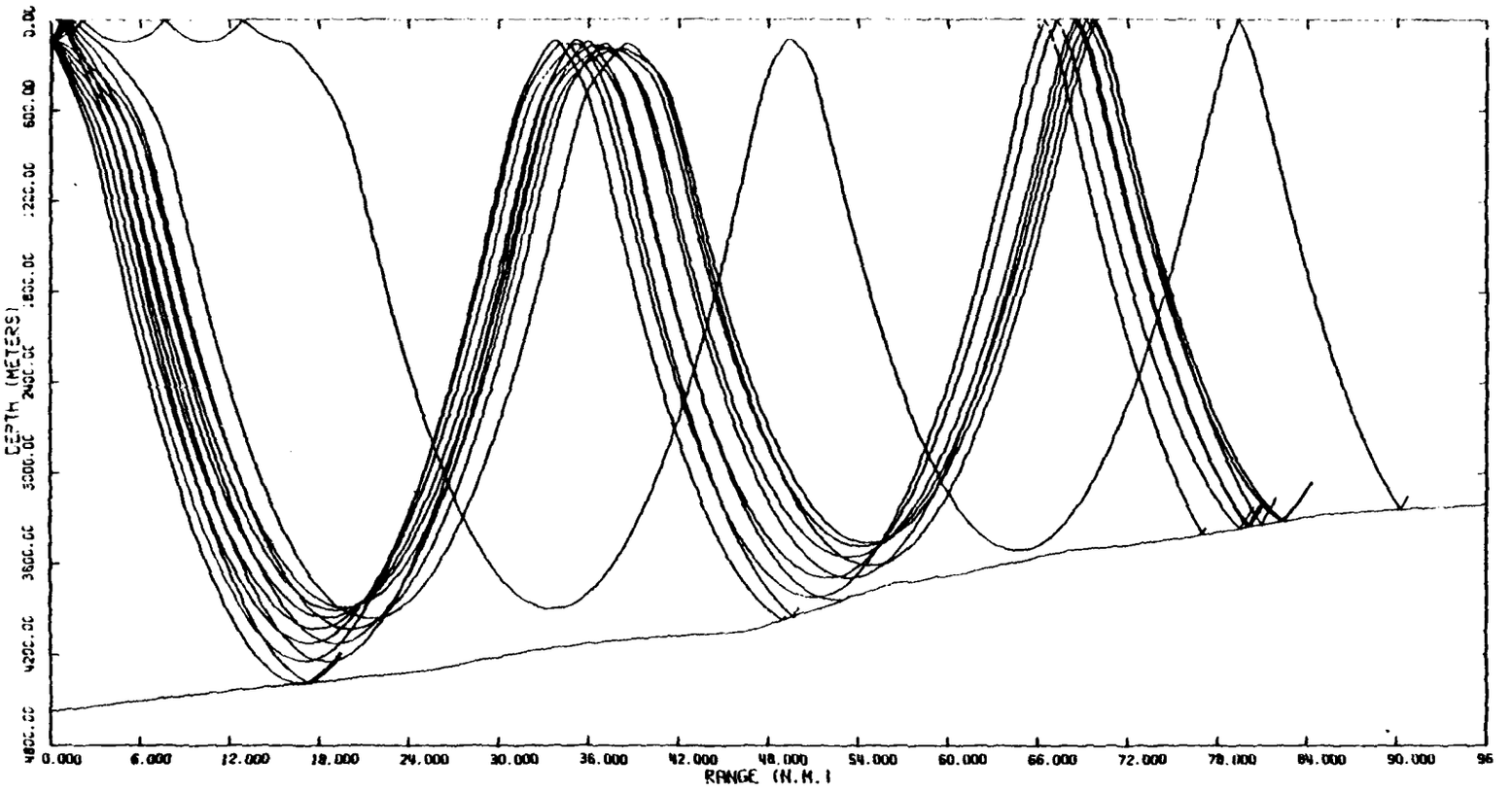

Figure A-7 SARGASSO/SLOPE Ray plot
Receiver = 140 m, Source = 140 m
Angles plotted 6^{O} to -6^{O}

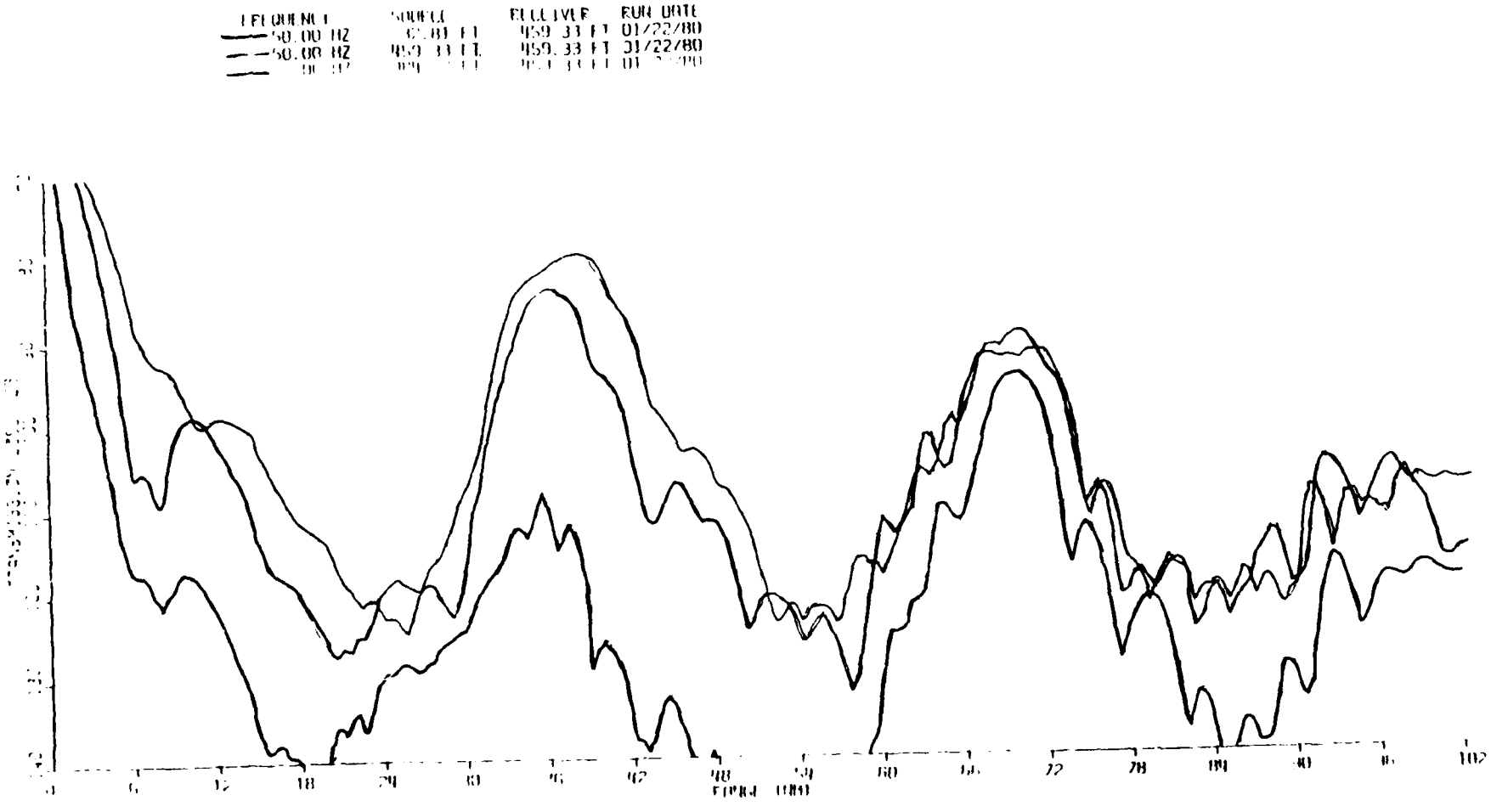

Figure A-8 SARGASSO/SLOPE Transmission Loss (PE)
Receiver = 140 m, 50 Hz

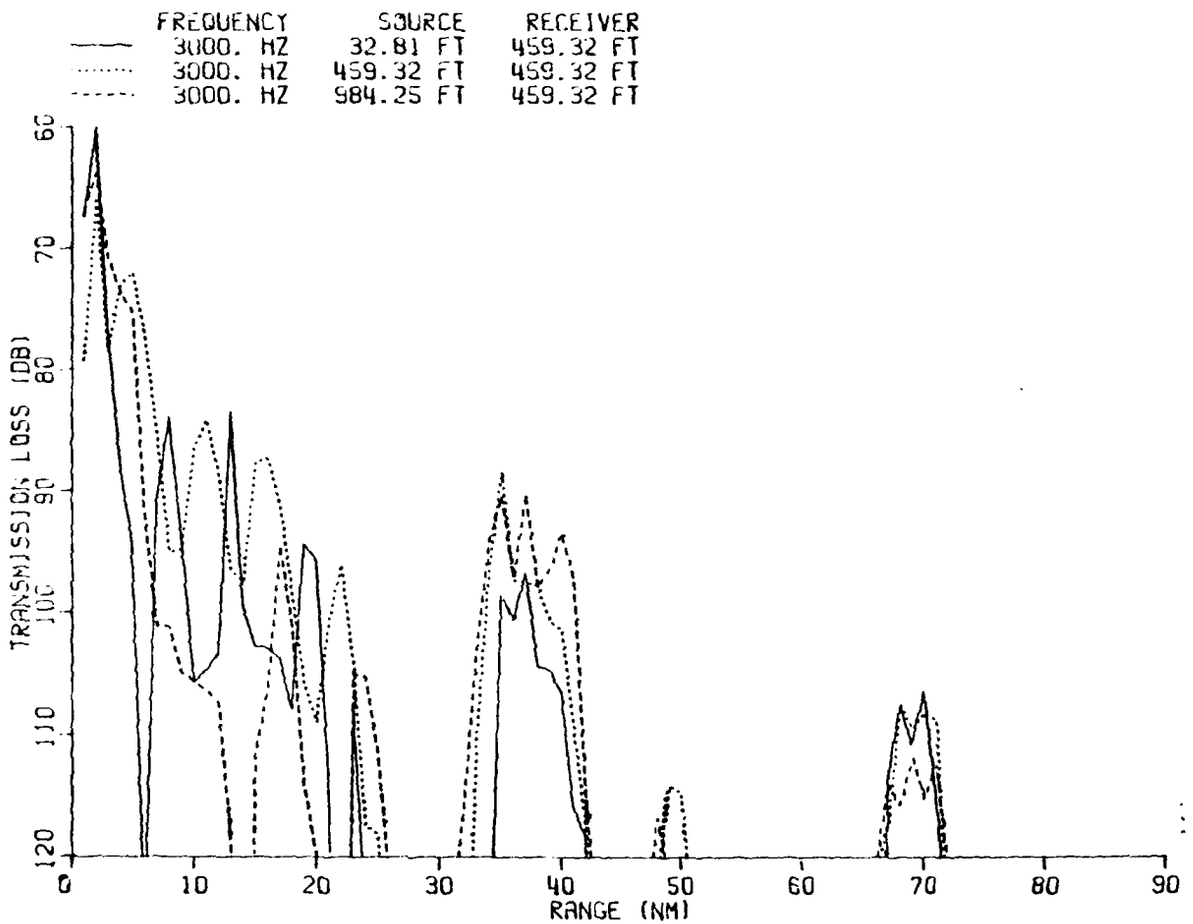

Figure A-9 SARGASSO/SLOPE Transmission Loss (MPP)
Receiver = 140 m, 3000 Hz

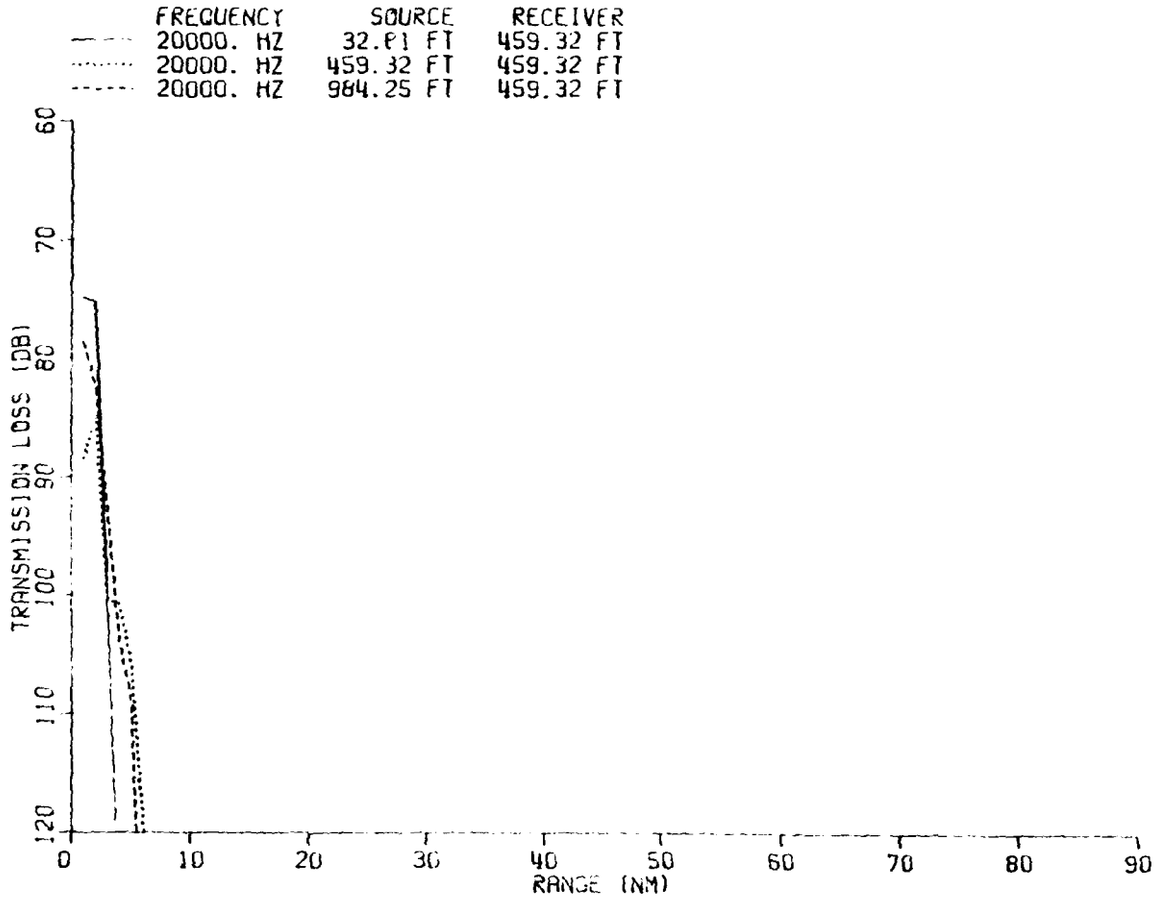

Figure A-10 SARGASSO/SLOPE Transmission Loss (MPP)
Receiver = 140 m, 20,000 Hz

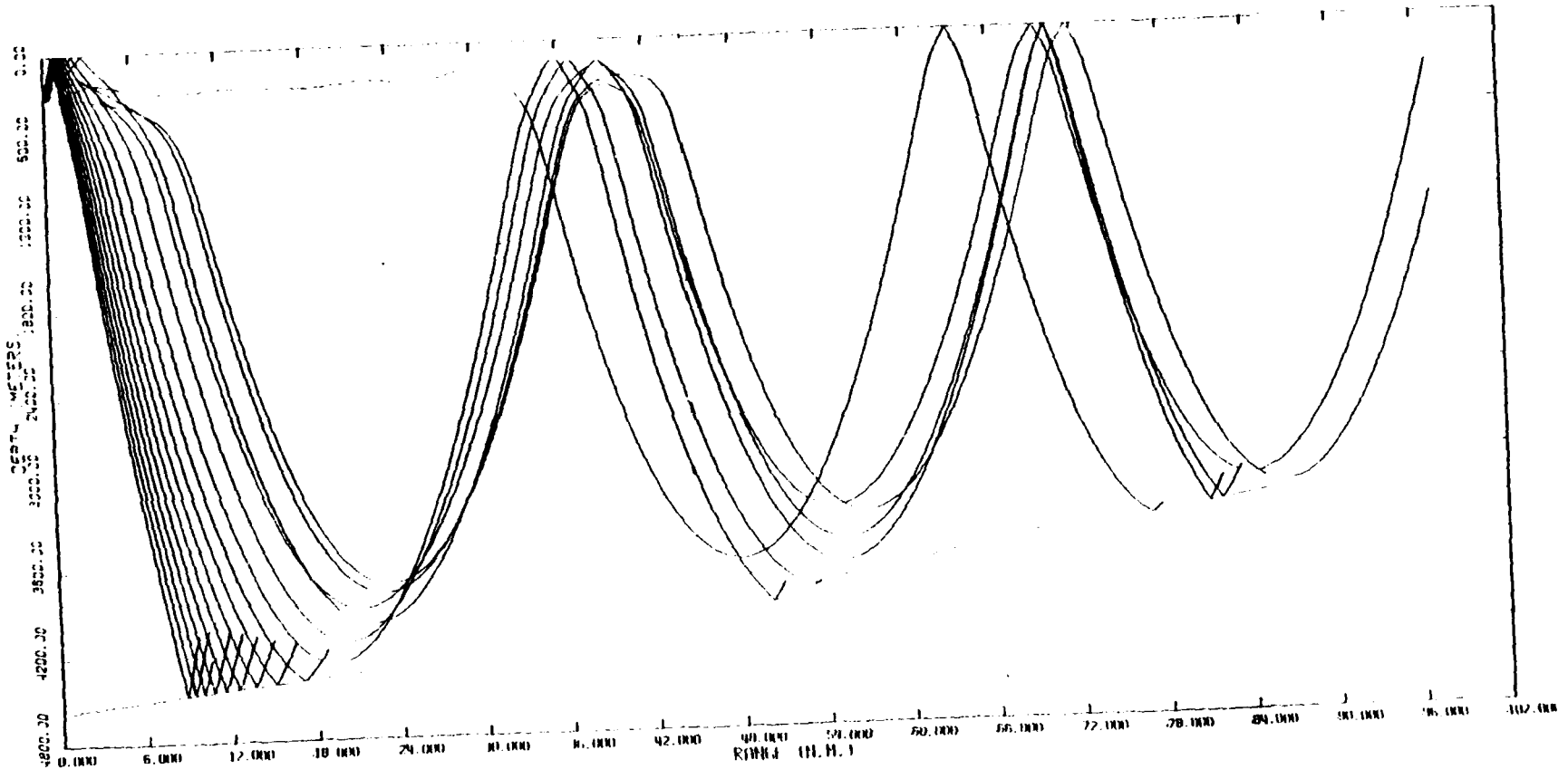

Figure A-11 SARGASSO/SLOPE Ray plot
Receiver = 300 m, Source = 140 m
Angles plotted 0^{o}-15^{o}

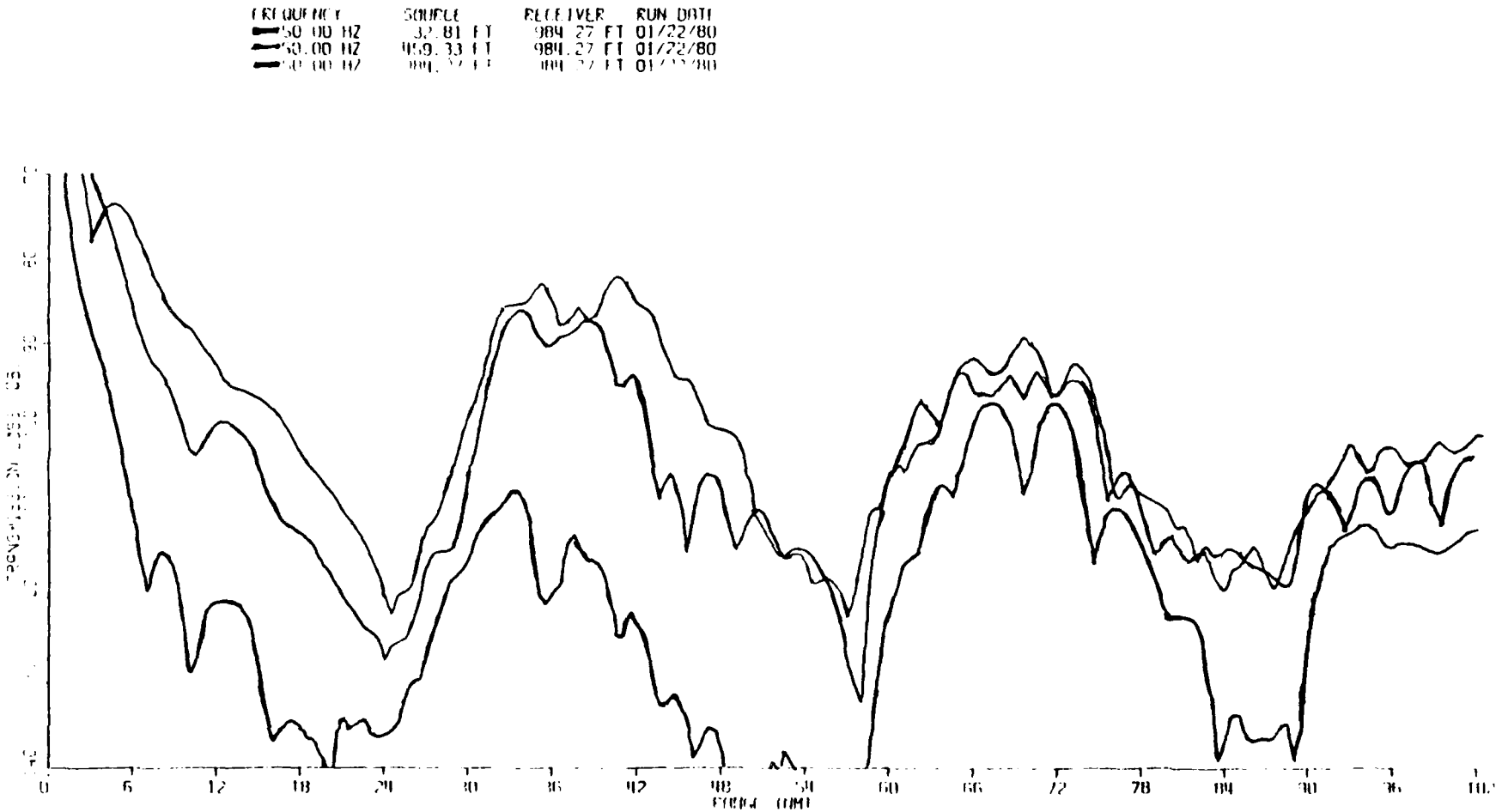

Figure A-12 SARGASSO/SLOPE Transmission Loss (PE)
Receiver = 300 m, 50 Hz

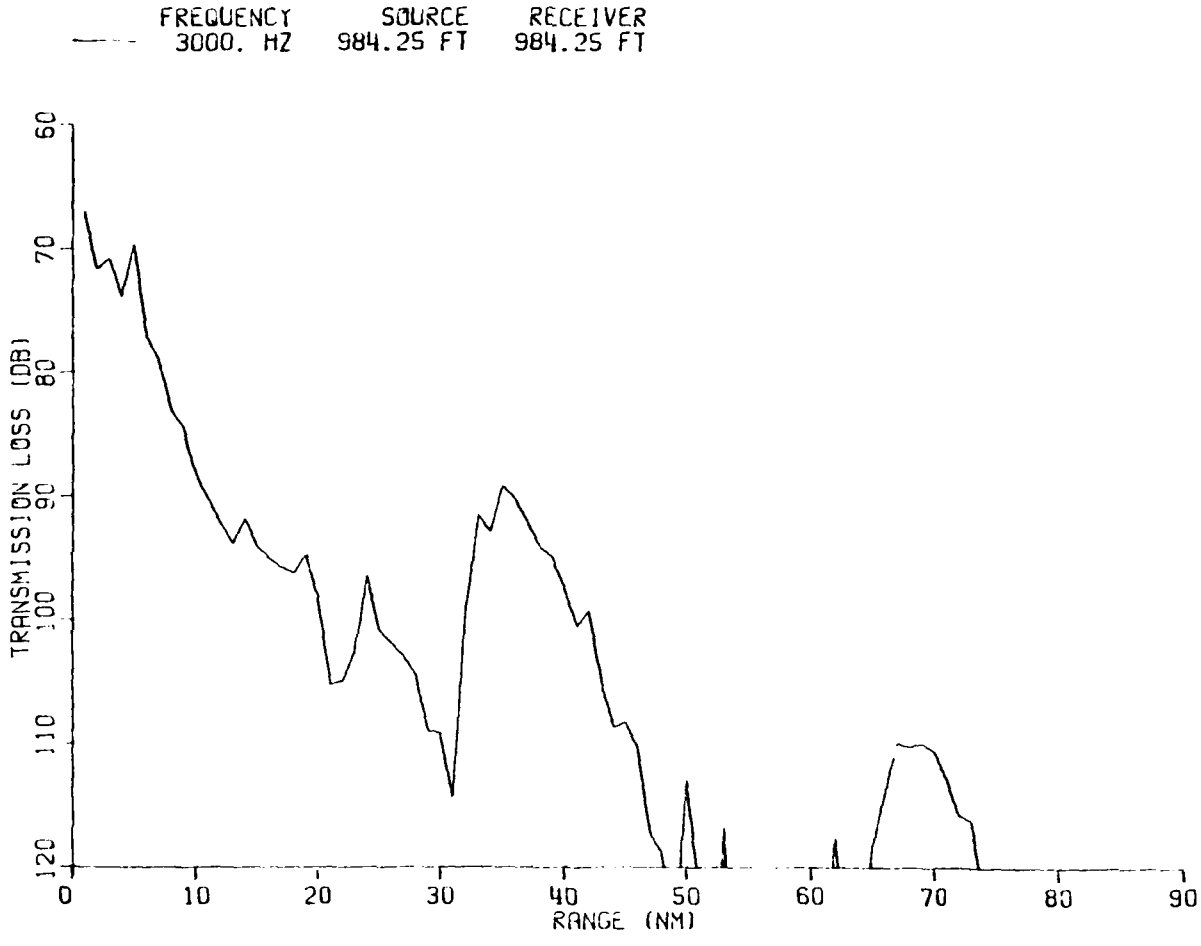

Figure A-13 SARGASSO/SLOPE Transmission Loss (MPP)
Receiver = 300 m, 3,000 Hz

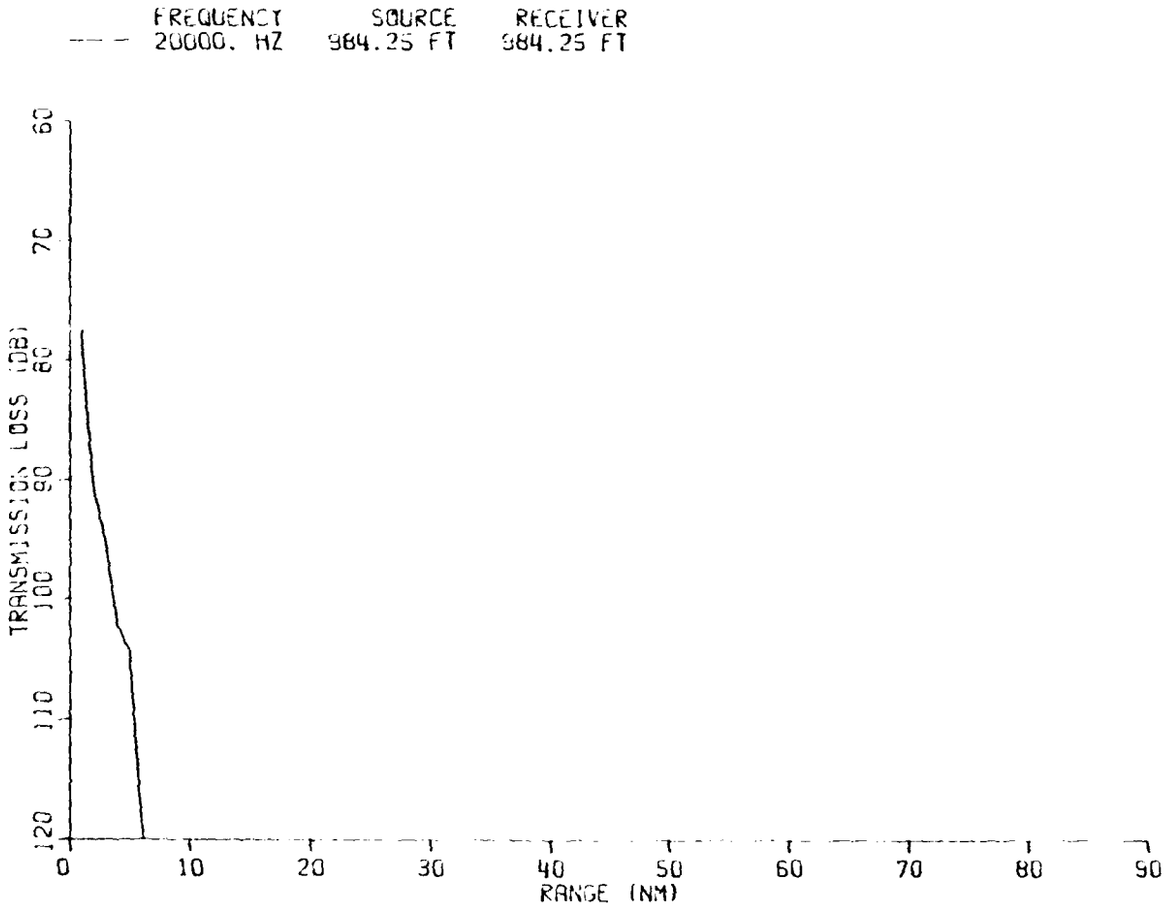

Figure A-14 SARGASSO/SLOPE Transmission Loss (MPP)
Receiver = 300 m, 20,000 Hz

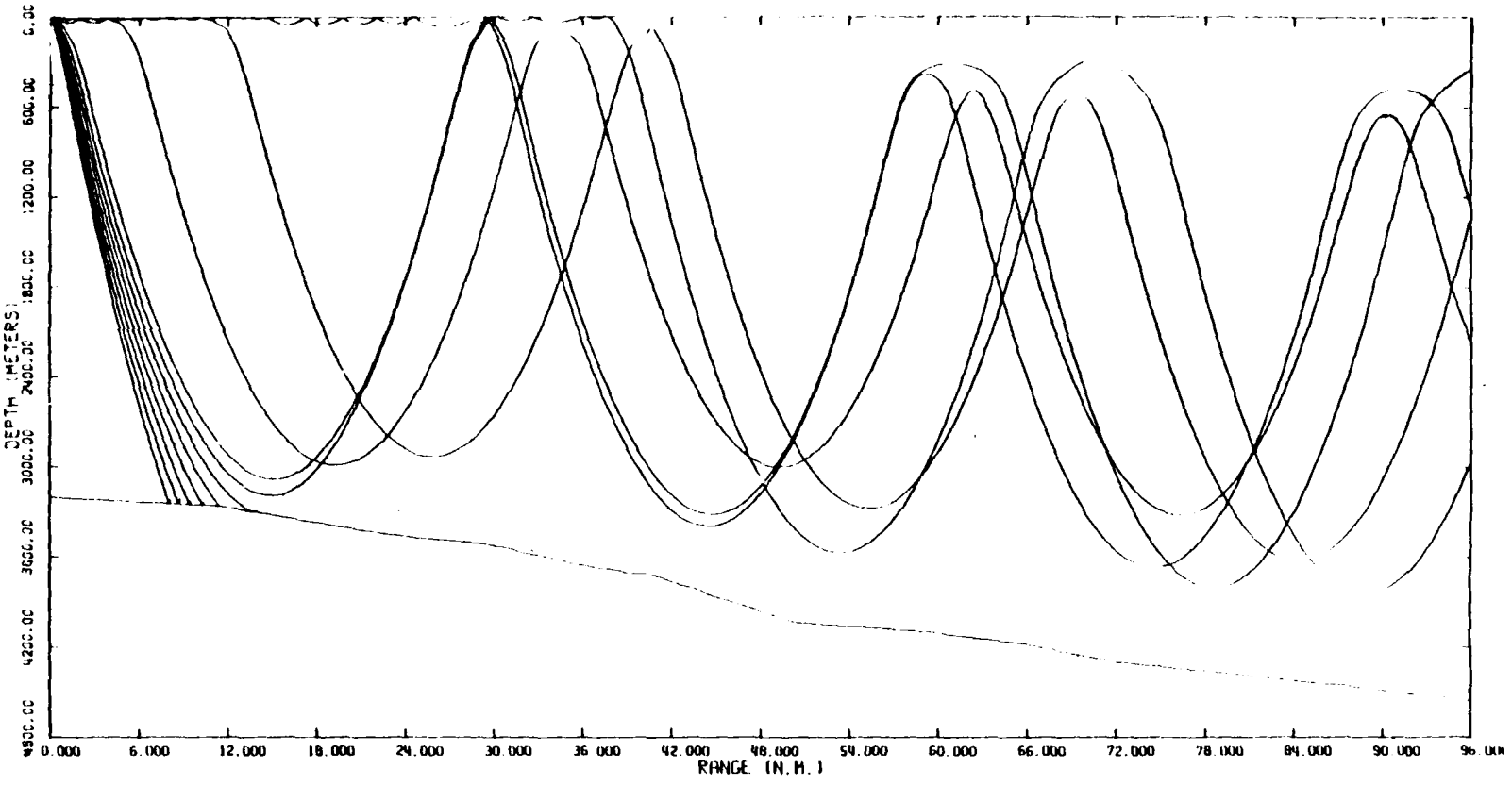

Figure A-15 SLOPE/SARGASSO Ray plot
Receiver = 10 m, Source = 140 Hz
Angles plotted 0^{o}-10^{o}

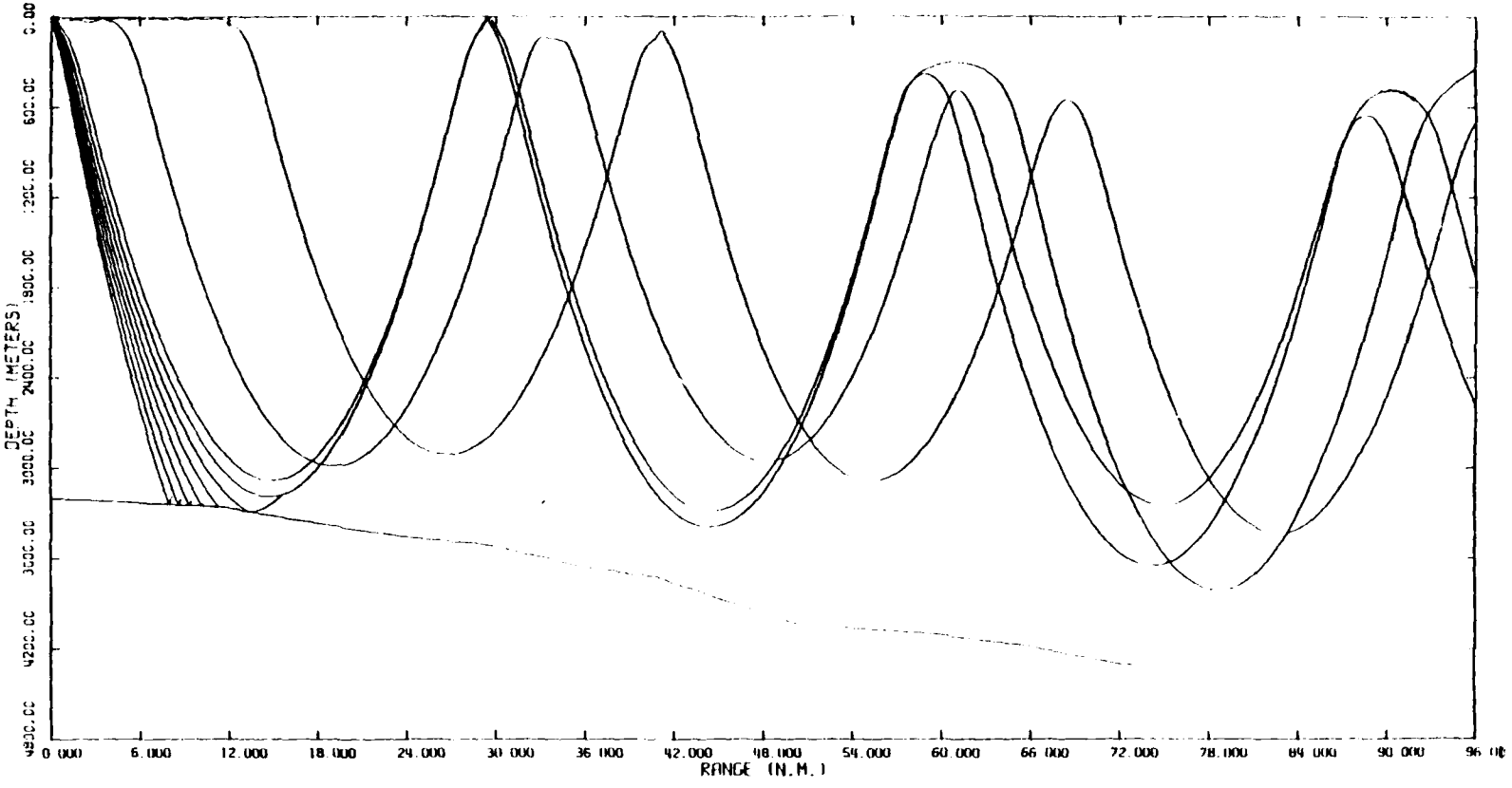

Figure A-16 SLOPE/SARGASSO Ray plot
Receiver = 10 m, Source = 140 m
Angles plotted -1^{o} to -10^{o}

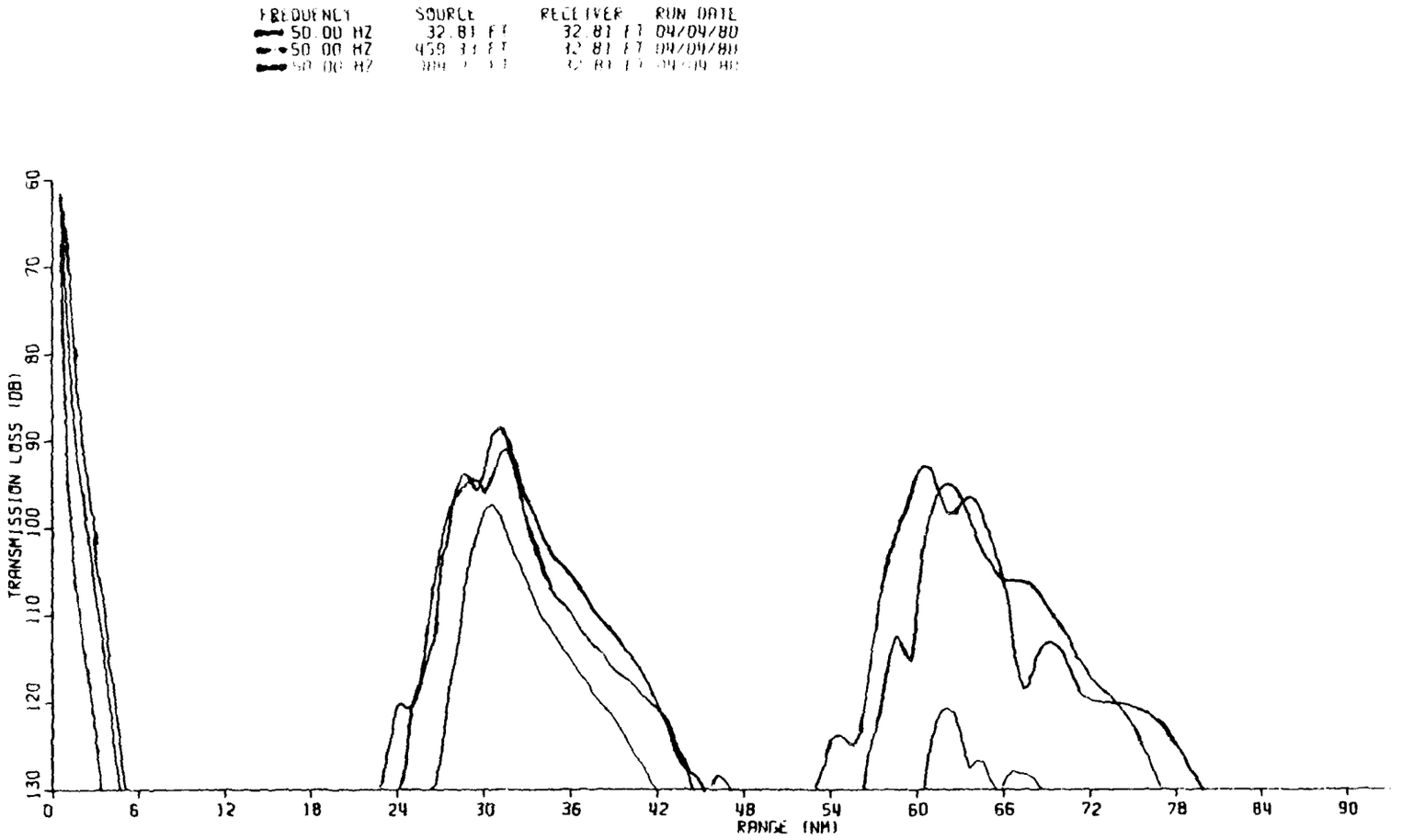

Figure A-17 SLOPE/SARGASSO Transmission Loss (PE)
Receiver = 10 m, 50 Hz

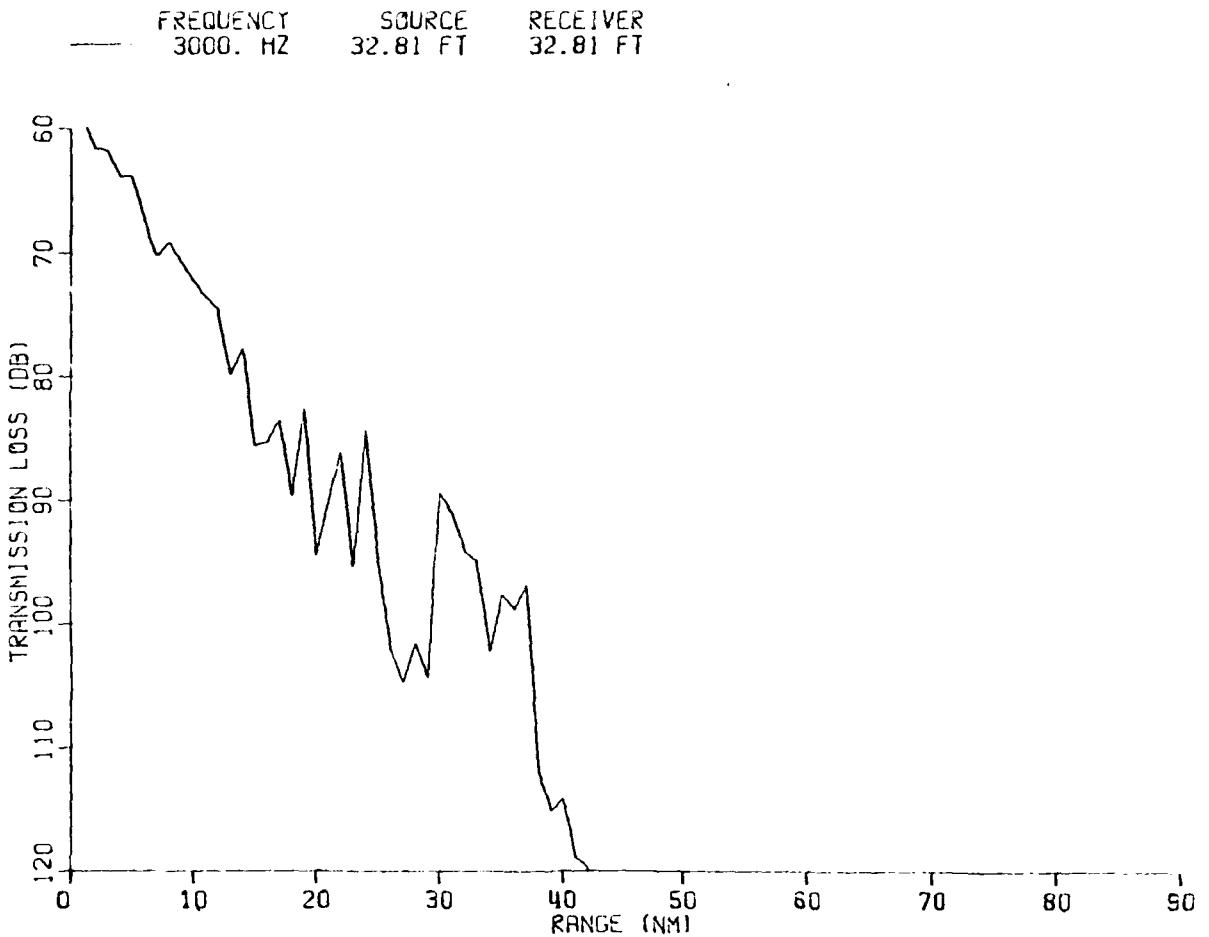

Figure A-18 SLOPE/SARGASSO Transmission Loss (MPP)
Receiver = 10 m, 3,000 m

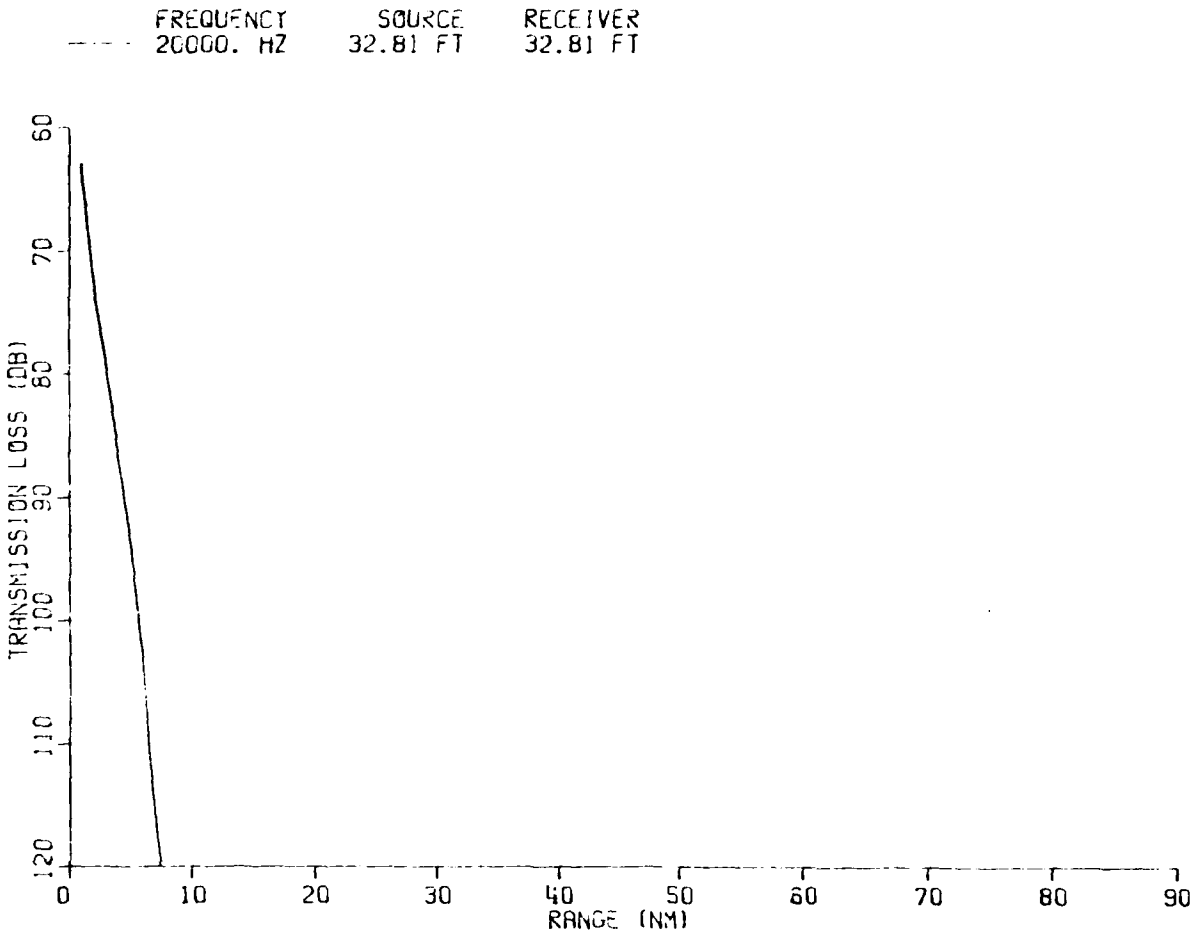

Figure A-19 SLOPE/SARGASSO Transmission Loss (MPP)
Receiver = 10 m, 20,000 Hz

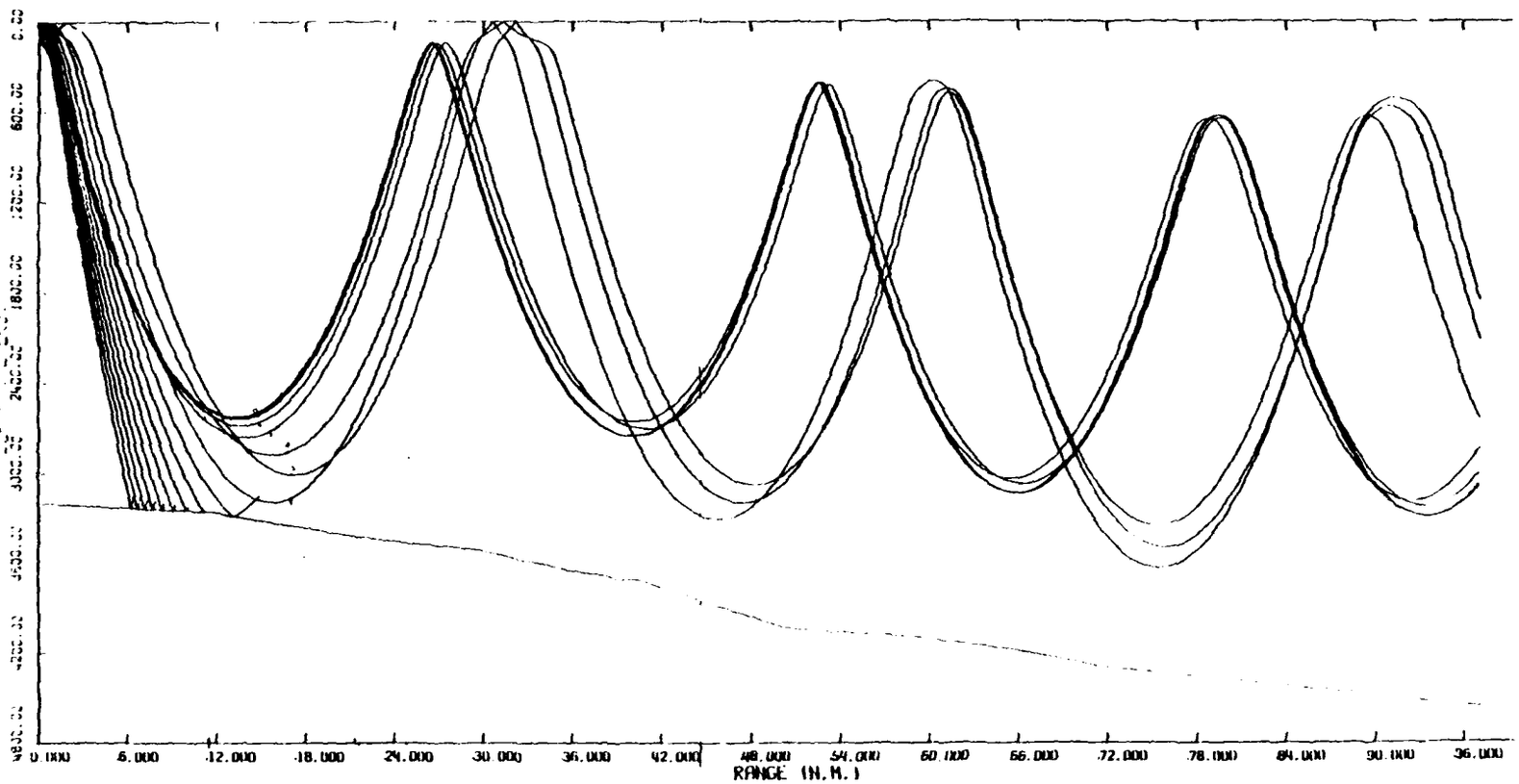

Figure A-20 SLOPE/SARGASSO Ray plot
Receiver = 140 m, Source = 140 m
Angles plotted 0^{o}-15^{o}

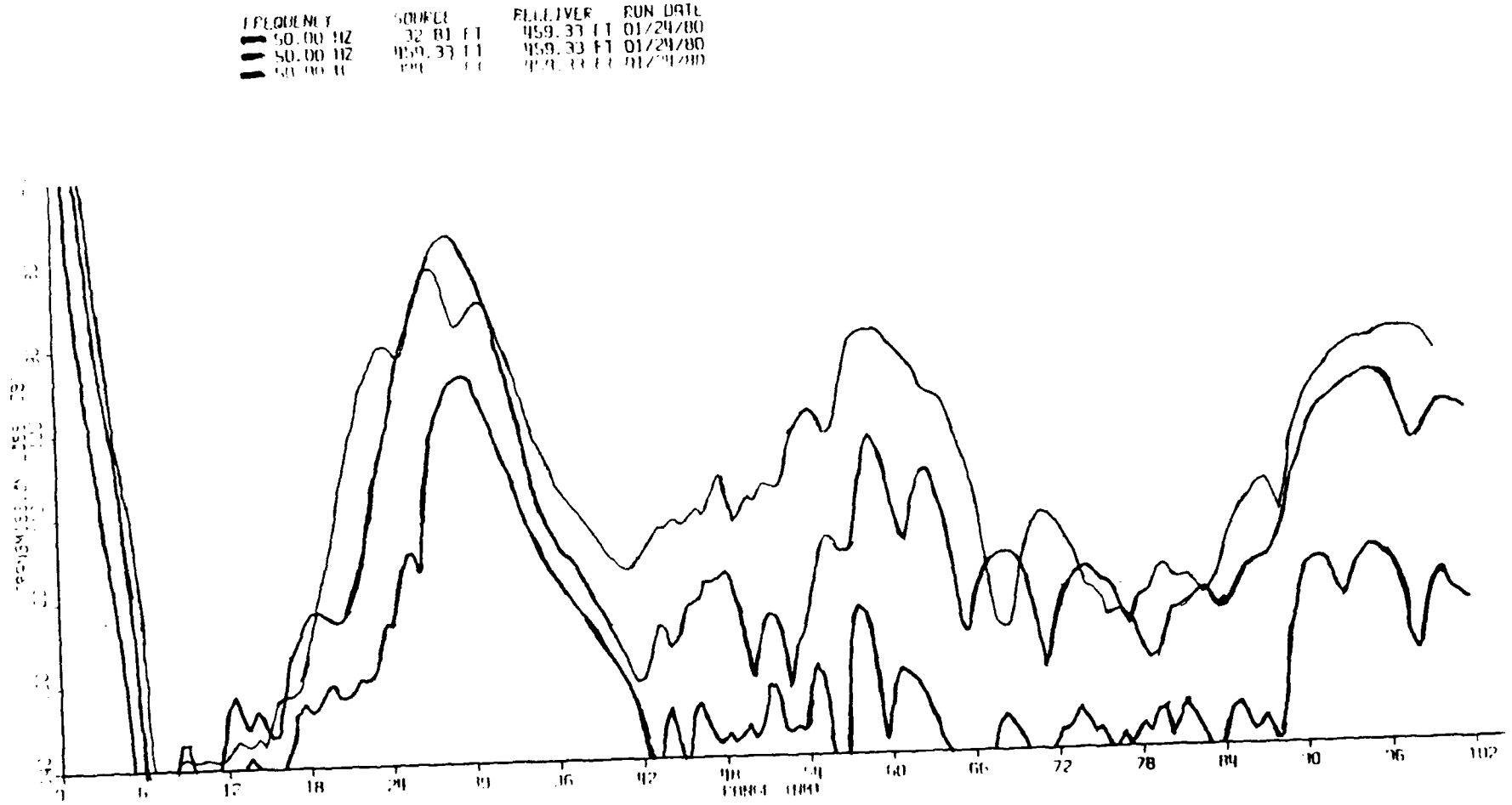

Figure A-21 SLOPE/SARGASSO Transmission Loss (PE)
Receiver = 140 m, 50 Hz

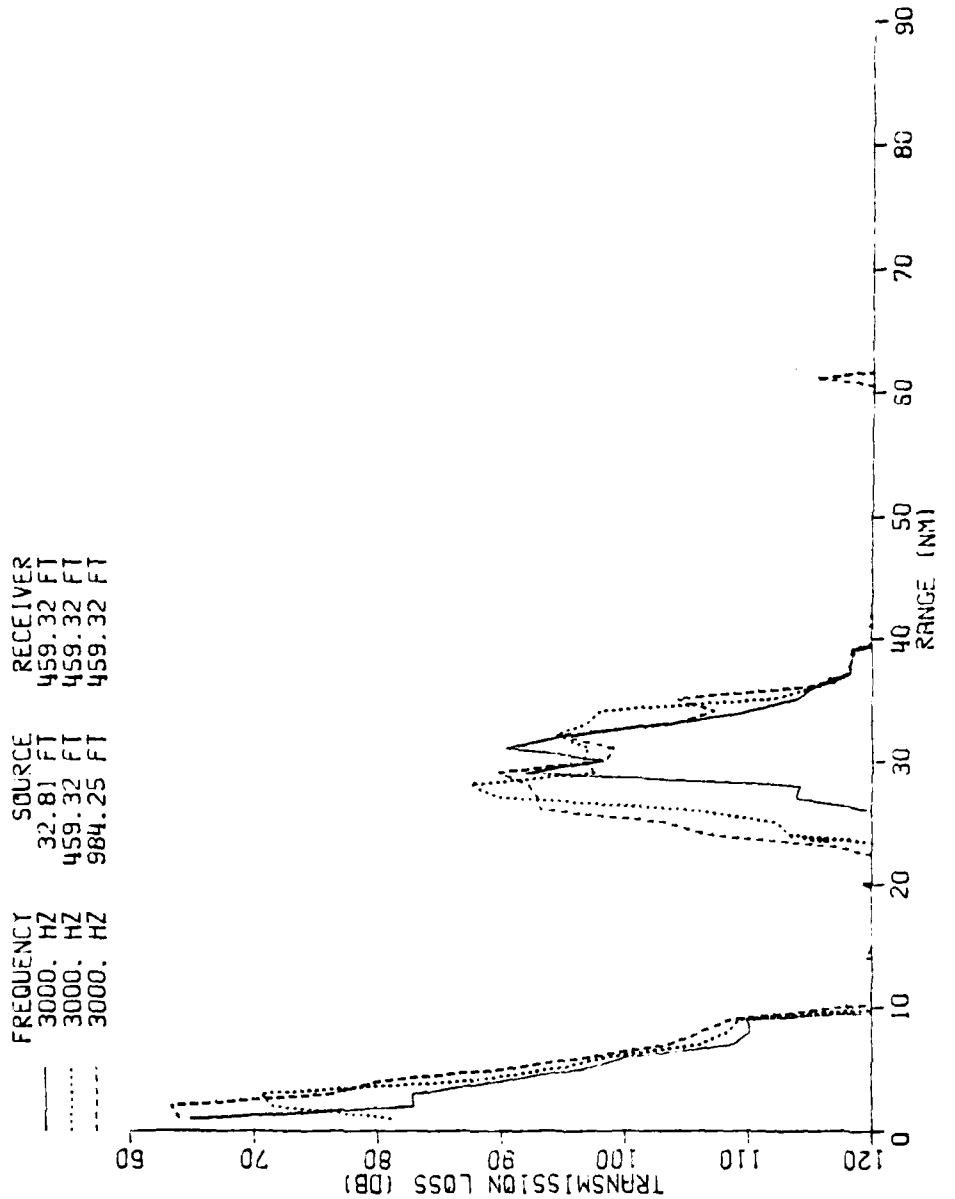

Figure A-22 SLOPE/SARGASSO Transmission Loss (MPP)
Receiver = 140 m, 3000 Hz

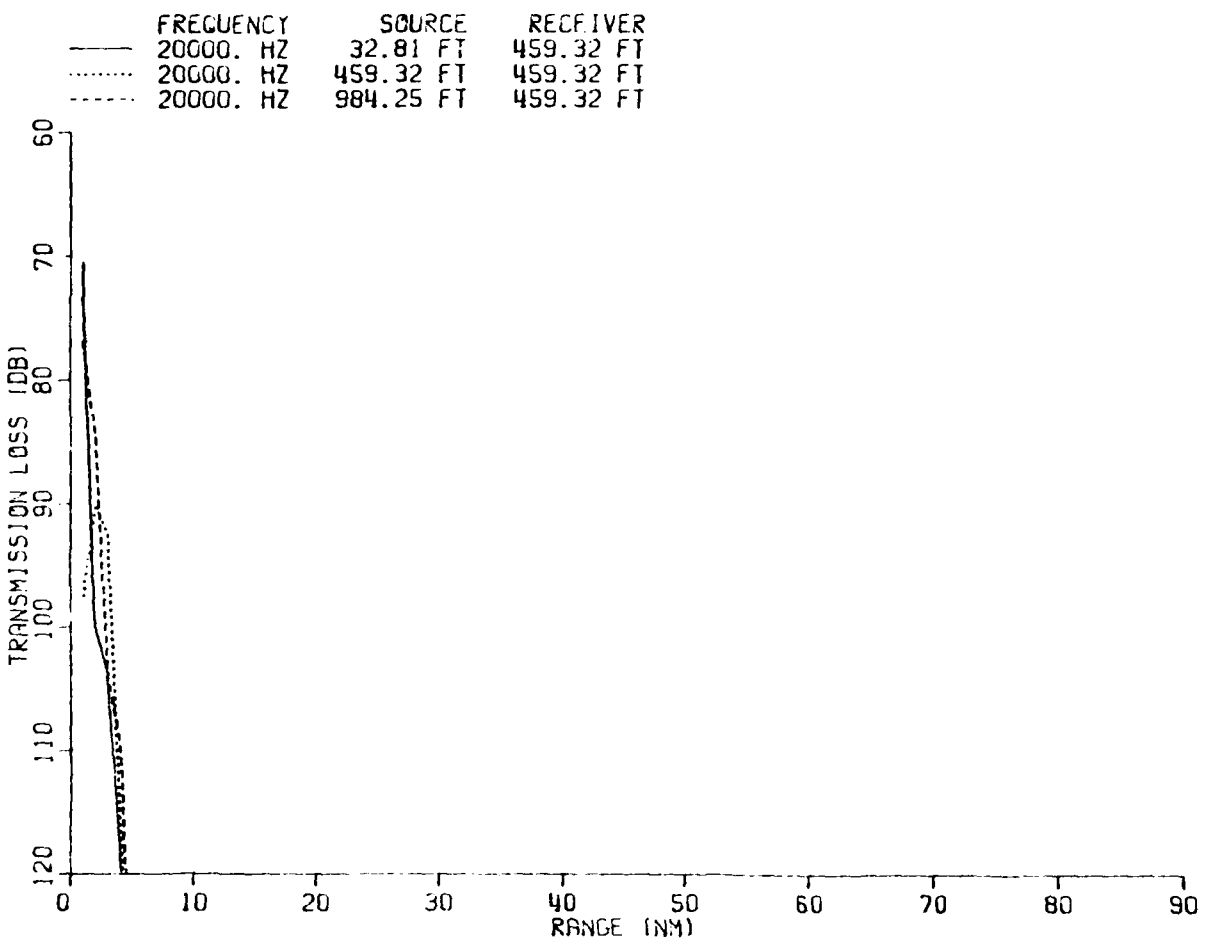

Figure A-23 SLOPE/SARGASSO Transmission Loss (MPP)
Receiver = 140 m, 20,000 Hz

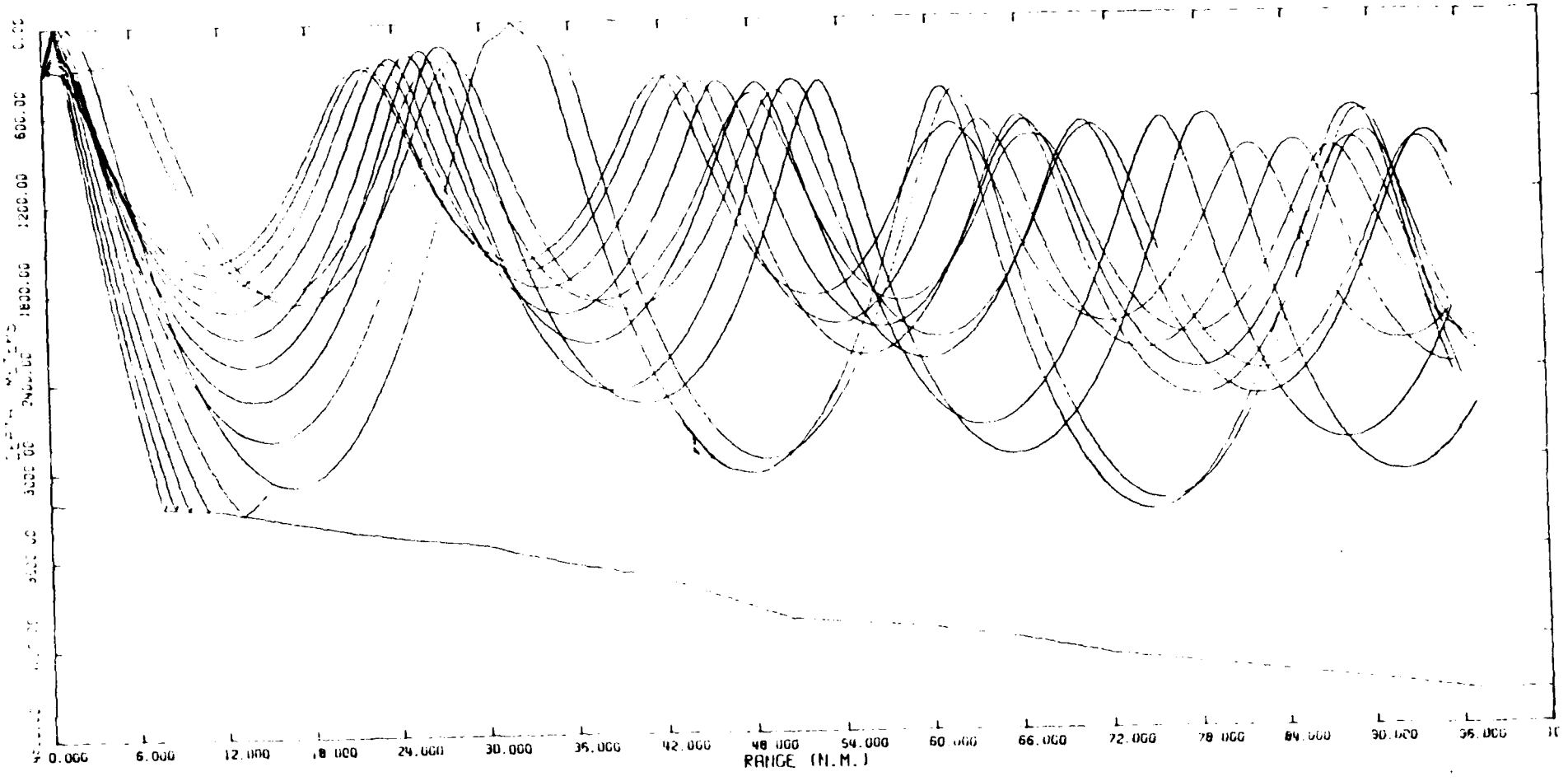

Figure A-24 SLOPE/SARGASSO Ray plot
Receiver = 300 m, Source = 140 m
Angles plotted 0^{o}-15^{o}

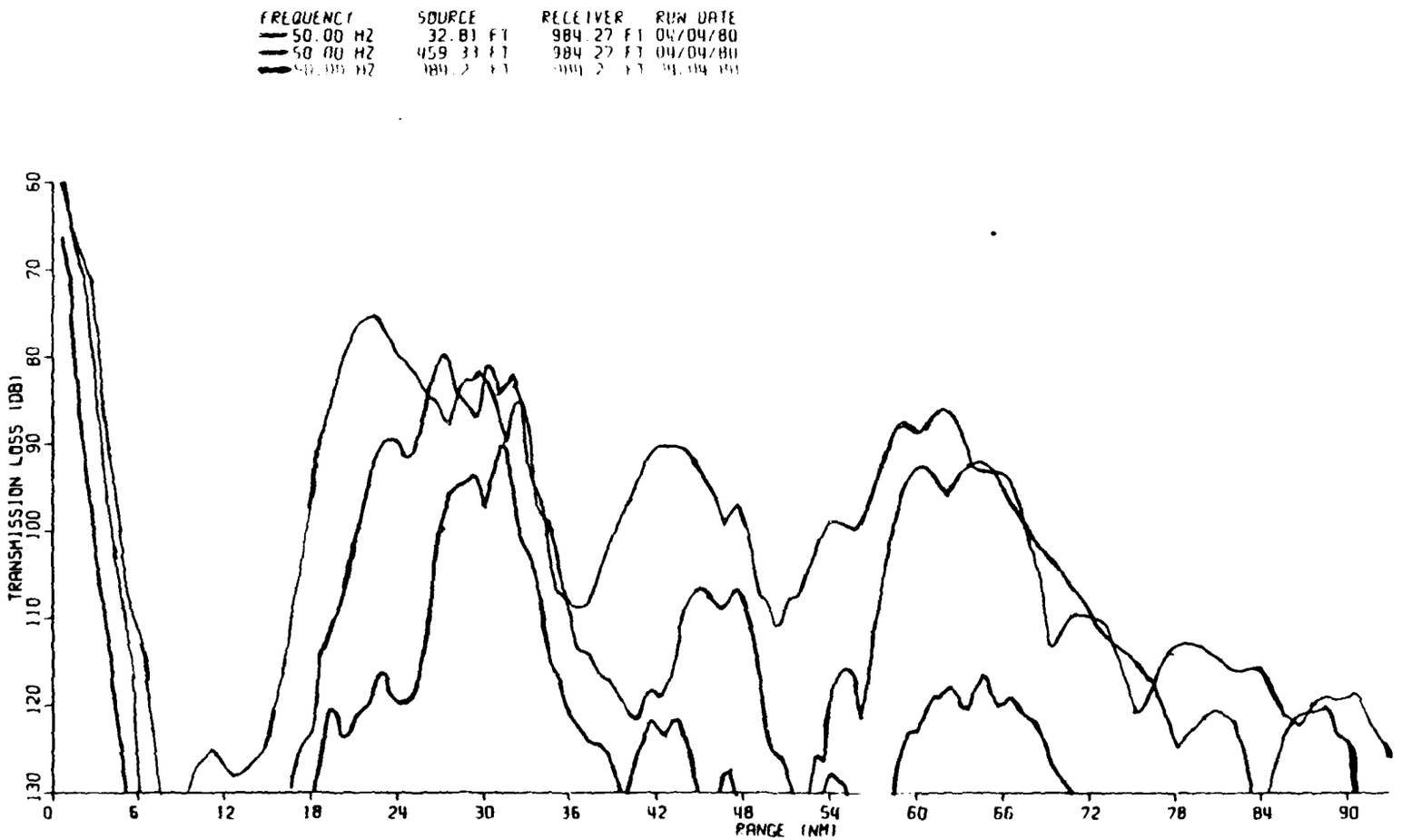

Figure A-25 SLOPE/SARGASSO Transmission Loss (PE)
Receiver = 300 m, 50 Hz

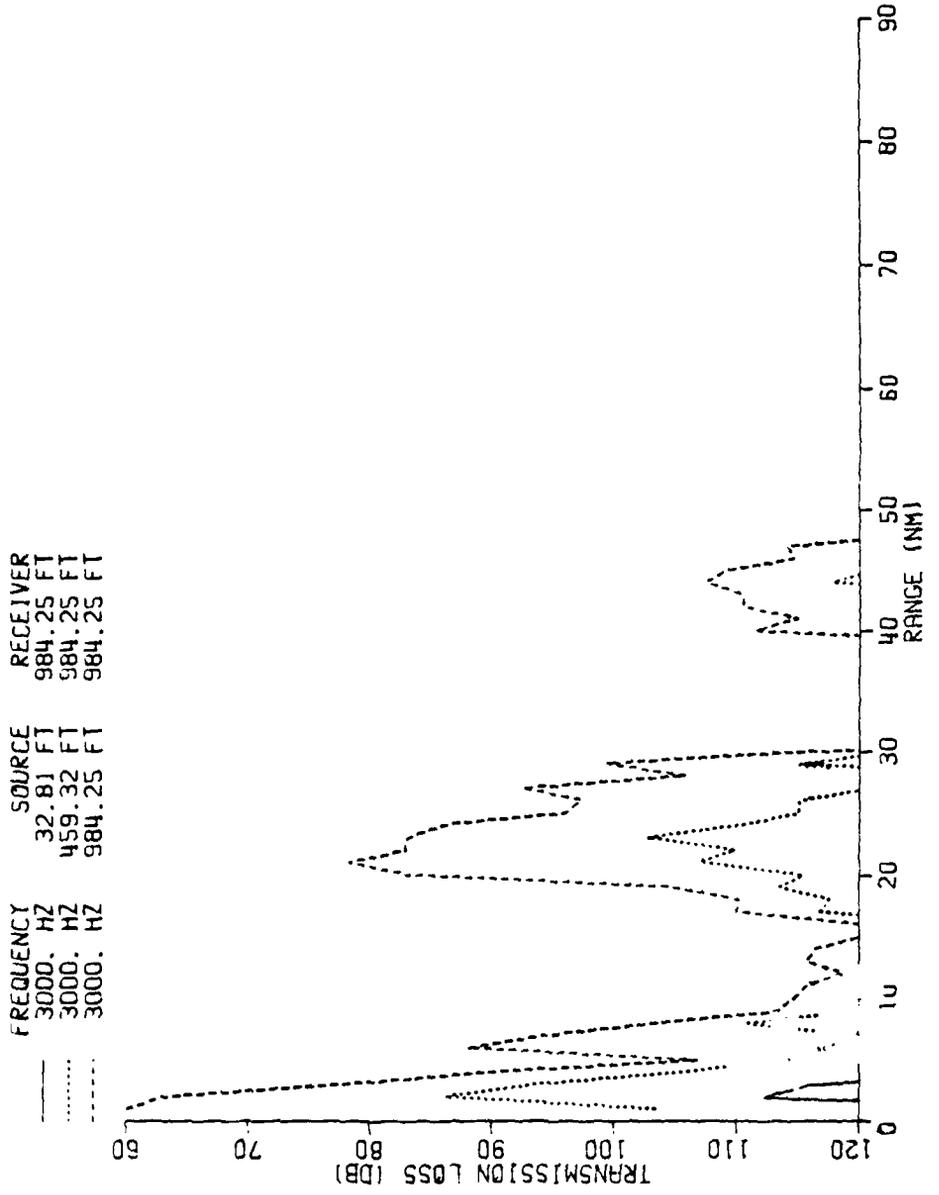

Figure A-26 SLOPE/SARGASSO Transmission Loss (MPP)
Receiver = 300 m, 3,000 Hz

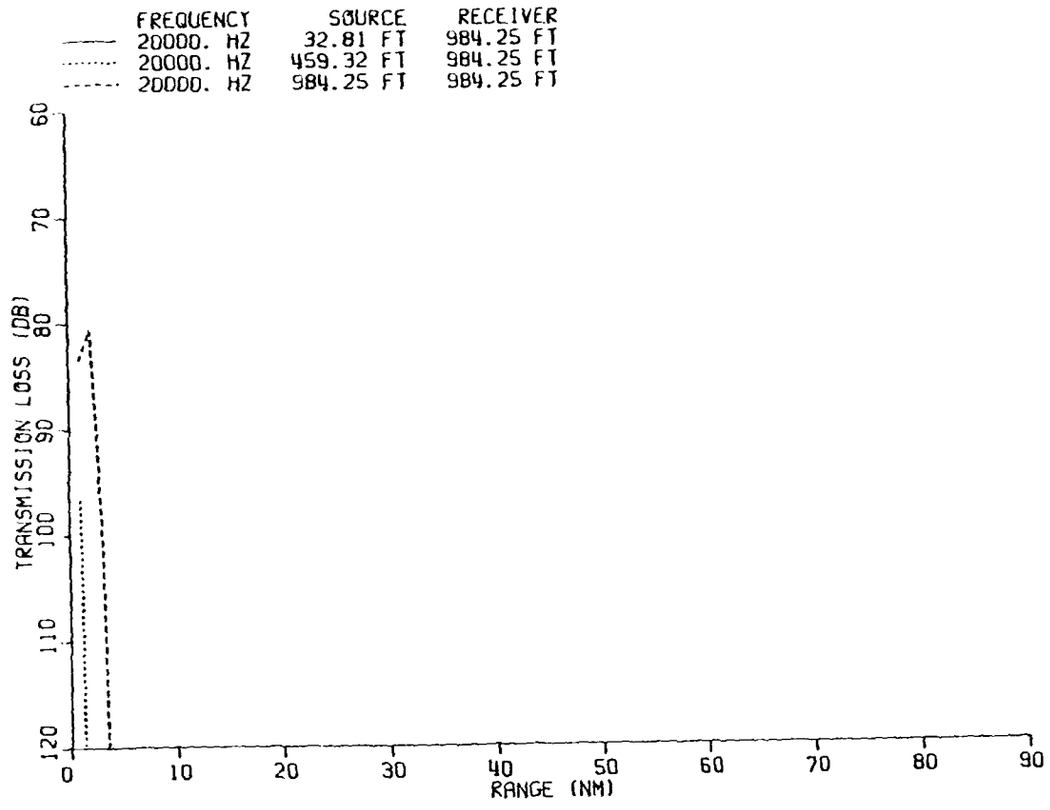

Figure A-27 SLOPE/SARGASSO Transmission Loss (MPP)
Receiver = 300 m, 20,000 Hz

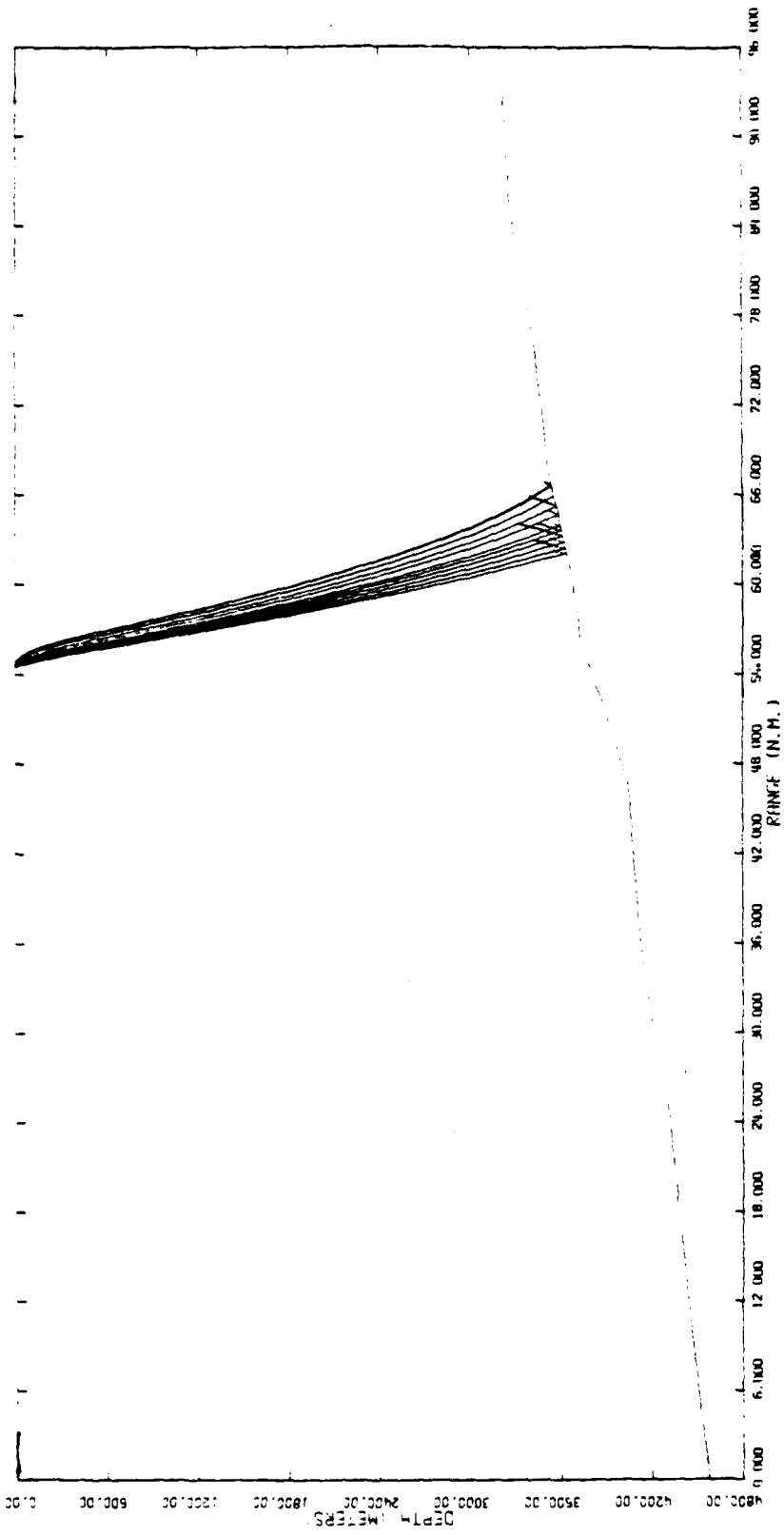

Figure A-28 NORTH WALL/SLOPE Ray plot
Receiver = 10 m, Source = 140 m
Angles plotted 0°-10°

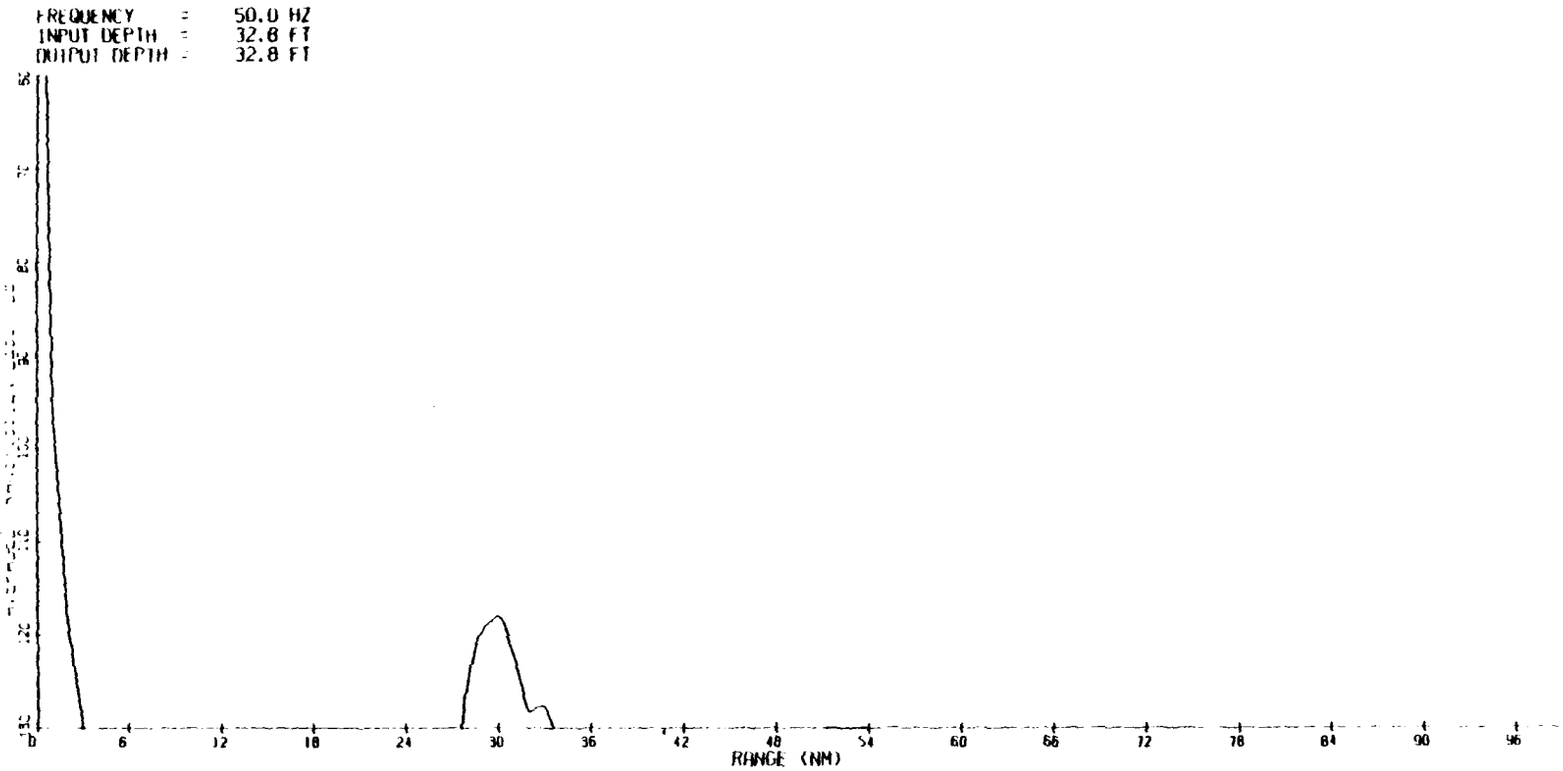

Figure A-29 NORTH WALL/SLOPE Transmission Loss (PE)
Receiver = 10 m, Source = 10 m 50 Hz

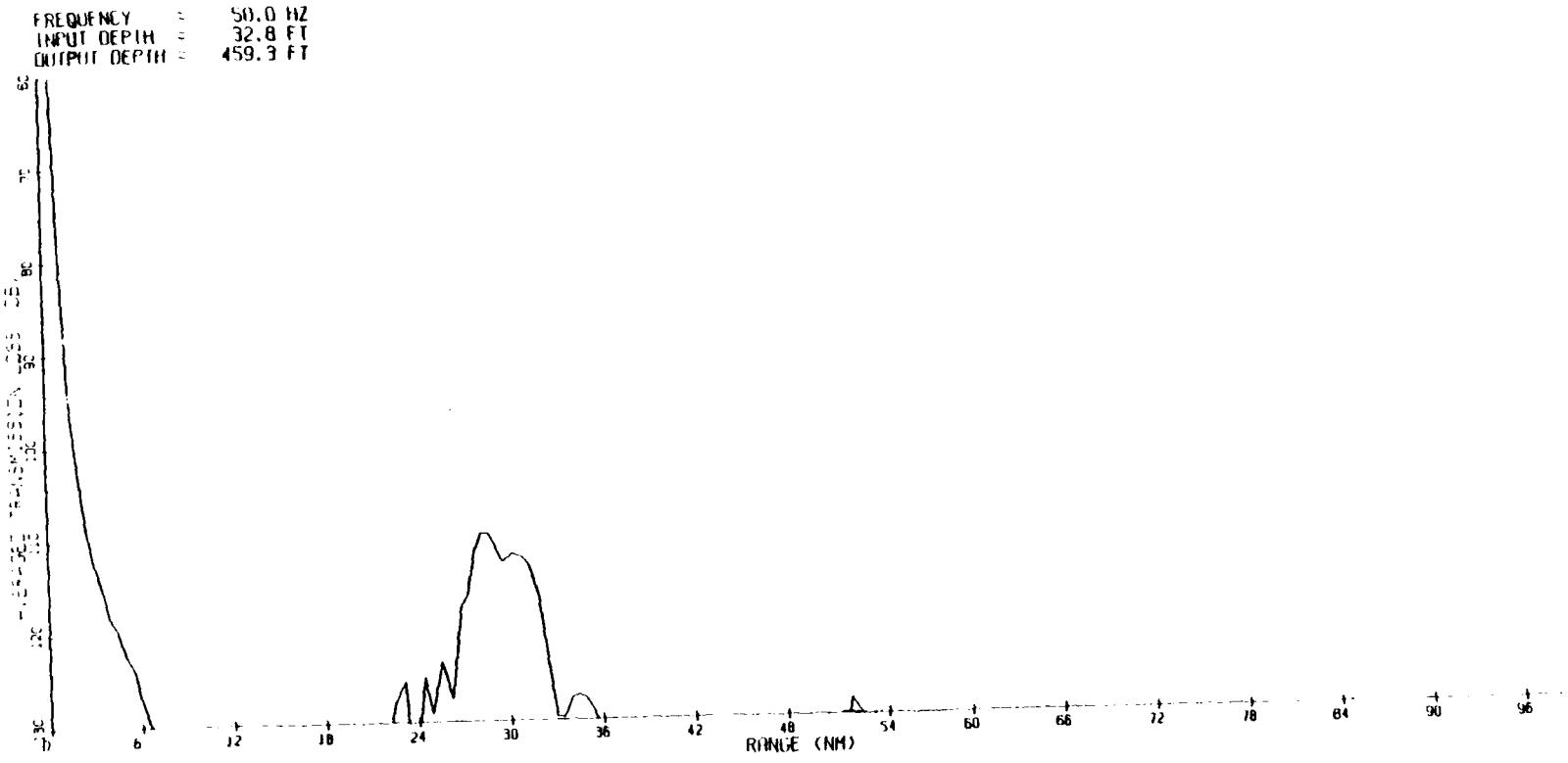

Figure A-30 NORTH WALL/SLOPE Transmission Loss (PE)
Receiver = 10 m, Source = 140 m 50 Hz

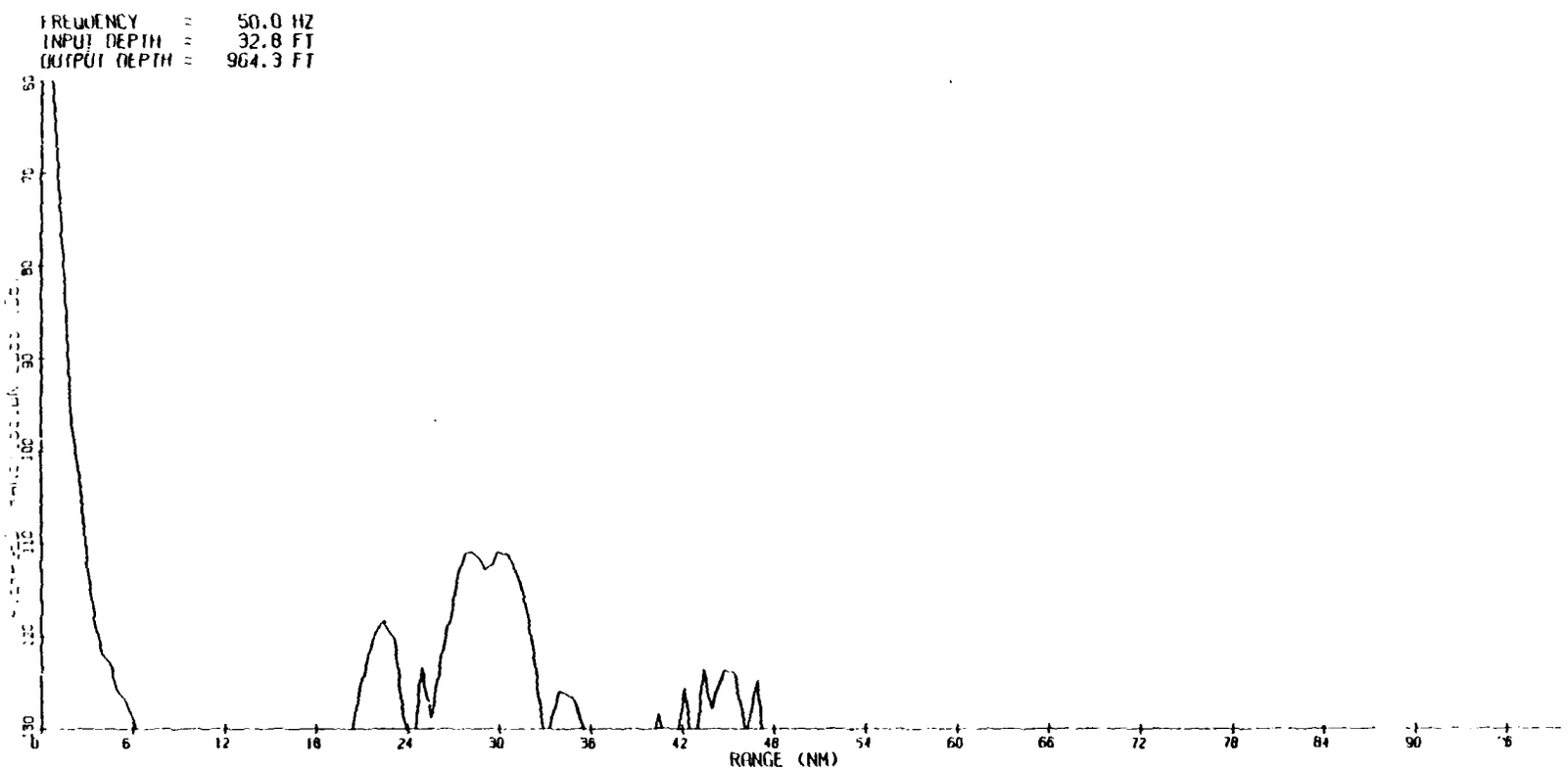

Figure A-31 NORTH WALL/SLOPE Transmission Loss (PE)
Receiver = 10 m, Source = 300 m 50 Hz

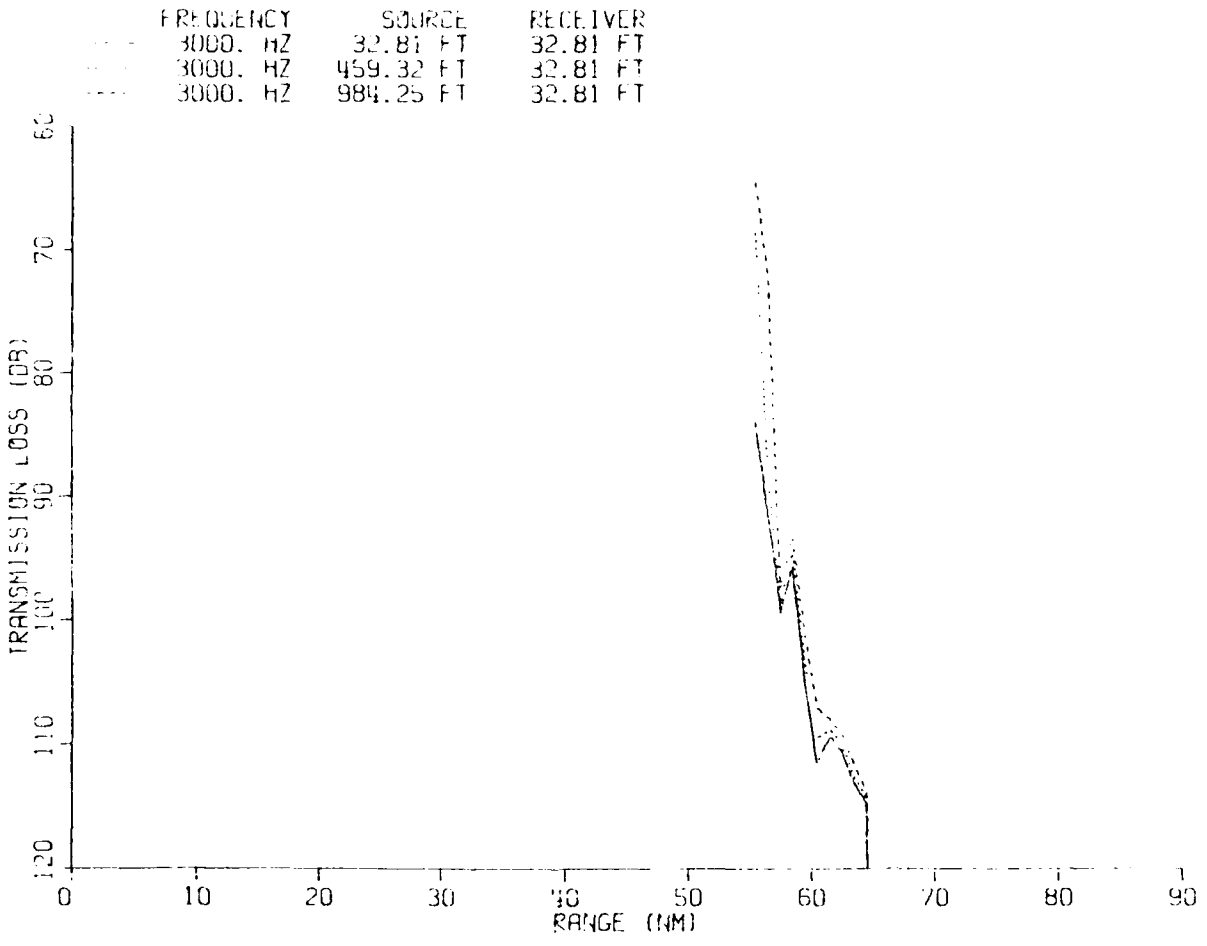

Figure A-32 NORTH WALL/SLOPE Transmission Loss (MPP)
Receiver = 10 m, 3,000 Hz

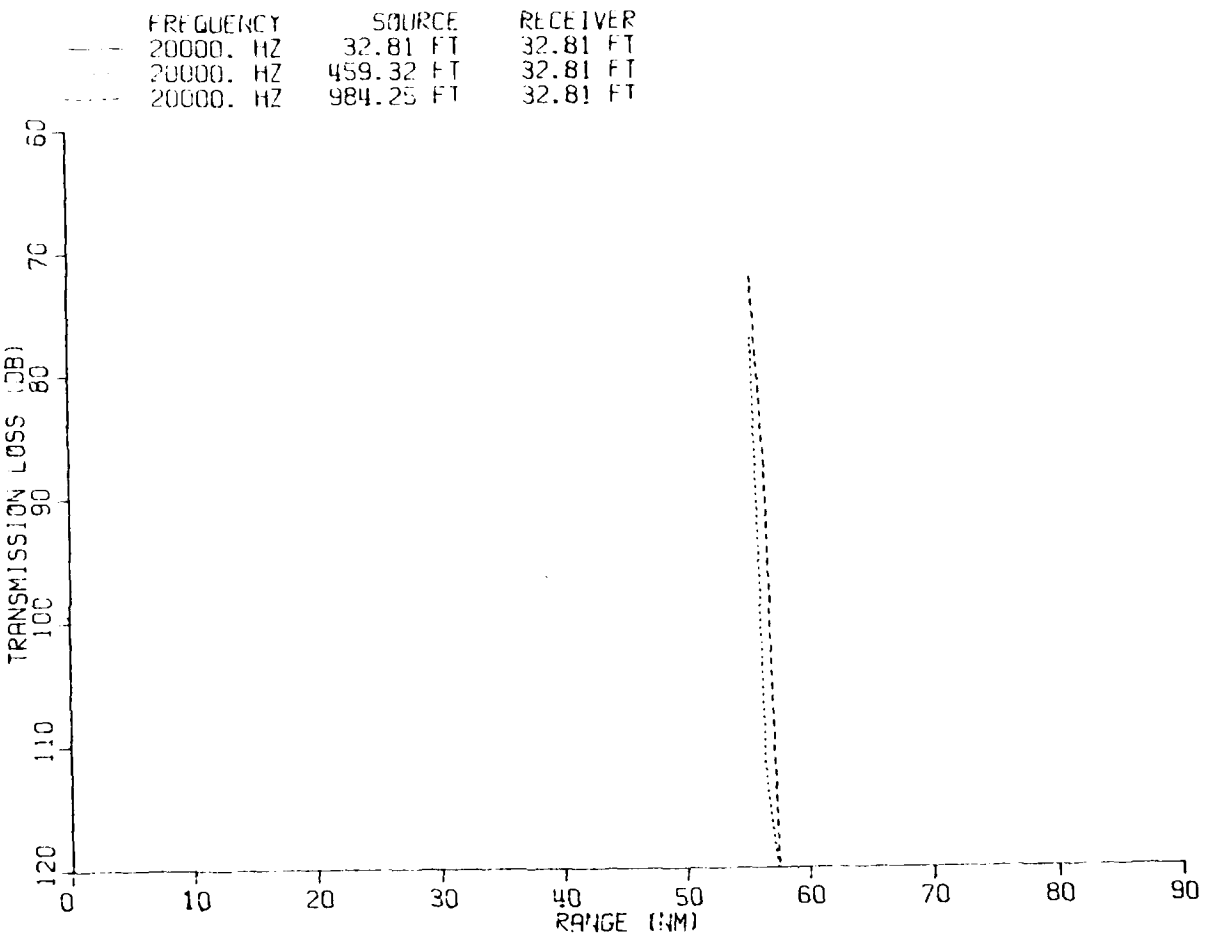

Figure A-33 NORTH WALL/SLOPE Transmission Loss (MPP)
Receiver = 10 m, 20,000 Hz

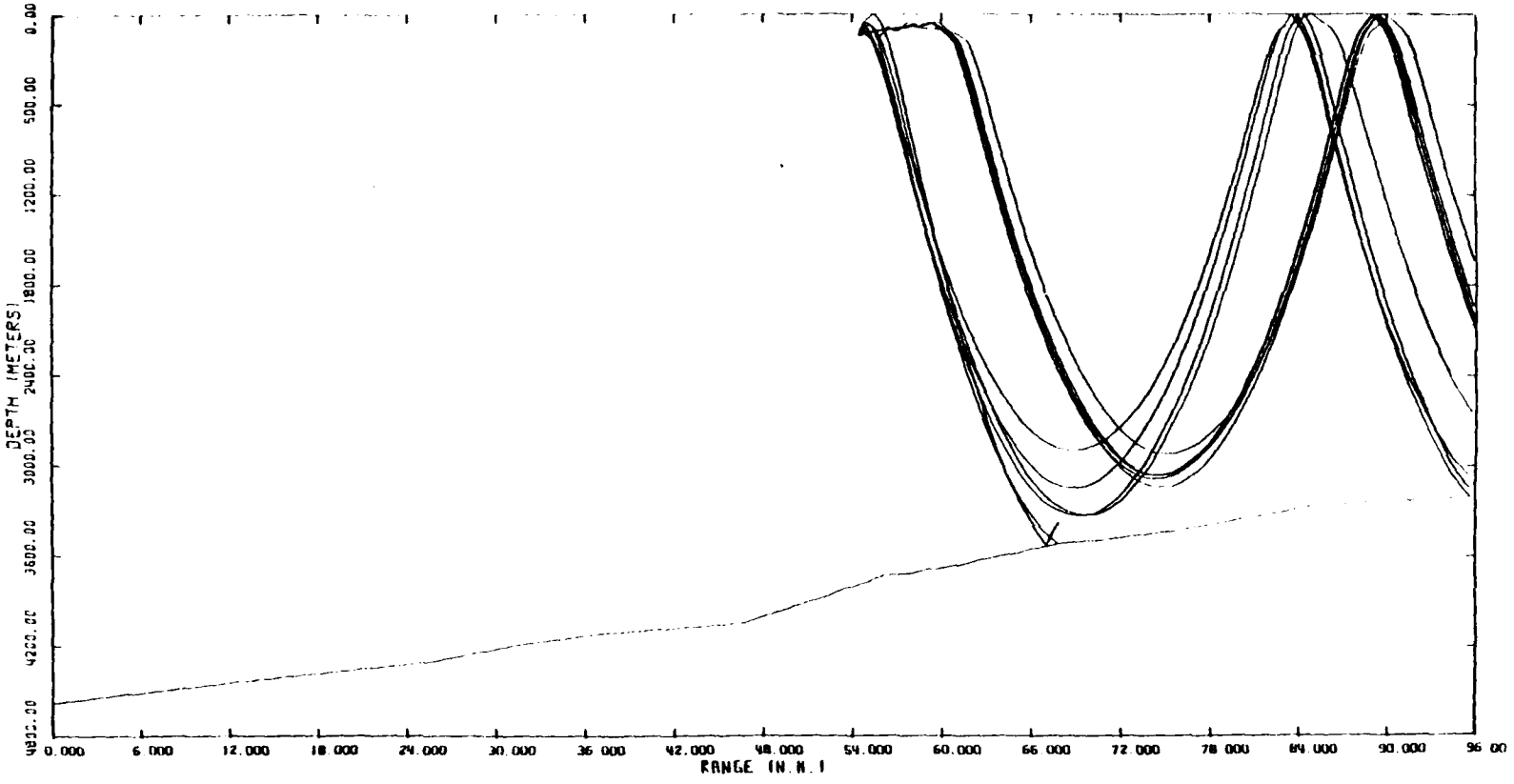

Figure A-34 NORTH WALL/SLOPE Ray plot
Receiver = 140 m, Source = 140 m
Angles plotted 0^{o}-10^{o}

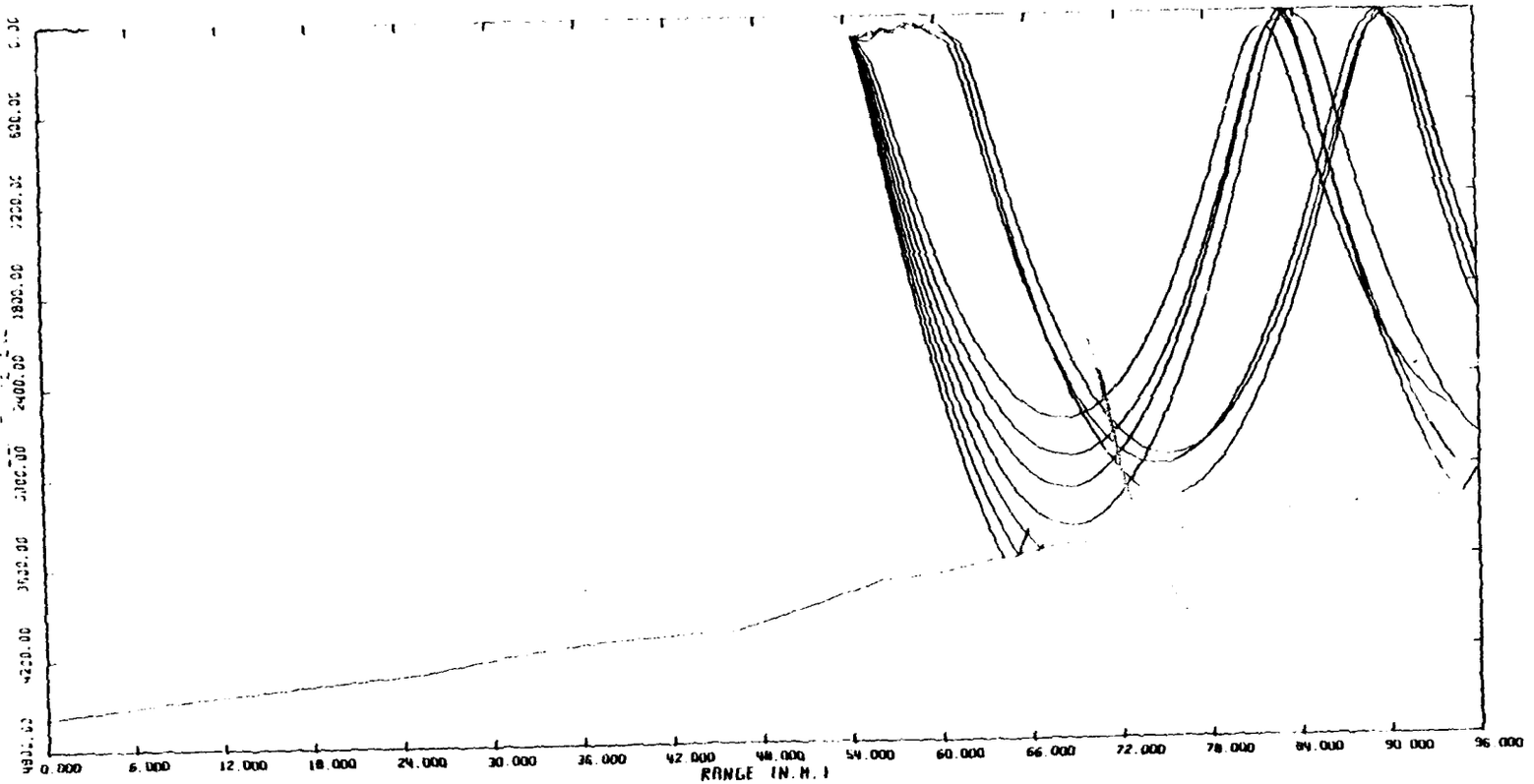

Figure A-35 NORTH WALL/SLOPE RAY plot
Receiver = 140 m, Source = 140 m
Angles plotted -1^{o} to -10^{o}

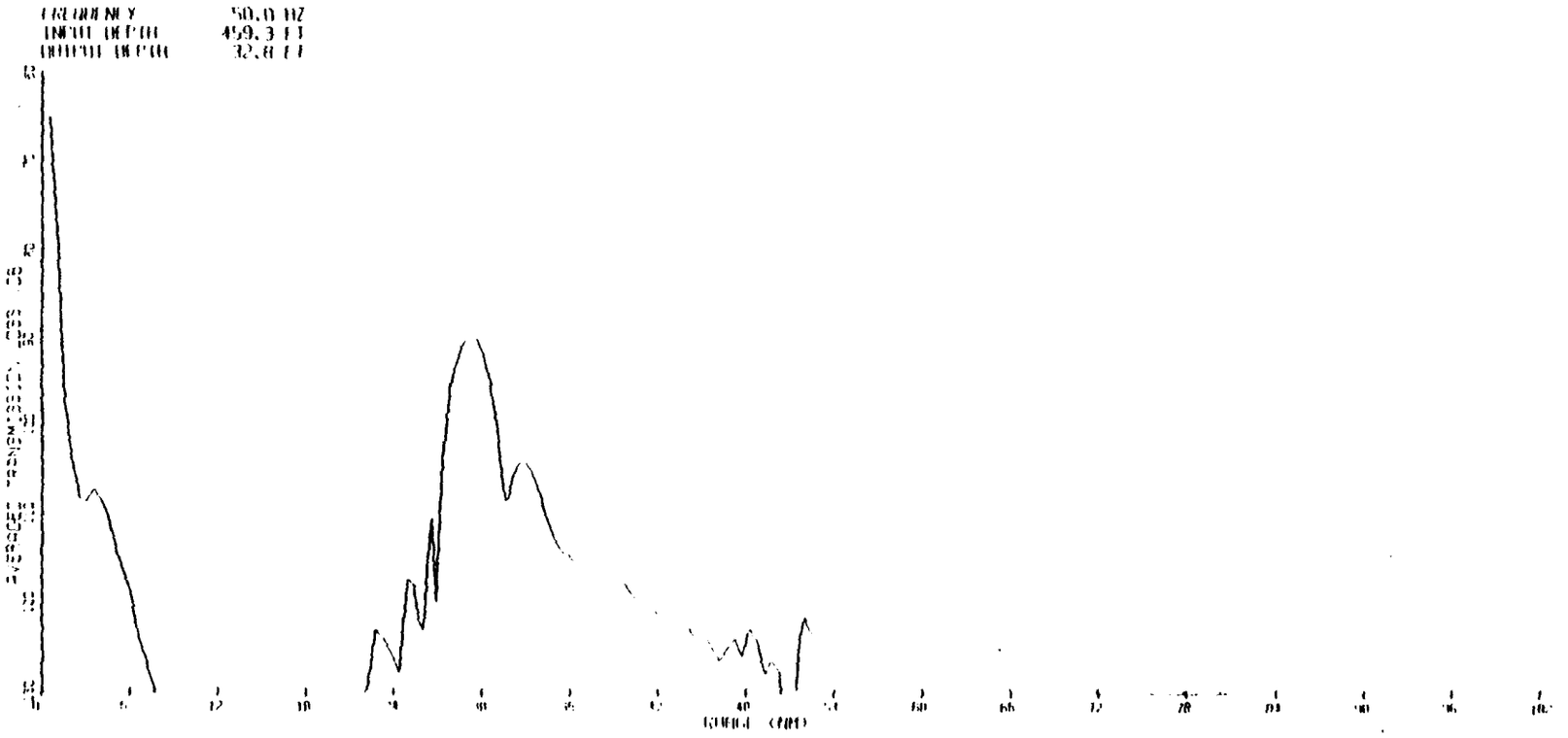

Figure A-36 NORTH WALL/SLOPE Transmission Loss (PE)
Receiver = 140 m, Source = 10 m 50 Hz

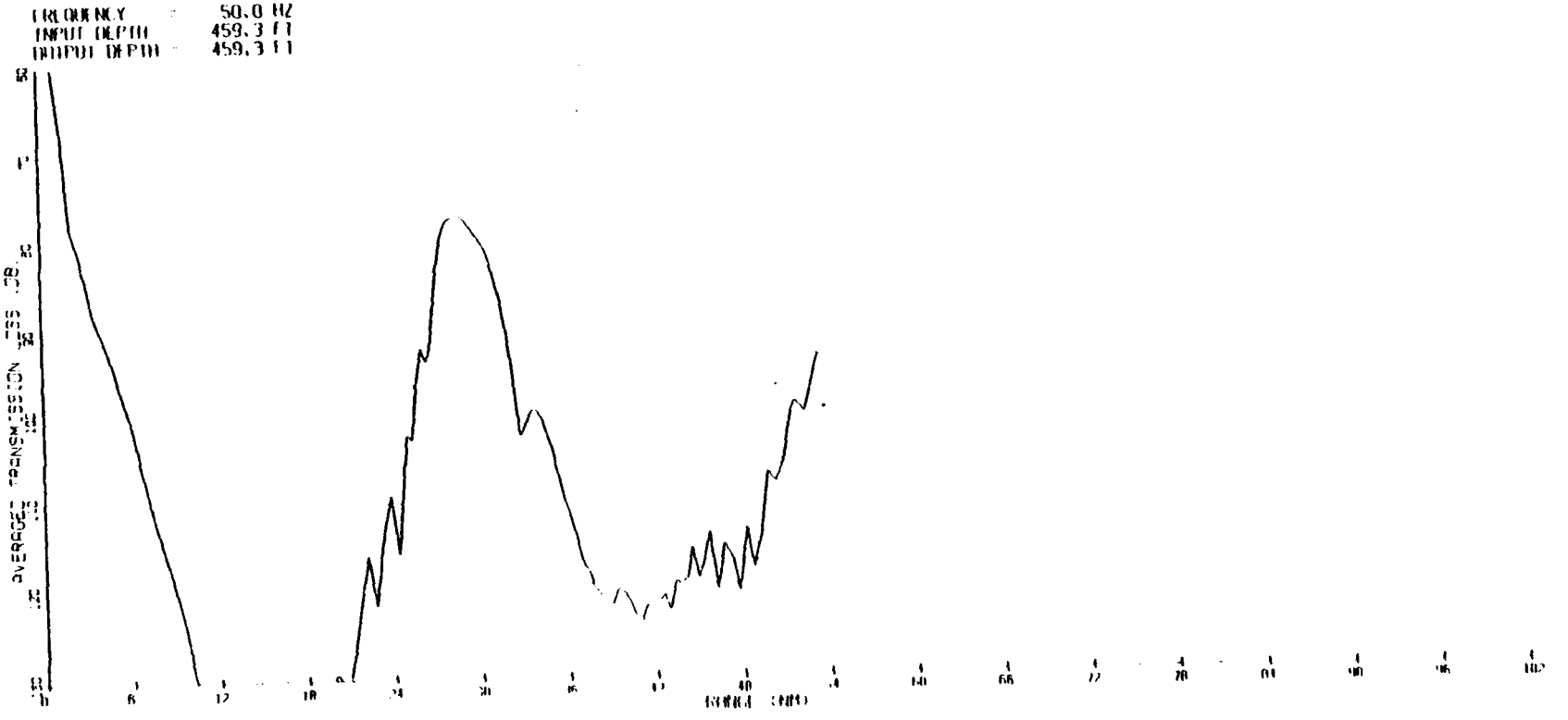

Figure A-37 NORTH WALL/SLOPE Transmission Loss (PE)
Receiver = 140 m, Source = 140 m 50 Hz

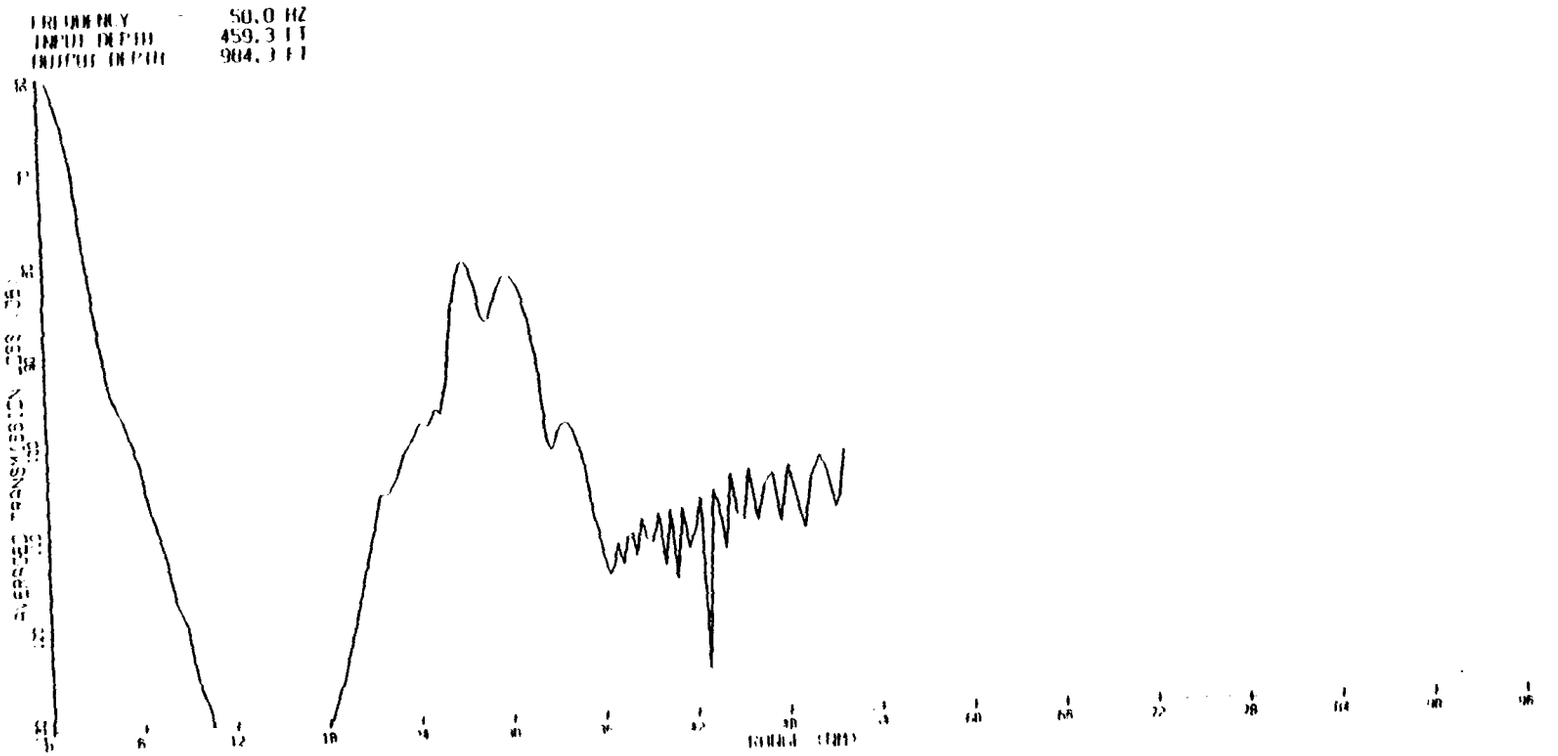

Figure A-38 NORTH WALL/SLOPE Transmission Loss (PE)
Receiver = 140 m, Source = 300 m 50 Hz

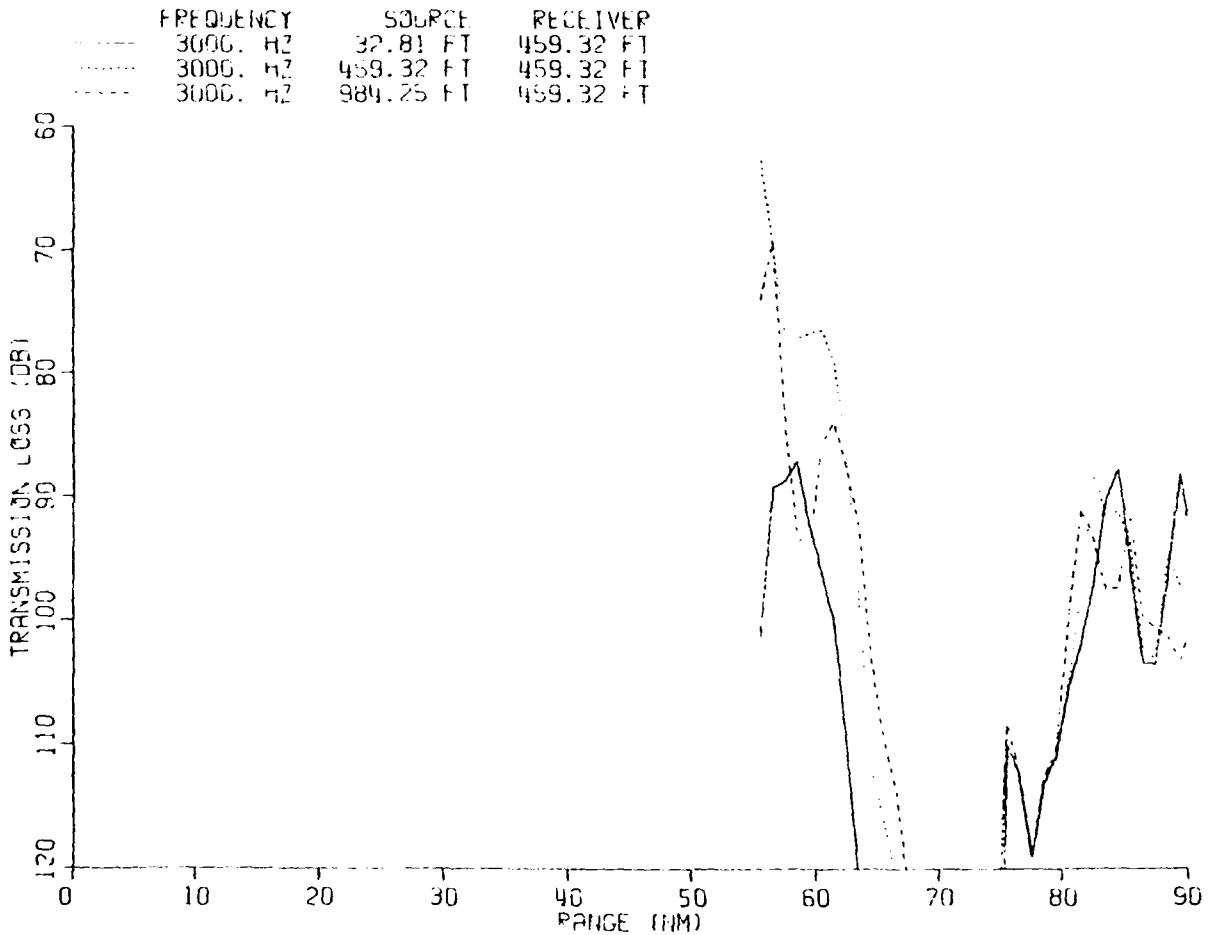

Figure A-39 NORTH WALL/SLOPE Transmission Loss (MPP)
Receiver = 140 m, 3,000 Hz

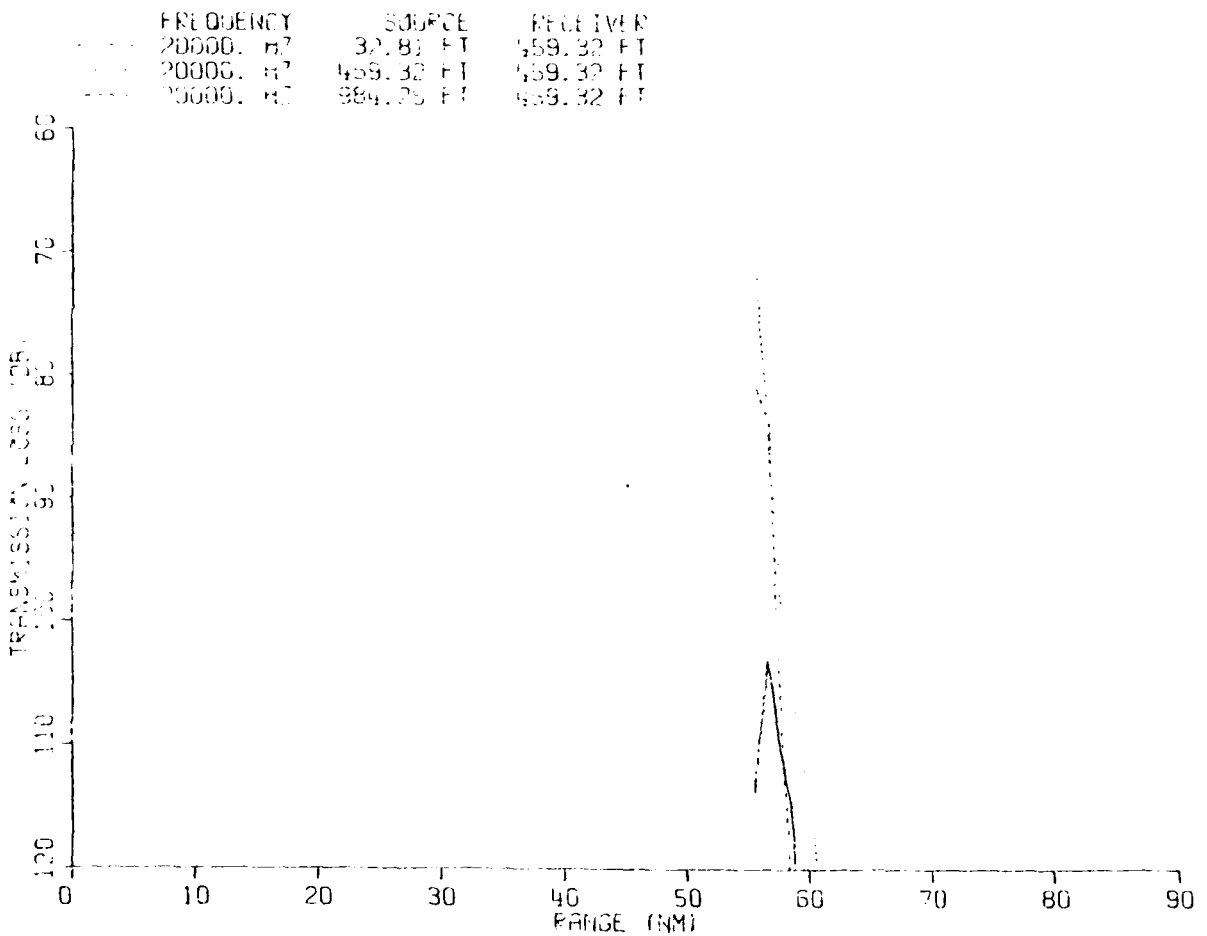

Figure A-40 NORTH WALL/SLOPE Transmission Loss (MPP)
Receiver = 140 m, 20,000 Hz

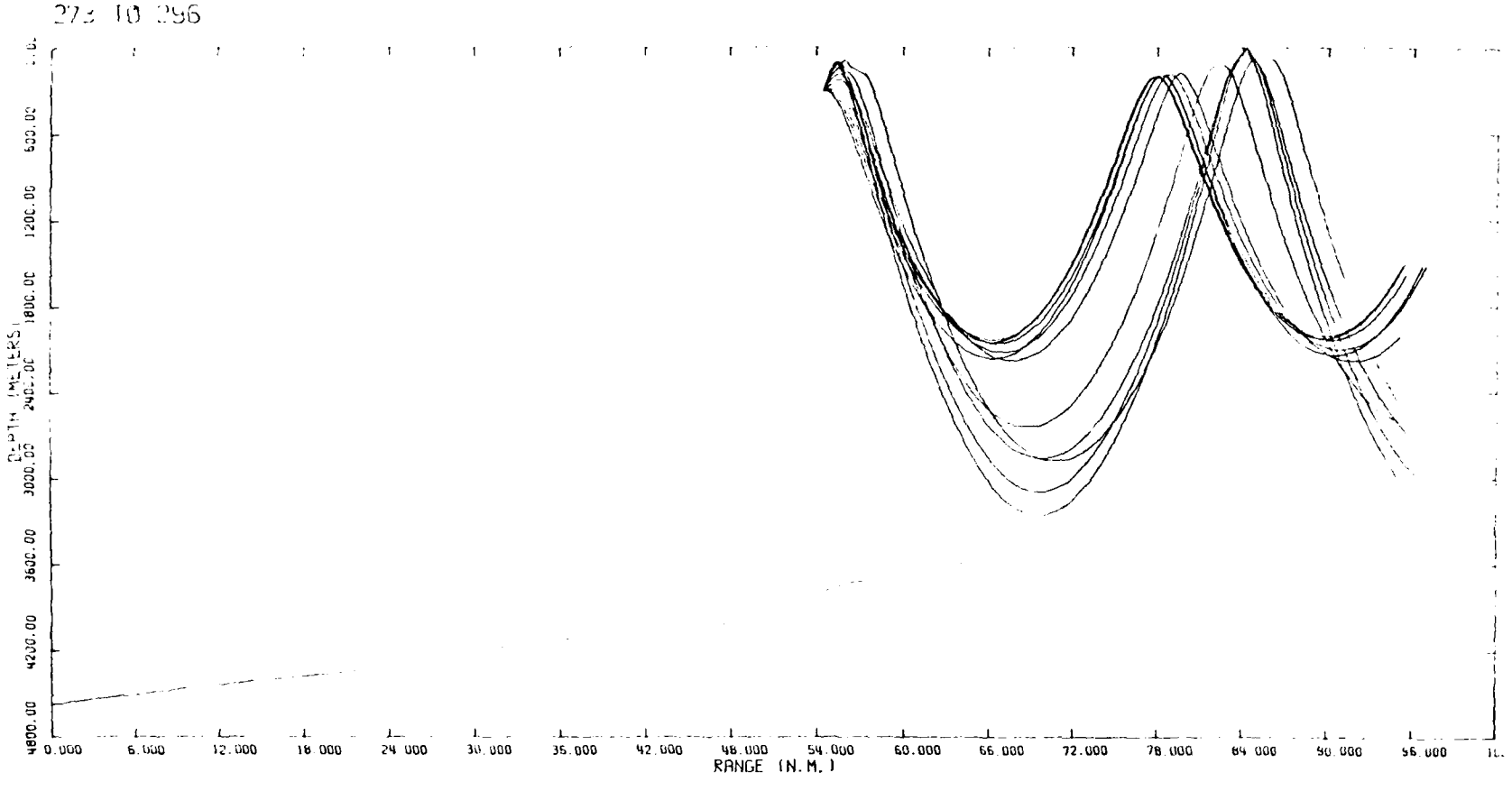

Figure A-41 NORTH WALL/SLOPE Ray plot
Receiver = 300 m, Source = 140 m
Angles plotted 0^{o}-10^{o}

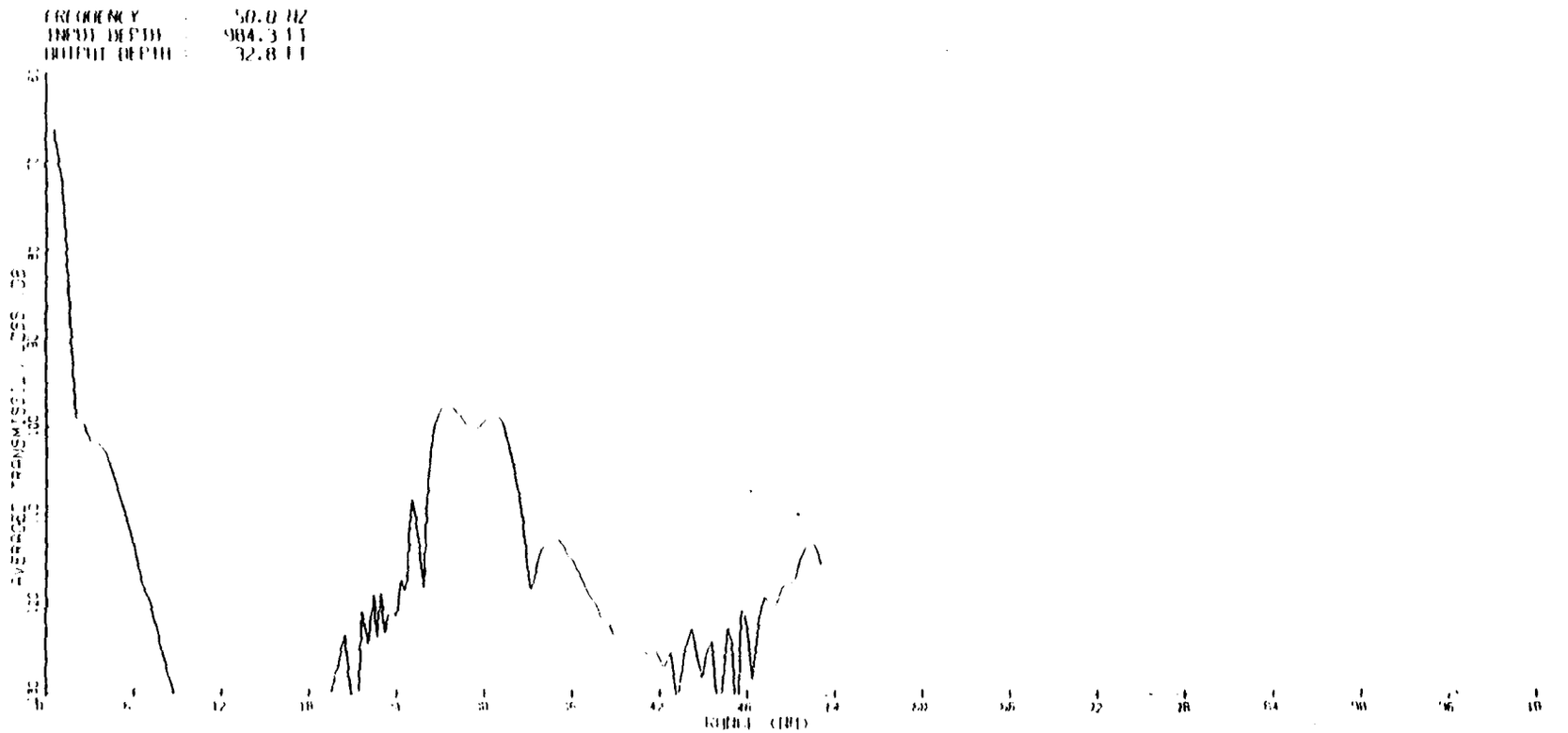

Figure A-42 NORTH WALL/SLOPE Transmission Loss (PE)
Receiver = 300 m, Source = 10 m 50 Hz

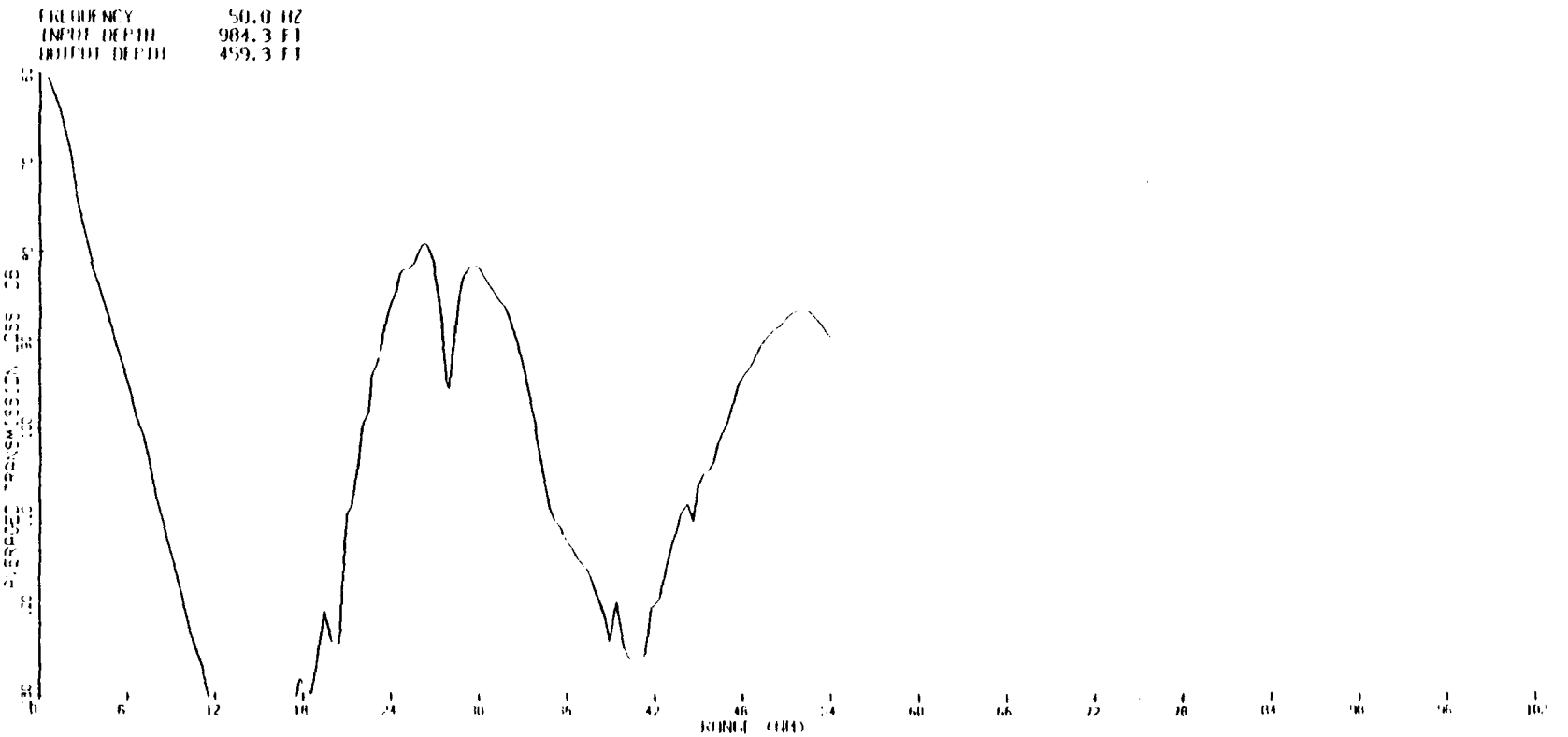

Figure A-43 NORTH WALL/SLOPE Transmission Loss (PE)
Receiver = 300 m, Source = 140 m 50 Hz

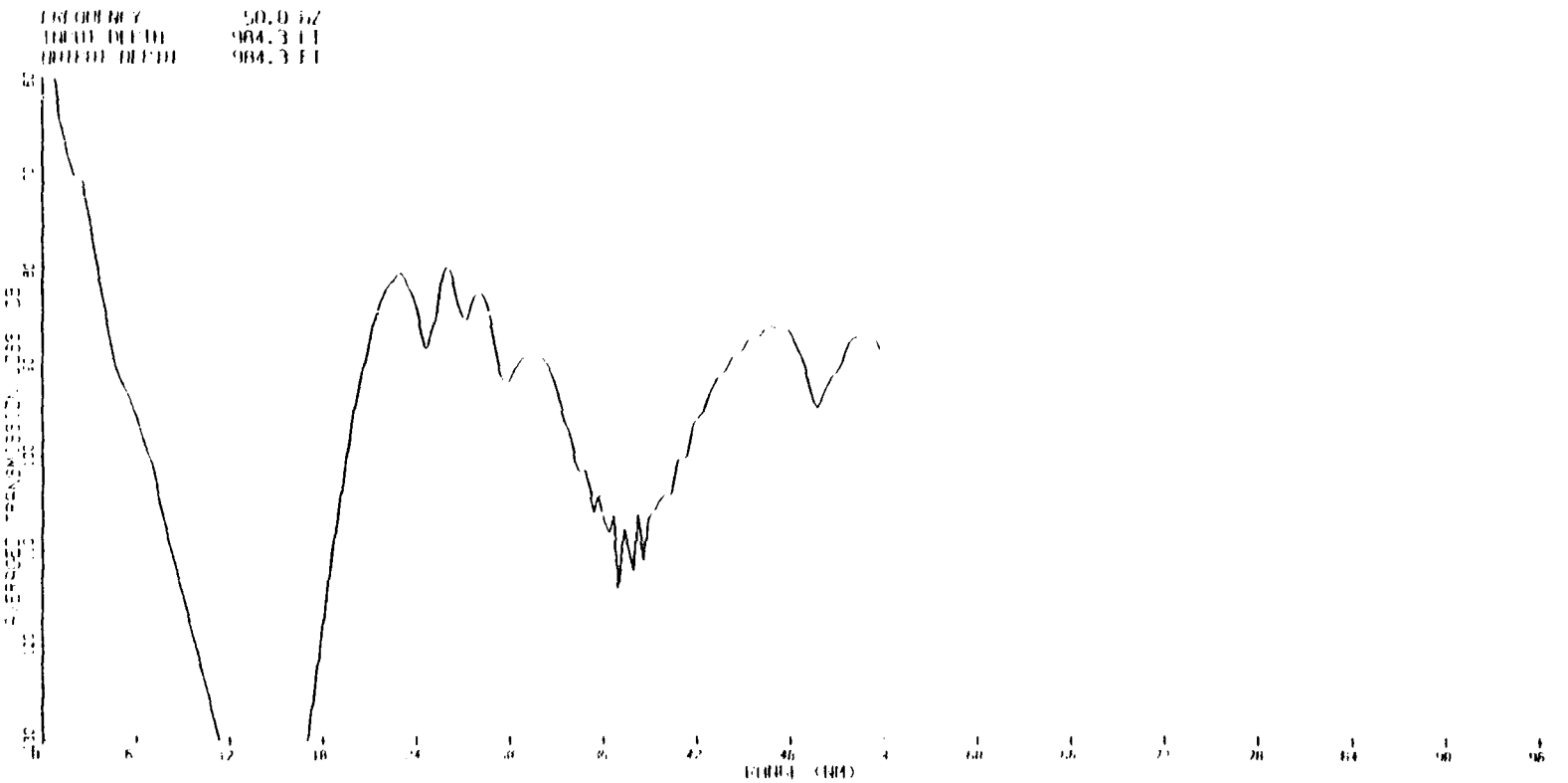

Figure A-44 NORTH WALL/SLOPE Transmission Loss (PE)
Receiver = 300 m, Source = 300 m 50 Hz

AD-A099 406 SCIENCE APPLICATIONS INC MCLEAN VA F/G 20/1
EFFECTS OF THE GULF STREAM ON ACOUSTIC PROPAGATION.(U)
JUL 80 A D'AMICO N00014-79-C-0481
UNCLASSIFIED SAI-81-221-WA NL

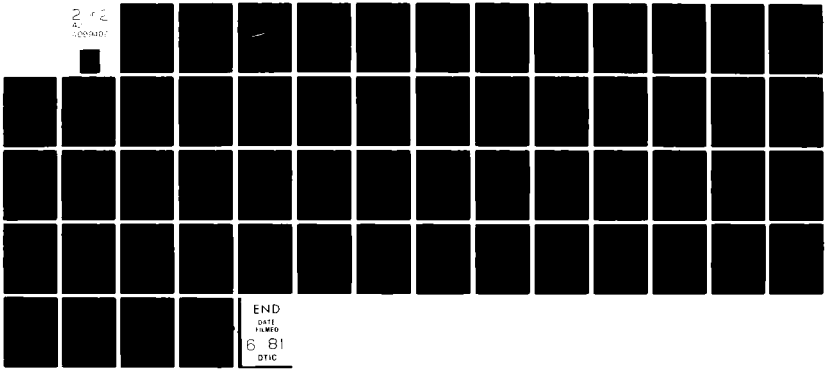

END
DATE FILMED
6 81
DTIC

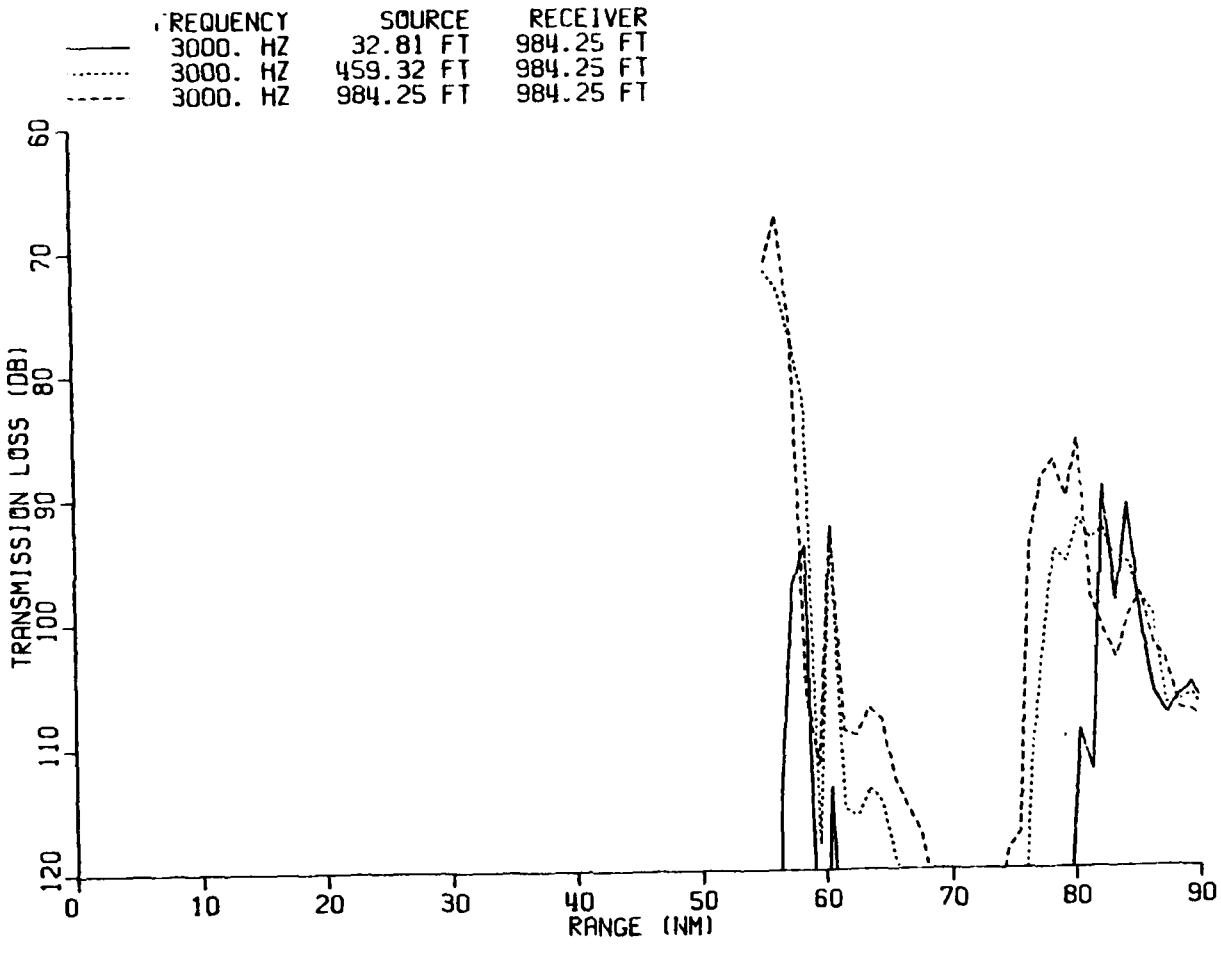

Figure A-45 NORTH WALL/SLOPE Transmission Loss (MPP)
Receiver = 300 m, 3,000 Hz

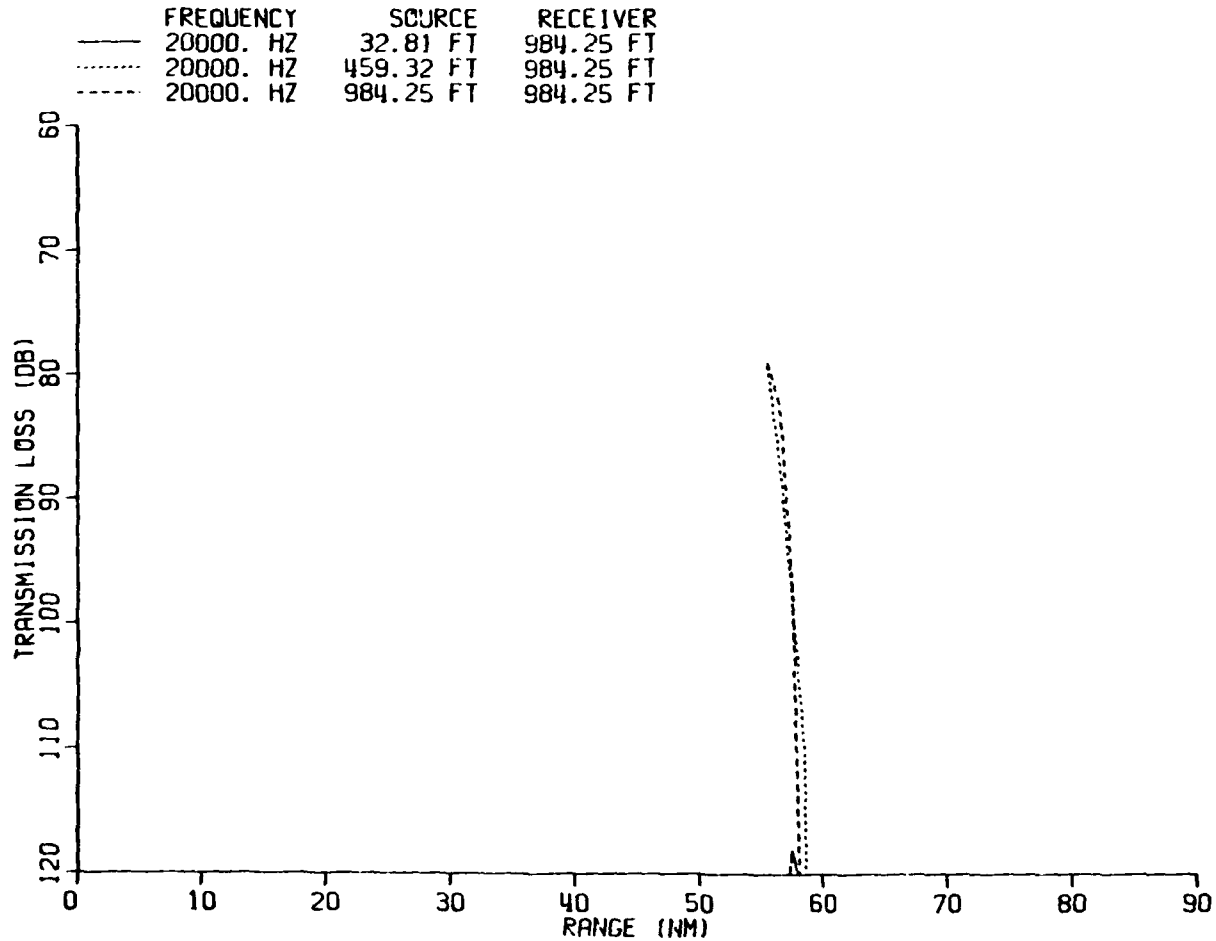

Figure A-46 NORTH WALL/SLOPE Transmission Loss (MPP)
Receiver = 300 m, 20,000 Hz

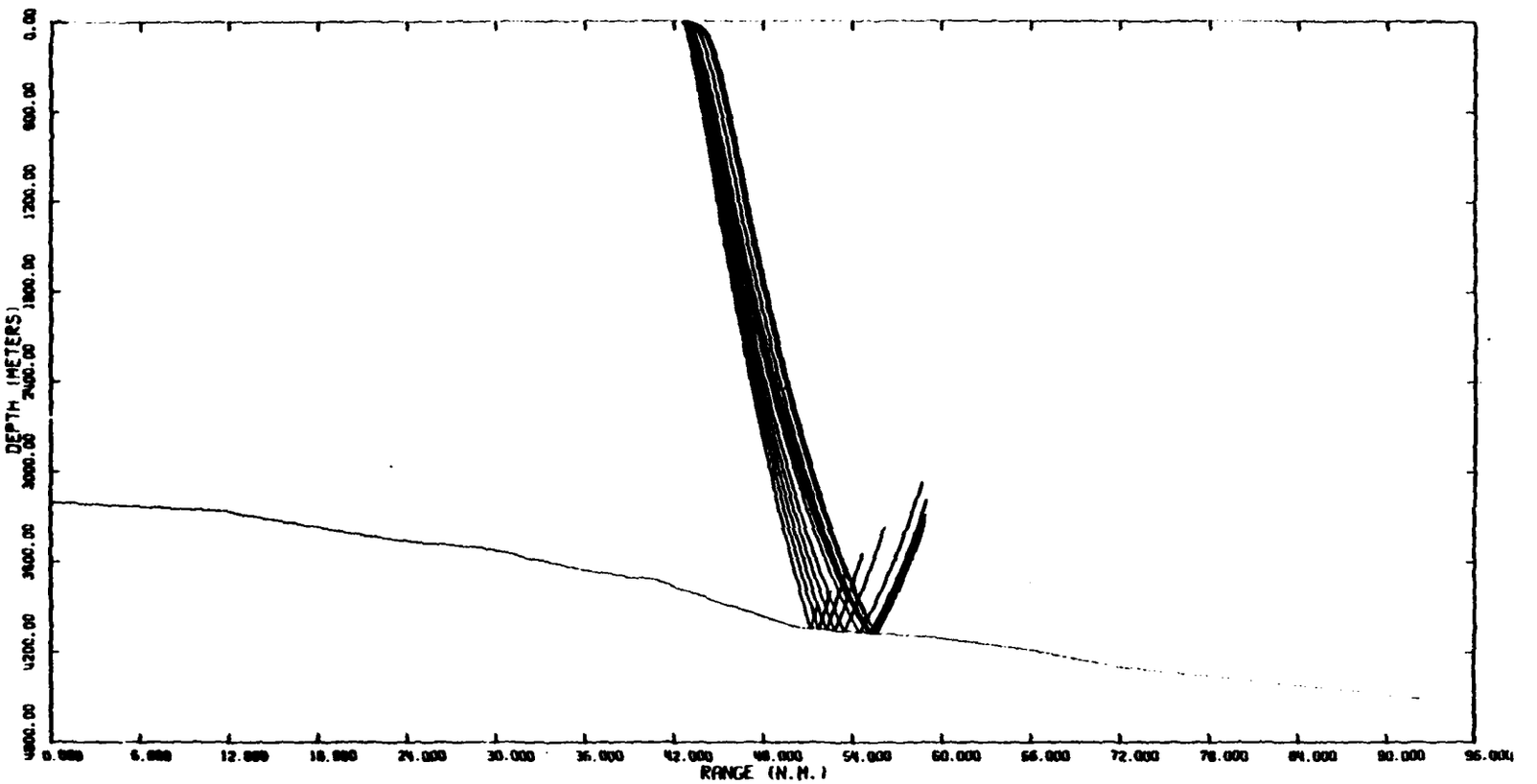

Figure A-47 NORTH WALL/SARGASSO Ray plot
Receiver = 10 m, Source = 140 m
Angles plotted 0^{o}-10^{o}

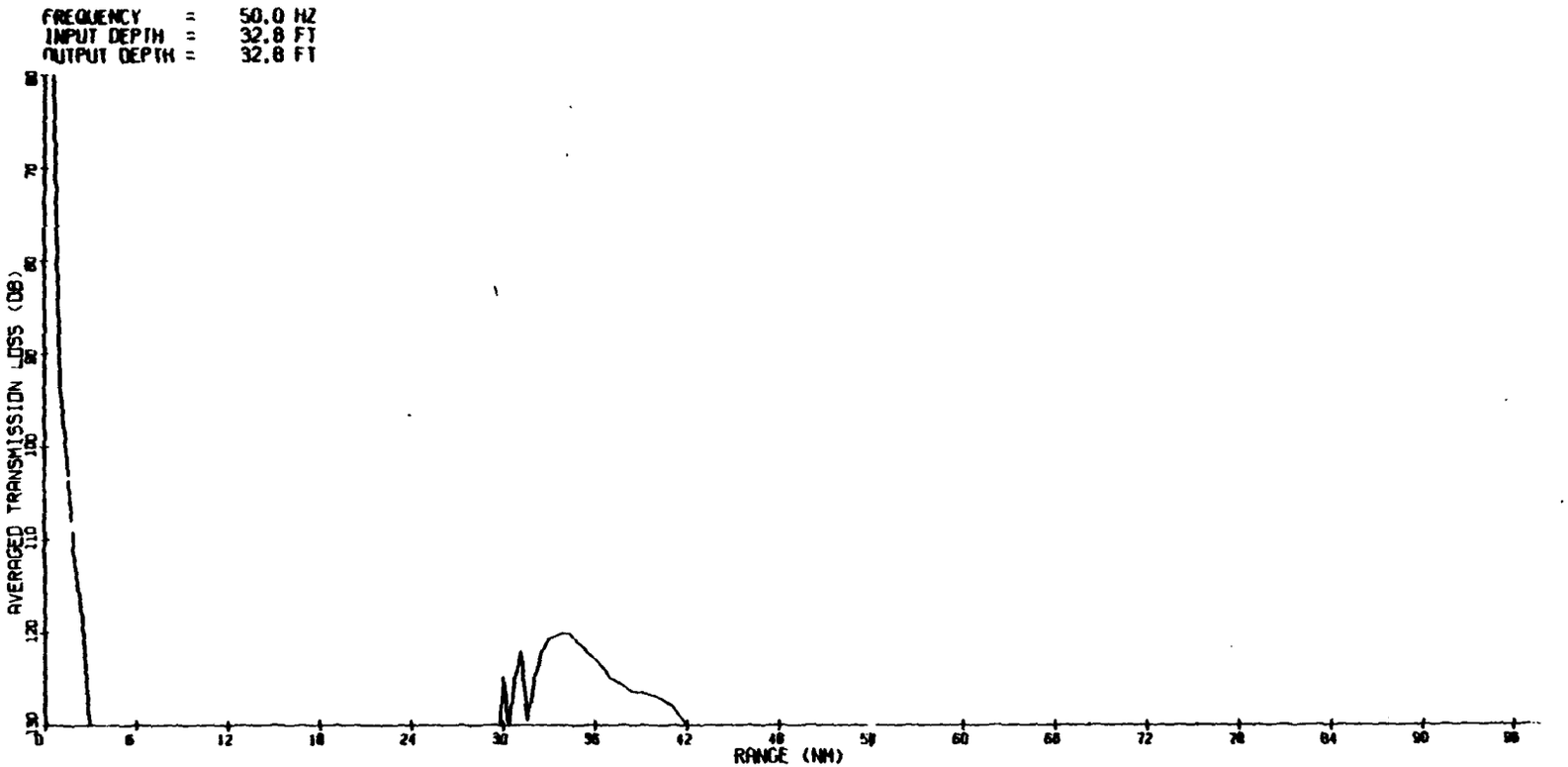

Figure A-48 NORTH WALL/SARGASSO Transmission Loss (PE)
Receiver = 10 m, Source = 10 m 50 Hz

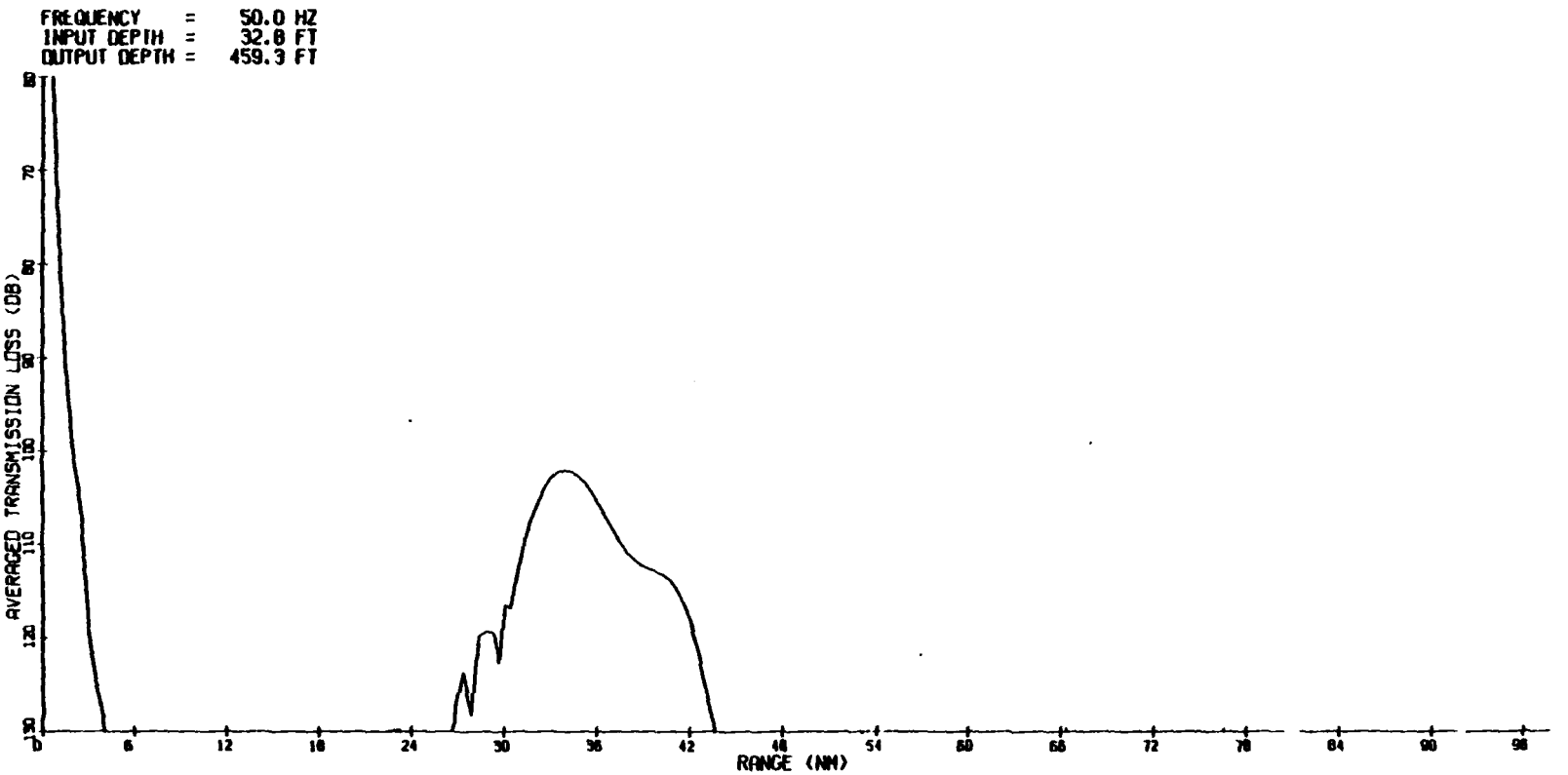

Figure A-49 NORTH WALL/SARGASSO Transmission Loss (PE)
Receiver = 10 m, Source = 140 m 50 Hz

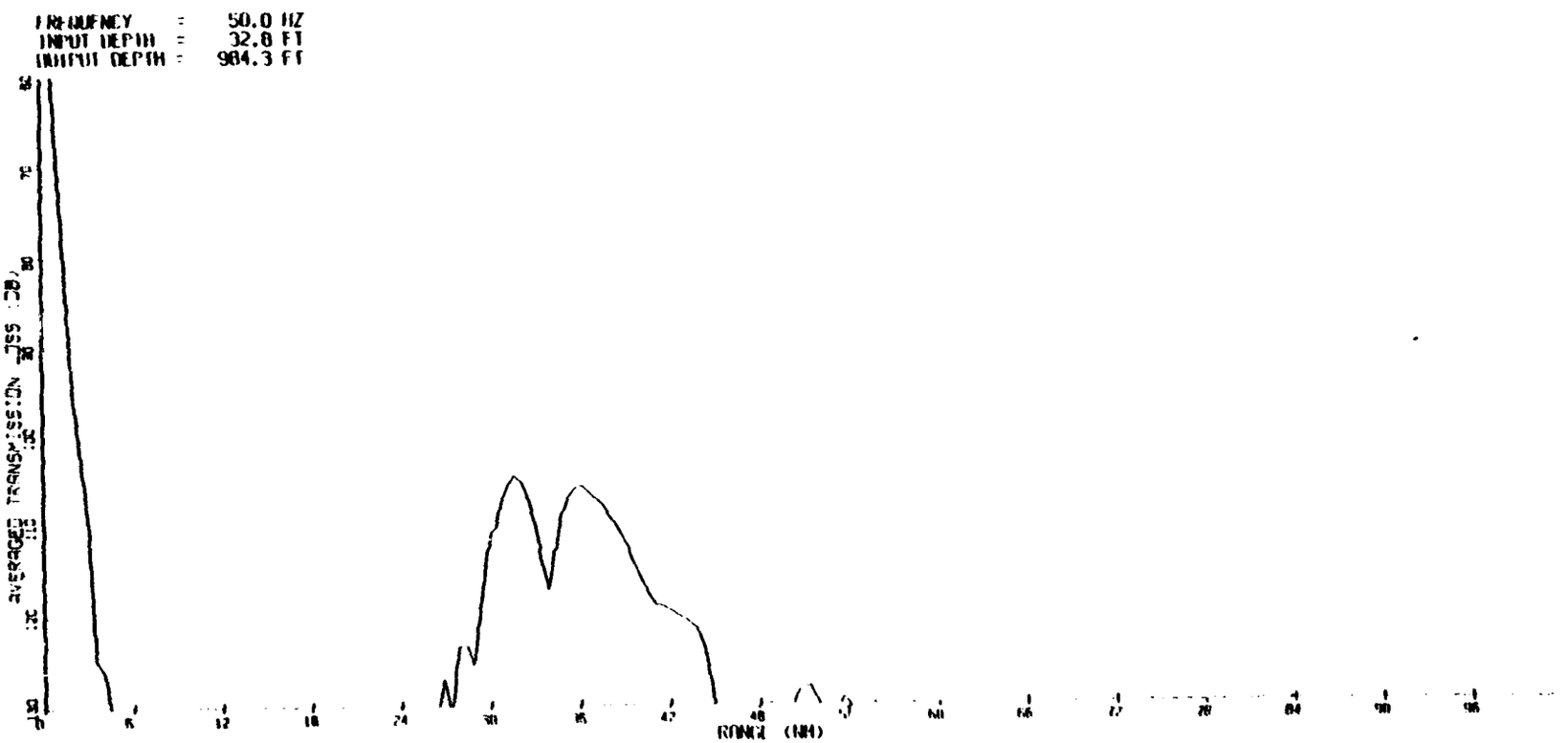

Figure A-50 NORTH WALL/SARGASSO Transmission Loss (PE)
Receiver = 10 m, Source = 300 m 50 Hz

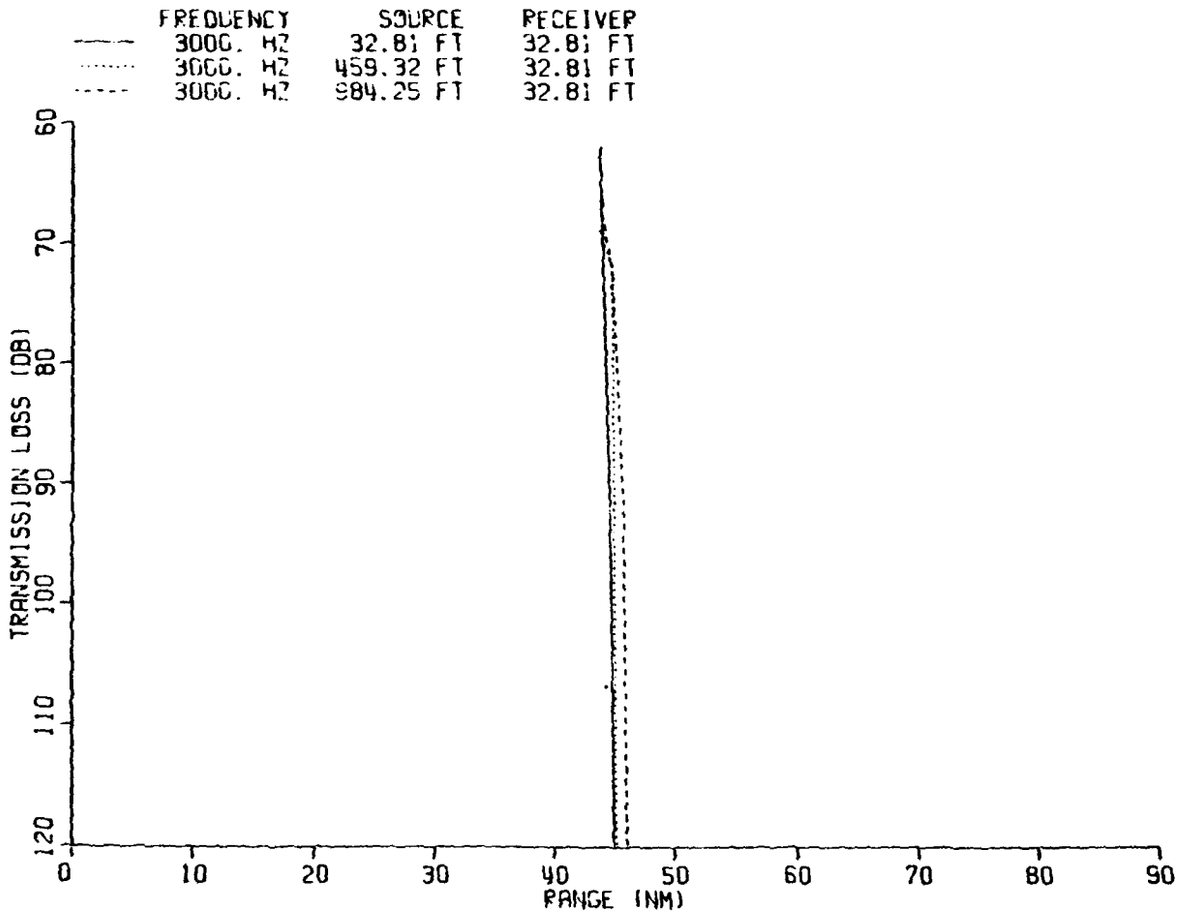

Figure A-51 NORTH WALL/SARGASSO Transmission Loss (MPP)
Receiver = 10 m, 3,000 Hz

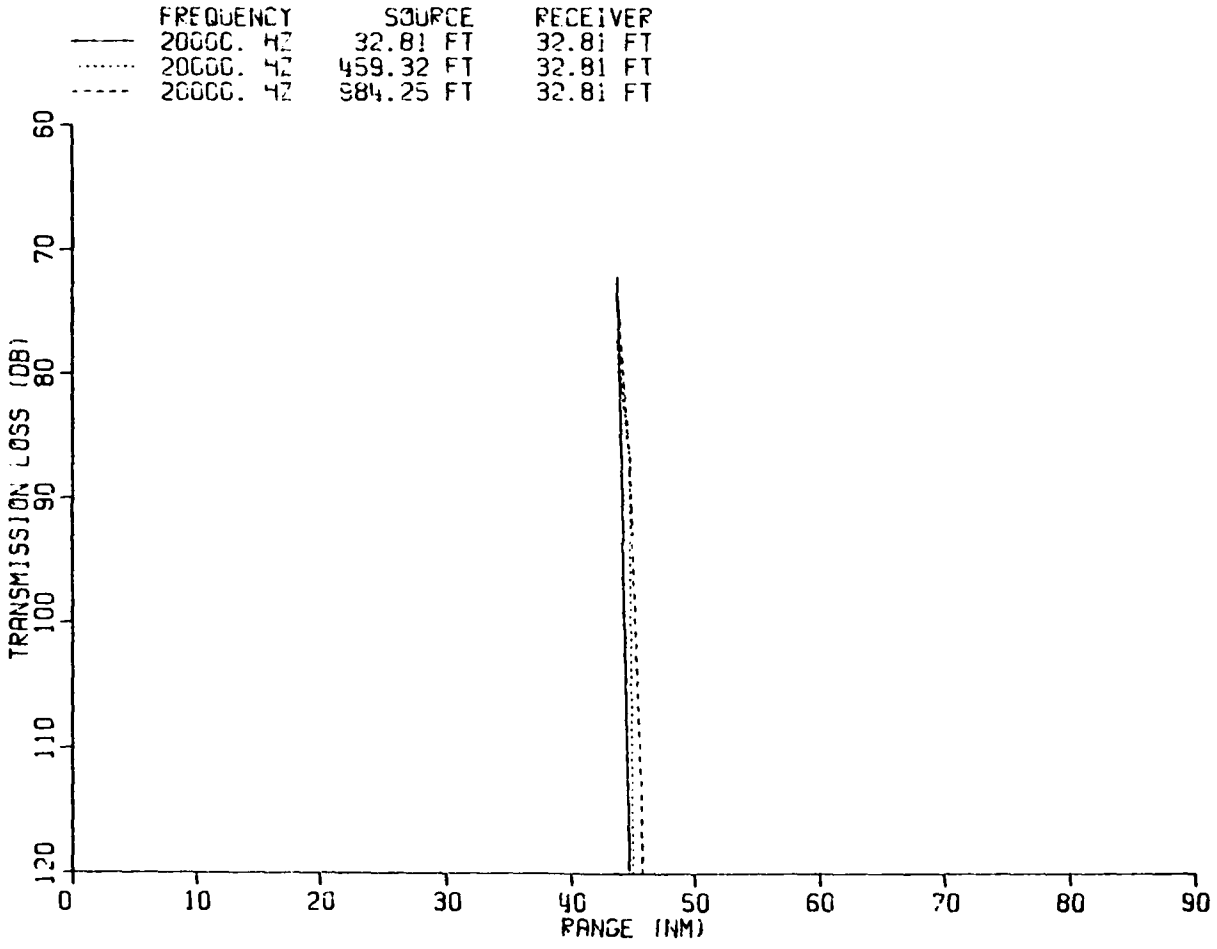

Figure A-52 NORTH WALL/SARGASSO Transmission Loss (MPP)
Receiver = 10 m, 20,000 Hz

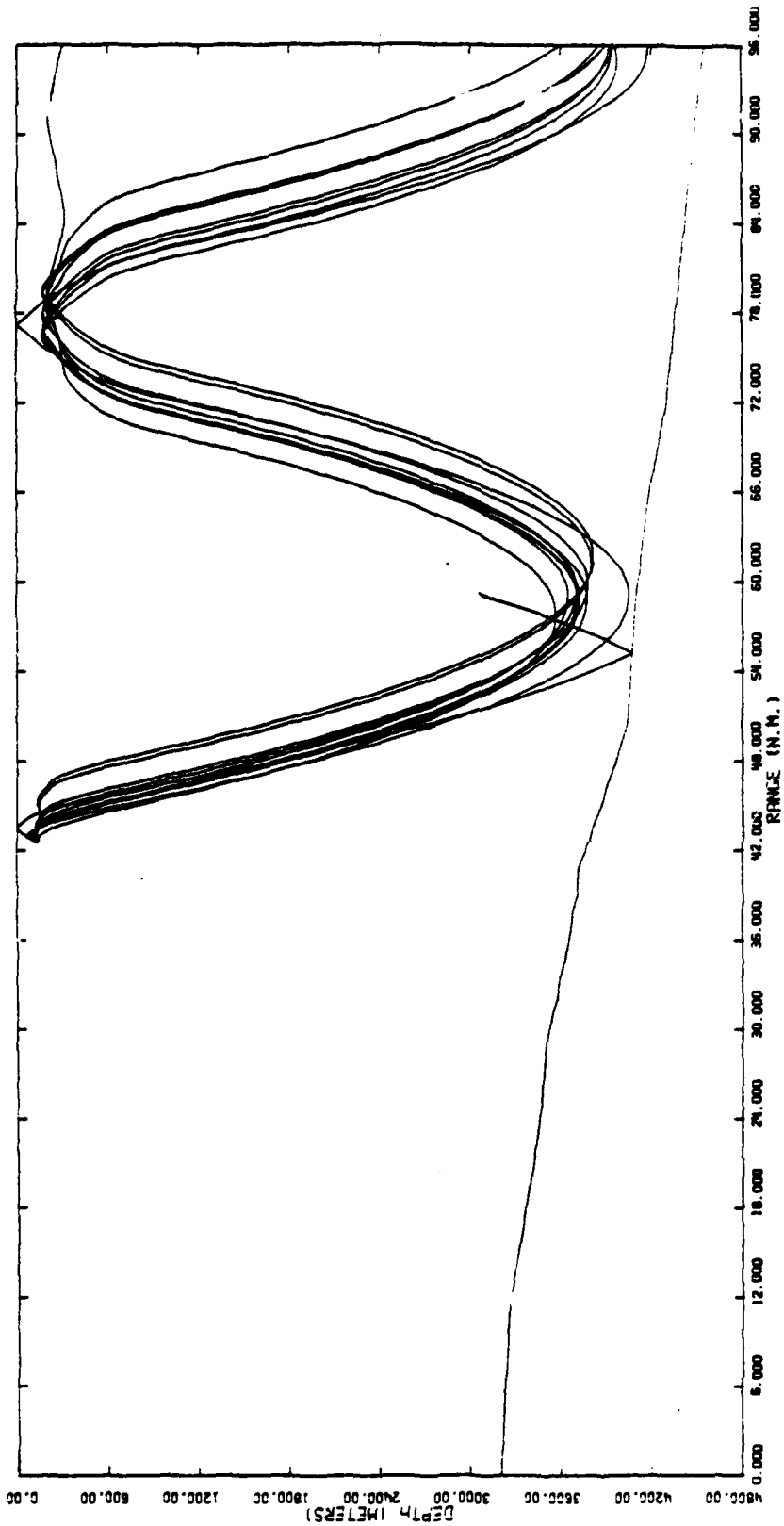

Figure A-53 NORTH WALL/SARGASSO Ray plot
Receiver = 140 m, Source = 140 m
Angles plotted 0^{o}-10^{o}

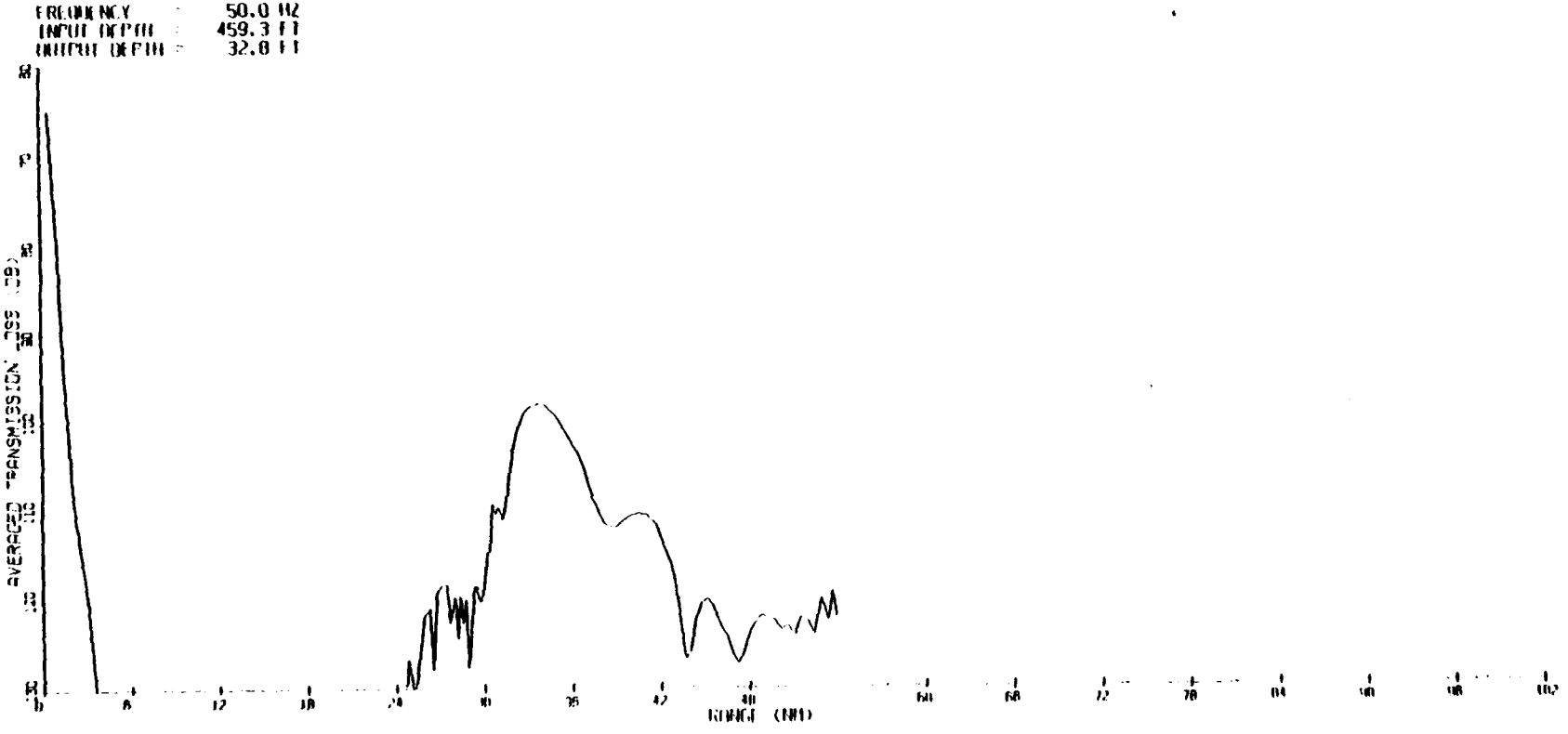

Figure A-54 NORTH WALL/SARGASSO Transmission Loss (PE)
Receiver = 140 m, Source = 10 m

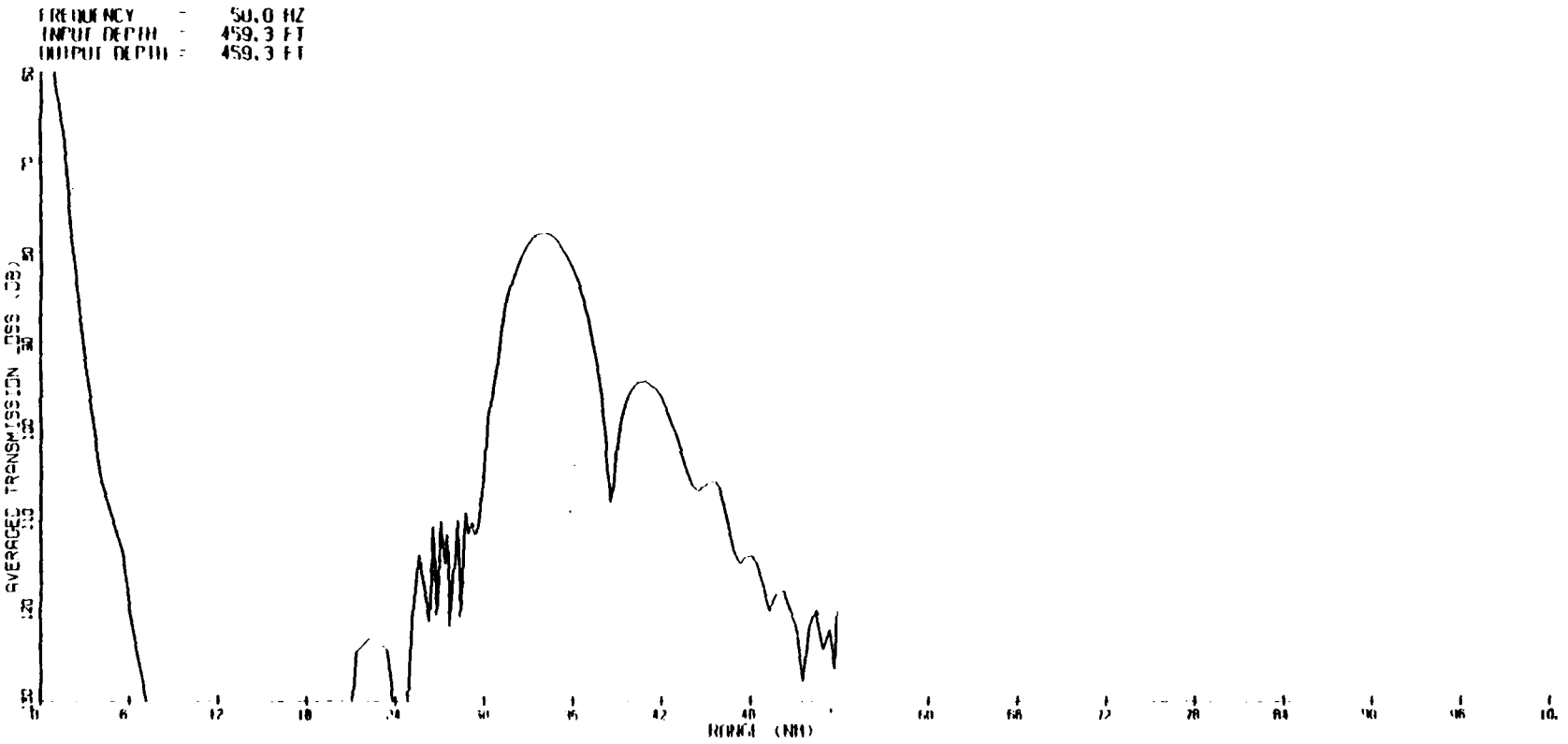

Figure A-55 NORTH WALL/SARGASSO Transmission Loss (PE)
Receiver = 140 m, Source = 140 m

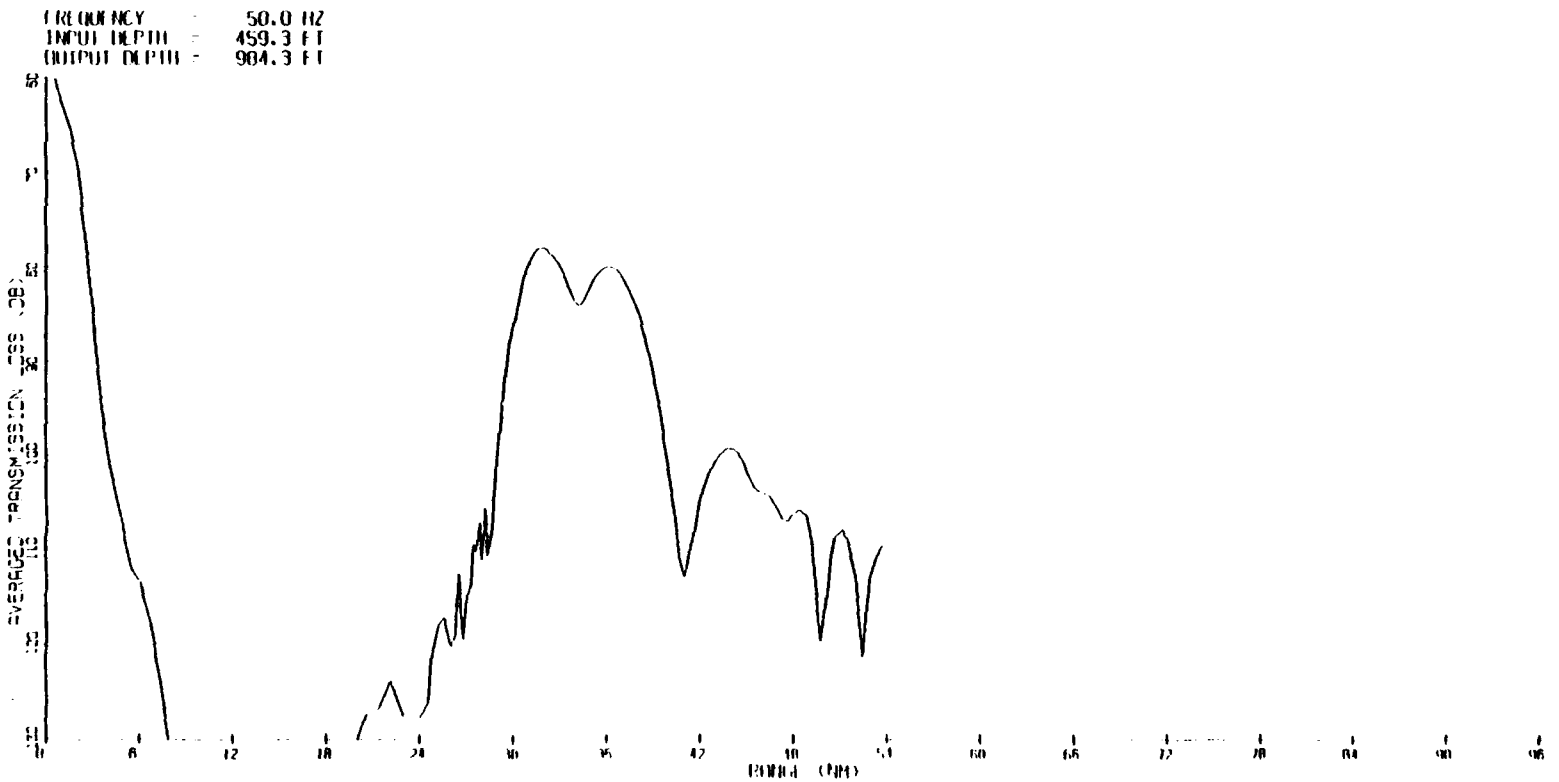

Figure A-56 NORTH WALL/SARGASSO Transmission Loss (PE)
Receiver = 140 m, Source = 300 m

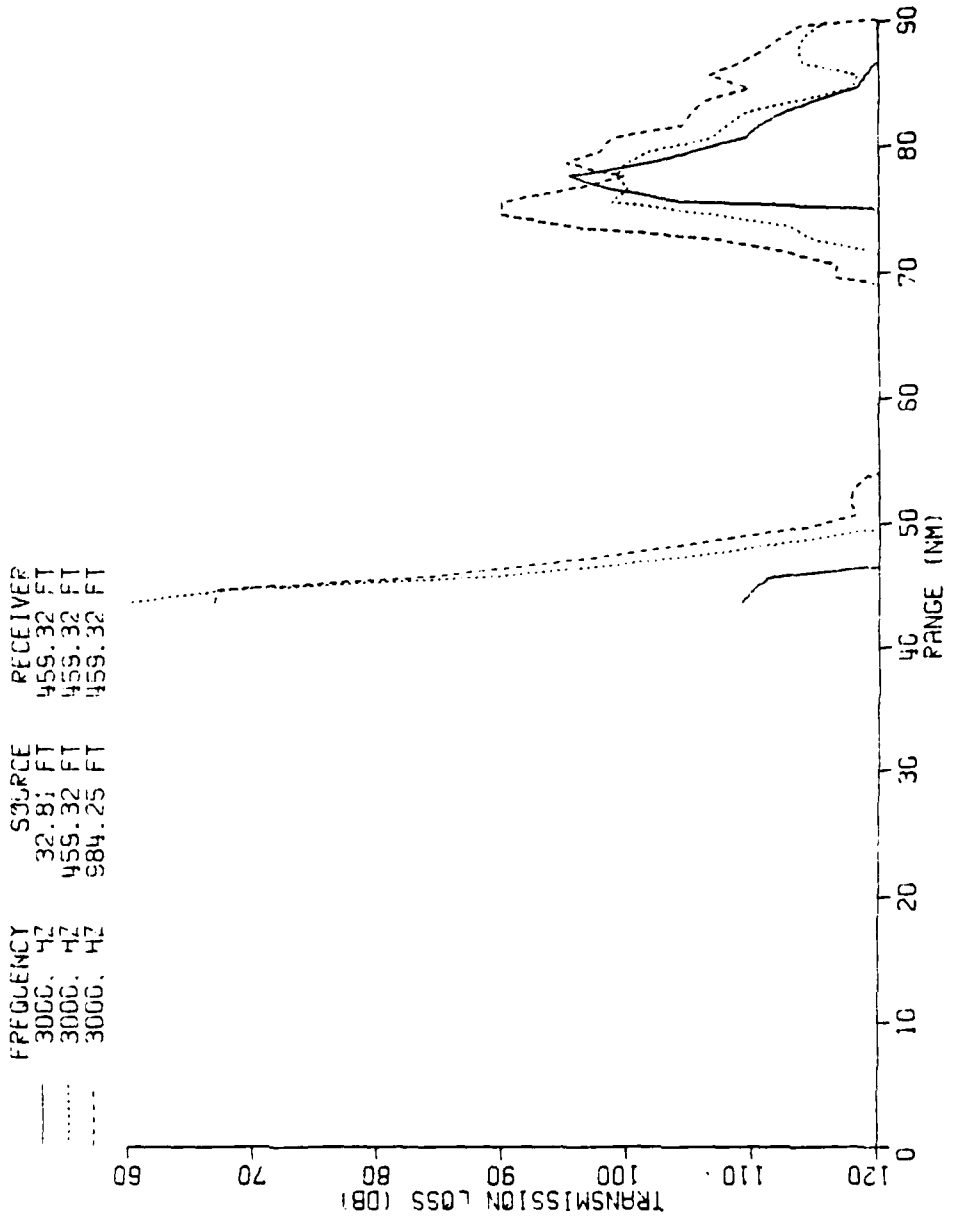

Figure A-57 NORTH WALL/SARGASSO Transmission Loss (MPP)
Receiver = 140 m, 3,000 Hz

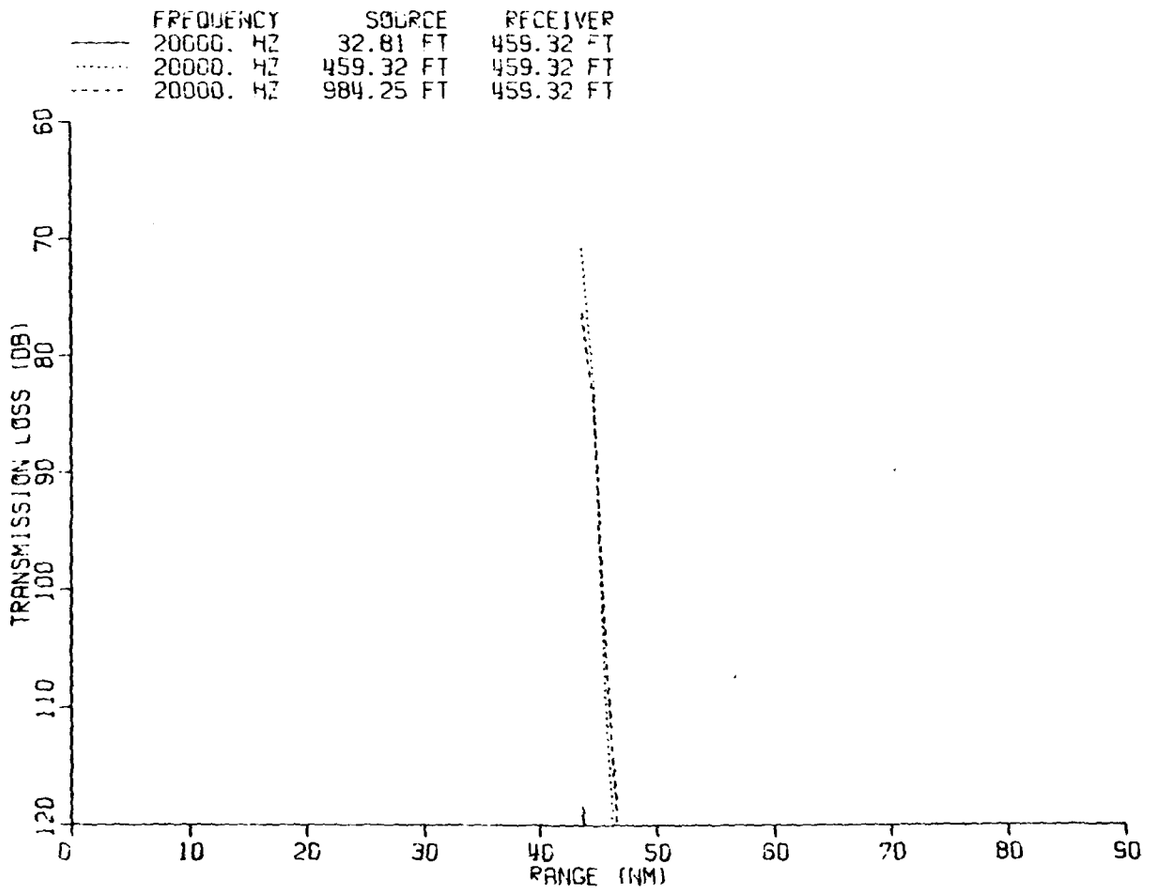

Figure A-58 NORTH WALL/SARGASSO Transmission Loss (MPP)
Receiver = 140 m, 20,000 Hz

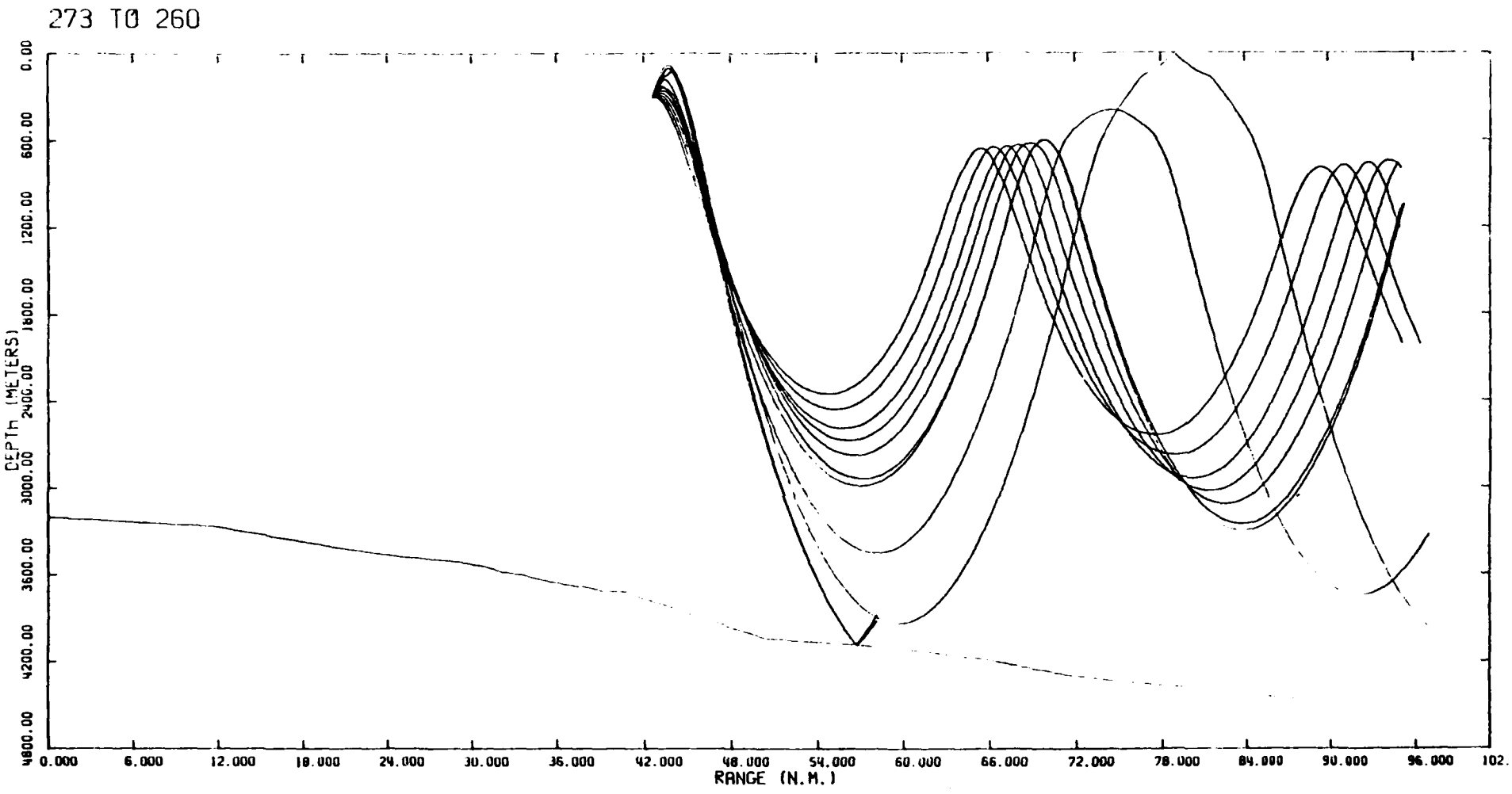

Figure A-59 NORTH WALL/SARGASSO Ray plot
Receiver = 300 m, Source = 140 m
Angles plotted 0^{o}-10^{o}

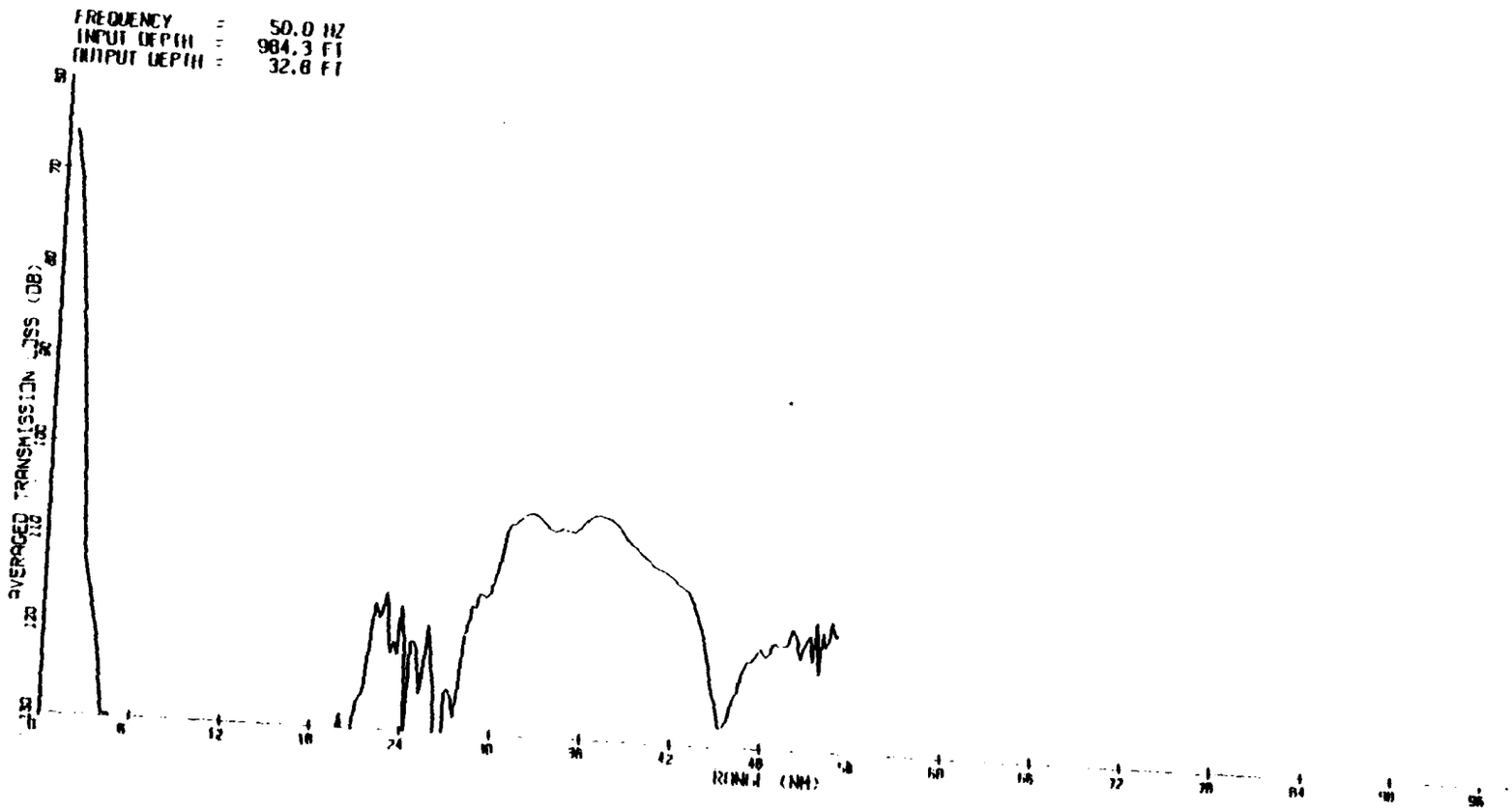

Figure A-60 NORTH WALL/SARGASSO Transmission Loss (PE)
Receiver = 300 m, Source = 10 m 50 Hz

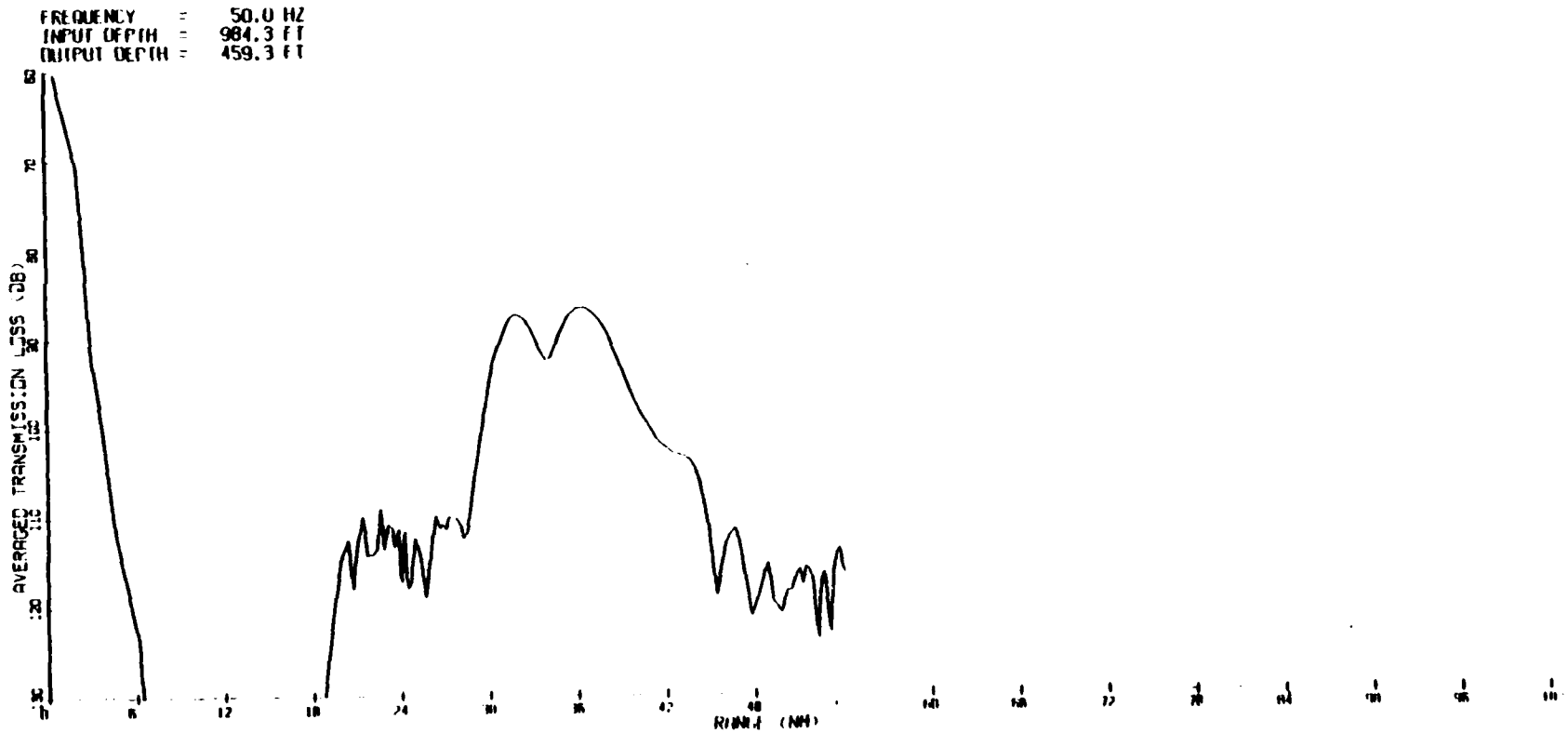

Figure A-61 NORTH WALL/SARGASSO Transmission Loss (PE)
Receiver = 300 m, Source = 140 m 50 Hz

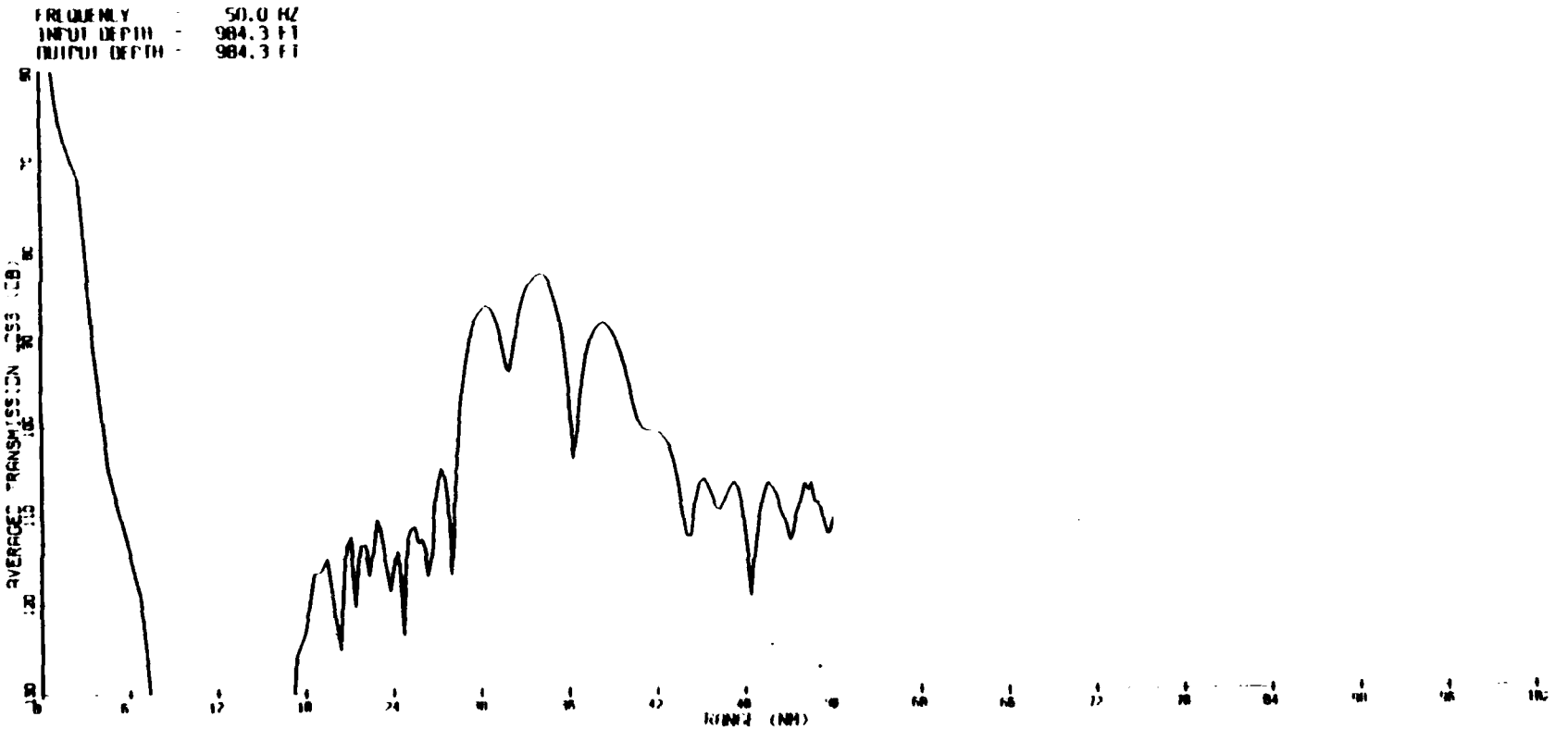

Figure A-62 NORTH WALL/SARGASSO Transmission Loss (PE)
Receiver = 300 m, Source = 300 m 50 Hz

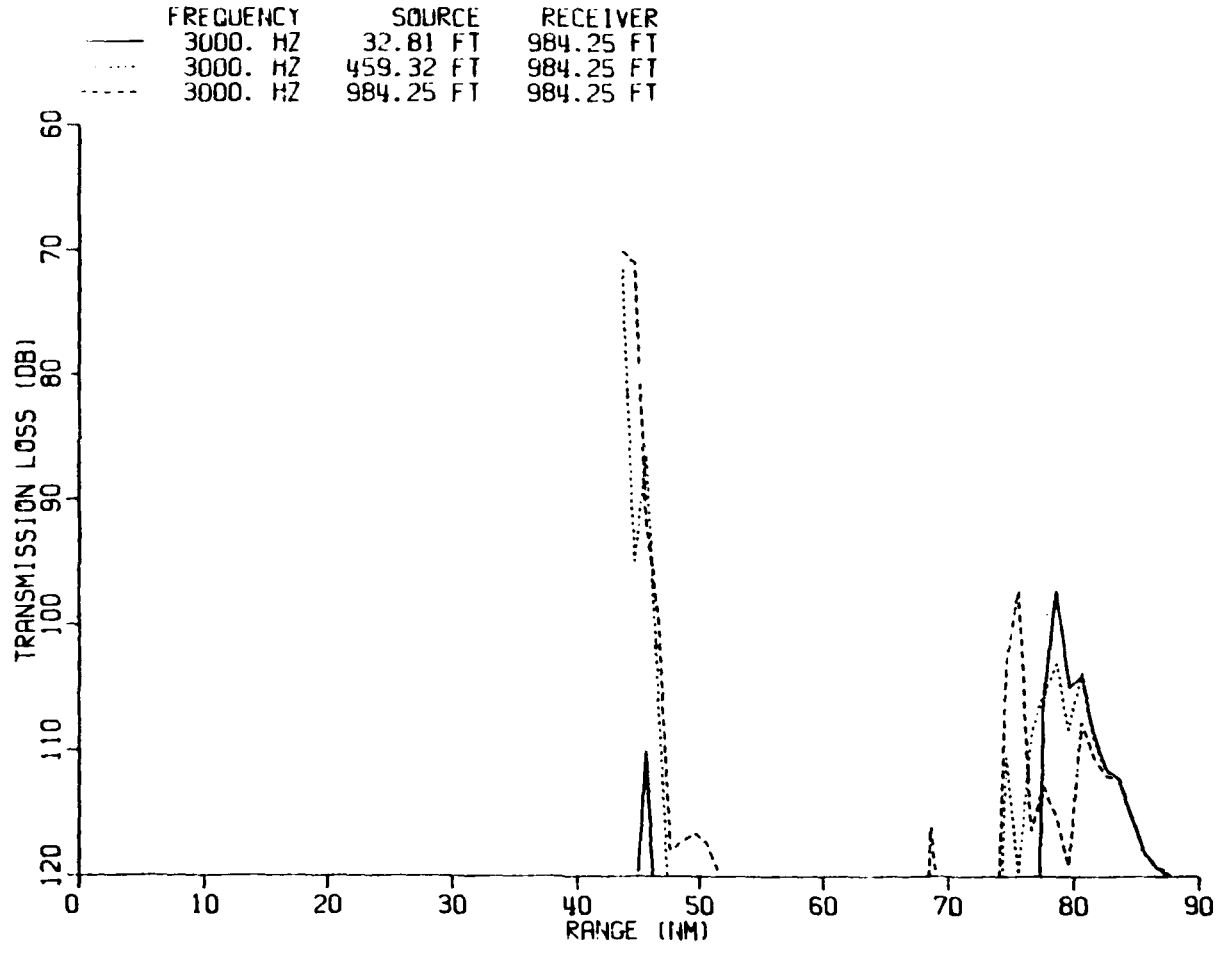

Figure A-63 NORTH WALL/SARGASSO Transmission Loss (MPP)
Receiver = 300 m, 3,000 Hz

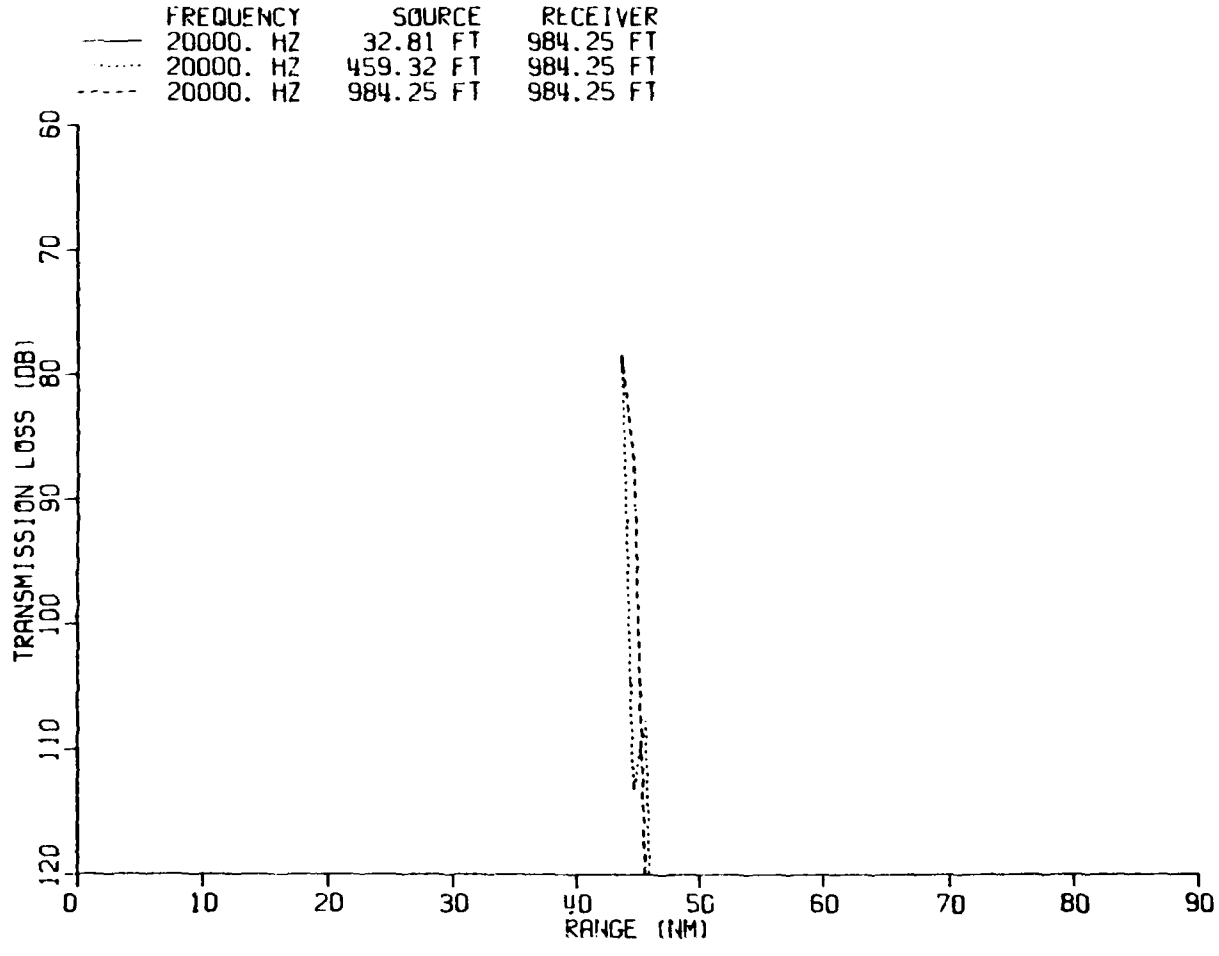

Figure A-64 NORTH WALL/SARGASSO Transmission Loss (MPP)
Receiver = 300 m, 20,000 Hz

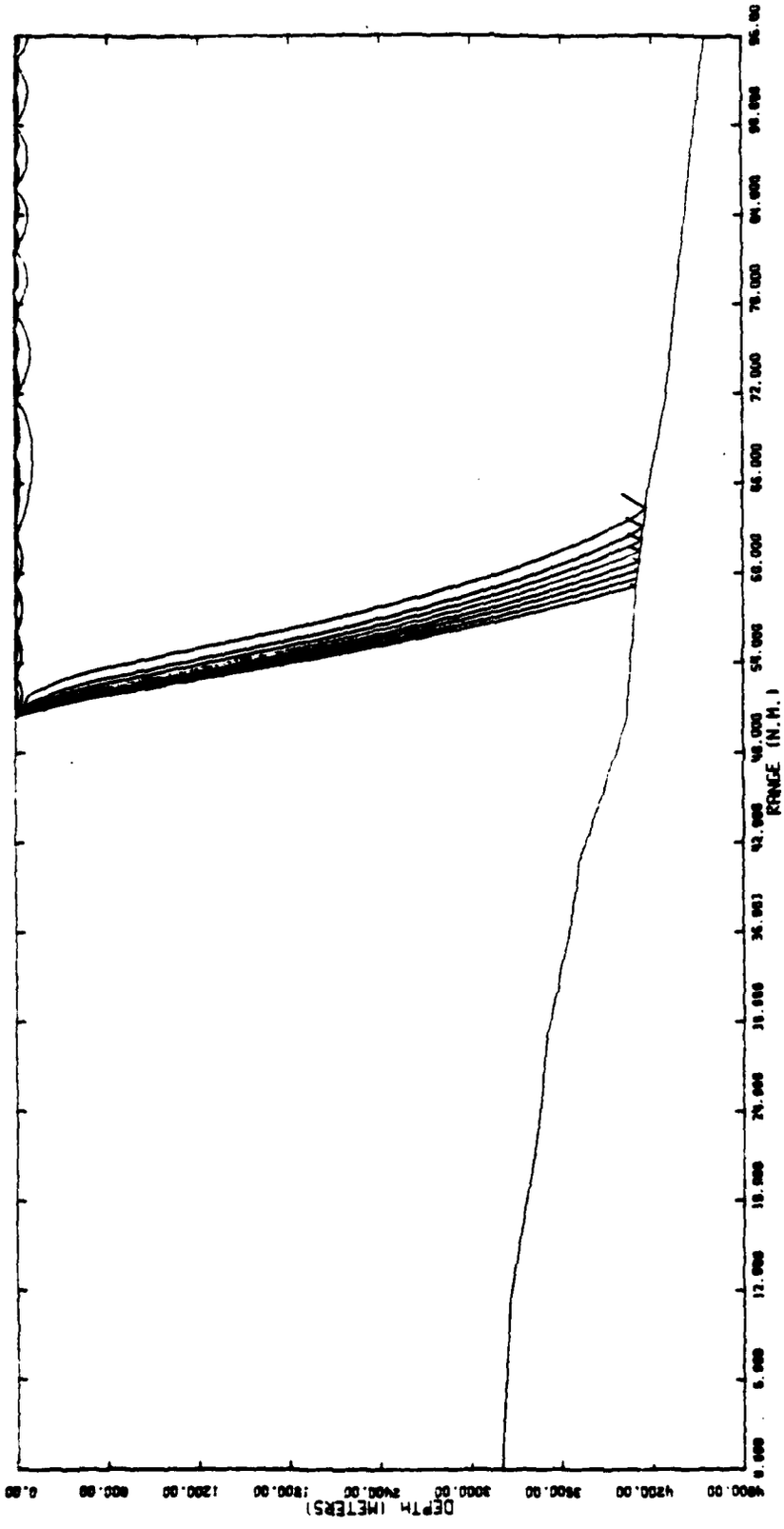

Figure A-65 WARM CORE/SARGASSO Ray plot
Receiver = 10 m, Source = 10 m
Angles plotted 0°-10°

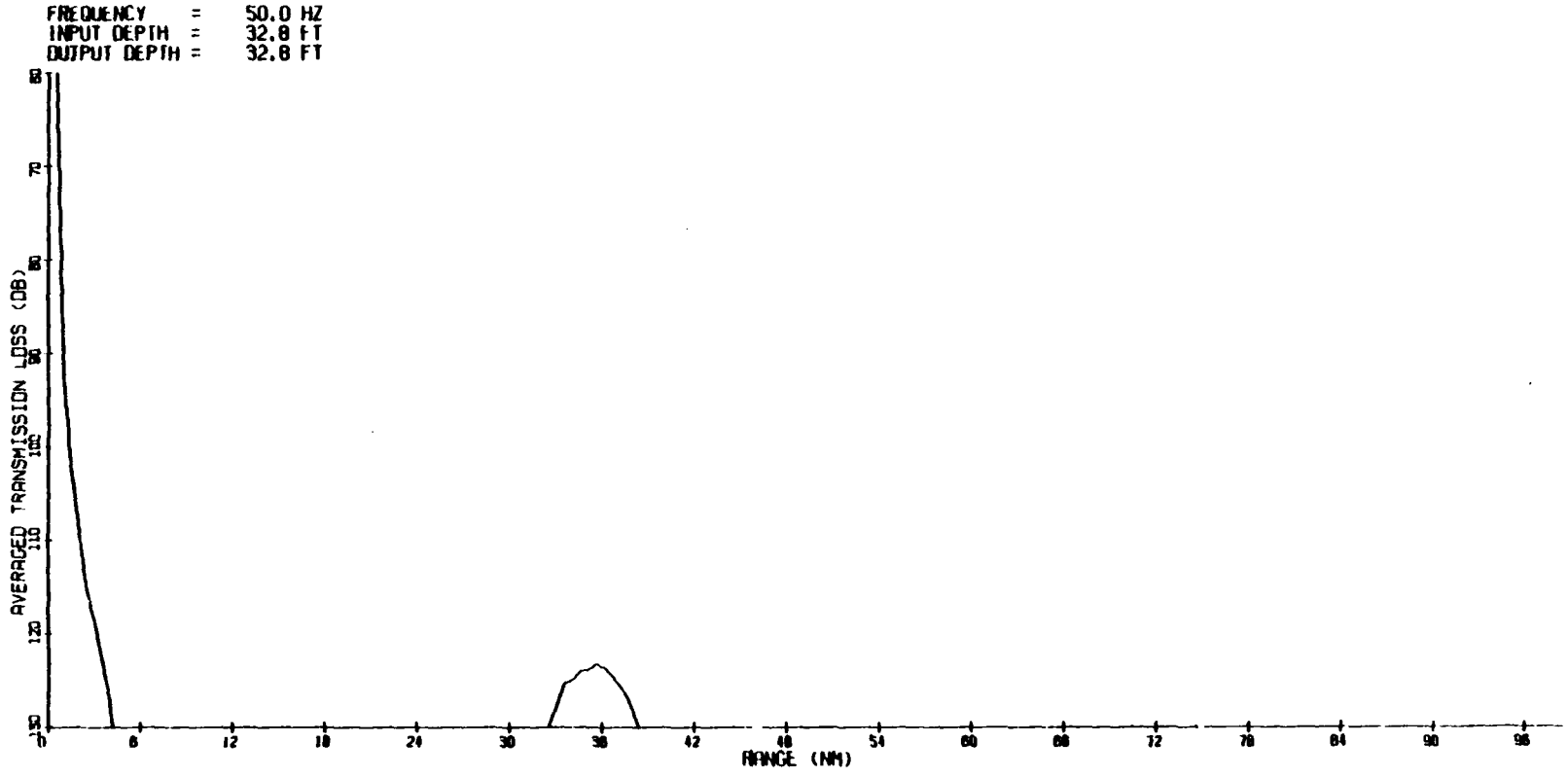

Figure A-66 WARM CORE/SARGASSO Transmission Loss (PE)
Receiver = 10 m, Source = 10 m 50 Hz

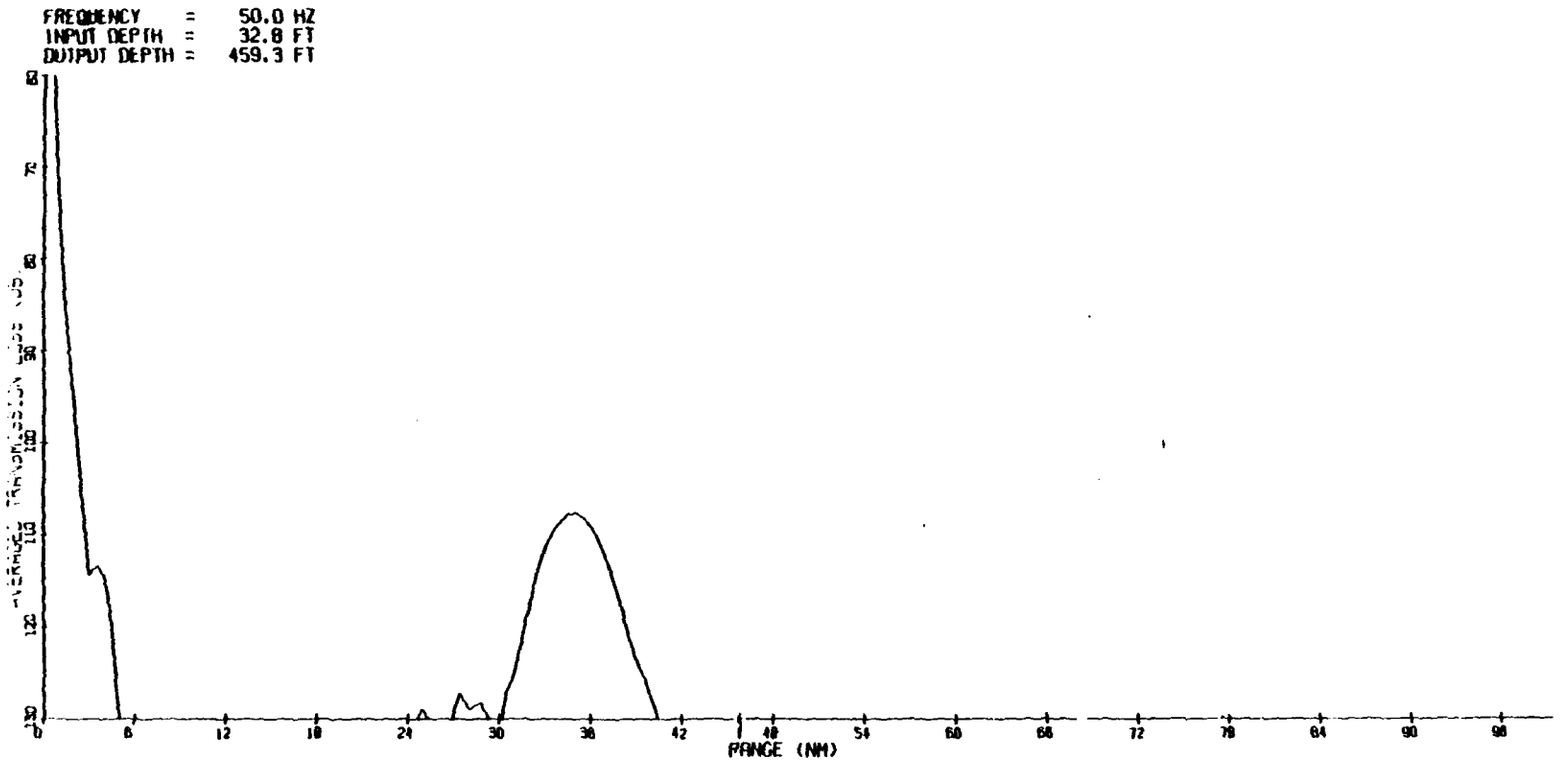

Figure A-67 WARM CORE/SARGASSO Transmission Loss (PE)
Receiver = 10 m, Source = 140 m 50 Hz

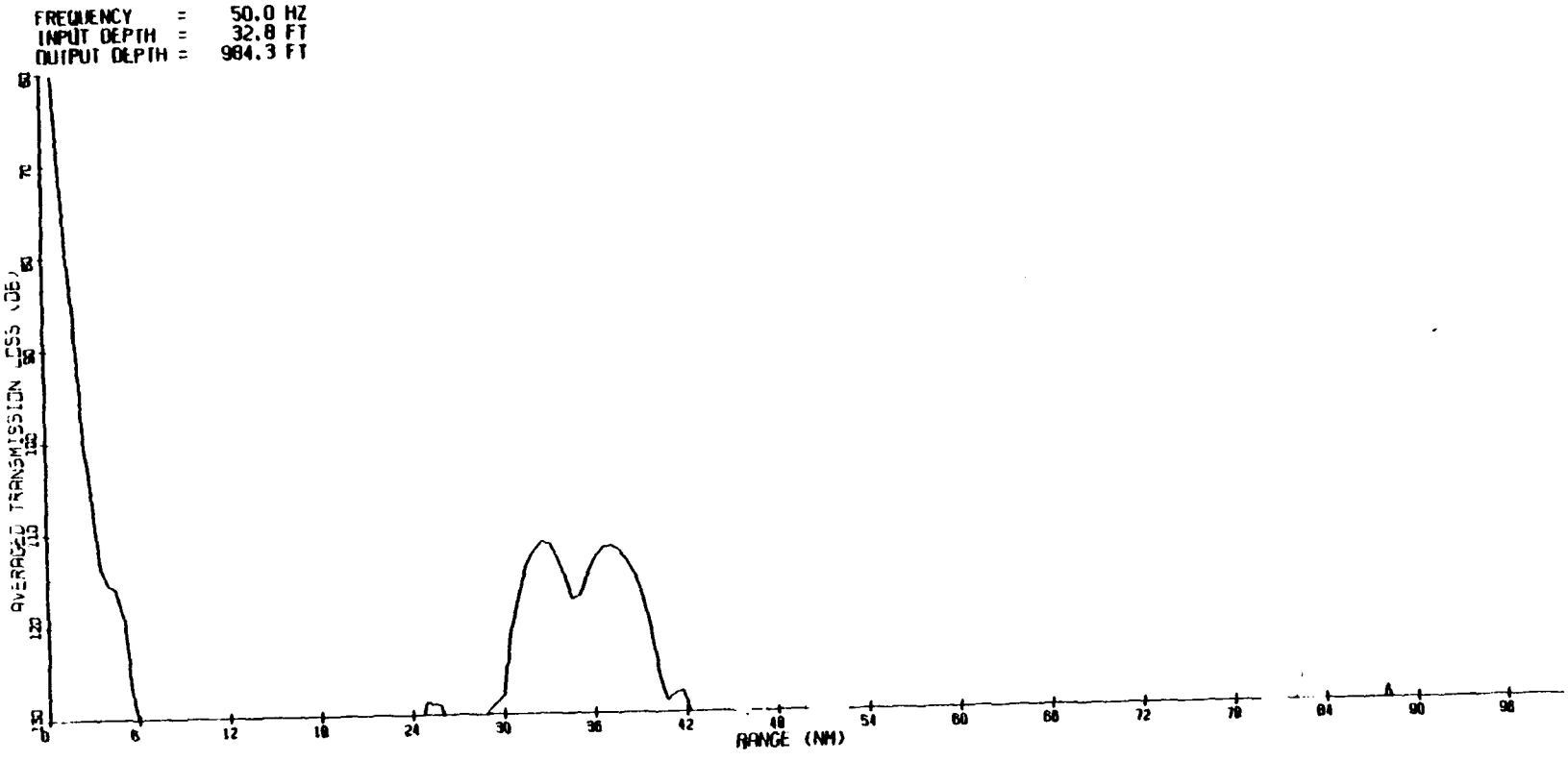

Figure A-68 WARM CORE/SARGASSO Transmission Loss (PE)
Receiver = 10 m, Source = 300 m 50 Hz

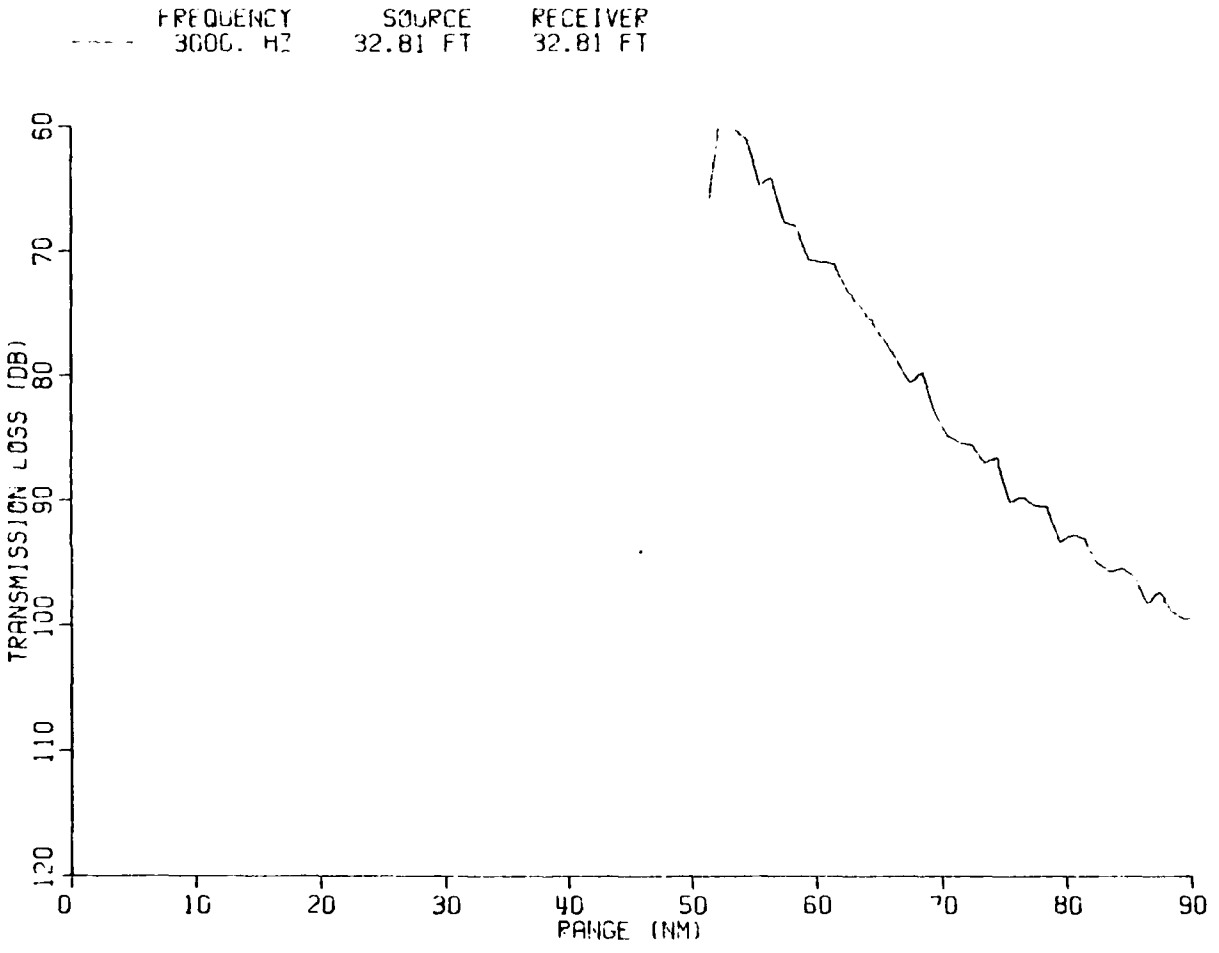

Figure A-69 WARM CORE/SARGASSO Transmission Loss (MPP)
Receiver = 10 m, 3,000 Hz

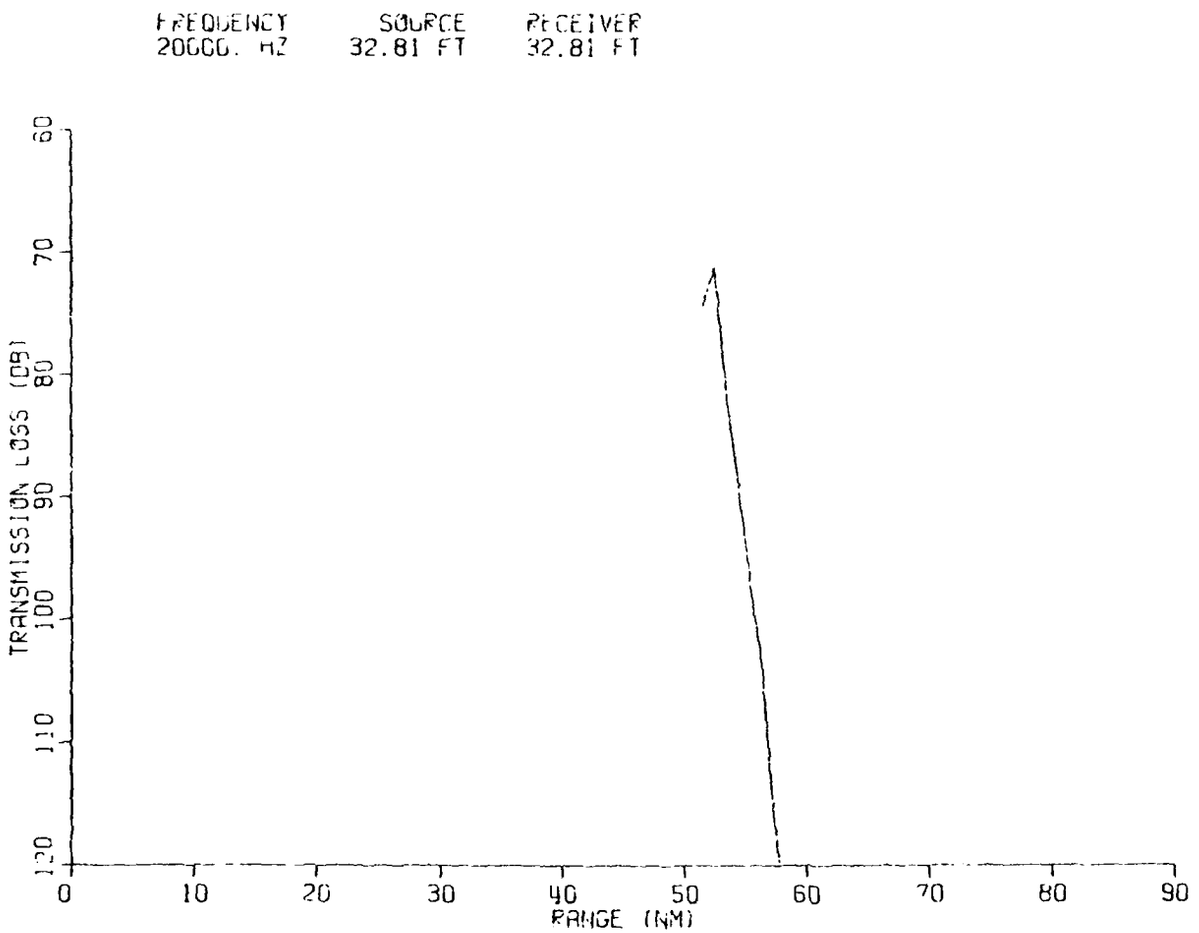

Figure A-70 WARM CORE/SARGASSO Transmission Loss (MPP)
Receiver = 10 m, 20,000 Hz

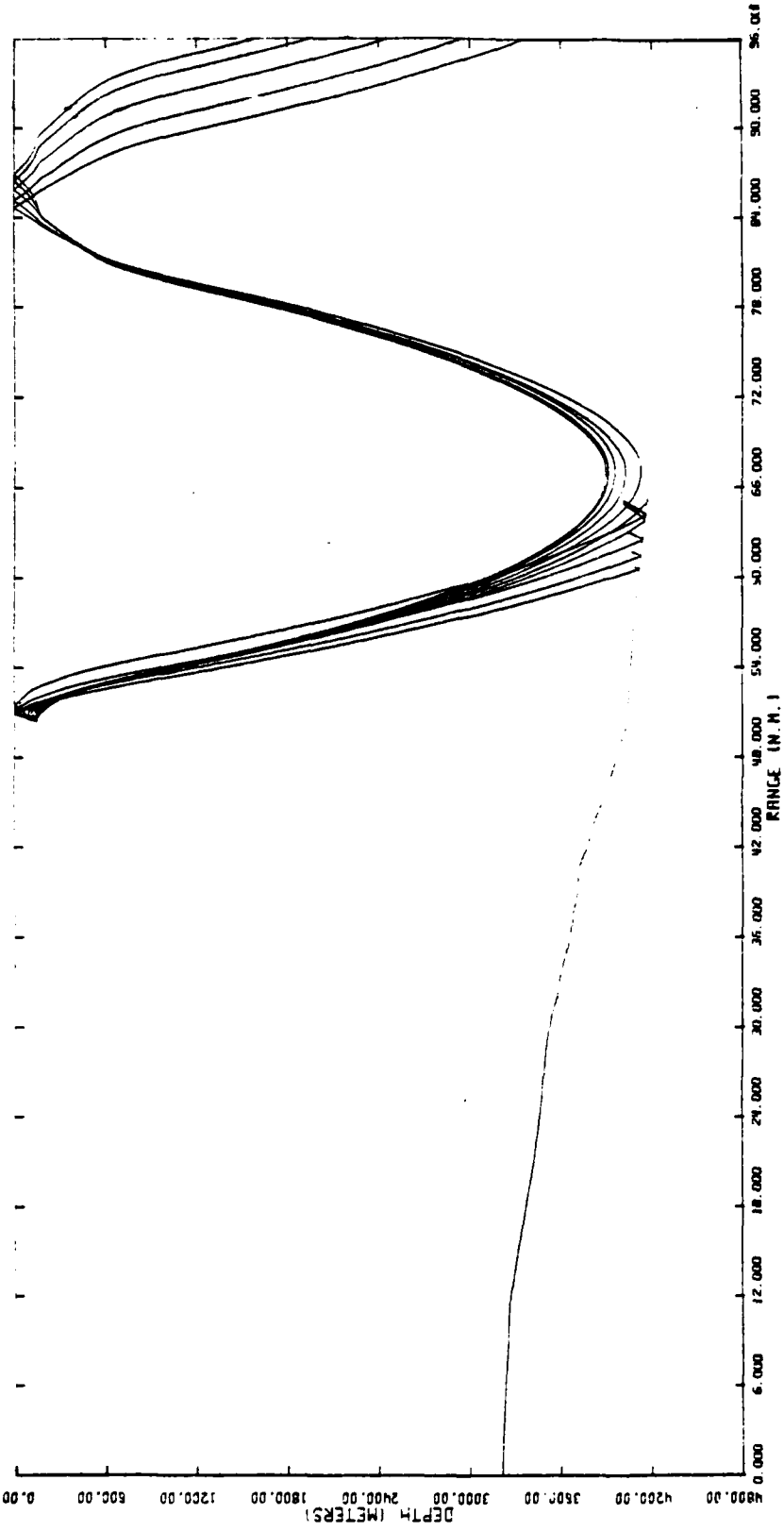

Figure A-71 WARM CORE/SARGASSO Ray plot
Receiver = 140 m, Source = 140 m
Angles plotted 0^{o}-10^{o}

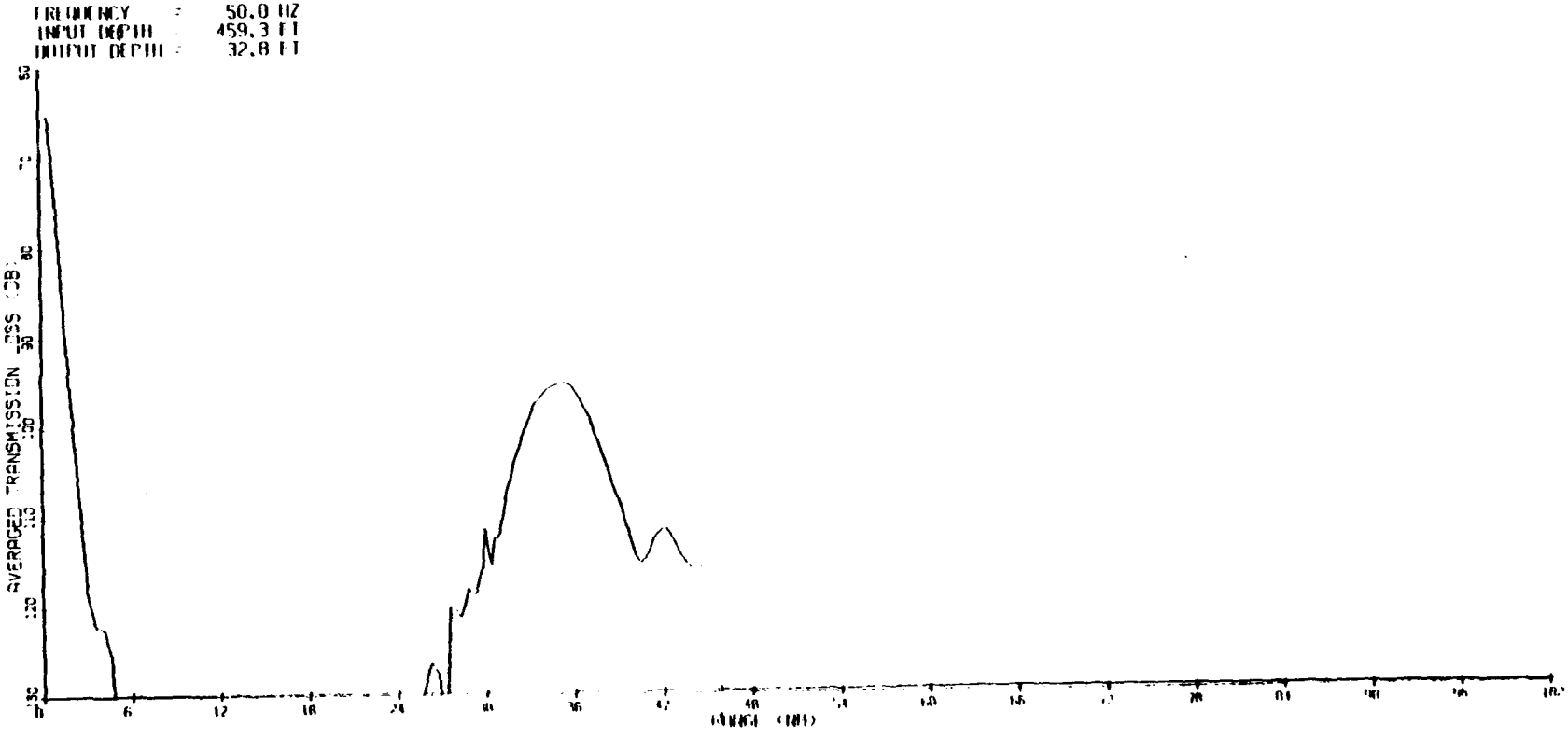

Figure A-72 WARM CORE/SARGASSO Transmission Loss (PE)
Receiver = 140 m, Source = 10 m 50 Hz

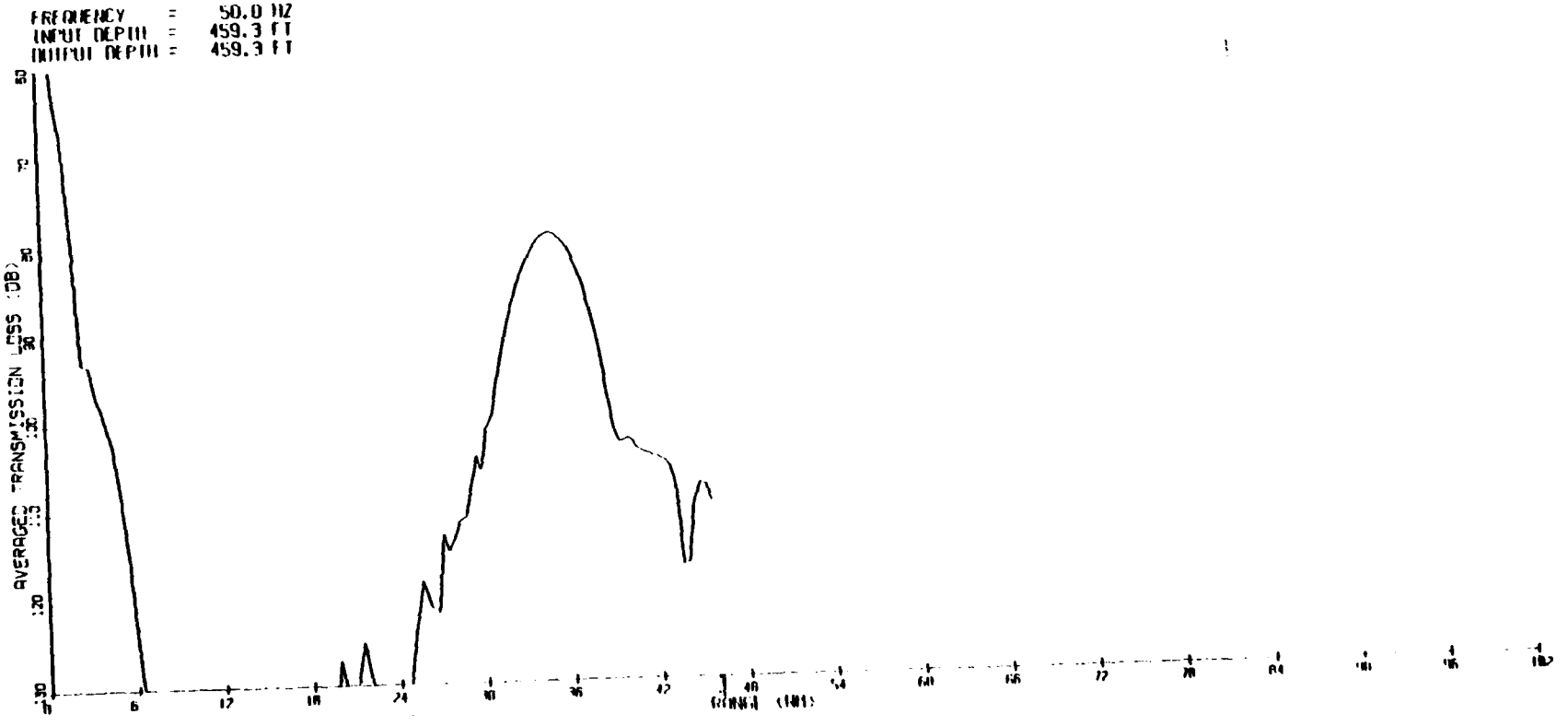

Figure A-73 WARM CORE/SARGASSO Transmission Loss (PE)
Receiver = 140 m, Source = 140 m 50 Hz

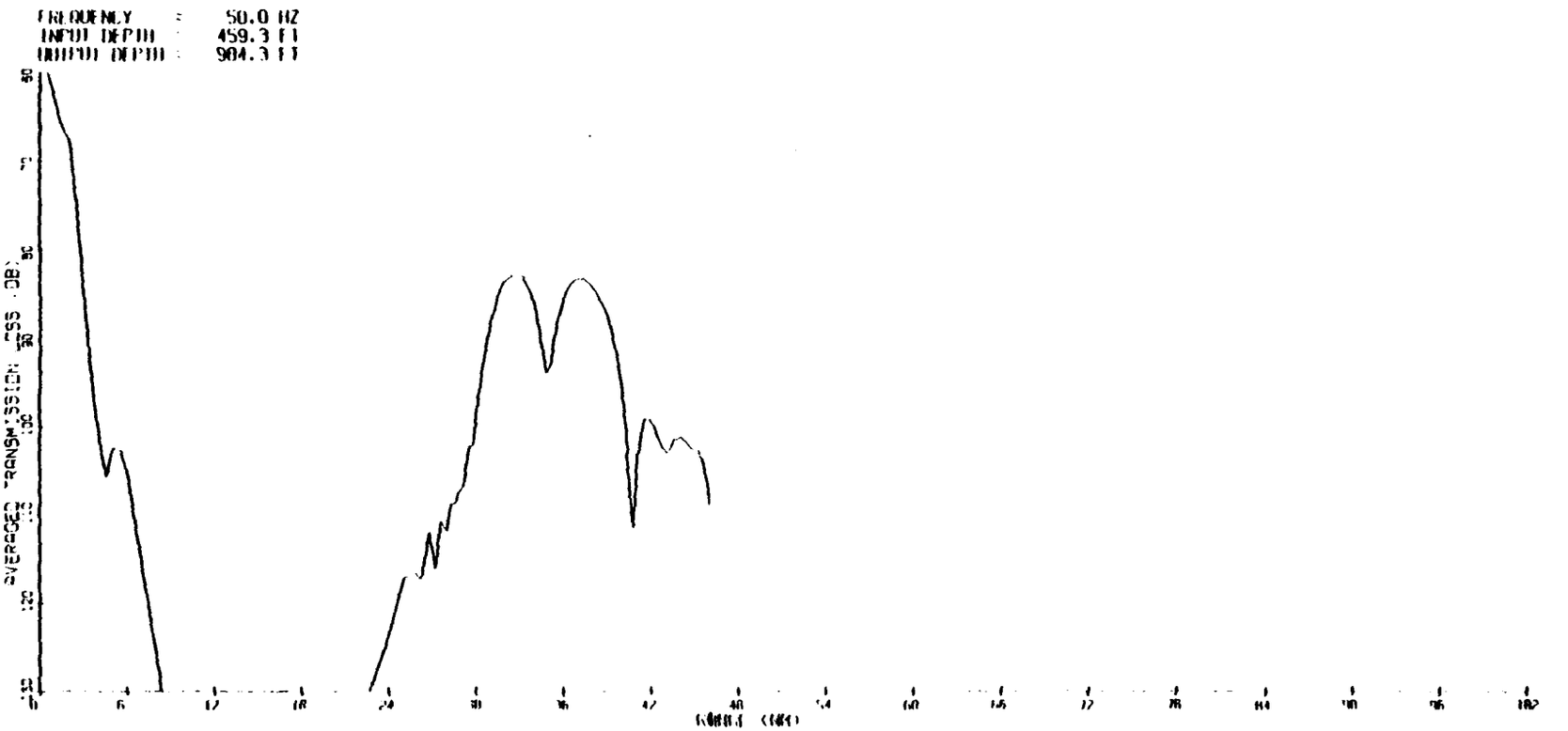

Figure A-74 WARM CORE/SARGASSO Transmission Loss (PE)
Receiver = 140 m, Source = 300 m 50 Hz

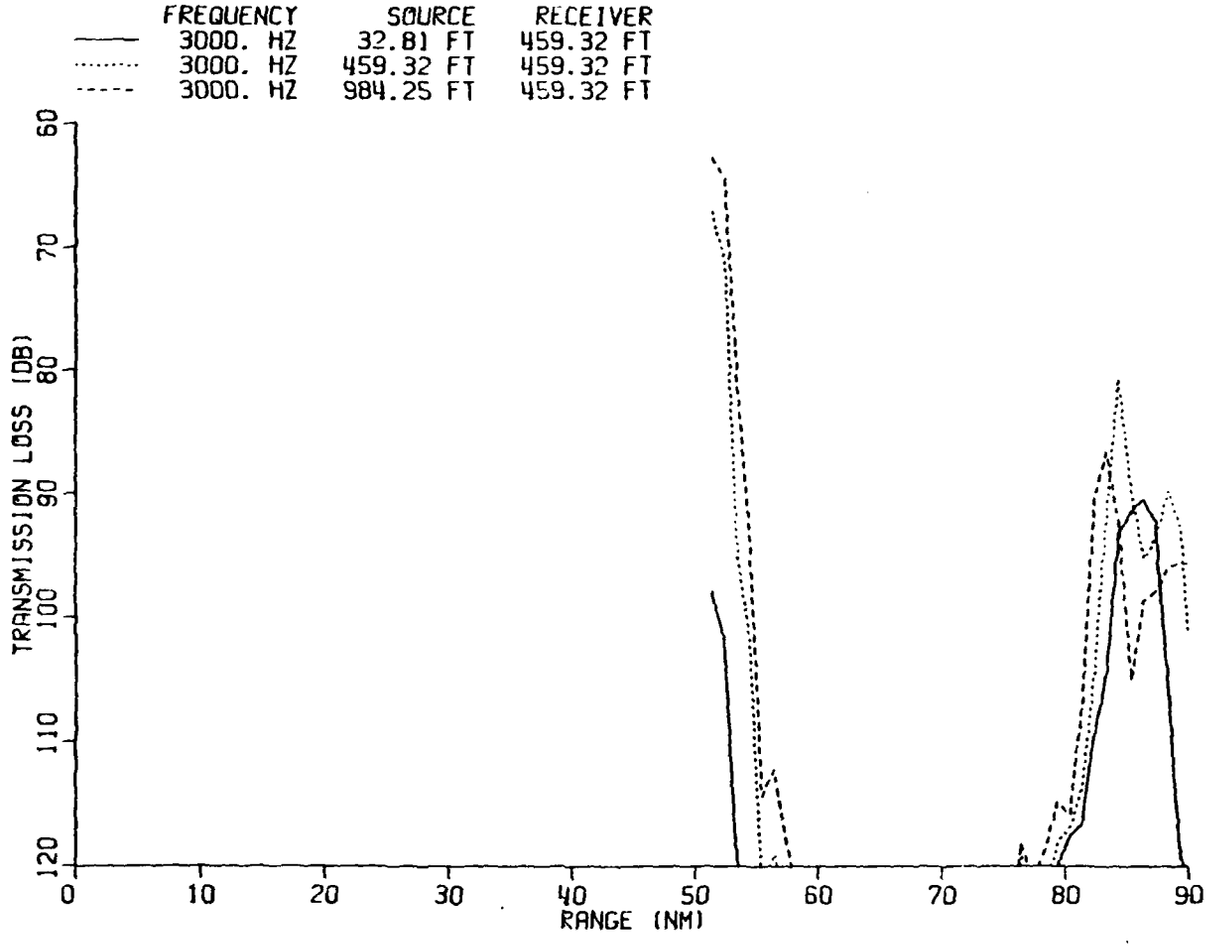

Figure A-75 WARM CORE/SARGASSO Transmission Loss (MPP)
Receiver = 140 m, 3,000 Hz

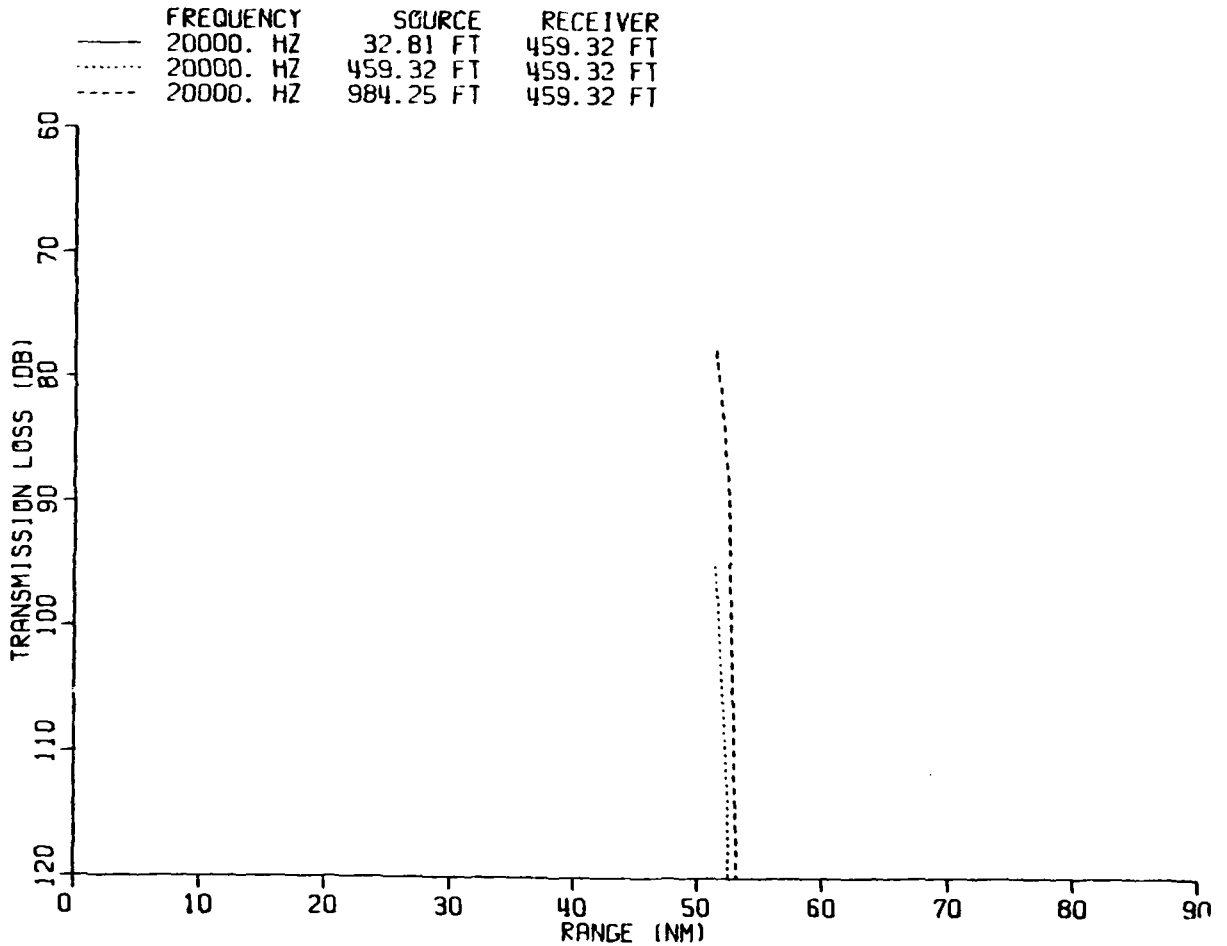

Figure A-76 WARM CORE/SARGASSO Transmission Loss (MPP)
Receiver = 140 m, 20,000 Hz

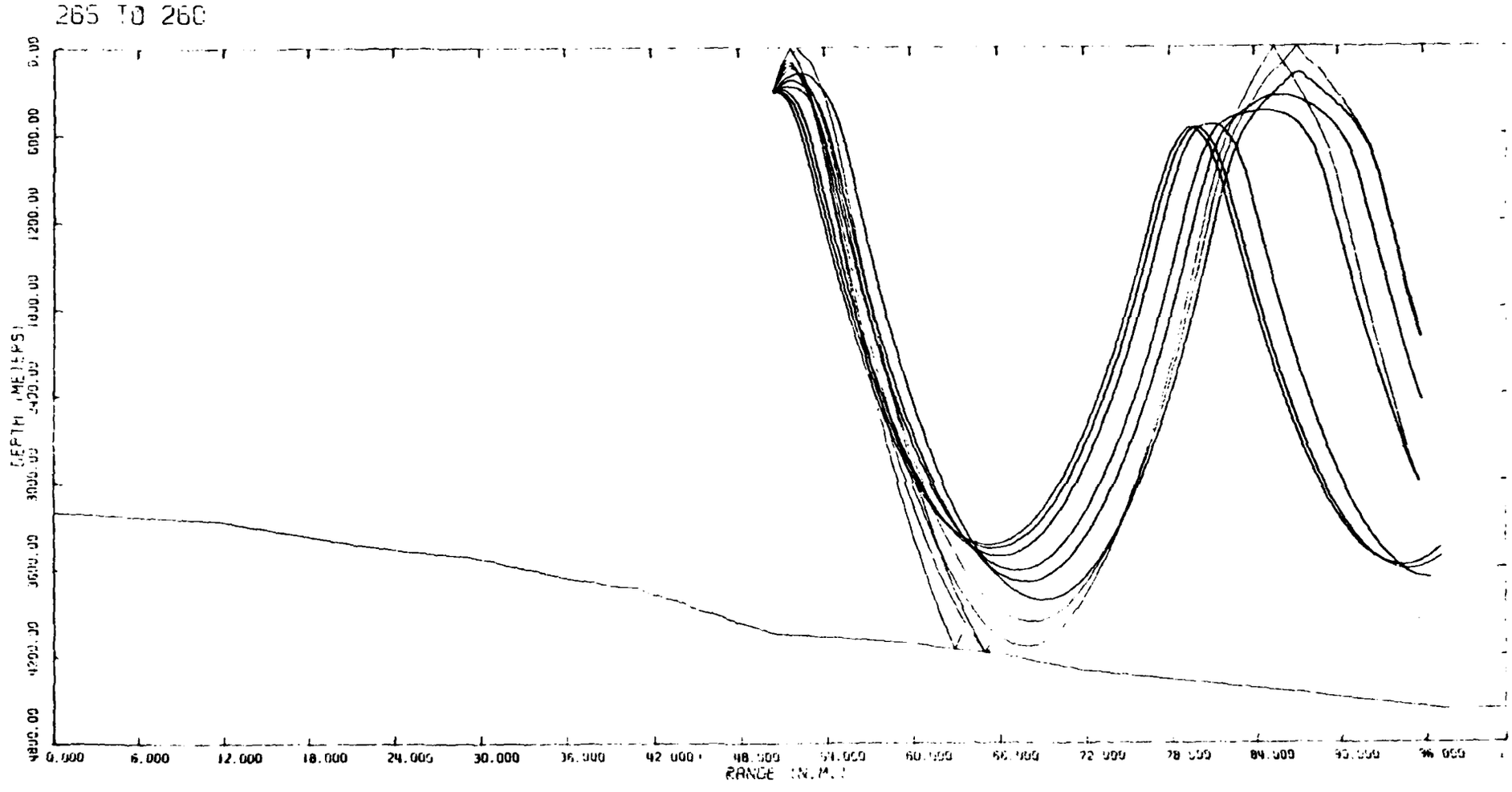

Figure A-77 WARM CORE/SARGASSO Ray plot
Receiver = 300 m, Source = 140 m
Angles plotted 0^{o}-10^{o}

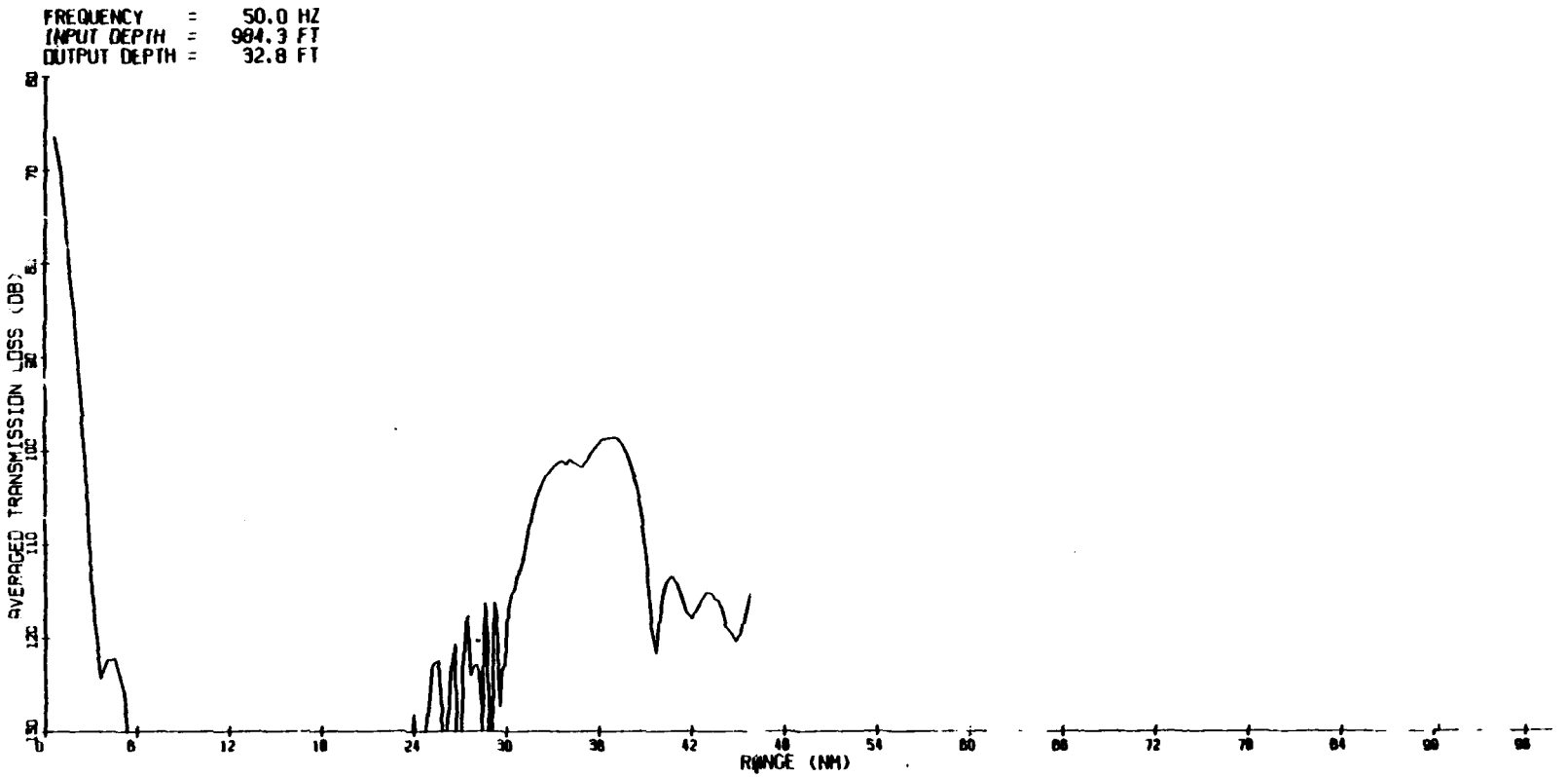

Figure A-78 WARM CORE/SARGASSO Transmission Loss (PE)
Receiver = 300 m, Source = 10 m 50 Hz

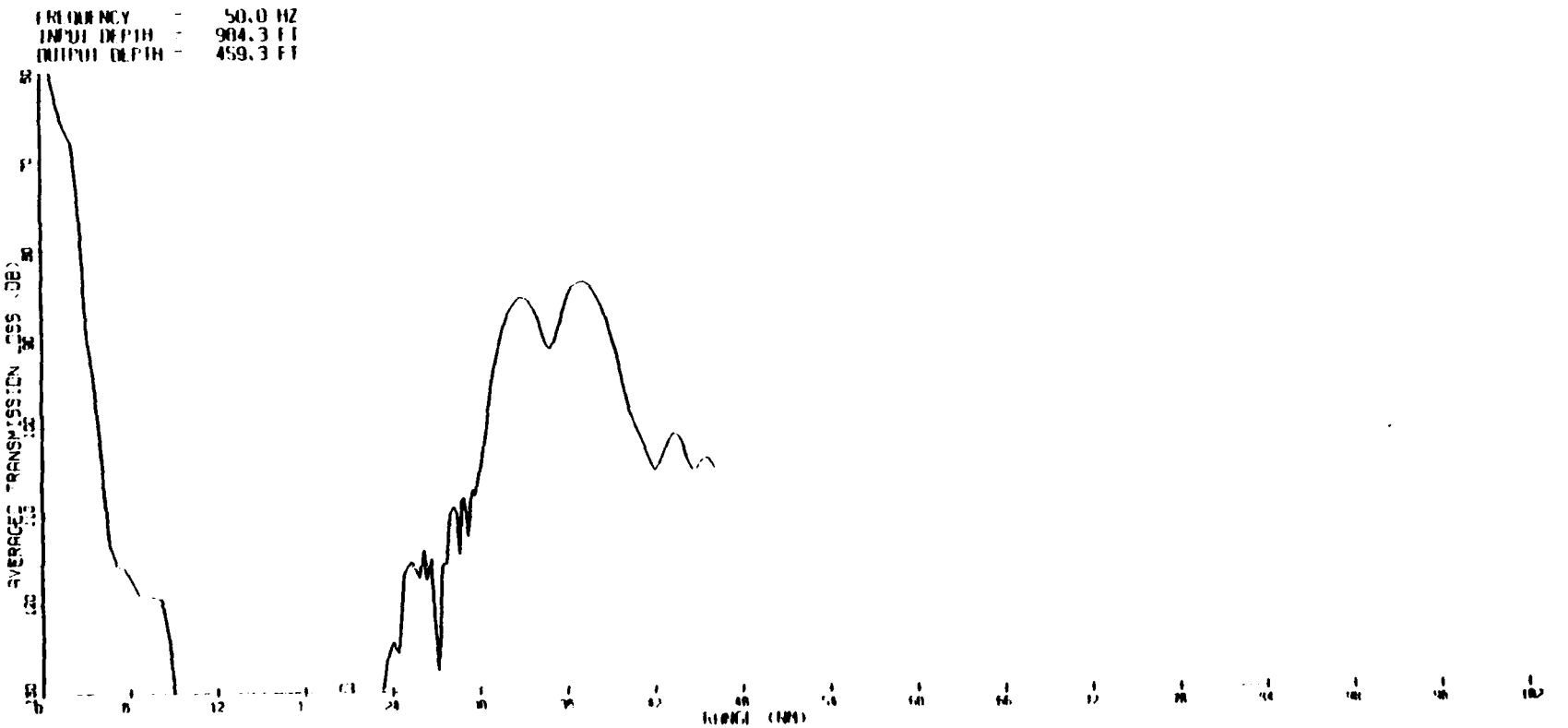

Figure A-79 WARM CORE/SARGASSO Transmission Loss (PE)
Receiver = 300 m, Source = 140 m 50 Hz

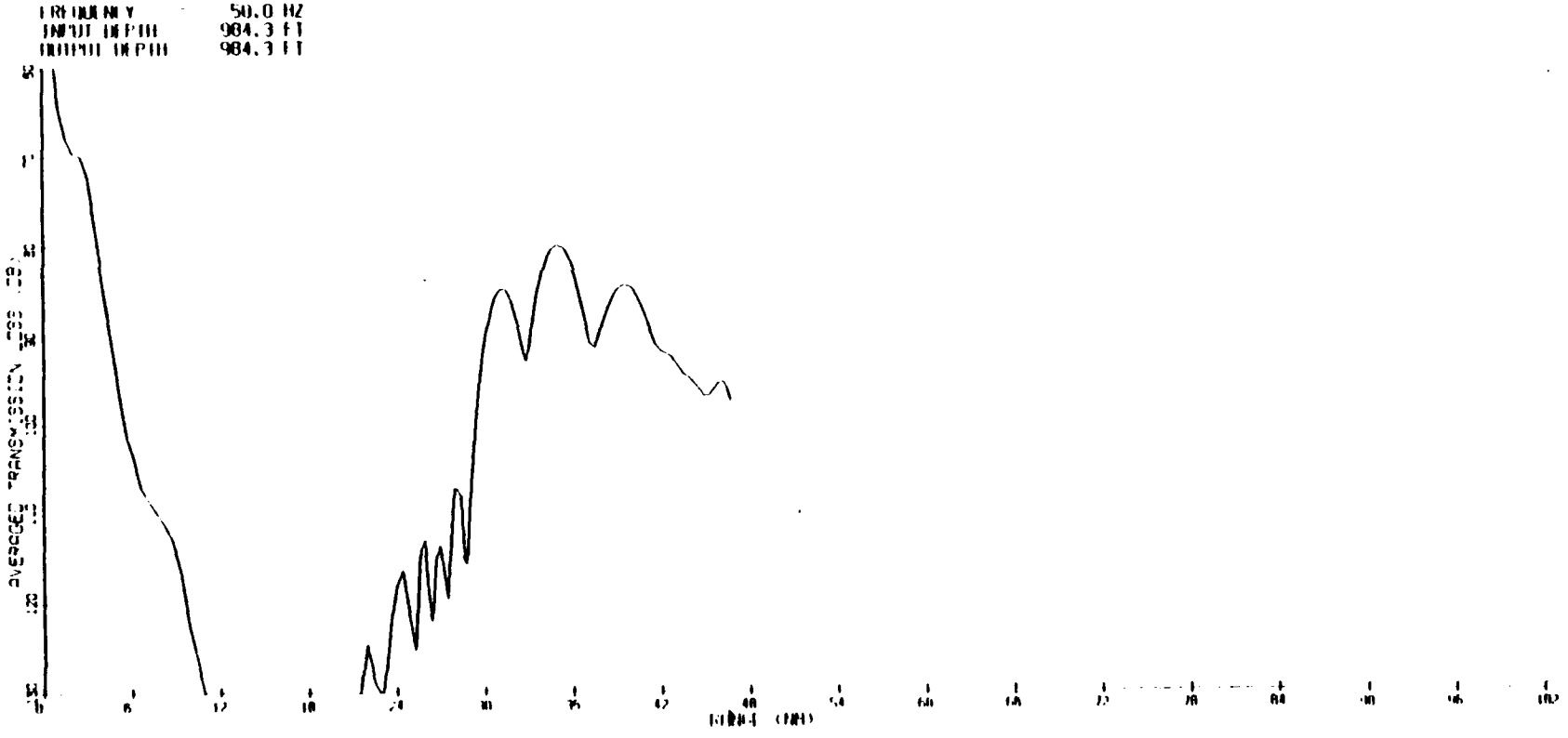

Figure A-80 WARM CORE/SARGASSO Transmission Loss (PE)
Receiver = 300 m, Source = 300 m 50 Hz

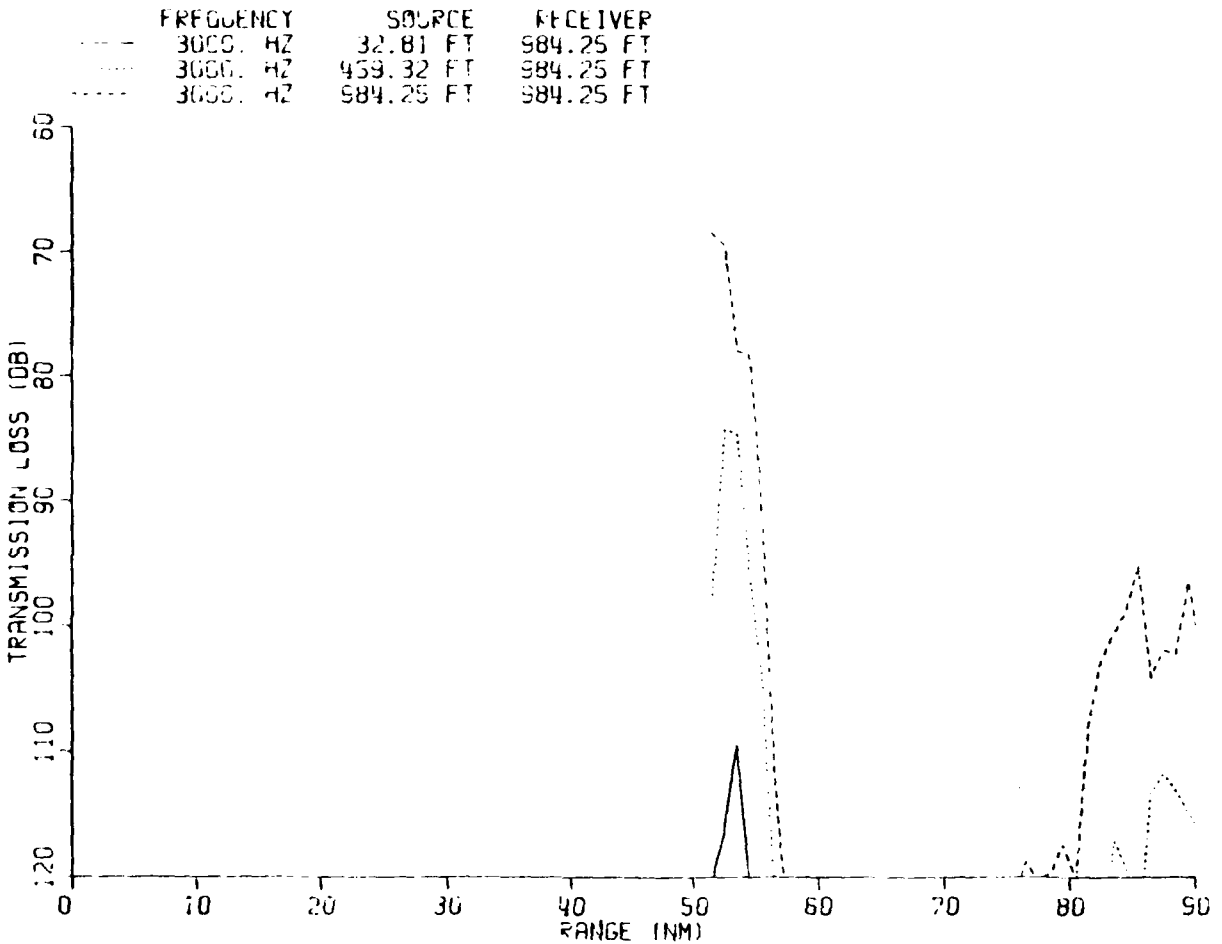

Figure A-81 WARM CORE/SARGASSO Transmission Loss (MPP)
Receiver = 300 m, 3,000 Hz

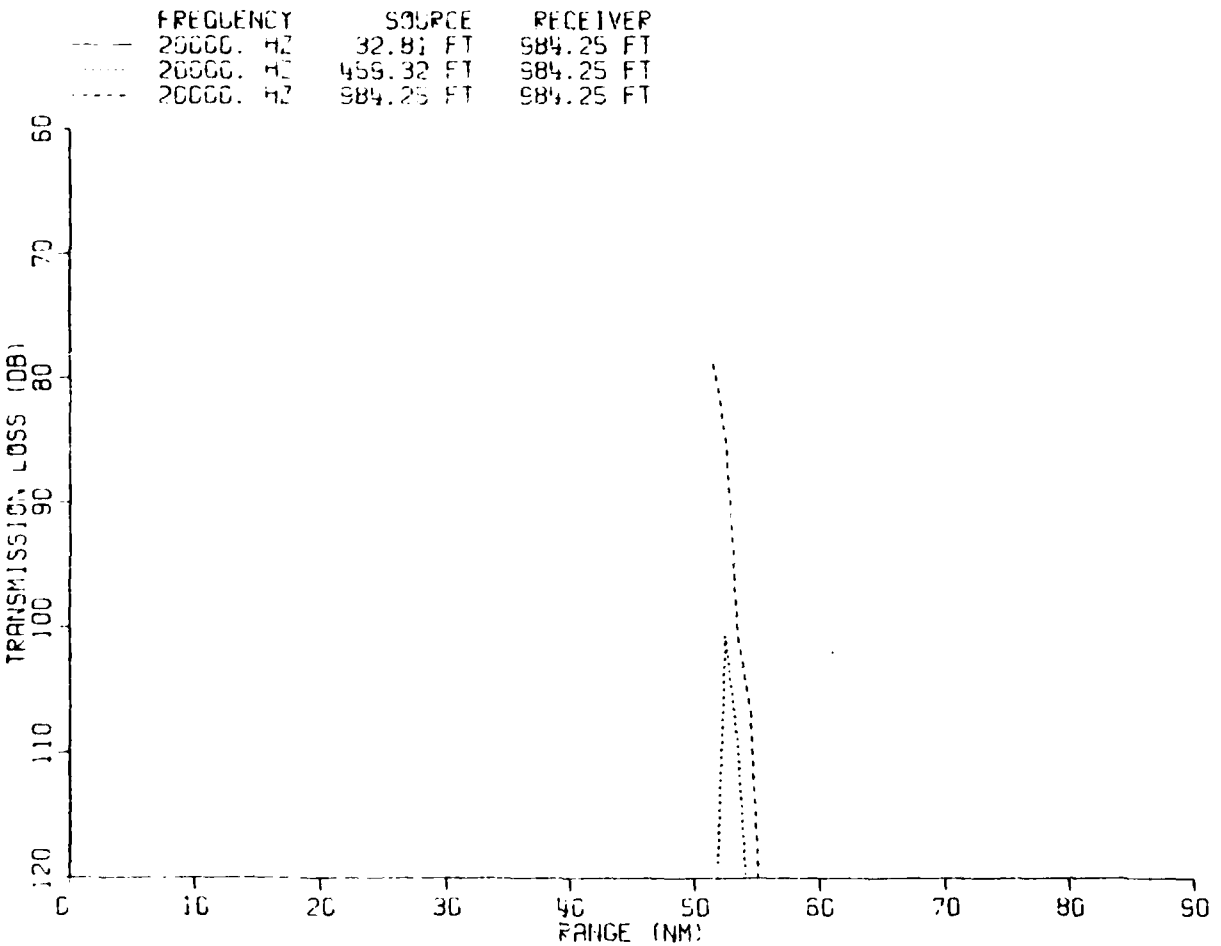

Figure A-82 WARM CORE/SARGASSO Transmission Loss (MPP)
Receiver = 300 m, 20,000 Hz

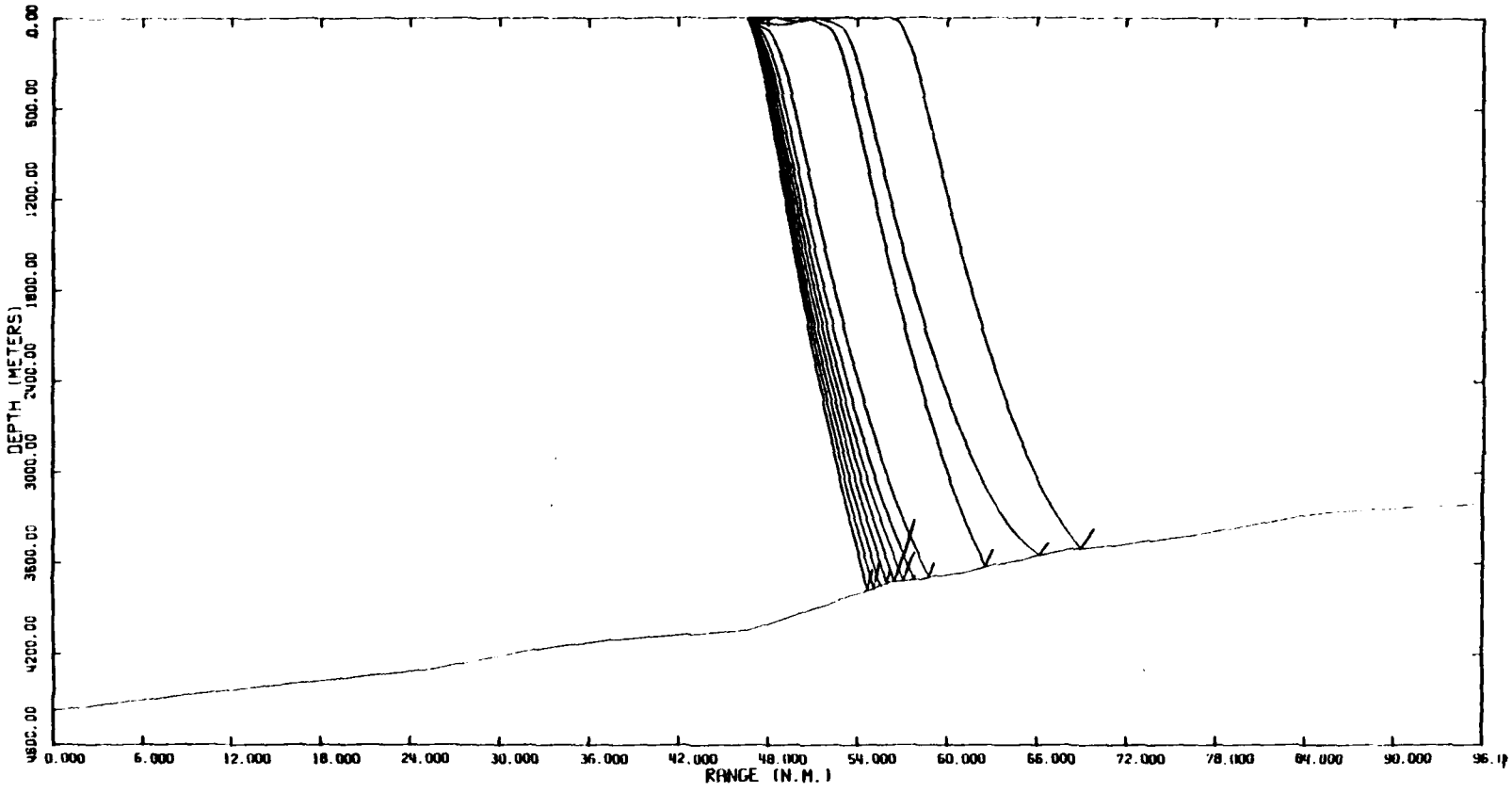

Figure A-83 WARM CORE/SLOPE Ray plot
Receiver = 10 m, Source = 140 m
Angles plotted 0^{o}-10^{o}

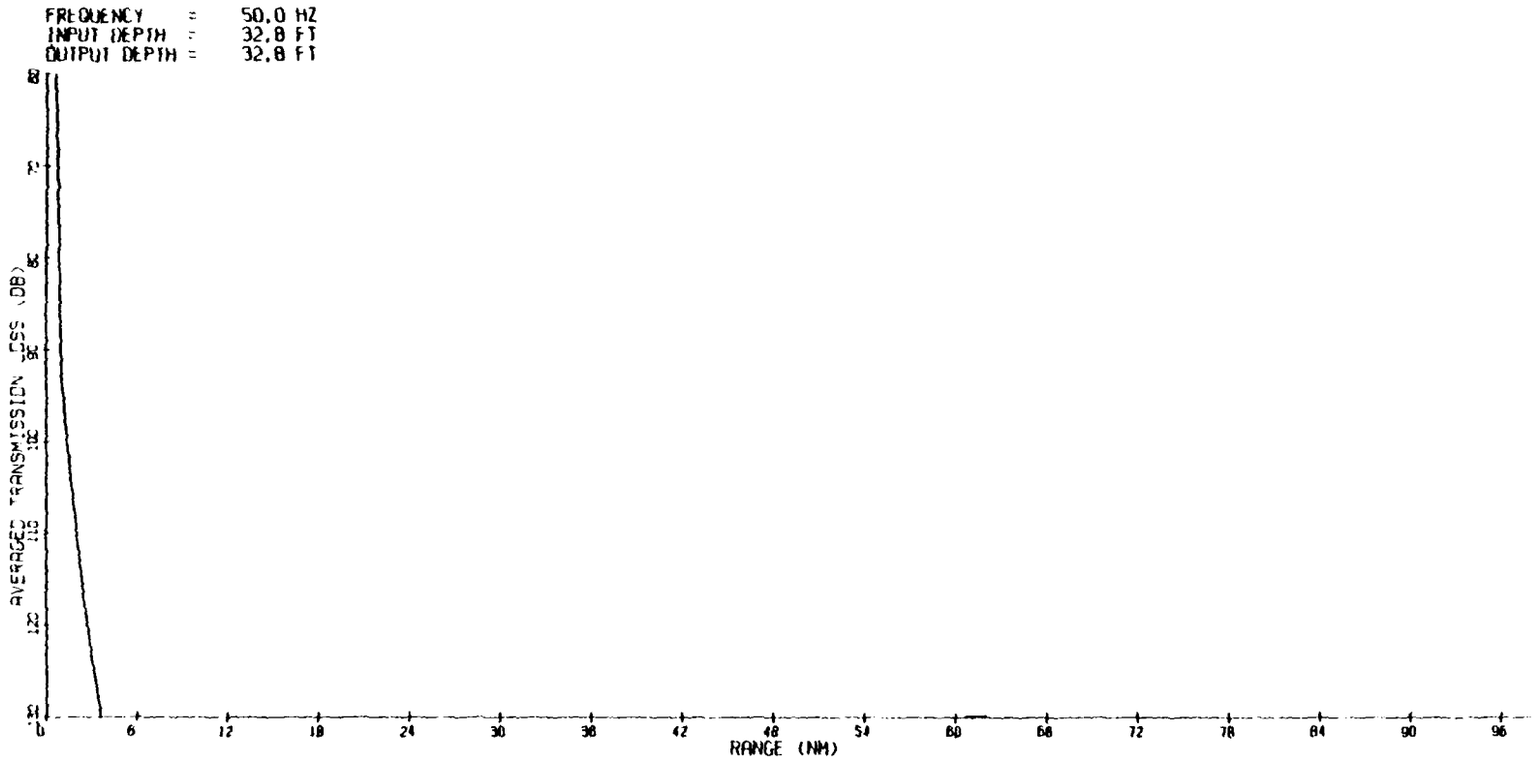

Figure A-84 WARM CORE/SLOPE Transmission Loss (PE)
Receiver = 10 m, Source = 10 m 50 Hz

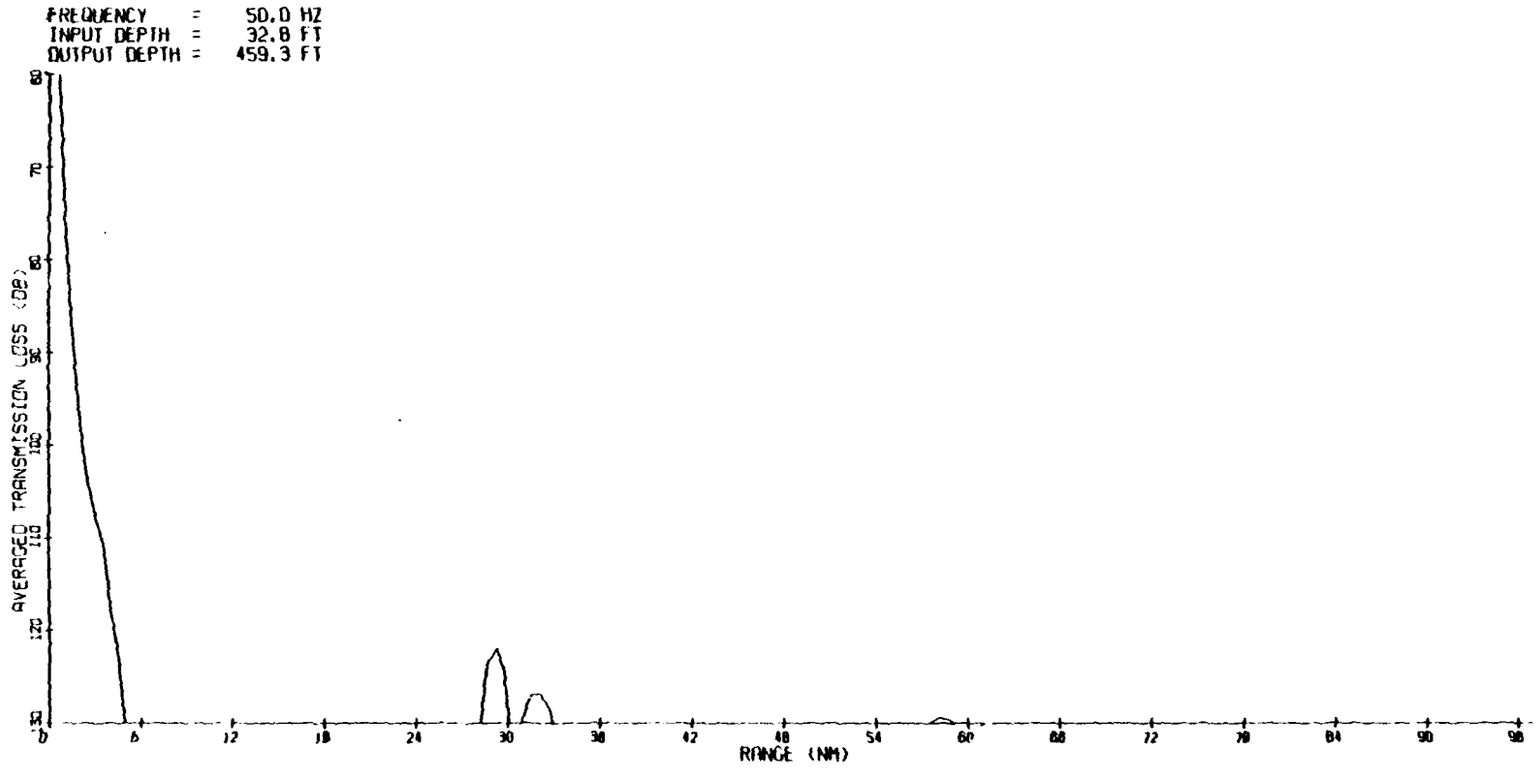

Figure A-85 WARM CORE/SLOPE Transmission Loss (PE)
Receiver = 10 m, Source = 140 m 50 Hz

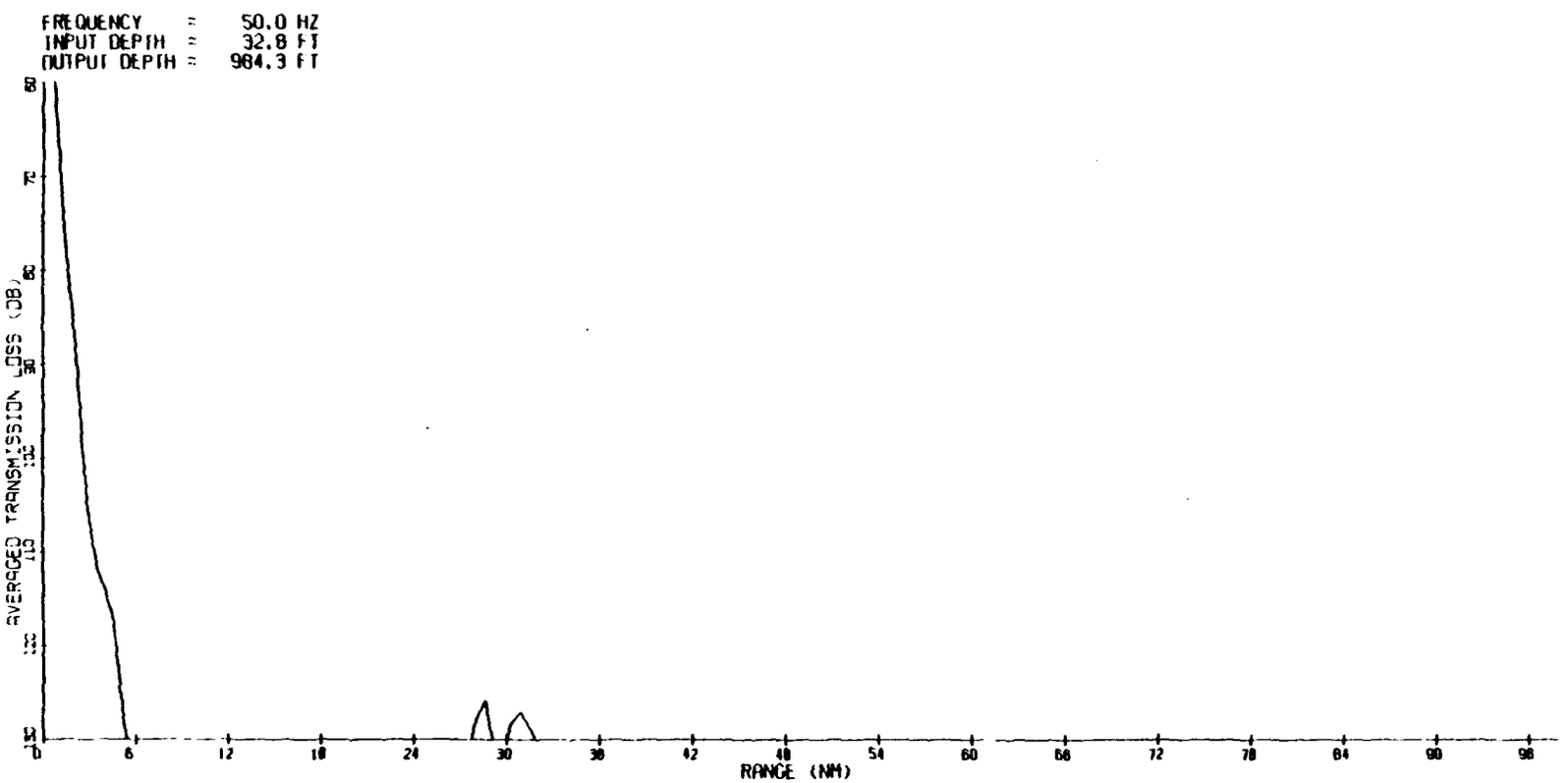

Figure A-86 WARM CORE/SLOPE Transmission Loss (PE)
Receiver = 10 m, Source = 300 m 50 Hz

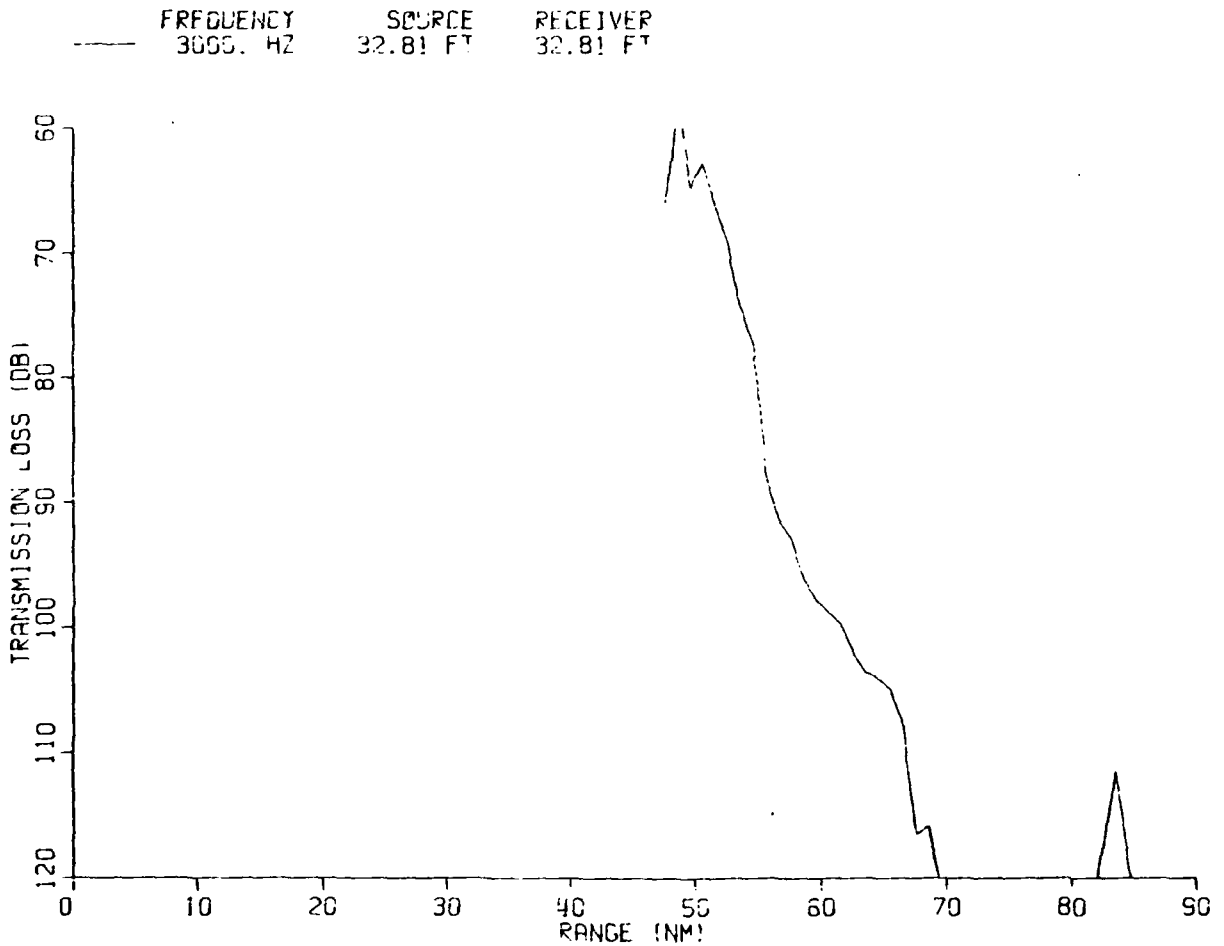

Figure A-87 WARM CORE/SLOPE *Transmission Loss* (MPP)
Receiver = 10 m, 3,000 Hz

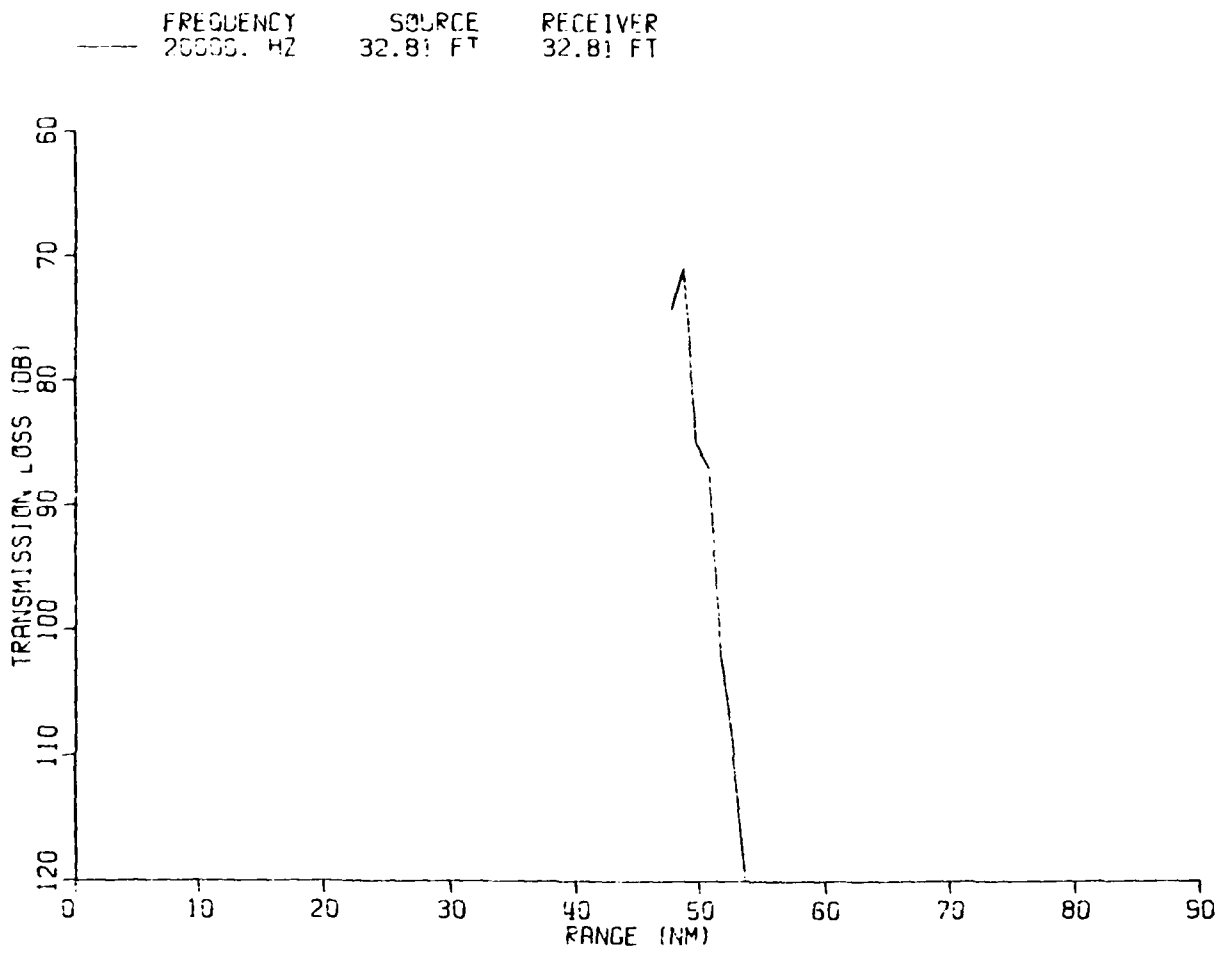

Figure A-88 WARM CORE/SLOPE Transmission Loss (MPP)
Receiver = 10 m, 20,000 Hz

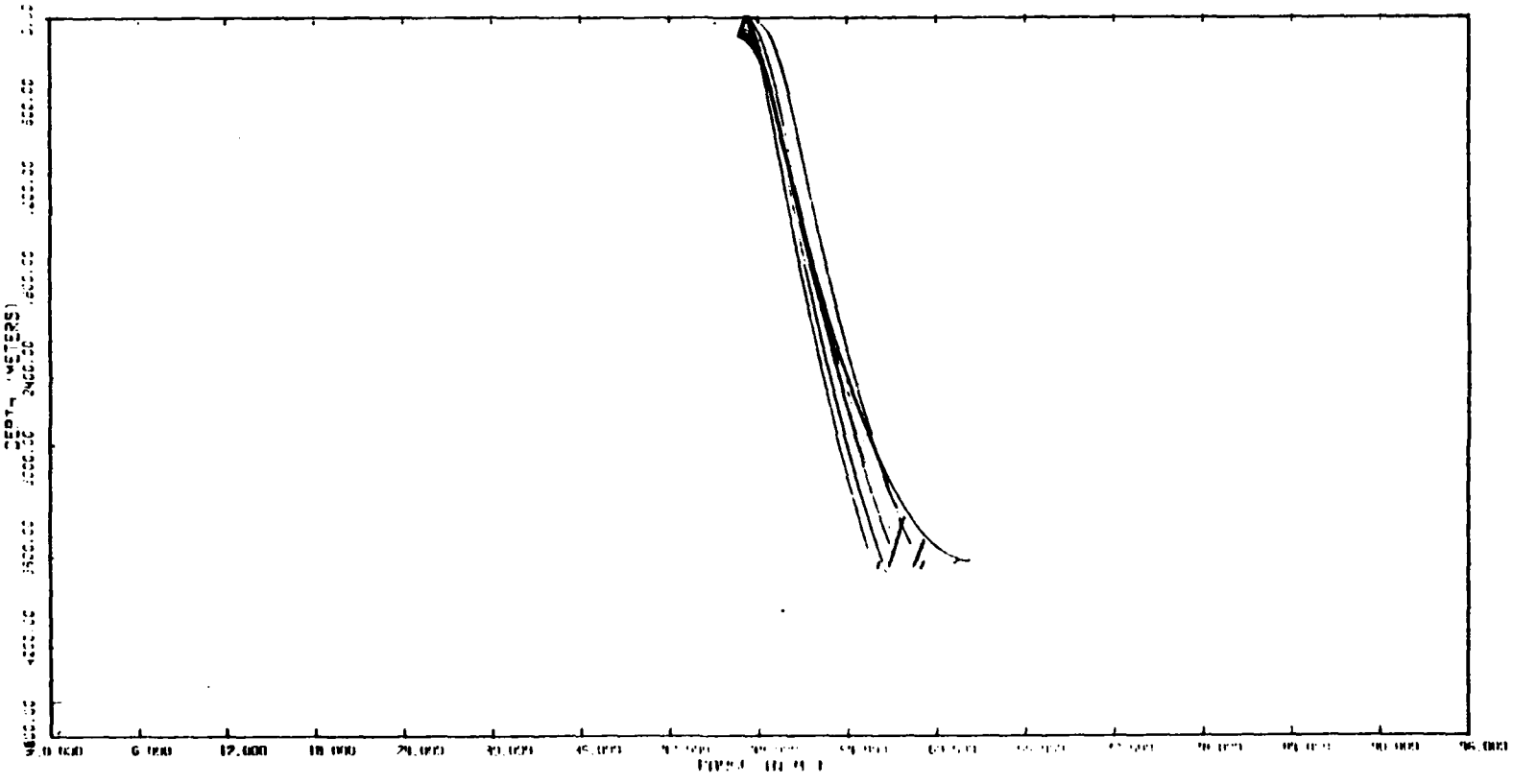

Figure A-89 WARM CORE/SLOPE Ray plot
Receiver = 140 m, Source = 140 m
Angles plotted 0^{o}-10^{o}

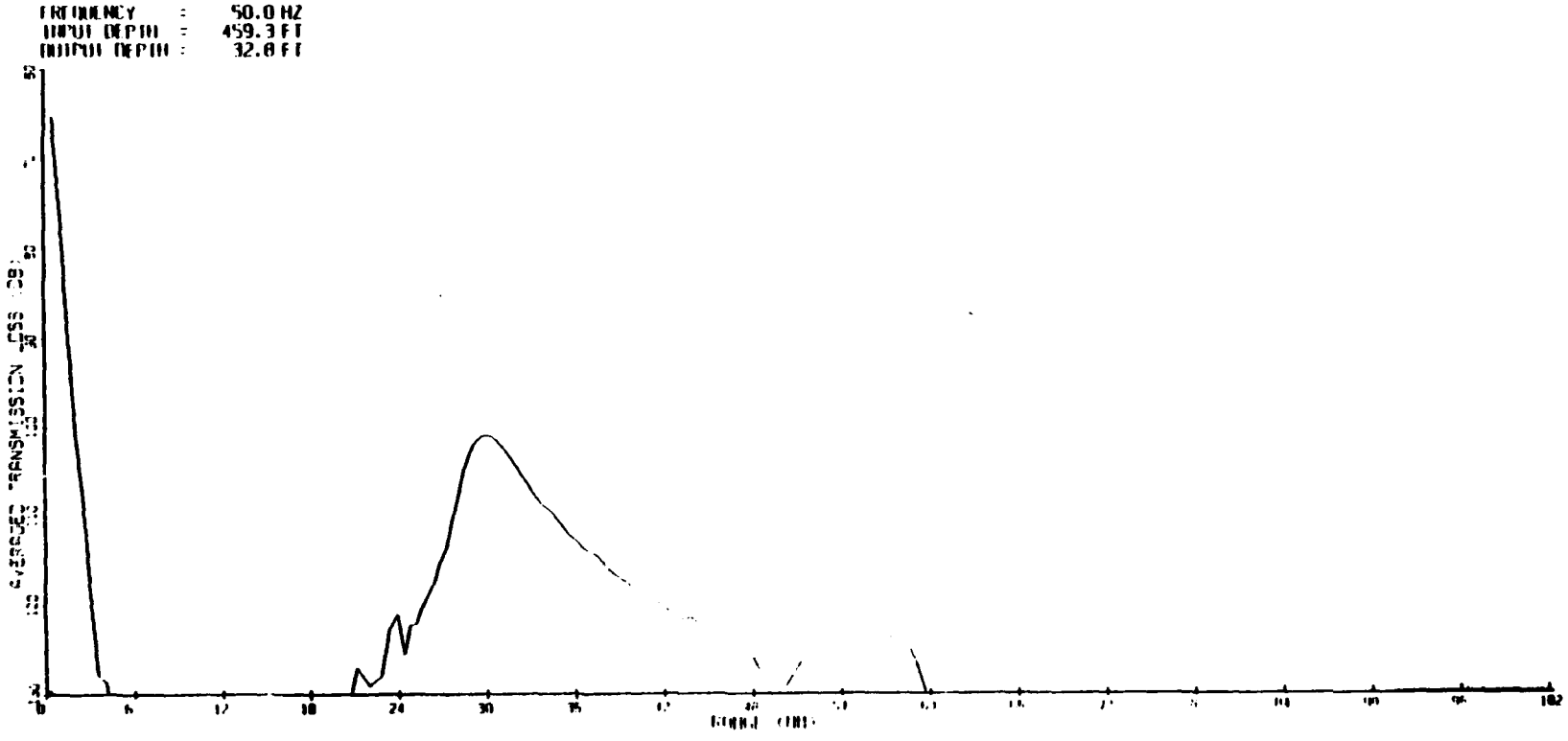

Figure A-90 WARM CORE/SLOPE Transmission Loss (PE)
Receiver = 140 m, Source = 10 m 50 Hz

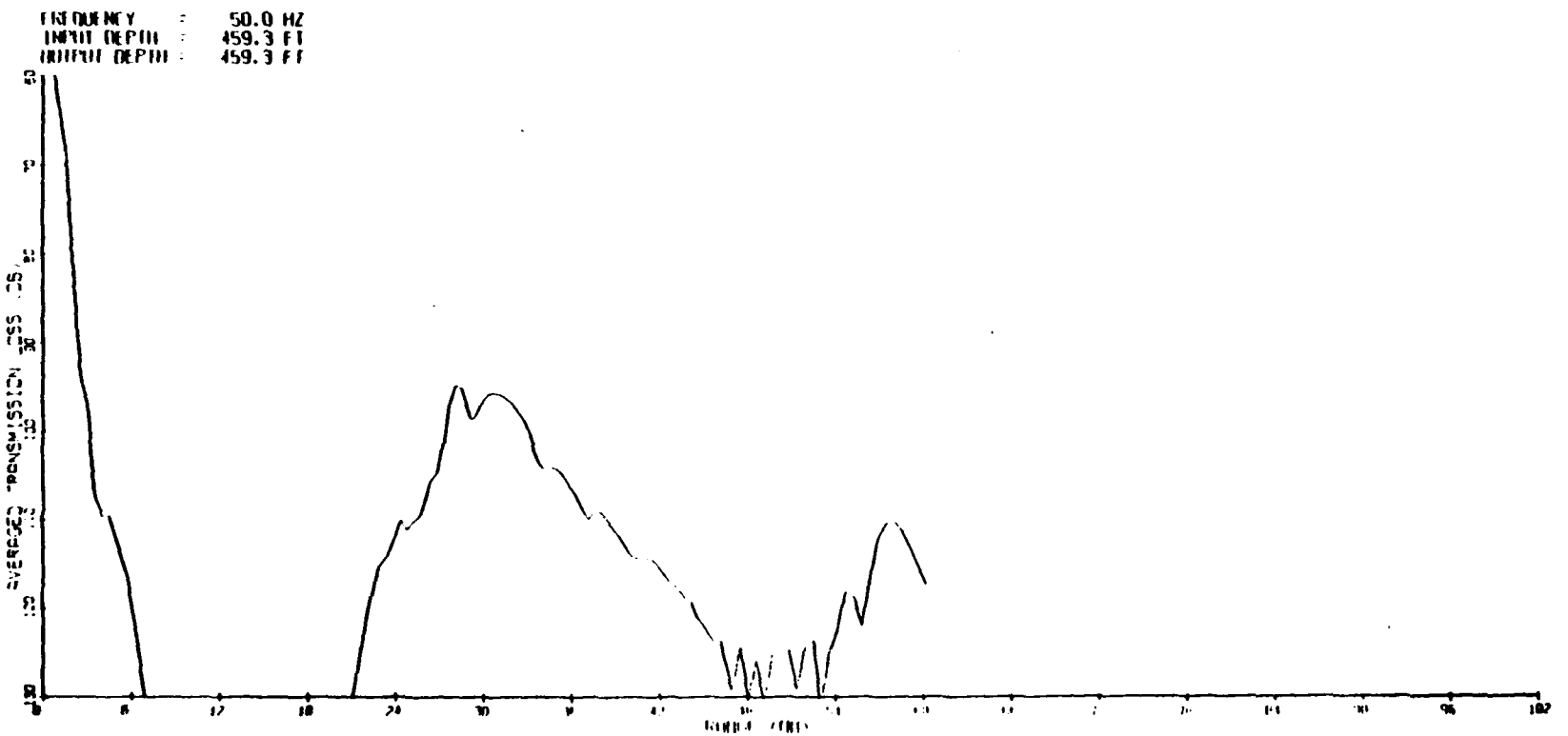

Figure A-91 WARM CORE/SLOPE Transmission Loss (PE)
Receiver = 140 m, Source = 140 m 50 Hz

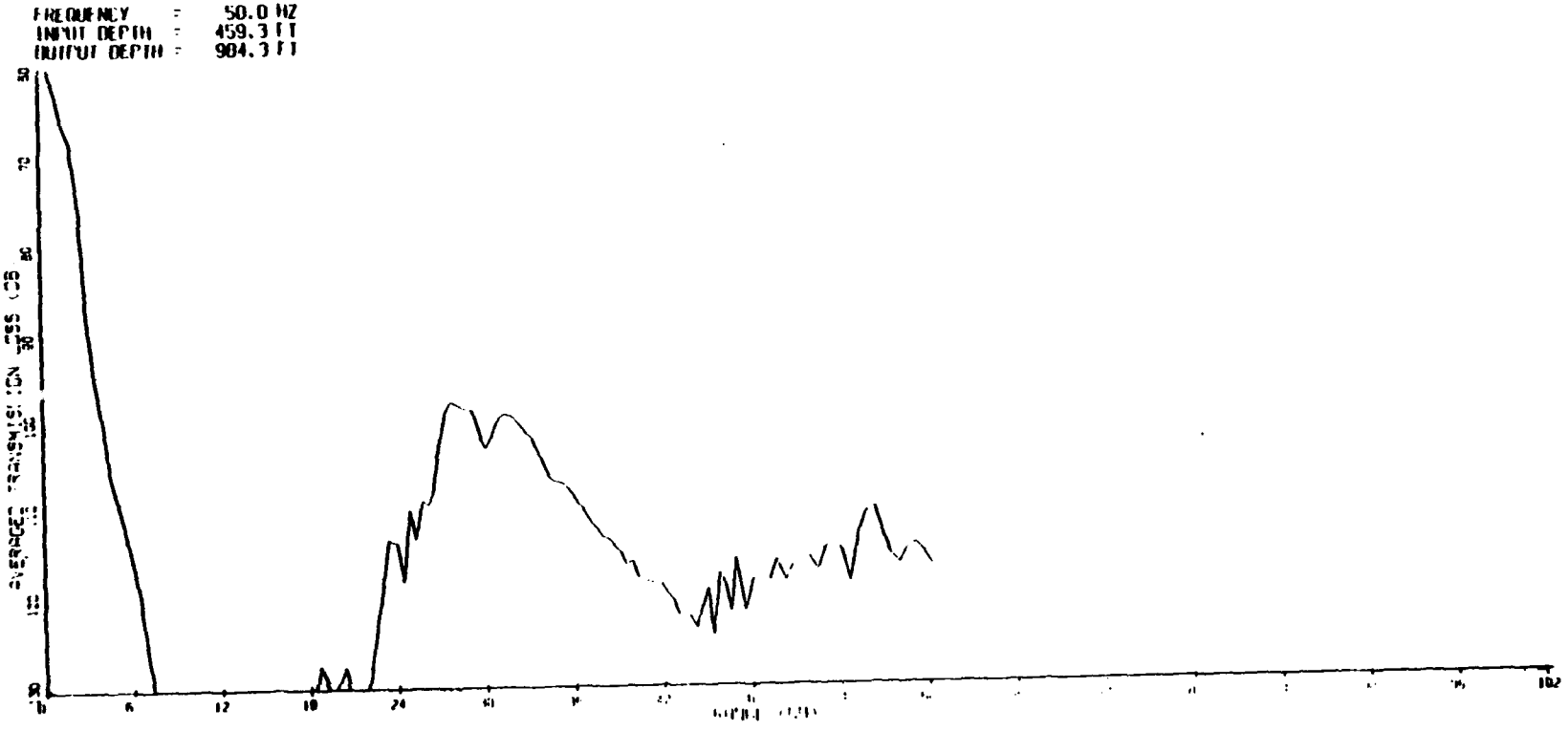

Figure A-92 WARM CORE/SLOPE Transmission Loss (PE)
Receiver = 140 m, Source = 300 m 50 Hz

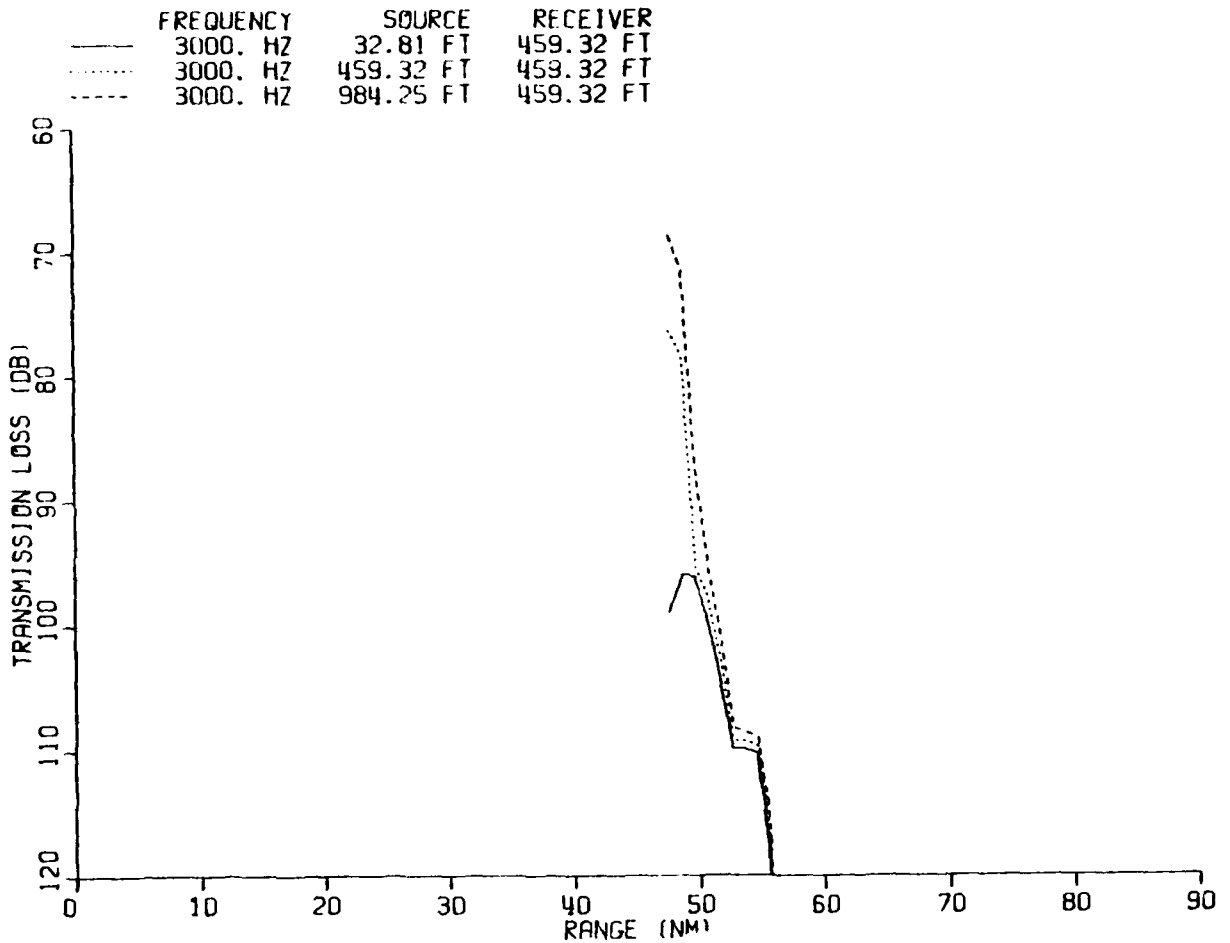

Figure A-93 WARM CORE/SLOPE Transmission Loss (MPP)
Receiver = 140 m, 3,000 Hz

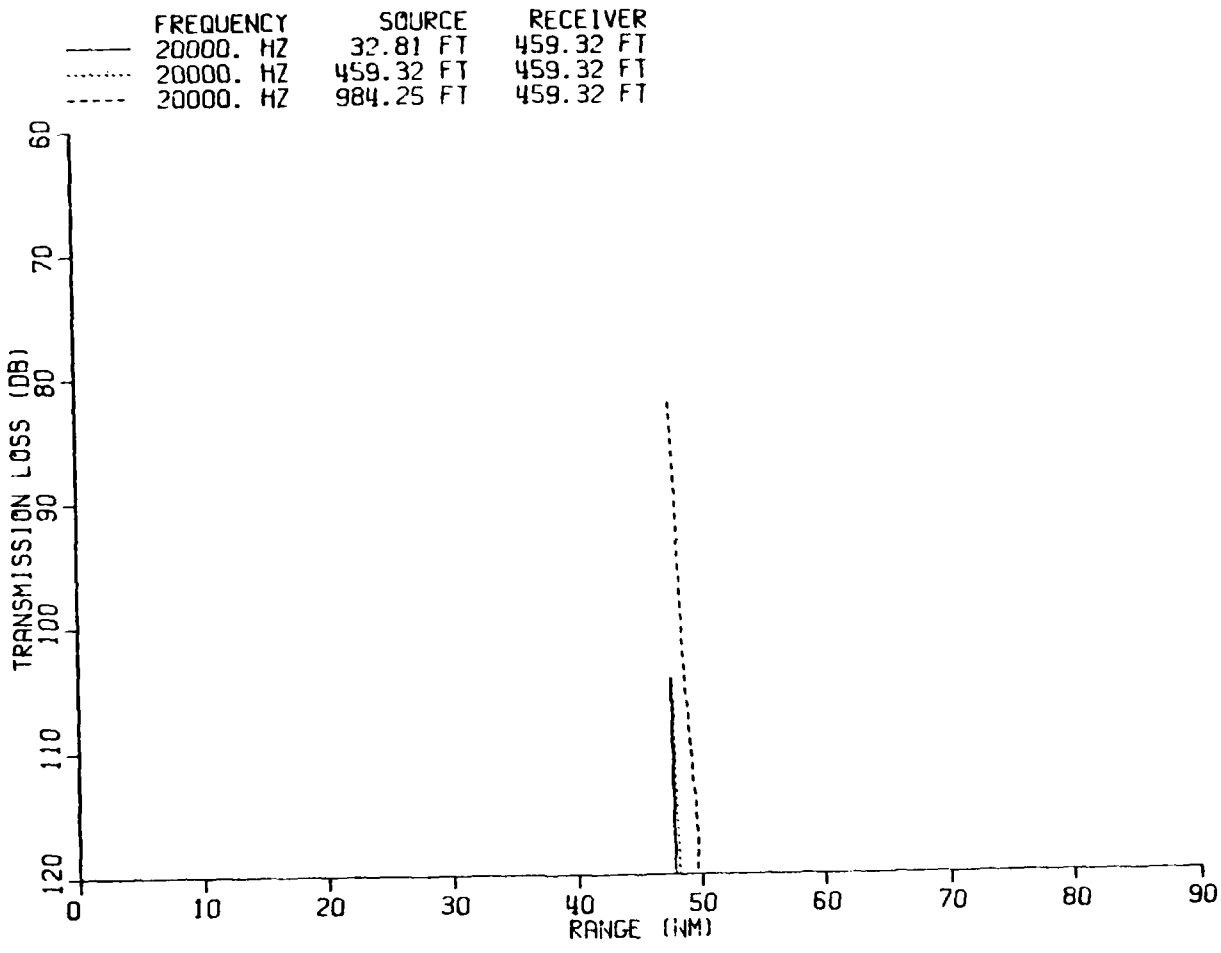

Figure A-94 WARM CORE/SLOPE Transmission Loss (MPP)
Receiver = 140 m, 20,000 Hz

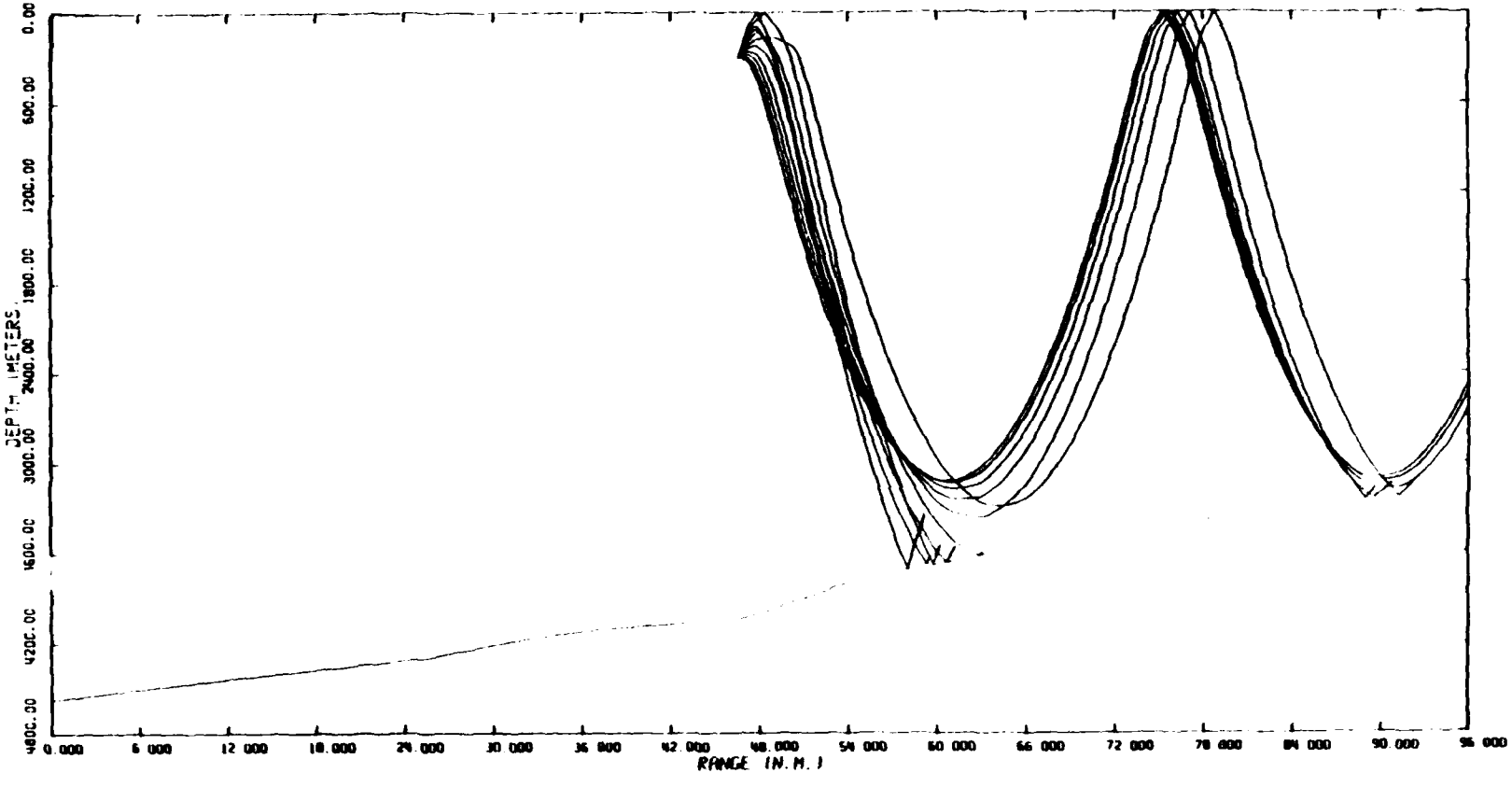

Figure A-95 WARM CORE/SLOPE Ray plot
Receiver = 300 m, Source = 140 m
Angles plotted 0^{o}-10^{o}

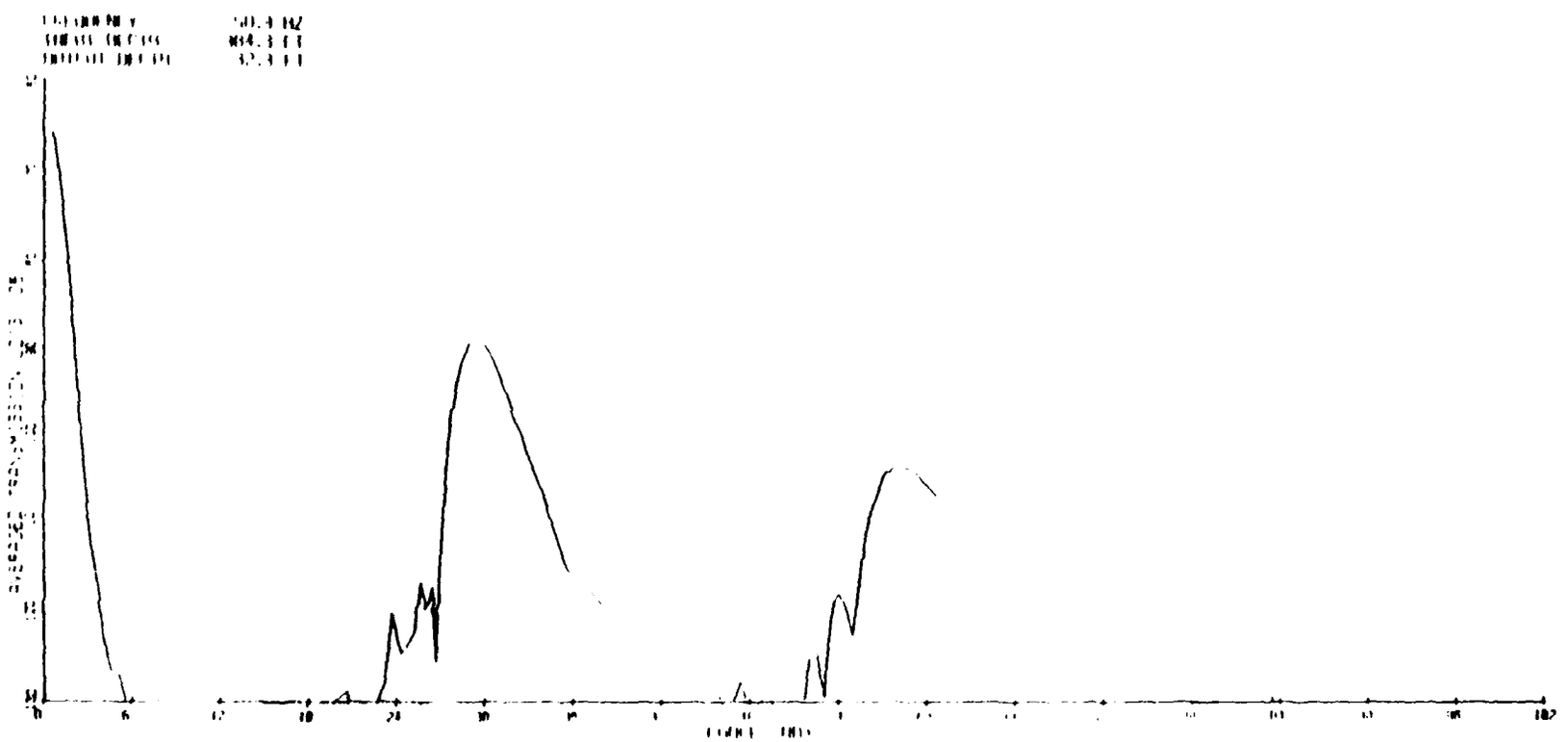

Figure A-96 WARM CORE/SLOPE Transmission Loss (PE)
Receiver = 300 m, Source = 10 m 50Hz

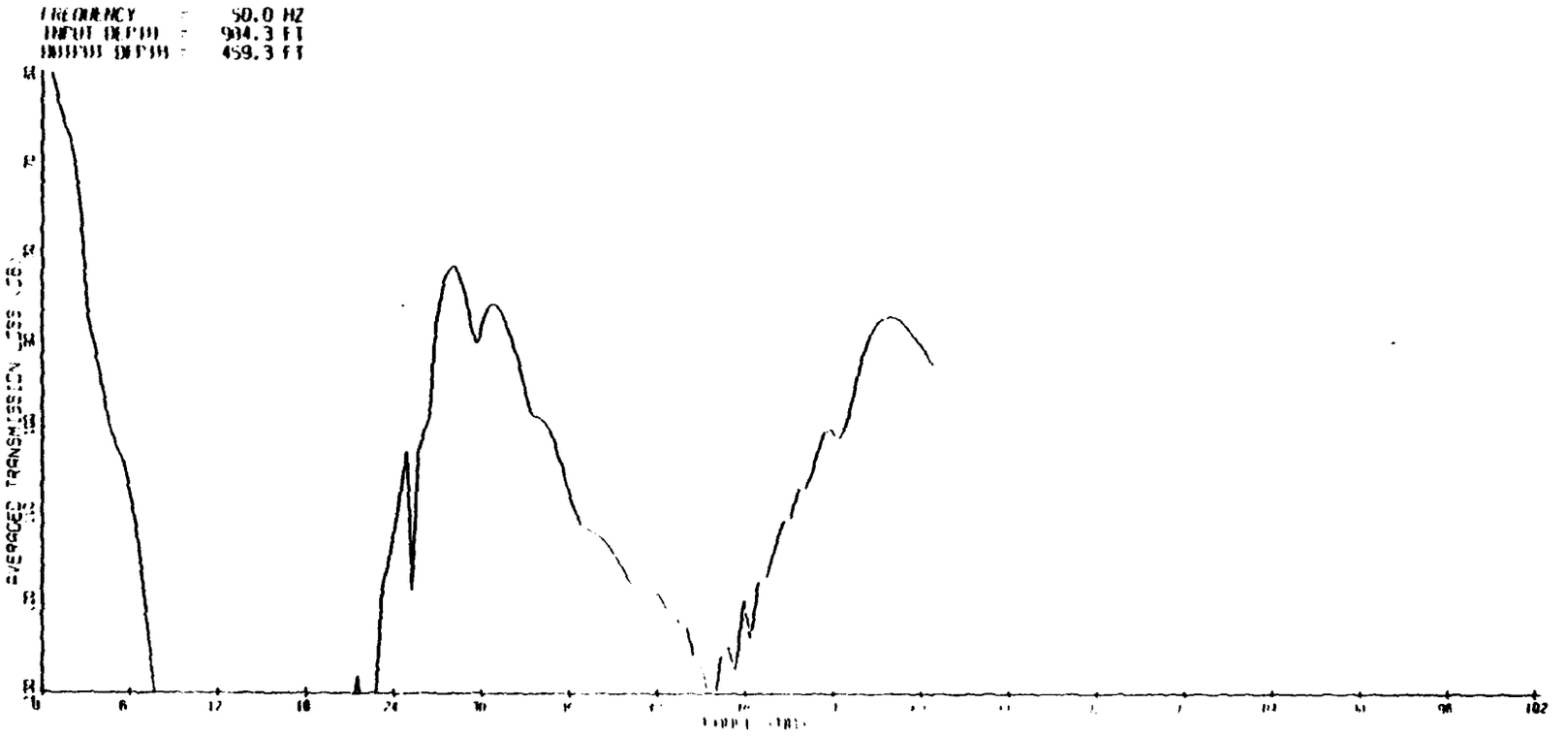

Figure A-97 WARM CORE/SLOPE Transmission Loss (PE)
Receiver = 300 m, Source = 140 m 50 Hz

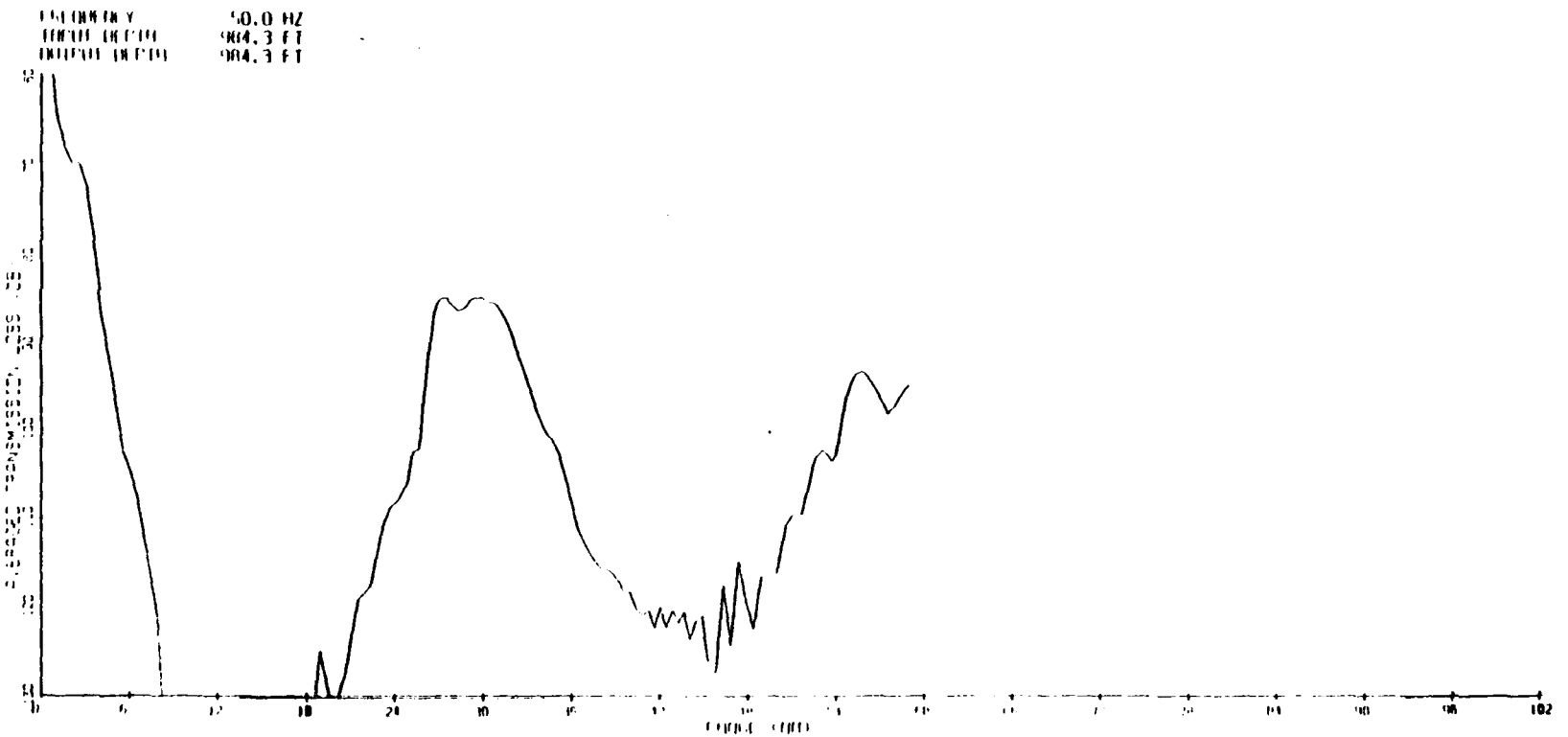

Figure A-98 WARM CORE/SLOPE Transmission Loss (PE)
Receiver = 300 m, Source = 300 m 50 Hz

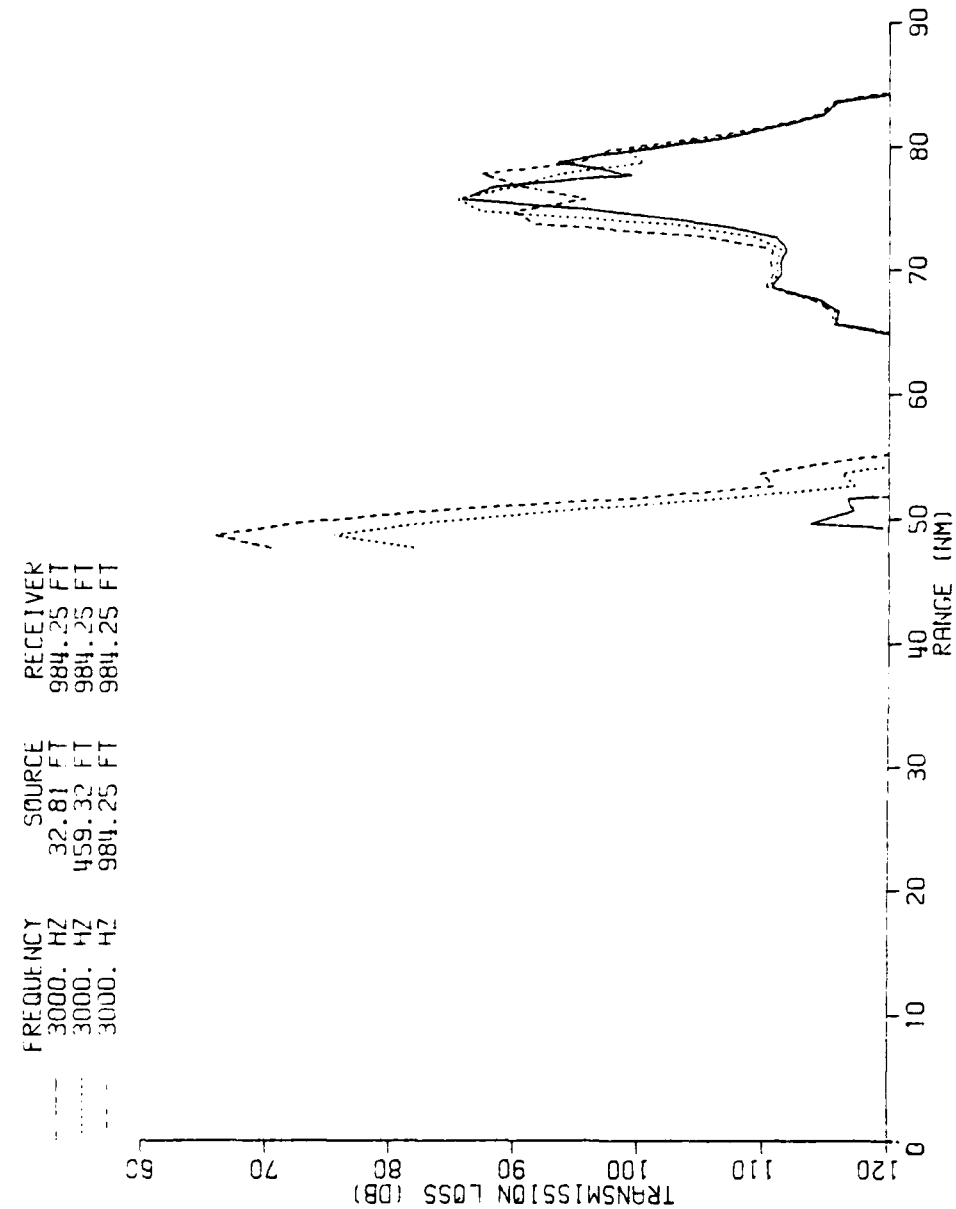

Figure A-99 WARM CORE/SLOPE Transmission Loss (MPP)
Receiver = 300 m, 3,000 Hz

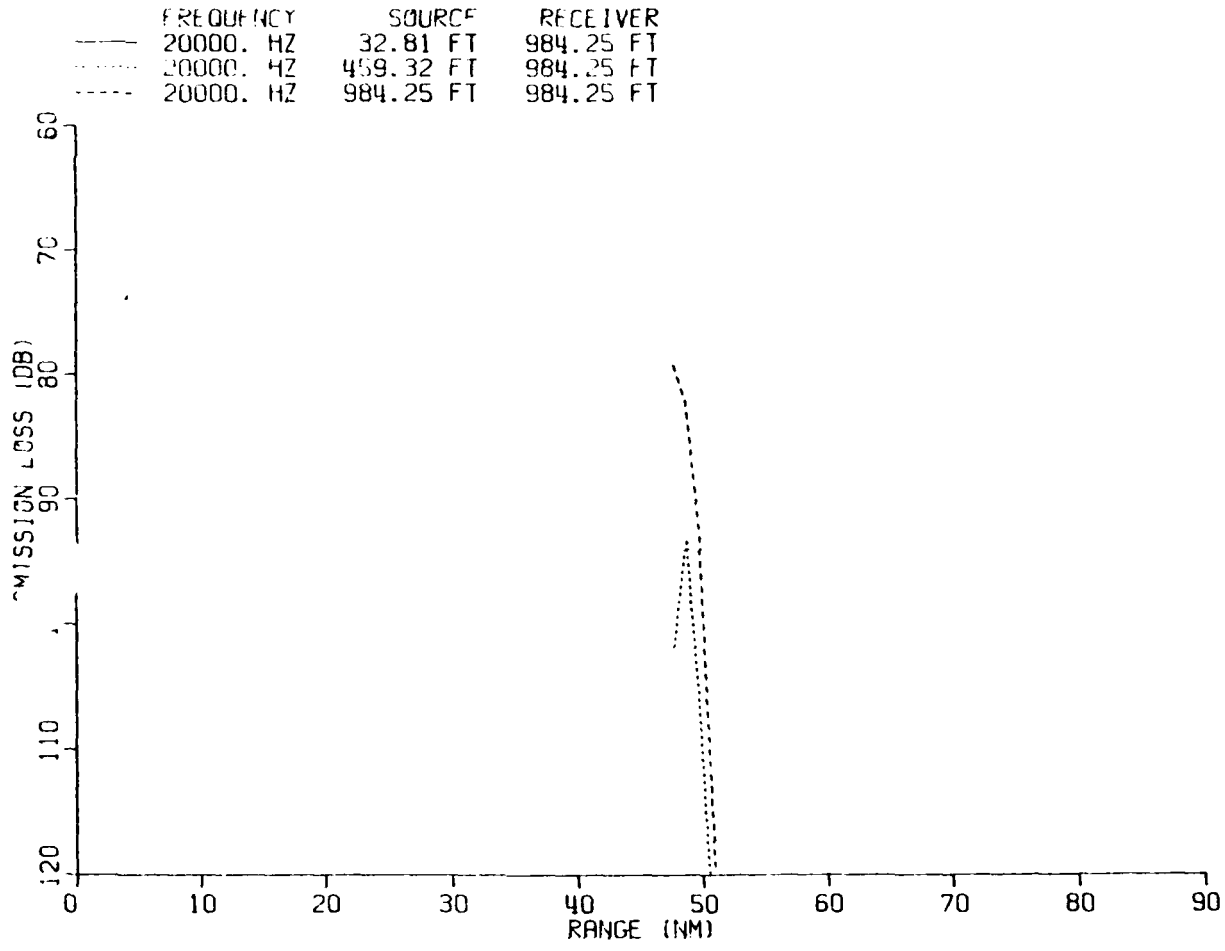

Figure A-100 WARM CORE/SLOPE Transmission Loss (MPP)
Receiver = 300 m, 20,000 Hz

REFERENCES

Brock, H. K., The AESD Parabolic Equation Model, internal report, AESD TN-75-07, ONR, Arlington, Va., 1975.

Cheney, R. E., Oceanographic Observations in the Western North Atlantic during FOX 1, May 1978, internal report, NAVOCEANO TN 370-79-78, U.S. Naval Oceanographic Office, Washington, D.C., 1978.

Cornyn, J. J., GRASS: A Digital-Computer Ray-Tracing and Transmission-Loss-Prediction System, Volume 1 - Overall Description, NRL Report 7621, Naval Research Laboratory, Washington, D.C., 1973.

Cornyn, J. J., GRASS: A Digital-Computer Ray Tracing and Transmission-Loss-Prediction System, Volume 2 - User's Manual, NRL Report 7642, Naval Research Laboratory, Washington, D.C., 1973.

D'Amico, A., and Blumen, L. S., Modeling the Impact of Oceanographic Variability on Acoustic Propagation in the Western North pacific, internal report, NAVOCEANO TN 3440-9-78, U.S. Naval Oceanographic Office, Washington, D.C., 1978.

Gold, B.A., Vigliotti, V., and Clark, J., Comparison Between Measured and Theoretical Transmission Loss Across the Gulf Stream, internal report, NAVOCEANO TN 9000-91-79, U. S. Naval Oceanographic Office, Washington, D.C., 1979.

Gulf Stream Monthly Summary, U.S. Naval Oceanographic Office, Washington, D.C., 1970 - 1974.

Hanna, J. S., Example of Acoustic Model Evaluation and Data Interpretation, J. Acoust. Soc. Am., 60, 1024 - 1031, 1976.

Huang, N.E., Leitao, C.D. and C. G. Parra, Large-Scale Gulf Stream Frontal Study Using Geos. 3 Radar Altimeter Data, Jour. of Geophy. Res., 83(c9), 1978, 4673-4682.

Istoshin, Y. V., Formative Area of the "Eighteen-Degree" Water in the Sargasso Sea, Okeanologiya, 1, 600-607 (trans. Deep-Sea Res., 9, 384-390) 1961.

Kedouri, E., and Cheney, R. E., Distribution, Characteristics, and some Acoustic Applications of Oceanic Fronts, paper presented at Acoustical Society of America, 95th meeting, Providence, R.I., May 1978.

Kupperman, S. L. and Garfield, N., Transport of Low-salinity Water at the Slope Water-Gulf Stream Boundary, Jour. of Geophys. Res., 82(24), 1977, 3481 - 3486.

Luyten, J. R., Scales of Motion in the Deep Gulf Stream and Across the Continental Rise, Jour. of Mar. Res., 35(1), 1977, 49 - 74.

Maul, G. A., deWitt, P. W., Yanaway, A., and Baig, S.R., Geostationary Satellite Observations of Gulf Stream Meanders: Infared Measurements and Time Series Analysis, Jour. of Geophys. Res., 83(C12), 1978, 6123 - 6135.

Robinson, A. R., Luyten, J. R., and Fulgister, F.C., Transient Gulf Stream Meandering. Part I: An Observational Experiment, Jour. of Phys. Ocn., 4(2), 1974, 237 - 255.

Stommel, H., The Gulf Stream. University of Calif. Press, Berkeley, 1966, 243.

Tappert, F. D. and Hardin, R. H., A Synopsis of the AESD Workshop on Acoustic Modeling by Non-Ray Techniques, 22 - 25 May, 1973, Washington, D.C., internal report, AESD TN-73-05, ONR, Arlington, Va., 1973.

Tappert, F. D., Parabolic Equation Method in Underwater Acoustics, J. Acoust. Soc. Am., 35, S34(A), 1974.

Thompson, R. O. R. Y., Observations of Rossby Waves Near Site D. In Progress in Ocn., Vol. 7, 1977, 135 - 162.

Vigoureaux, P. and Hersey, J. B., Sound in the Sea, In The Sea, Vol. 1, 1962, 476 - 497.

Worthington, L. V., The 18° Water in the Sargasso Sea, Deep-Sea Res., 5, 1959, 297-305.

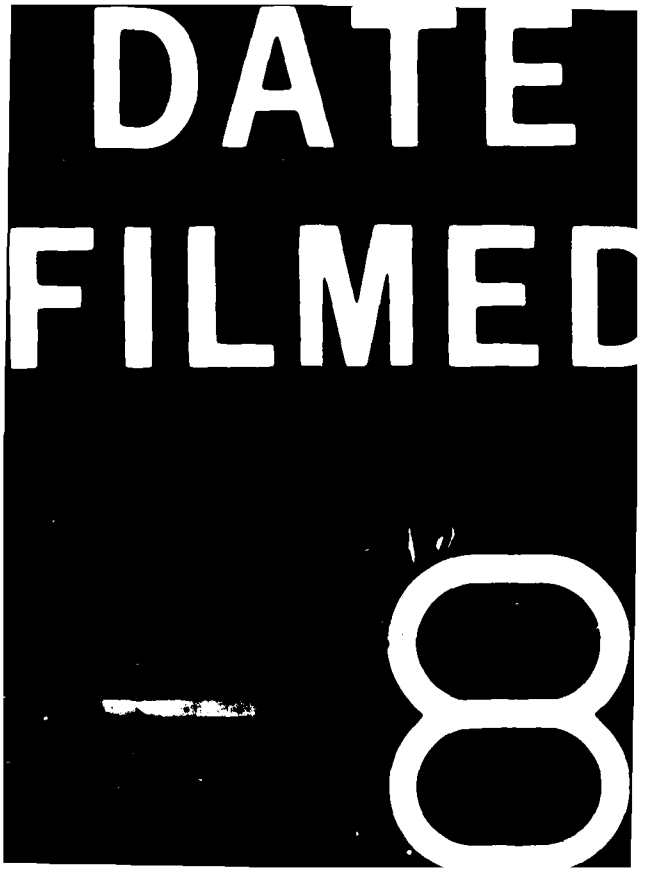
DATE
FILMED
8